emen ta zabal zazu
Universidad del País Vasco
Euskal Herriko Unibertsitatea
CSIC
Consejo Superior de Investigaciones Científicas
Instituto Biofisika Institutua

Interaction between colicin A pore-forming domain and its cognate immunity protein

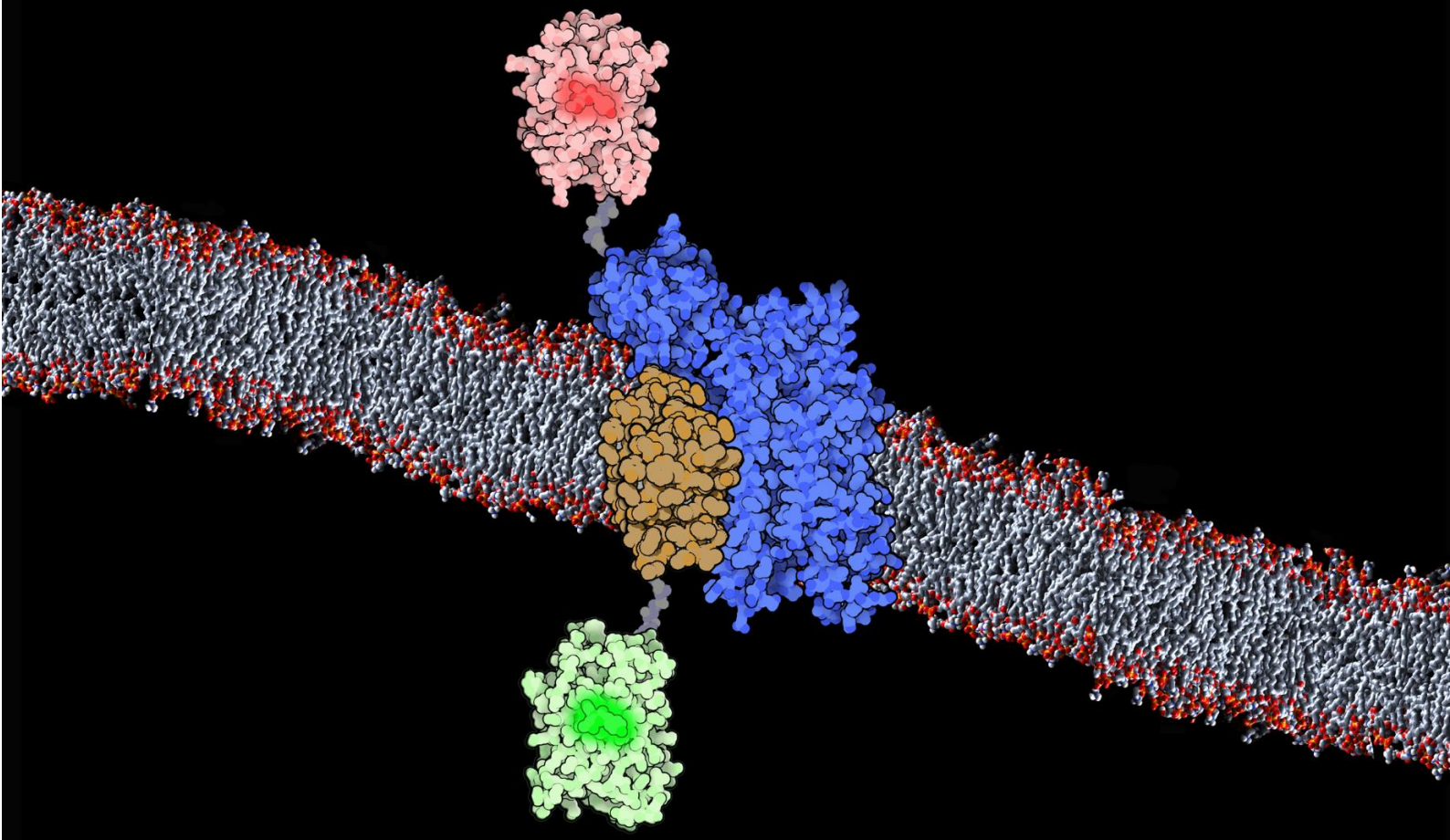

Doctoral Thesis

Ane Metola Martinez

Interaction between colicin A pore-forming domain and its cognate immunity protein

Biofisika Institute (UPV/EHU, CSIC)
Department of Biochemistry and Molecular Biology
Faculty of Science and Technology
University of the Basque Country (UPV/EHU)

Doctoral Thesis

Ane Metola Martinez

Leioa 2017

INDEX

INDEX i

ACKNOWLEDGMENTS iii

ABBREVIATIONS v

1. **INTRODUCTION AND OBJECTIVES** 1

1.1 Membrane proteins in the bilayer 1

1.1.1 Membrane lipid bilayers 1

1.1.2 Membrane protein types 4

1.1.3 Folding and stability of α–helical integral membrane proteins 6

1.1.4 Methods to study membrane protein stability 11

1.2 Colicins 14

1.2.1 Genetic organization of colicins 16

1.2.2 Colicin A 17

1.2.3 The pore-forming domain of ionophoric colicins 19

1.2.4 Channel formation 22

1.2.5 Immunity to pore-forming colicins 28

1.3 Objectives 33

2. **EXPERIMENTAL PROCEDURES** 37

2.1 Molecular biology 37

2.1.1 DNA constructs and cloning 37

2.1.2 Protein overexpression and purification 40

2.2 Membrane model systems 42

2.2.1 Detergent micelles 43

2.2.2 Lipid vesicles 45

2.3 Circular dichroism (CD) 48

2.4 Nuclear magnetic resonance (NMR) 51

2.5 Protein stability by equilibrium unfolding 53

2.6 Ion conductance assay in liposomes 55

2.7 Cai/pfColA binding assays 56

2.7.1 Binding assays by fluorescence anisotropy 57

3. Characterization of Cai in detergent micelles 65
3.1 Expression and purification of Cai 66
3.2 Solubility and stability of Cai under different solubilization conditions 67
3.3 Oligomerization state of Cai 74
3.4 Conformational stability of Cai 77
3.5 Functional analysis of Cai in micelles 84
3.6 pfColA conformations in micelles 87
3.7 Discussion 91
4. **Functional reconstitution of Cai/pfColA in lipid vesicles** 99
4.1 Reconstitution of Cai in proteoliposomes 99
4.2 pfColA incorporation to liposomes 103
4.3 pfColA activity in liposomes of *E. coli* lipids 108
4.4 Inhibition of pfColA activity by Cai in liposomes of *E. coli* lipids 111
4.5 Discussion 114
4.6 Supplementary information 116
5. **The Cai/pfColA complex *in vivo:* co-expression and isolation** 125
5.1 Optimization of ColA pore-forming domain and immunity protein co-expression 129
5.2 Membrane extraction of the ColA pore-forming domain and immunity protein complex 136
5.3 Discussion 140
6**. Studying the Cai/pfColA complex *in vitro*: stability, stoichiometry, binding affinity and sequence dependence** 145
6.1 Formation and co-purification of Cai/pfColA complex 145
6.2 Stoichiometry of ColA pore forming domain/immunity protein complex 150
6.3 Stability and conformational analysis of Cai/pfColA complex 152
6.4 Equilibrium binding of Cai with pfColA 161
6.5 Cai - pfColA binding kinetics 166
6.6 pfColA mutants in complex formation 168
6.7 Discussion 173
7. OVERVIEW AND CONCLUSIONS 179
7.1 Conclusions 184
7.2 RESUMEN Y CONCLUSIONES 185
8. **BIBLIOGRAPHY** 193

ACKNOWLEDGMENTS

This PhD thesis has been carried out at the Biofisika Institute (UPV/EHU, CSIC) under the supervision of Dr. Ana Rosa Viguera Rincón and Prof. Félix M. Goñi Urcelay. This work has been supported by the Basque Government (IT852-13, ELKARTEK15/20, IE14-384). The candidate was granted a research fellowship from the Basque Government and she was also supported by Fundación Biofísica Bizkaia.

We are indebted to Dr. Ana Bouchet for her contribution to this work during her postdoctoral period in the lab, to Marián Alonso BSc. for technical assistance, to Maria Fariña BSc. for her contribution to chapter 5, to Dr. Tammo Diercks and Dr. Francisco Blanco (CIC bioGUNE, Bizkaia Technology Park) for the help with NMR experiments included in chapter 3, to the group of Prof. Lena Mäler (Department of Biochemistry and Biophysics, Stockholm University) for the collaboration and support during the research stay and to Dr. Alain Ibáñez de Opakua (CIC bioGUNE, Bizkaia Technology Park) who constructed the pfColA mutants used in chapter 4 and 6.

ABBREVIATIONS

λ	wavelength
Δψ	transmembrane potential
ANTS	8-aminonapthalene-1,3,6 trisulfonic acid
BS^3	bis(sulfosuccinimidyl)suberate
Cai	colicin A immunity protein
$C_{12}E_9$	dodecyl nonaethylene glycol ether
CCCP	carbonyl cyanide m-chlorophenyl hydrazone
CD	circular dichroism
CHAPS	3-[(3-cholamidopropyl)-dimethylammonio]-1- propanesulfonate
CHAPSO	3-[(3-cholamidopropyl)dimethylammonio]-2-hydroxy-1-propanesulfonate
Cholate	3α,7α,12α-Trihydroxy-5β-cholan-24-oic acid sodium salt
CL	Cardiolipin
ColA	colicin A
CPM	N-[4-(7-diethylamino-4-methyl-3-coumarinyl)phenyl]-maleimide
dansyl-DOPE	1,2-dioleoyl-*sn*-glycero-3-phosphoethanolamine-Nstearoyl-*sn*-glycero-3-phosphocholine
DDAO	n-Decyl-N,N-Dimethylamine-N-Oxide
DDM	n-dodecyl-*β*-D-maltopyranoside
DPX	p-xylene-bis-pyridinium bromide

DH_6PC	1,2-dihexanoyl-*sn*-glycero- phosphocholine
DH_7PC	1,2-diheptanoyl-*sn*-glycero-phosphocholine
DM	n-decyl-*β*-D-maltopyranoside
DOPG	1,2-dioleoyl- *sn* -glycero-3-phosphatidyl-glycerol
DPC	n-dodecylphosphocholine
FITC	fluorescein isothiocyanate
FRET	fluorescence resonance energy transfer
GFP	green fluorescent protein
HEPES	N-2-hydroxyethylpiperazine-N'-2-ethane sulfonic acid
HMQC	Heteronuclear Multiple Quantum Coherence
HSQC	Heteronuclear Single Quantum Coherence
IPTG	isopropyl α-D-thiogalactopyranoside
LAPAO	3-dodecylamido-N,N'-dimethylpropyl amine oxide
LDAO	n-Dodecyl-N,N-Dimethylamine-N-Oxide
LUV	large unilamellar vesicle
NM	n-nonyl-*β*-D- maltopyranoside
NMDG	N-methyl-D-glucamine
NMR	nuclear magnetic resonance
NTA	nitrilotriacetic acid
OG	n-octyl-β-D-glucopyranoside
OLPC	lyso-oleoyl-sn-Glycero-3-phosphatidyl-choline

OLPG lyso-oleoyl-sn-glycero-3-phosphatidyl-glycerol

PBS Phosphate Buffered Saline

PDC protein detergent complex

PE Phosphatidylethanolamine

PG Phosphatidylglycerol

pfColA pore forming C-terminal domain of colicin A

Ri lipid-to-protein ratio

SDS sodium dodecyl sulphate

SDS-PAGE sodium dodecyl sulphate (SDS) polyacrylamide gel electrophoresis (PAGE)

SEC size exclusion chromatography

TCEP Tris (2-carboxyethyl) phosphine

TDAO n-Tetradecyl-N,N-Dimethylamine-N-Oxide

TROSY Transverse Relaxation Optimized Spectroscopy

TX-100 *α*- [4-(1,1,3,3-tetramethylbutyl)phenyl]-*w*-hydroxy-poly(oxy-1,2-ethanediyl)]

Zwittergent 3.12 n-dodecyl-N, N-dimethyl-3-ammonio-1-propanesulfonate

Zwittergent 3.14 n-tetradecyl-N, N-dimethyl-3-ammonio-1-propanesulfonate

CHAPTER 1

Introduction and objectives

1. INTRODUCTION AND OBJECTIVES

1.1 Membrane proteins in the bilayer

The emergence of membrane-delimited life forms is understood as one of the fundamental events in the evolution of cells and organisms. Biomembranes are a requisite for essential life functions such as homeostasis, organization, metabolism, adaptation or reproduction. The primary role of a membrane as a selective permeability barrier imposes the nature of the bilayer as a dynamic, fluid and anisotropic environment. Therefore, the physical and chemical properties of membranes and membrane constituting lipids and proteins (and their glycoconjugates), represent major constraints which define structure, function and regulation at the bilayer level. Establishing the forces that govern membrane protein structure and interactions with the surrounding lipids and proteins is one of the current challenges in the biochemical field hindering further understanding of cellular processes.

1.1.1 Membrane lipid bilayers

Biological membranes are continuous bilayers constituting a two-dimensional liquid composed by amphipathic lipid molecules in which membrane proteins are embedded or peripherally associated. The bilayer is a spontaneously assembled structure as a result of the tendency of the acyl chains to minimize the exposure to water combined with repulsion between head groups. Membrane fluidity is crucial for most membrane functions. The bilayer is fluid as a consequence of the lateral diffusion of lipid molecules within the monolayer as well as lipid rotation, flexion and monolayer migration. The most abundant lipids in biological membranes are phospholipids which can have different polar heads and hydrophobic hydrocarbon tails. The tails are most commonly fatty acids and have usually 14-24 carbons. One of the two acyl chains in the phospholipid is usually cis-unsaturated, which creates a kink in its structure and makes packing more difficult. Both acyl chain length and unsaturation strongly affect bilayer packing, fluidity and phase separation (Fig. 1.1).

The amphipathic nature of the phospholipids creates a polarity gradient along the normal of the bilayer with a strong position-dependent anisotropy. The hydrocarbon core at the centre is dominated by the hydrophobic acyl chains while polar head groups define a broad and dynamic interfacial region with a considerable amount of bound water (Fig. 1.1).

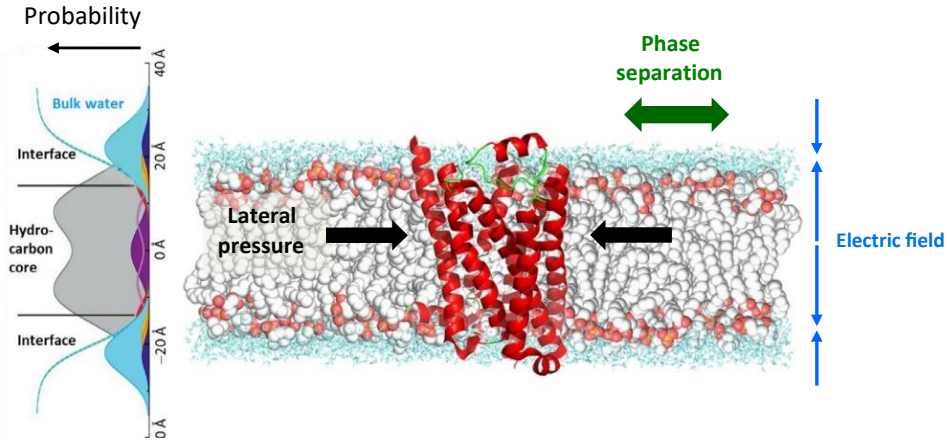

Figure 1.1 Biological membranes are mainly composed of phospholipids and embedded proteins involved in many different physicochemical interactions to reach a stable thermodynamic free energy minimum. (Left) Probability distribution of various chemical moieties of a phospholipid bilayer in a liquid crystalline phase. Methyls (purple), methylenes (grey area), double bonds (light purple line), carbonyls (red), glycerol (yellow), phosphate (brown), and choline (dark blue). Modified from White and von Heijne (2008). (Right) Schematic representation of numerous physico-chemical interactions that affect he structural stability of membrane proteins. Adapted from Hong, (2014).

The proportion of proteins and lipids varies considerably between different types of membranes as shown in Table 1.1. Even if lipids are free to diffuse in the two dimensional space of the bilayer, lipid domains differentially enriched in certain proteins and lipids are formed in many biomembranes. The membrane is crowded with protein super-assemblies that extend not only laterally but transversally out of the membrane. Some bilayers contain high concentrations of the same protein going beyond the formation of protein-clusters and becoming quasi-crystalline as in the case of bacteriorhodopsin or outer membrane porins.

The particular physicochemical properties of the phospholipid matrix are known to influence protein structure to a great extent but a growing number of studies indicate that proteins might be more important in determining general bilayer properties. Some proteins are able to adjust to membranes of different thickness to overcome what is known as the hydrophobic mismatch (Williamson et al., 2002). Nevertheless, several examples exist in which the thickness of the bilayer as well as the lipid composition and polymorphism is

adjusted to the requirements of the protein effectors (Mitra et al., 2004). The structural diversity present among membrane proteins attributed to different functional requirements may have resulted in a wider range of lipid species during evolution. This provides the potential to cope with protein-induced curvature elastic strain, global curvature deformation (fusion and fission) (Kozlov et al., 2010) or accommodation of functionally important polar moieties.

Table 1.1 Composition of membrane preparations by percent dry weight. From (Guidotti, 1972).

Membrane	Protein (%)	Lipid (%)	Carbohydrate (%)
Plasma membrane			
Red blood cell	49	43	8
HeLa cells	60	38	2
Sarcoplasmic reticulum	67	33	-
Chloroplast lamellae	64	30	6
Mitochondrial inner membrane	76	24	1
Myelin	30	70	-
Gram-positive bacteria	75	20-25	1-5
Gram-negative bacteria (*E. coli*)	70	20-30	5-10

Apart from determining general bilayer properties, specific lipids are found bound to certain proteins and act as important cofactor for function and stability (Contreras et al., 2011). Many crystal structures revealed the presence of tightly bound lipid molecules like in the case of cytochrome C oxidase (Shinzawa-Itoh et al., 2007), mitochondrial ADP/ATP carrier (Nury et al., 2005) or potassium channel KcsA (Valiyaveetil et al., 2002).

1.1.1.1 Bacterial membranes

The lipid composition of membranes is very diverse, comprising phospholipid head groups that differ in shape, charge and size. Different acyl chain combinations arise from varying chain length and saturation. Eukaryotic membranes contain a high variety of phospholipids, while prokaryotic membranes lack sterols and sphingolipids and are often composed of one main type of phospholipid. In the absence of cholesterol, the external cell wall provides mechanical stability to bacteria. The anionic phospholipids cardiolipin (CL) and phosphatydil glycerol (PG) are found in bacterial plasma membranes but not in eukaryotic membranes other than mitochondria. In *E. coli*, the common phospholipid composition includes 70-80%

of phosphatidyl ethanolamine (PE), 20-25% PG and less than 5% of CL, all produced from a phosphatidic acid precursor (Raetz, 1978). Anionic lipids PG and CL are essential in bacteria, they are involved in many cellular functions in some through direct binding to particular proteins. Bacteria that cannot produce PE, however, are still viable. The abundant lipid PE seems to be important for membrane polymorphism determining the global and nonspecific properties of the bilayer. The non-lamellar lipid PE, together with CL are essential to maintain the bilayer in a narrow window between lamellar and the inverted hexagonal phase (Andersson, 1996). Cardiolipin appears to be important in the dynamic lateral organization of the membrane and several lines of evidence indicate that multi-protein complexes exist in CL-enriched domains are assembled during in cell division, energy metabolism and membrane (Mileykovskaya and Dowhan, 2000, 2009; Renner and Weibel, 2011).

As previously stated, membrane fluidity is strongly dependent on lipid composition. Many microorganisms are exposed to ever changing environments, so they are able to regulate the fluidity of the bilayer in response to external temperature changes. They do so by modifying the fatty acid composition of the membrane, most commonly by changing the saturation of the acyl chain to ensure a relatively constant fluidity (Andersson, 1996). Indeed as more membrane related processes are studied it is becoming apparent that some protein activities require lipid mixtures that are able to mimic physiological acyl chain and head group heterogeneity to the detriment of pure synthetic lipid mixtures.

1.1.2 Membrane protein types

Singer and Nicolson originally classified membrane proteins into two groups based on the conditions necessary to extract them from the membrane. Different types of membrane proteins are summarized in Figure 1.2. Peripheral membrane proteins do not interact with the hydrophobic core of the membrane and can be extracted from the membrane applying mild treatments like high pH or high salt concentrations. They are temporarily attached either to the lipid bilayer or to integral membrane proteins by hydrophobic, electrostatic, and other non-covalent interactions. This enables specific proteins to be recruited and concentrated at specific sites of the membrane.

Integral or intrinsic proteins are found to be embedded in the membrane, requiring more drastic treatments, such as the use of detergents to be extracted from the bilayer. Depending on the segments inserted in the membrane, integral membrane proteins can be separated into 3 groups: monotopic, in contact with only one side of the membrane; bitopic, when they cross the membrane only once; and polytopic, if they cross the membrane several times. Integral and peripheral proteins might get anchored to the membrane upon post-translational modification trough covalent bonds to fatty acids, prenyl chains, or glycols GPI (glycosylphosphatidylinositol).Integral polytopic membrane proteins can adopt two different architectures: α-helical bundles, present in all types of biological membranes and β-barrels, which can be found in the outer membrane of Gram-negative bacteria, mitochondria and chloroplasts and as part of the cell-wall of some Gram-negative bacteria. Amphitropic proteins can be considered as a special type of membrane proteins, including polypeptide toxins such as colicins, haemolysins or diphtheria toxin and many antibacterial peptides; and certain proteins involved in apoptosis. These proteins are water-soluble but can bind and insert into the lipid bilayer becoming reversibly or irreversibly membrane-associated (Burn, 1988; Goñi, 2014).

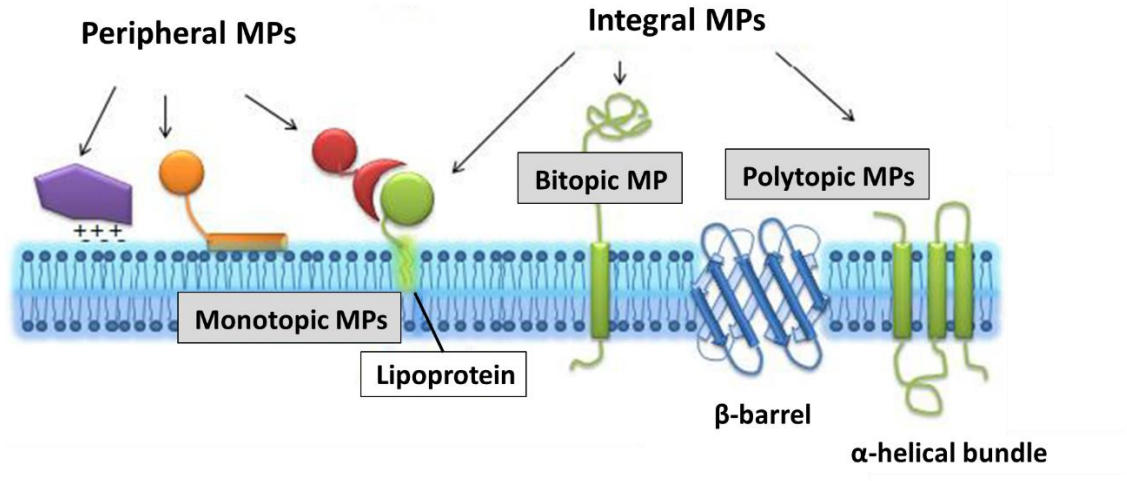

Figure 1.2 Schematic representation of different membrane protein types. Peripheral proteins are weakly associated to the membrane, integral proteins are tightly bound and depending on how many times they cross the membrane we find: monotopic, bitopic or polytopic proteins. Proteins get anchored to the membrane by covalent bonds mainly with fatty acids or glycols.

1.1.3 Folding and stability of α–helical integral membrane proteins

Around 30% of all open-reading frames in the genome of various organisms are predicted to encode integral membrane proteins (Krogh et al., 2001). But despite being important for many cell functions our understanding of membrane proteins lags behind that of soluble proteins, as reflected by the low amount of high resolution structures available to date. Strikingly, at least 50% of approved drugs elicit their therapeutic effects by selectively targeting G-protein coupled receptors, an extended family of membrane proteins (Müller, 2000).

Due to the high hydrophobicity of membrane proteins, this class of molecules are resistant to most of the clasical approaches employed to procure knowledge of their soluble counter-parts. Protein unfolding studies have provided very valuable information about the thermodynamic rules that drive folding and, in some cases, allowed to propose kinetic pathways of folding. They were based on equilibrium denaturation assays of purified small soluble proteins *in vitro*. In the majority of studies protein unfolding takes place in aqueous solution in the absence of additional cell components. Because folding and bilayer insertion are coupled processes during integral membrane protein biogenesis, *in vitro* folding studies require the insertion of the protein into a bilayer, detergent micelle or other membrane model. Thus before biochemical studies can be carried out, considerable efforts have to be devoted to find the specific solubilization conditions necessary for structural and functional integrity of every particular protein.

The fact that the denaturation methods commonly used to unfold soluble proteins frequently cause irreversible aggregation of membrane proteins, precluding the extraction of thermodynamic parameters, does not imply that membrane proteins cannot exist as equilibrium structures. Evidence supporting the thermodynamic control of membrane protein folding were first presented for unfolding and refolding of bacteriorhodopsin. Since then, many other examples continue to emerge (Harris and Booth, 2012; Harris et al., 2014; Klug et al., 1995; Schlebach et al., 2011). In that first approach bacteriorhodopsin was unfolded in organic solvents or SDS and refolded into mild detergent or lipid vesicles, upon which it recovered its native conformation (Huang et al., 1980; London and Khorana, 1982). Furthermore, proteolytically cleaved bacteriorhodopsin fragments could be independently reconstituted into lipid vesicles where they reassemble yielding a functional protein (Huang et al., 1981; Popot et al., 1986) supporting the hypothesis that membrane protein folding is indeed a thermodynamically driven process. Thus, in theory it is possible to study membrane protein folding *in vitro* provided that the simplified system devised takes into account the major forces involved in membrane protein stability (Min et al., 2015). In an attempt to define the framework of membrane protein folding mechanisms it is still very useful to apply the two-stage

model proposed by Popot and Engelman (1990). This model identifies a first step in which helix formation and simultaneous bilayer insertion occurs. A second step involves packing forces such as tertiary and quaternary contacts between different helices leading to the native state (Fig. 1.3). This model has proved to be relevant for both *in vitro* and *in vivo* folding experiments, since, unlike soluble proteins, secondary structure elements of membrane proteins can be separated from tertiary contacts in what seems to be an intrinsic feature of proteins localized at the hydrophobic bilayer. In the cellular context, the insertion of nearly all helical-bundle membrane proteins is mediated by a protein-conducting channel or translocon in a co-translational manner. This facilitates hydrophobic interactions and shields polar moieties from the cytoplasmic non-polar environment. We can estipulate that protein insertion and topology are dictated both by the translocon and the sequence itself, as the polypeptide chain comes out of the ribosome. Membrane protein assembly is a complex process that goes beyond the two-stage model. But this approach provides the theoretical framework to assess the basic thermodynamic forces that drive membrane protein folding, which are also relevant to understand how the reaction works when it is catalysed by the translocon (Fig. 1.3).

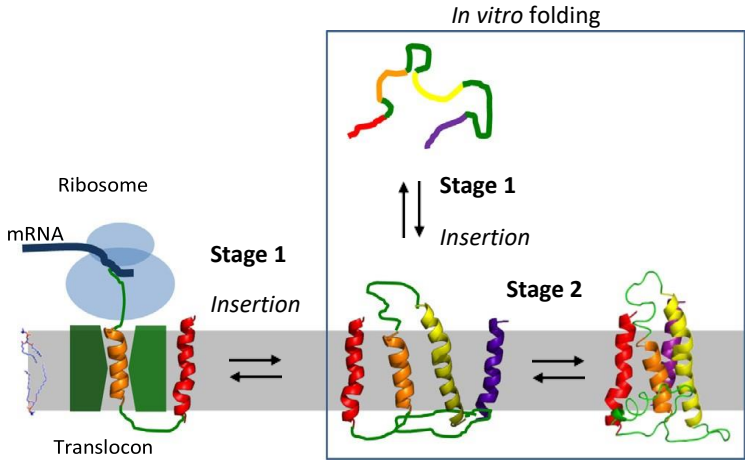

Figure 1.3 Two-stage model in the folding of α-helical membrane proteins. The majority of membrane proteins are co-translationally inserted into the membrane through a translocon. The steps in the box are the *in vitro* biophysical representation of the two-stage model. The steps in the vertical direction represents stage 1, the steps in the horizontal direction represent stage 2. Adapted from Hong, 2014).

In stage 1, the hydrophobic character of transmembrane segments triggers membrane partitioning owing to the hydrophobic effect and the apolar environment of the bilayer forces protein backbone groups into hydrogen bonds. For soluble peptides, however, the helix-coil transition is approximately isoenergetic as far as the peptide backbone competes with water for hydrogen bonds. This explains why membrane proteins make for a very stable hydrogen bonded secondary structure as unfolding

the peptide backbone inside the membrane is greatly unfavourable (White and Wimley, 1999). In this regard, denatured states of different membrane proteins are shown to remain highly helical.

Apart from backbone hydrogen bonding, side-chain hydrophobicity is an important parameter that defines transmembrane helices which triggers not only the insertion but also the maintenance of the protein within the bilayer. In order to predict membrane insertion capacity, different hydrophobicity scales were calculated compiling the free energies for transferring different amino acids in pentapeptides from water to n-octanol (Wimley et al., 1996) or POPC bilayers (Wimley and White, 1996). Later on these propensities were further tested *in vivo*, to compare membrane partitioning tendencies when the insertion is directed by the translocon under physiological conditions. Substituting each of the 20 amino acids into a test transmembrane segment, allowed to derive apparent free energy of partition into the membrane (Hessa et al., 2005a). Surprisingly, the resulting biological hydrophobic scale correlates well with those scales mentioned above, which implies that the translocon-mediated insertion obeys similar physicochemical principles established by the simple apolar partitioning models. In this sense it has been proposed that transmembrane segments may interact directly with the membrane interface as the protein comes out of the ribosome, suggesting that membrane protein folding and topology might not depend solely on protein mediated translocation (Cymer et al., 2015).

Although these scales turned out to be quite accurate for predicting membrane partitioning probabilities, they did not consider that the localization of a certain side chain along a transmembrane segment could greatly alter its insertion capacity. This is especially true considering the hydrophobicity variations occurring along the bilayer normal. In this regard, position-dependent contributions of different amino acids to translocon-mediated transmembrane insertion revealed that insertion of polar residues is particularly unfavourable in a position dependent manner (Hessa et al., 2007). Even if the insertion of polar residues within the hydrocarbon core of the membrane is generally unfavourable, functionally significant residues are found at the centre of transmembrane helices in some cases (Bañó-Polo et al., 2012; Jiang et al., 2003; Kim et al., 2011; Murata et al., 2000). A possible explanation is that compensating structural changes in both the lipid and protein components can occur as observed in the case of snorkelling polar moieties (Hessa et al., 2005b). Another way of introducing functionally important charged residues into the interior of the bilayer is through the formation of salt bridges. In fact, the low permittivity of the hydrophobic environment implies that if formed, electrostatic interactions would be strong. It has already been shown that the insertion of polyleucine peptides with a lysine and an aspartate is only possible when a salt bridge can be formed i.e. when both residues are found on the same side of the helix separated by a turn

(Chin and von Heijne, 2000). After all the energetic cost of partitioning charged residues appears to be lower than previously believed (Ulmschneider et al., 2017) .

From a thermodynamic stand point, stage I can be separated into three sub-stages, which considers partitioning, folding and insertion individually (White and Wimley, 1999). As discussed above the apolar nature of the side chains triggers membrane partitioning as the hydrophobic effect dominates over the changes in solvation, perturbation of the membrane or the loss of entropy in the protein. Folding of the polypeptide helix is concomitant with partitioning provided that the partition itself is energetically favourable. This would mean that the favourable gain of dehydrating hydrophobic side chains should outbalance the unfavourable cost of partitioning the peptide bond, which is reduced by H-bonded secondary structure formation (Ladokhin and White, 1999). In the last step, the helix acquires the membrane spanning conformation driven by the hydrophobic effect which compensates for the entropic loss of the surrounding lipids as well as the helix itself (Fig. 1.4).

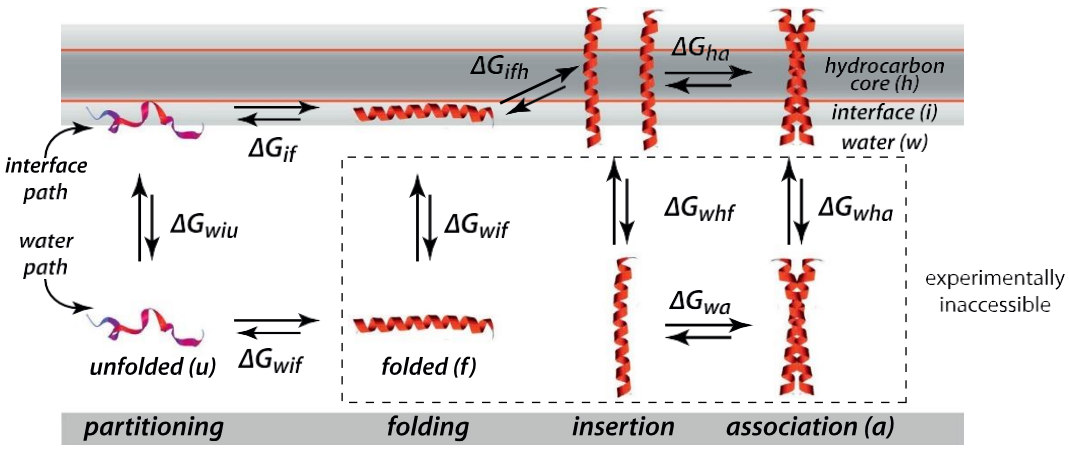

Figure 1.4 Schematic representation of the thermodynamic cycle of partitioning, folding, insertion, and association of an α-helix in a lipid bilayer. In theory, the assembly can follow an interfacial path, a water path, or a combination of the two. Studies of folding along the interfacial path are experimentally more tractable. The ΔG symbols indicate standard transfer free energies. The subscript labelling indicates a specific step in the cycle. The subscript letters are defined as follows: w, water; i, interface; h, hydrocarbon core; u, unfolded; f, folded; a, association. The dashed box indicates cycle steps that cannot be tested experimentally. From (Cymer et al., 2015) adapted from (White and Wimley, 1999).

In stage II, helix-helix interactions trigger lateral association to form α-helical bundles. This is mediated by packing forces, electrostatic effects and interactions with additional components (soluble loops, prosthetic groups, surrounding protein/lipids). As mentioned above, considerable limitations exist in the application of the approach used to study soluble protein folding, mainly because the all-or-none highly cooperative reaction does not apply for membrane proteins. As a first approximation, we can say that the 3D structure might be more conditioned by the primary

structure, both in the determination of transmembrane helical stretches and helix distortions, such as kinks or short stretches of π or 3_{10} helices (Cordes et al., 2002; Riek et al., 2001). Because the secondary structure stability is not compromised, helix topology and orientation is believed to be dramatically constrained upon insertion. In many cases, this aspect challenges the determination of tertiary contacts which could assess membrane protein stability in simplified systems. Given the architecture of the bilayer the magnitude of free energy responsible for helix-helix contacts is expected to be low. Additional stabilizing forces arising from the confinement of the helices within the bilayer can presumably contribute to membrane protein stability. This global effect of the membrane is often difficult to mimic *in vitro*, as in the case of detergent solubilized proteins where the non-fixed tertiary structure might be futile. Several examples of solubilized proteins with secondary but no tertiary structure have been reported (Cross et al., 2011; Hirota et al., 1997; Taylor et al., 2000). Nevertheless, numerous experiments with membrane protein fragments indicate that after insertion helix association is guided by equilibrium thermodynamics, as fragments are able to reassemble upon which functionality is recovered (Bibi and Kaback, 1990, 1990; Groves and Tanner, 1999).

Helix packing is believed to be important to drive membrane proteins into a native compact state. The narrow distribution of tilt angles found in membrane-embedded proteins (a clear preference for 20 °(Bowie, 1997)) together with the optimization of van der Waals interactions triggers tight inderdigitation of side chains in adjacent helices. Even if van der Waals interactions do not necessarily have a higher energetic contribution compared with soluble proteins (Joh et al., 2009), shape complementarity could provide specificity to reach the native conformation in membrane proteins. Evidence demonstrating the importance of van der Waals driven knob-into-hole packing were derived mainly from the studies of bacteriorhodopsin, made up of left handed coiled-coils (Langosch and Heringa, 1998; Walshaw and Woolfson, 2003) and the GxxxG motif in glycophorin A (MacKenzie et al., 1997; Walther et al., 1996).

Additionally, membrane protein oligomers are commonly stabilized by hydrogen bonds as this kind of bond is expected to be very stable within the hydrocarbon core. Examples of hydrogen bonded oligomers are the GCN4-LZ and ζζ membrane proteins for which the disruption of hydrogen bond partners by mutation, prevents dimer formation (Call et al., 2006; Choma et al., 2000). In fact, mutations that disrupt hydrogen bonds between transmembrane segments are the cause of many severe diseases (Sanders and Myers, 2004). The contribution of single intramolecular hydrogen bonds in the stability of polytopic proteins, however, turned out to be lower than originally predicted (Joh et al., 2008). As it happens in soluble proteins, the global stability of the fold can be envisioned as the result of many weak interactions which simultaneously allows for dynamic flexibility required

for function. Actually Cao and Bowie showed that hydrogen bonding interactions might be rather flexible in the apolar environment of the bilayer. They showed how introducing a single mutation which disrupts a natively kinked helix, causes multiple transitions between distinct distorted helix conformations by shifting of backbone hydrogen bonding partners at a low energetic cost (Cao and Bowie, 2012). This and other studies exemplify how transmembrane helix kinks and distortions might be important for membrane protein structure, function and dynamics (Riek et al., 2001). Prolines are residues frequently linked to these helix distortions and are usually good predictors of kinks within transmembrane helices.

Aromatic side chains participate in the stabilization of transmembrane helix interactions not only by contributing to the hydrophobic effect, but forming π-π interactions between them and cation-π with lysine residues. Aromatic residues like tryptophan and tyrosine, are engaged in aromatic-aromatic interactions with a strong positional preference for the bilayer interface while phenylalanine residues are particularly effective in triggering lateral association of helices (Unterreitmeier et al., 2007).

1.1.4 Methods to study membrane protein stability

In order to extract stability information, denaturation studies have to fulfil a set of conditions. Ideally denaturation has to be a reversible two-state reaction and denatured proteins must be able to refold to reach their native folded state. Similar equilibrium constants should be derived independently of the denaturation method used. Several examples exist in which reversible unfolding of polytopic membrane proteins has been achieved but up to date, none of the methods implemented so far proved to be effective for helical membrane proteins in general. A number of theoretical limitations have not been solved so far exemplified by the difficulty to define what a denatured state of a membrane protein is, which will obviously differ from what we call the unfolded state in soluble proteins.

As mentioned before many of the initial membrane protein studies were based on analysing helix oligomerization in membrane-mimicking environments. In this respect the set of available tools is quite broad, including double-mutant cycle analysis, analytical ultracentrifugation, fluorescence resonance energy transfer (FRET), and oligomerization-dependent transcription activation systems such as TOXCAT, POSSYCAT, GALLEX or AraTM.

1.1.4.1 SDS denaturation

The first integral membrane protein to be fully unfolded and refolded back into its active conformation was bacteriorhodopsin for which the anionic detergent SDS was used as the denaturing agent. The addition of SDS renders the protein inactive after triggering chromophore dissociation, this allows to follow the refolding process into non-denaturing micelles or bilayers spectroscopically (Huang et al., 1981). A protocol was later established to standardise SDS-induced denaturation experiments (Hong et al., 2009; Lau and Bowie, 1997). The folded membrane protein is solubilized in non-denaturing detergent micelles and is subsequently denatured by increasing the mol-fraction of SDS out of a total detergent concentration. Reversely, from the SDS-denatured protein the refolding can be tested by increasing the fraction of non-denaturing detergents to shift the equilibrium in favour of the folded state (Fig. 1.5A). In many cases, the unfolding transition curves were consistent with a two-state model, and the free energies of unfolding calculated from the extrapolation to zero SDS concentration. This method has been effectively applied to numerous membrane proteins that provided valuable insights into the kinetic parameters and folding transition states (Otzen, 2003). The validity of the linear extrapolation to zero SDS is, however, a matter of debate as the free energy cost of transferring the polypeptide to SDS might not be linearly correlated to SDS concentration over the whole range of SDS concentrations tested (Chang and Bowie, 2014).

1.1.4.2 Urea and GdnHCl denaturation

Reversible folding has been achieved for some membrane proteins using the traditional chaotropic agents, urea or guanidinium chloride (GdnHCl) (Figure 1.4B). This approach has been tested in both detergent micelles, like in the case of major facilitator proteins or the multidrug transporter EmrE (Miller et al., 2009) and in lipid vesicles, in the case of lactose permease (LacY). Addition of urea or GdnHCl to LacY reconstituted into lipid vesicles disrupted the tertiary structure of the protein. Upon removal of the denaturant, the protein was able to recover transport activity (He and Kaback, 1998). Interestingly, proton-deuterium exchange experiments showed that most of amide protons were accessible to the solvent while backbone amide protons, responsible for the secondary structure, were not exchangeable. It is worth noticing that most of the proteins in which polar denaturants cause reversible unfolding have transport functions which contain hydrophobic cavities inside the protein. This suggests that chaotropic agents are able to denature membrane proteins in the same way as they denature soluble proteins even if the denatured state is not necessarily comparable (Moon et al., 2013).

1.1.4.3 Pulse-proteolysis

In theory, the use of proteolysis combined with destabilization can be very useful to study stability and intermediate conformations of membrane proteins. The method is based on the selective proteolysis of the fraction of the protein that becomes unfolded as a consequence of the gradual addition of a physical or chemical denaturant (Fig 1.4C). After rapid protease inactivation quantification of the protease-resistant fraction is assessed and the stability of the protein can be estimated. The use of pulse-proteolysis as a conformational probe has been successful in measuring thermodynamic stability and folding kinetics of several membrane proteins. The stability value obtained for bacteriorhodopsin through pulse-proteolysis was consistent with stability values obtained in previous spectroscopy-based assays (Schlebach et al., 2012).

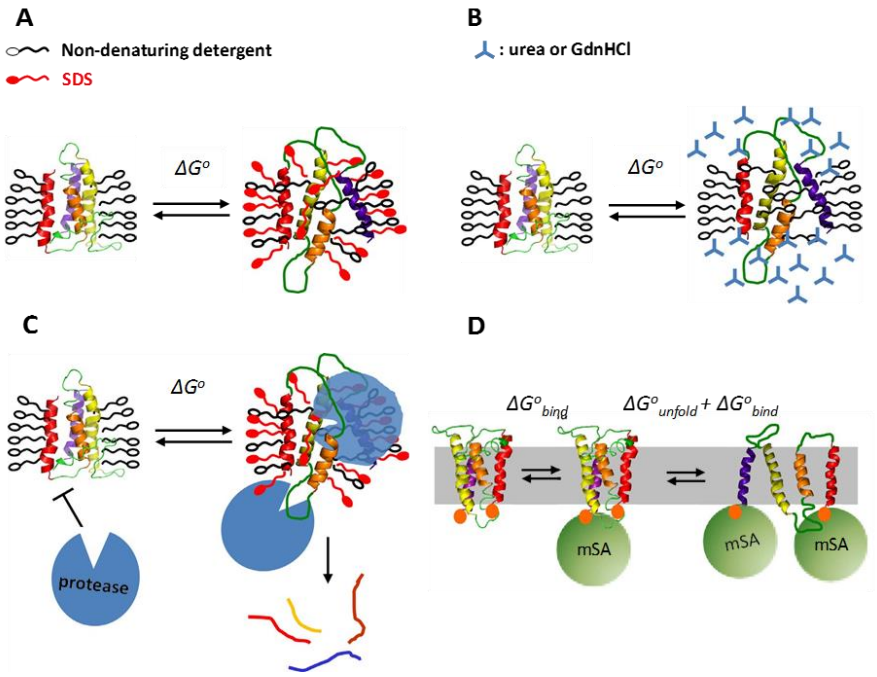

Figure 1.5. Schematic representation of different methods used to study the folding of α-helical membrane proteins. (A) SDS denaturation: a native membrane protein solubilized in non-denaturing detergents or detergent-lipid mixed micelles can unfold in increasing mol-fractions of SDS, reversible refolding can be achieved by diluting the SDS-unfolded proteins with non-denaturing detergents. (B) Urea or GdnHCl denaturation: for several membrane proteins, reversible unfolding is possible in increasing concentration of urea or GdnHCl, refolding is achieved by diluting the unfolded protein back into a native buffer solution. (C) Detection of unfolded state by pulse proteolysis: fractions of the unfolded and folded membrane protein can be determined by a short period of proteolysis reaction under denaturing conditions. (D) Steric trapping: reversible unfolding of a doubly-biotinylated membrane protein can be driven by coupling to the binding of monovalent streptavidin (mSA). From Hong, 2014).

1.1.4.4 Steric trapping

Steric trapping represents an innovative approach to measure equilibrium unfolding in the absence of denaturants. It has been validated for soluble proteins (Blois et al., 2009), for the dimerization of glycophorin A (Hong et al., 2013) and most importantly for unfolding of polytopic proteins including bacteriorhodopsin, which constitutes one of the model polytopic membrane proteins for which more stability and conformational information is available. In this method the protein is labelled with two biotin tags that are close in the 3D structure, monovalent streptavidin is then added which binds to one of the sites according to its intrinsic affinity. Binding of a second monovalent streptavidin is less favourable unless the protein is unfolded due to steric overlap and this second event is coupled to the unfolding free energy (Fig. 1.5D). Under these conditions, equilibrium unfolding is directed by affinity and concentration of the ligand which allows for obtaining ligand binding isotherms. This approach allows not only to study membrane protein stability and folding under native conditions but also to understand how other membrane protein denaturation methods work, as streptavidin binding can be tested under different conditions (in micelles, bicelles, adding SDS…).

1.2 Colicins

Prokaryotic organisms have developed different defence mechanisms to adjust to highly diverse ecological niches in an attempt to get competitive advantage for resources and space. During evolution a huge array of antimicrobial molecules emerged ranging from broad-spectrum antibiotics, to exotoxins, bacteriocins or lysozymes (Riley and Wertz, 2002). Unlike antibiotics, the bacteriocin family includes ribosomally synthesized protein toxins with different biochemical properties and cytotoxic strategies directed against the same or closely related bacterial species. Colicins are bacteriocins produced by *Escherichia coli* and other enteric bacteria which are usually lethal only for a narrow range of related strains (Fredericq, 1964). The killing action of colicins ranges from endonuclease activity (Boon, 1971), the formation of pores in the inner membrane (Schein et al., 1978) or the enzymatic degradation of peptidoglycan precursors (colicin M) (Ghachi et al., 2006). Colicinogenic strains are widely distributed in nature and it is estimated that up to 99% of bacteria produce at least one kind of bacteriocin (Klaenhammer, 1988; Raloff, 1998). Recently, an increasing attention is devoted to the use of colicin-bearing bacteria to complement or even replace antibiotics and chemical preservatives (Dobson et al., 2012; Gillor et al., 2008; Montalbán-López et al., 2011; Rivera and Boucher, 2011).Colicinogenic bacteria commonly harbour plasmids coding for a certain colicin, specific immunity proteins which protect producing strains, and lysis proteins which aid in colicin release. Colicins enter the target cells binding to outer membrane receptors and reaching the

inner membrane through either the Tol or Ton translocation machineries (Table 1.1). Based on the translocation system they use, colicins are classified into group A and group B colicins (Davies and Reeves, 1975a, 1975b). The genetic organization of colicinogenic plasmids is also different for group A (type I plasmids) and group B (type II plasmids) colicins. Type I plasmids are low molecular weight (6-10 kb) multi-copy plasmids containing few other genetic determinants which can be amplified and transmitted in the presence of a conjugative plasmid. Type II plasmids are high molecular weight (40 kb) monocopy plasmids that carry many additional genes and are self-transmissible by conjugation.

Table 1.2 Colicin characteristics, cellular import and cytotoxicity. Colicins are grouped into two groups, A and B based on Tol and Ton translocation mechanisms respectively. (Braun et al., 2002; Kim et al., 2014; Lazdunski et al., 1998; Lazzaroni et al., 2002)

Colicin	Receptor	Translocation	Activity
Group A			
A	BtuB	OmpF, Tol ABQR	Pore-forming
E1	BtuB	TolC, Tol AQ	Pore-forming
E2-E7-E8-E9	BtuB	OmpF, Tol ABQR	DNase
E3-E4-E6	BtuB	OmpF, Tol ABQR	16S RNase
E5	BtuB	OmpF, Tol ABQR	tRNA-(Y-H-N-D)-specific RNase
K	Tsx	OmpF, OmpA, Tol ABQR	Pore-forming
N	OmpF	OmpF, Tol AQR	Pore-forming
U	OmpA	OmpF, Tol ABQR	Pore-forming
S4	OmpW	OmpF, LPS, Tol ABQR	Pore-forming
28b	OmpA	OmpF, LPS, Tol ABQR	Pore-forming
Cloacin D13	IutA	OmpF, Tol AQR	16S RNase
Group B			
B	FepA	TonB-ExbBD	Pore-forming
D	FepA	TonB-ExbBD	tRNA-(R)-specific RNase
Ia-Ib	Cir	TonB-ExbBD	Pore-forming
M	FhuA	TonB-ExbBD	Degradation of peptidoglycan
5-10	Tsx	TolC, TonB-ExbBD	Pore-forming

1.2.1 Genetic organization of colicins

The genetic organization of different colicin operons is summarized in Figure 1.5. The first open reading frame in practically all colicin operons corresponds to the colicin structural gene (named *cxa* for colicin x activity) and it is expressed under a SOS response inducible promoter (P_{SOS}). Thus the expression of colicins is repressed by LexA dimers bound to the operator region (SOS box) while physical as well as chemical agents as UV light, bacteriolytic molecules or stress conditions would trigger LexA self-cleavage and thereby colicin production (Lwoff et al., 1952). For the case of nuclease enzymatic colicins downstream of *cxa* gene is the gene coding for the immunity protein (*cxi*, named colicin x immunity) which apart from P_{SOS} it is under the regulation of its own constitutive promoter P_{im}, ensuring that bacteria are protected at all times. Some operons of group B colicins also contain a gene encoding the lysis protein *cxl* (termed colicin x lysis), involved in the extracellular release of colicins through cell lysis (Baty et al., 1987; Cavard et al., 1985). For pore-forming colicins, the immunity gene is located in a separate operon on the opposite DNA strand, specifically in the intergenic gap between the colicin and lysis genes (Fig. 1.6) and is constitutively transcribed ensuring constant protection against the colicin (Bishop et al., 1985; Lloubes et al., 1986).

The genetic organization of immunity proteins reflects the different inhibition mechanisms developed for nuclease and pore-forming colicins. For nuclease colicins, after activation of SOS response, the colicin and immunity genes are transcribed together in a single mRNA, coordinately translated and immediately associated to form an inactive protein complex. This is an essential requirement to avoid cytotoxicity in the producing bacteria. It is generally accepted that only a subset of the bacterial population will be responsible for toxin overproduction as colicin expression and release by cell lysis will ultimately result in cell death of the producing cell (Bayramoglu et al., 2017; Riley and Wertz, 2002). Therefore, after cell lysis, virtually all released nuclease toxins are inactive until they reach the cytoplasm of target cells. The additional promoter, P_{im}, ensures that the immunity protein is present in the cytoplasm of the rest of the cells to block nuclease activity. In the mode of action of pore-forming colicins, however, activation of the SOS response induces only the production

of high amounts of the toxin in the cytoplasm by a small fraction of the bacterial population. These pore-forming colicins are not toxic to the producing cell owing to the negative membrane potential (Geli et al., 1986), but for the colicinogenic population to survive, all neighbouring bacteria must be immunized against the action of the secreted toxin. This is consistent with the simultaneous gene expression for enzymatic colicins, while the immunity and colicin genes are independently expressed in the case of pore-forming colicins.

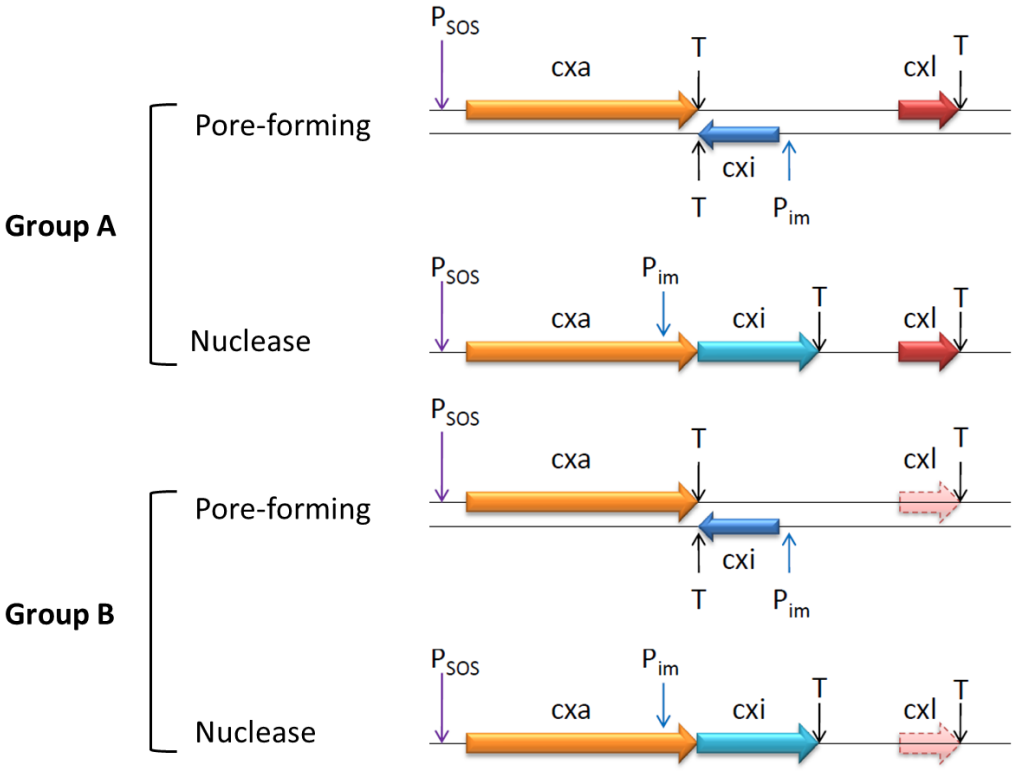

Figure 1.6 Genetic organization of colicin operons. Arrows represent different genes, P_{SOS} : SOS promoters, P_{im}: constitutive promoter of immunity gene, T: transcription terminator. Gene nomenclature follows a three letter code, the colicin gene (*cxa*, in which *x* is specific to the colicin), immunity gene (*cxi*) and lysis protein gene (*cxl*).

1.2.2 Colicin A

A common aspect of colicin toxins is their modular organization, they contain three different functional domains related to the three steps in their mode of action: reception, translocation and cytotoxicity (colicin import stages are detailed in Fig 1.7). The receptor binding domain (R) located in the central region of the protein, comprises almost one third of the protein and interacts with a β-barrel transporter in the outer membrane. Table 1

shows different cell envelope proteins involved in colicin import, for colicin A (ColA) the transporter used is BtuB, whose primary function is the vitamin B12 active translocation to the periplasmic space. Upon binding to the receptor on the bacterial cell surface, colicin undergoes a partial unfolding and the N-terminal domain or translocation domain (T) gets access to the periplasmic space through the porin OmpF where it interacts with the Tol machinery. The T domain is divided into two parts, an intrinsically unstructured T domain (IUTD) and a larger structured T domain (STD). Intrinsically disordered regions can be found in proteins that are required to interact with several partners, as coupling folding transitions to protein binding allows for the formation of different intermolecular interfaces contributing to the specificity and rate of molecular recognition (Dyson and Wright, 2005). Several studies with colicins have highlighted the important role of disordered regions in the complex translocation process that drive cellular uptake of these proteins (Collins et al., 2002; Zhang et al., 2010b). The exact function of the Tol system in the cell is not clear but, based on colicin import experiments, it was concluded that the TolB, Pal, TolA, TolQ, and TolR proteins can function as a transmembrane protein translocation portal or translocon (Zakharov et al., 2004).

Once the toxin has reached the inner membrane, the C-terminal domain, harbouring the cytotoxic activity (A), approaches its cellular site of action, in the case of colicin A it inserts into the inner membrane (Fig. 1.7 Stage 4). The exact translocation mechanism of the pore-forming domain is unknown but the fact that it can only happen after the T domain recruits and interacts with translocation components suggests that it could be facilitated by tol-dependent translocation (Cascales et al., 2007; Dover et al., 2000; James et al., 1996). Alternatively, different outer membrane destabilization phenomena that could facilitate cytotoxic domain entry have been proposed. Deprez et al. postulated that changes in the arrangement of Tol components upon T domain translocation might create outer membrane defects (Deprez et al., 2002). Moreover Mosbahi et al observed that colicins undergo conformational changes upon binding to phospholipids (Mosbahi et al., 2004). Nevertheless, what appears to be clear from the work done in bacteria, as well as in model membranes, is that the pore-forming domain has to undergo a considerable conformational change or partial unfolding to get inserted into the membrane (Bénédetti et al., 1992; Dunkel et al., 2015; van der Goot et al., 1991). This biophysical process would not necessarily involve specific binding to Tol proteins, as fusing the pore-forming domain of colicin A to a SEC-

dependent signal sequence brings about a functional pore localized in the inner membrane (Duché et al., 1999; Nardi et al., 2001).

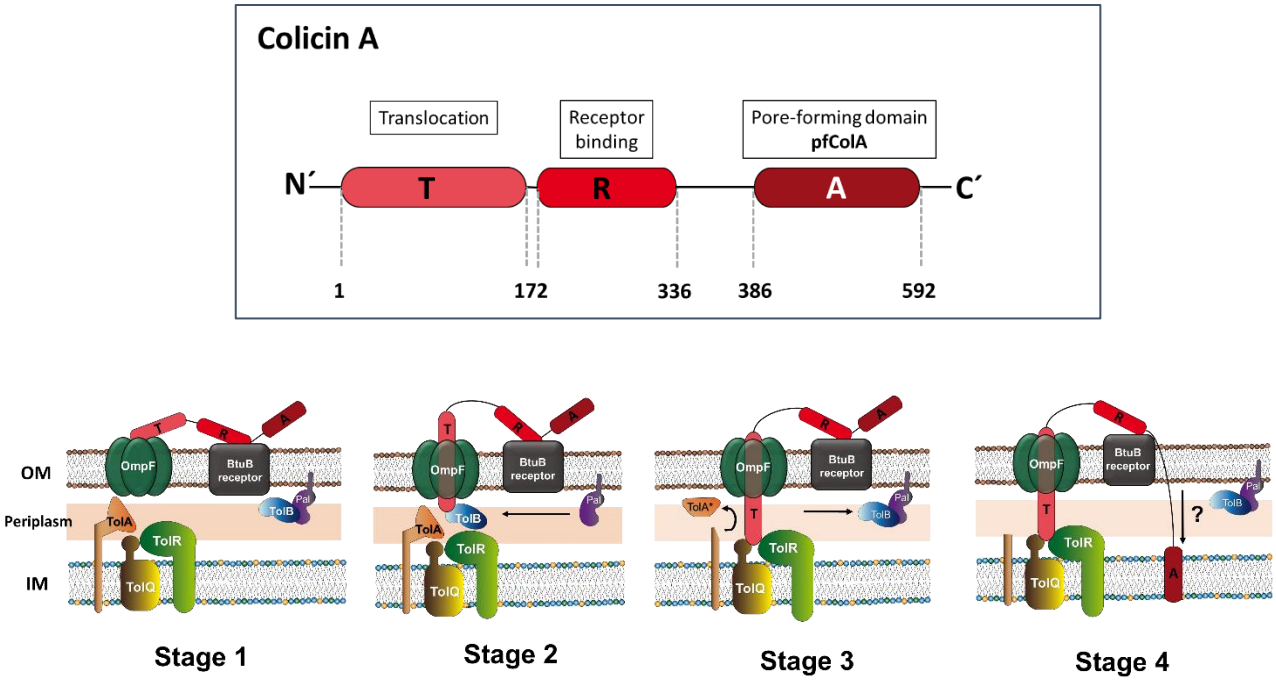

Figure 1.7 Modular organization of colicin A and putative import model for group A pore-forming colicins. Stage 1: The central domain (R) binds to the outer membrane receptor, BtuB and triggers the recruitment of the translocation machinery. Stage 2: the N-terminal domain is partially unfolded during the translocation through the OmpF porin and protrudes into the periplasm where it interacts with TolB, thus dissociating the TolB-Pal complex. Stage 3: the N-terminal domain dissociates from TolB to interact with TolA, causing TolA degradation (TolA *) and allowing the colicin to interact with TolR and/or TolQ. Stage 4: the C-terminal domain, carrying the lethal activity, is translocated by an unknown mechanism (?) and forms a pore in the inner membrane. Colicin depicted in red (T: translocation domain, R: receptor binding domain, A: activity domain) OM: outer membrane, IM: inner membrane.

1.2.3 The pore-forming domain of ionophoric colicins

In contrast with the divergence found in the N-terminal and central domains of various ionophoric colicins related to the various receptors and translocation systems involved, the pore-forming domain show a much higher structural similarity. Based on the sequence alignment, ionophoric colicins are classified into two distinct groups: group A (Colicin A) and group E1 (colicin E1).

The crystallographic structure of the colicin A pore-forming domain (pfColA) was the first structure of a colicin pore-forming domain to be solved (Parker et al., 1989) an revealed a

fold that later on was confirmed to be common for all pore-forming colicins (Fig. 1.9). It contains a hydrophobic domain surrounded by amphipatic helices (Fig. 1.8). To date, the three-dimensional structures of the C-terminal domain of several ionophoric colicins are available and exhibit a strong structural similarity. The structure can be described as a bundle of ten α-helices which are arranged in three layers resembling a classical three-on-three helical sandwich (Parker et al., 1989). The N-terminal region forms a pair of antiparallel amphipathic helices (H1-H2) followed by a long loop connecting to the next layer of two pairs of antiparallel helices, H3-H4 and H6-H7. Connecting these two helical pairs is a short helix, H5. Buried in the middle of the protein are the hydrophobic helices H8-H9 (in red in Fig. 1.9). Based on hydropathy profiles this hydrophobic stretch was predicted to be a membrane-spanning region (Pattus et al., 1985) which was extensively evidenced experimentally (Lakey and Slatin, 2001; Padmavathi and Steinhoff, 2008). The mechanism of insertion into the membrane thus involves the exposure of the hydrophobic hairpin buried within the protein in its water soluble conformation.

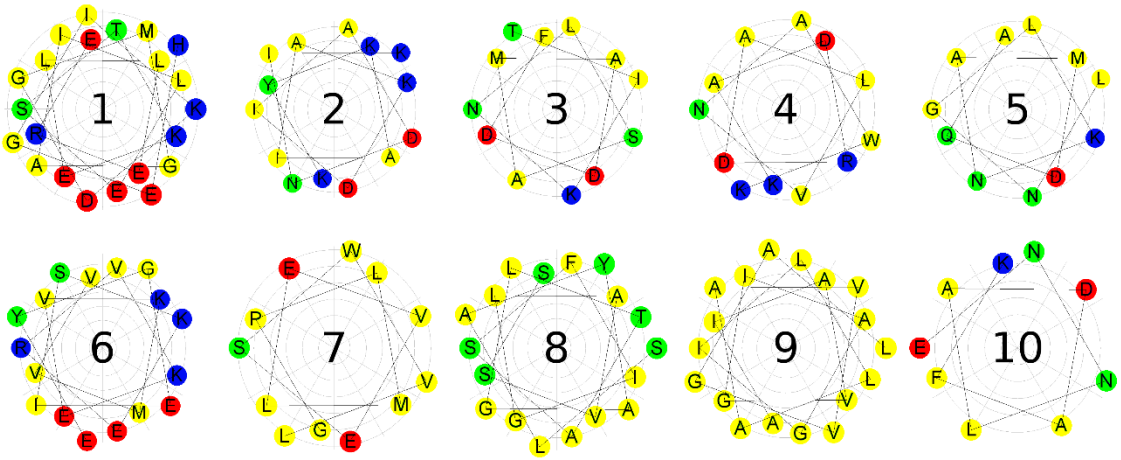

Figure 1.8 Helical wheel projections of the helices composing colicin A pore-forming domain, pfColA. In yellow hydrophobic residues (Leu, Ile, Val, Ala, Phe, Trp, Met, Pro and Gly), in green uncharged polar residues (Asn, Gln, Ser, Thr and Tyr), in blue positively charged residues (Lys, Arg and His) and negatively charged residues in red (Asp and Glu). The hydrophobic character of helices 8 and 9 becomes apparent as well as the amphipatic nature of the surrounding helices.

The similarity of the pore-forming domain of different colicins (Tol-dependent or TonB-dependent) suggests that the lethal activity of these colicins is independent of the translocation pathway. This has been demonstrated by the construction of chimeric toxins

exchanging the active domain of colicins A and B which do not use the same translocation system (Geli and Lazdunski, 1992) or by fusing the C-terminal domain of colicin A to a signal sequence targeting it to the periplasm of the producing bacteria. The C-terminal domain produced in this way has been found to be active even in bacterial strains which do not produce the Tol machinery required for colicin A translocation (Espesset et al., 1994a, 1996).

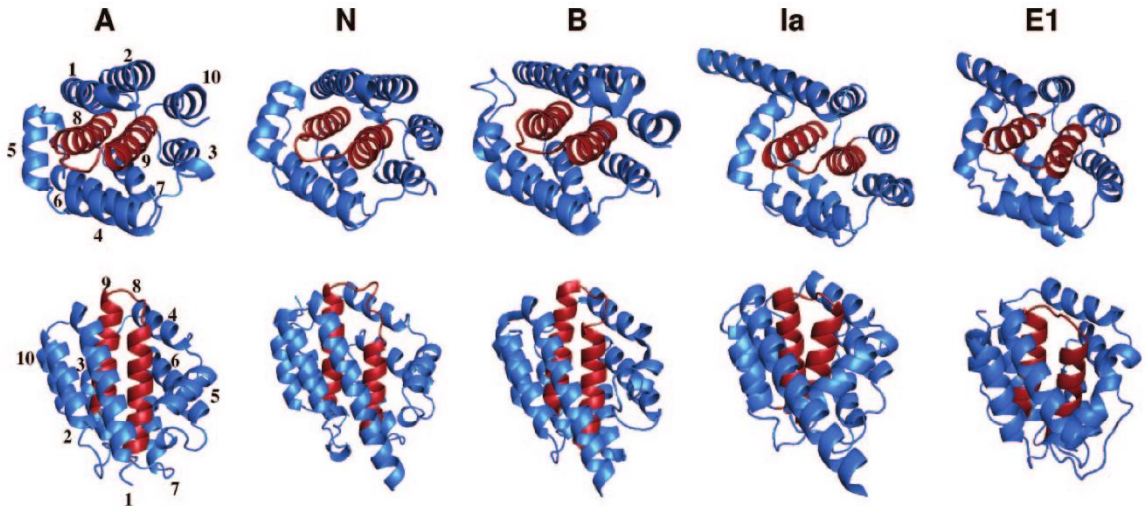

Figure 1.9 Comparison of the structures of the pore-forming domains of colicin A (1COL), colicin N (1A87), colicin B (1RH1), colicin Ia (1CII) and colicin E1 (2I88). Each molecule is shown in two orientations: one approximately perpendicular to the hydrophobic hairpin (upper) and the other parallel to it (lower). The localization of helices 1-10 are indicated for colicin A, the buried hydrophobic hairpin is depicted in red.

Despite the efforts no atomic resolution structure of the membrane-bound conformation of any colicin has been obtained to date, suggesting that the membrane inserted form might be highly dynamic (Anderluh and Lakey, 2008; Huster et al., 2001). Even if the hydrophobic nature of the central hairpin will facilitate bilayer penetration, the helices are shorter than average transmembrane helices and lack charged residues at the tip of the connecting loop to maintain the trans bilayer conformation. This suggests that the hydrophobic hairpin might not adopt a fixed conformation within the membrane.

Soon after the publication of the pfColA structure, its similarity with the extensively characterized globular topology was revealed (Holm and Sander, 1993). In this topology, different helical pairs lay perpendicular to each other forming three layers, a similar

structural architecture can be found in five different families: globins, phycocyanins, TipA class proteins, diphtheria toxin and pore-forming colicins. More generally, this orthogonal bundle topology can also be found in other membrane binding proteins like the Bcl-X family, uteroglobins, amoebapores, granulysins and antimicrobial peptides known as NK-lysins (Anderluh and Lakey, 2008). All these proteins share the mode of action of colicins to some extent, even though they have unrelated sequences and act in varying cellular contexts. This represents a good example of convergent evolution towards a folding motif that is simultaneously stable in aqueous solution as well as in the membrane environment. As a consequence these proteins are able to populate an ample conformational spectrum.

The apoptosis regulators Bax/Bcl-XL formed by members of the Bcl-X family, are surprisingly similar to pore-forming colicins (Cosentino et al., 2016). Although the molecularity and mechanism of pore-formation is not well understood, these apoptosis-related proteins undergo conformational rearrangements reminiscent of colicin A (Aisenbrey et al., 2007; Thuduppathy et al., 2006). As suggested by other authors, unravelling the molecular mechanism of bacterial pore-forming toxins can contribute to the understanding of the molecular function of structurally related proteins (Anderluh and Lakey, 2008; Cosentino et al., 2016).

1.2.4 Channel formation

The formation of a transmembrane channel by pore-forming colicins is believed to occur in two stages. The first step is voltage-independent and it is characterized by the adsorption of the pore-forming domain into the surface of the membrane followed by the insertion of the hydrophobic hairpin into the bilayer. The orientation the helices 8 and 9 and membrane arrangement of the rest of amphipatic helices is still elusive. This conformation of the pore-forming domain associated with the membrane and in the absence of membrane potential constitutes the closed state of the channel. The second stage is voltage-dependent and consists of the insertion of voltage-sensing helices into the membrane. The application of an electric potential would not only be accompanied by the insertion of helices into the membrane but would also cause the passage of several helices to the other side of the

membrane (Cascales et al., 2007). The channel is then opened causing the depolarization of the membrane that will be lethal for the cell.

1.2.4.1 The closed channel

The initial interaction between the pore-forming domain and the membrane is electrostatic in nature. This initial electrostatic binding is followed by a hydrophobic interaction that stabilizes the bound state and renders the interaction irreversible (W A Cramer et al., 1995) . Thus the hydrophobic segment would interact with the hydrophobic core of the bilayer while the amphipatic helices interact with the surface of the membrane, keeping their secondary structure. The need to undergo several conformational changes during membrane insertion and pore formation speaks in favour of a rather dynamic structure in which very stable secondary structure elements are able to move independently (Zakharov and Cramer, 2002a). In the case of colicin E1, the hydrophobic nucleus (Helix 8 and Helix 9) would adopt an orientation perpendicular to the plane of the membrane (Merrill et al., 1990; Rath et al., 1991; Zhang and Cramer, 1992). A similar insertion of hydrophobic helices has been described for the related diphtheria toxin and δ-endotoxin pore-forming domains (Parker and Pattus, 1993). By interacting with the membrane, the pore-forming domain of colicins A and B loses part of its tertiary contacts to adopt an insertion-competent state that promotes and accelerates its insertion into the bilayer (Evans et al., 1996; van der Goot et al., 1991) The requirement of a partly unfolded state for activity was shown by the dependence of activity onset of the channel measured for 4 different lipid compositions with the decrease in near-UV CD amplitude as a function of pH. This intermediate conformation was not found for colicin E1 (Schendel and Cramer, 1994; Zakharov and Cramer, 2002a) nor colicin N (Evans et al., 1996).

Two models have been proposed for the closed channel of pore-forming colicins. The first model, called the umbrella model, was proposed by Parker et al. in 1989 from the crystal structure of colicin A. In this model, the hydrophobic hairpin is inserted perpendicularly into the membrane. The amphipatic helices split into two parts and elongate along the surface of the inner membrane (Parker et al., 1989). Fluorescence Resonance Energy Transfer (FRET) studies between probes placed in helices 1, 2 and 10 of pfColA in the presence or absence

of lipid bilayers provided evidence for this model (Lakey et al., 1991). The second model described as the penknife model comes from a second series of FRET studies on colicin A (Lakey et al., 1993). In this study, the fluorescent probes were also bound to different sites at the hydrophobic hairpin. In this model, the helices H1 and H2 separate from the rest of the molecule when the protein is attached to the membrane. The rest of the protein is also adsorbed on the membrane surface with helices 3 to 7 and helix 10 covering the hydrophobic helices H8 and H9. This model was then confirmed by the insertion of disulfide bridges between different helices of pfColA. Only the disulfide bonds connecting the helices 1 or 2 to the other helices prevented the membrane insertion of colicin A. Disulphide bridges connecting helices 8 or 9 to helices 3 to 7 did not interfere with the insertion of colicin A into the membrane showing that the helices 8 and 9 do not penetrate perpendicularly into the membrane (Duché et al., 1994a, 1994b). As noted by Padmavathi and Steinhoff (2008), these structural models were determined under experimental conditions that do not allow for the protein to be fully inserted into the membrane, in particular, the experiments were performed with liposomes of 100% anionic lipids at pH 5.0 in which the protein is shown to be adsorbed rather than inserted (Padmavathi and Steinhoff, 2008). Furthermore, colicins were shown to be non-functional under these conditions (Lindeberg et al., 2000).

Similar FRET studies performed on colicin E1 made it possible to measure the distance between helix 9 and the rest of the helices. Based on this data the authors proposed an alternative umbrella model (Lindeberg et al., 2000). An electron paramagnetic resonance (EPR) study of pfColA was carried out by Böhme *and cols.* (2009) in which a model of the closed channel was proposed according to the inter-spin distances between the amphipathic helices and helix 9 (Böhme et al., 2009). This data are in agreement with the hydrophobic helices being anchored in the bilayer forming a transmembrane segment, similar to the model proposed for E1.

The current opinion regarding the insertion of a pore-forming colicin domain in the absence of voltages assumes that this is a dynamic process during which several conformations can be populated. The different models proposed would reflect different stages of membrane insertion under different physicochemical conditions.

1.2.4.2 The open channel

When applying a trans-negative potential (Δψ) to the cell membrane (*cis* = outside; *trans* = inside), the colicin ion channel opens (Cramer, et al., 1990). The conductance of the channel is small compared with highly selective eukaryotic channels, and generally pH-dependent (15 pS for colicin A at pH 7) (Spach et al. 1983) . All colicin channels exhibit a high selectivity for protons over other cations. The opening of the channel is induced by the insertion of several helices in the membrane but is also accompanied by the passage of a part of the colicin molecule to the other side of the membrane (Qiu et al., 1996; Slatin et al., 1994). Small peptides or proteins inserted between helices 3 and 4 by directed mutagenesis in colicins A and Ia were shown to be transported to the *trans* side of the membrane upon channel opening (Jakes et al., 1998) (Slatin et al., 1994, 2002).

One of the essential questions concerning channel formation by pore-forming colicins relates to the identification of the helices that line up and form the channel. The pore-forming domain of colicins is composed of 10 α-helices, but not all appear to be necessary for channel formation. Deletion studies within the cytotoxic domain of colicin A have shown that the last 5 helices of colicin A are sufficient to form a channel *in vivo* and *in vitro*, possessing close characteristics relative to the channel formed by the whole colicin (Nardi et al., 2001). Based on this study, the channel would be formed only by helices 6, 7, 8 and 9 (Slatin, et al., 2002). Extensive efforts to identify different steps in channel formation in planar lipid bilayer membranes led to the proposal of the following model for colicin Ia channel formation. Initially the H8-H9 hairpin inserts into the membrane in a voltage-independent manner to form two transmembrane segments. Then, in response to a cis-positive voltage, an additional portion of the C domain inserts, so that parts of helices H1 and H6-H7 contribute the third and fourth transmembrane segments. Concomitantly, helices H2-H5 are translocated across the membrane to the opposite, *trans* side. This voltage-dependent insertion results in the opening of a conductive channel through the membrane (Kienker et al., 2000; Qiu et al., 1996). Recently a model of the channel-lining residues of colicin Ia has been proposed based on cysteine accessibility. Mutations in the cis end of the channel (residues 577-609) showed altered conductance and selectivity of the channel. The residues involved in the formation of the ion channel have been identified and are organized on the same face of H8 and H9 (Fig. 1. 10) even if the channel would also

involve H6 and H7. Thus these residues would be responsible for the proton passage from the cis side to the *trans* side of the membrane (Kienker et al., 2008).

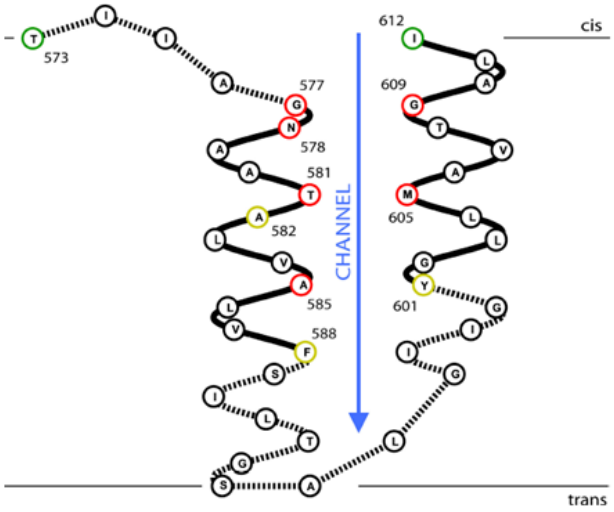

Figure 1.10 Schematic model of the colicin Ia hydrophobic hairpin the open channel state. Orientation of helices 8 and 9 of colicin Ia forming the ion channel in the membrane. The position of the residues accessible to the probe are indicated. The residues accessible only from the cis side in green, those accessible only from the *trans* side in yellow; and those accessible from both sides in red. The dotted line shows that the secondary structure of this part could change in the open channel. According to (Kienker, et al., 2008).

The diameter of the channel formed by colicin A is estimated to reach 10 Å (Raymond et al., 1985). For colicin Ia, this value is estimated to be around 7 Å (Krasilnikov, et al., 1998). This channel lumen is much larger in comparison with other well-characterized voltage-gated channels (Doyle et al., 1998). Trials with monovalent ions of different sizes showed that none of these ions is too large to cross the channel (Bullock and Kolen 1995, Bullock, et al 1992, Raymond, et al., 1985). Even tetraethyl ammonium (TEA), a cation of about 8 Å, permeates easily the channel formed by colicin Ia (Slatin, et al., 2008). Most of the pore-forming toxins, which have the capacity to form large ion channels, are oligomeric. However, almost all the results obtained so far show that the ion channel formed by ionophoric colicins is most probably monomeric (Lakey and Slatin 2001). Experiments carried out in planar lipid bilayers, showed that colicin K (Schein et al., 1978) and E1 (Slatin, 1988) formed channels in direct proportion to their concentration, implying a monomeric structure for the channels. The question arises of how we can reconcile these two contradictory results. One explanation could be that colicins recruit lipids to participate in the formation of the pore. This hypothesis has already been demonstrated for certain proteins forming oligomeric pores (Fradin et al., 2009; Gilbert, 2016; Lin and Baumgaertner, 2000; Matsuzaki et al., 1996).

Results obtained with colicin E1 support this hypothesis (Sobko et al., 2006, 2009, 2010). They showed that the activity of colicin E1 is dependent on the lipid composition of the membrane model used. With a thin membrane consisting of 1,2-dieicosanoyl-*sn*-glycero-3-phosphocholine (C20), channel conductance of colicin E1 is 60 pS and its size is 12 Å. With a thicker membrane, consisting of 1,2-dierucoyl-*sn*-glycero-3-phosphocholine (C22), the conductance is 600 pS, and the channel size is then 16 Å. In the case of the colicin E1, for instance, the presence of lysophosphatidylcholine has been shown to increase the ability to form channels by the protein because of the positive curvature conferred by the presence of this lipid to the membrane (Sobko et al., 2006). Additionally, it has been found that this protein induces transbilayer (flip-flop) processes in membranes (Sobko et al., 2010).
A 2D crystallography study of colicin Ia reconstituted into liposomes revealed the presence of a putative hexagonal arrangement of the protein. This complex is visualized by electron microscopy with a 17 Å resolution. All previous results suggest that the channel is monomeric, so it is not clear whether the contacts found in the crystal have physiological relevance. The authors proposed that such an oligomeric structure could facilitate the translocation of the helices upstream of the hydrophobic hairpin through the membrane (Greig et al., 2009).

The structure of the diphtheria toxin T domain shows structural similarities with the C-terminal domain of pore-forming colicins. This similarity has been demonstrated not only for the soluble form (Choe et al., 1992), but also for the topology of the ion channel formed (Kienker and Slatin, 2003). Despite the obvious similarities with colicins, diphtheria toxin was not chosen as a reference for colicins since its cytotoxic mechanism is fundamentally different. While diphtheria toxin does form low conductance channels, its lethal action consists on the translocation of a water-soluble enzymatic domain to the cytoplasm where it blocks protein synthesis. The translocation of such a large protein domain occurs without the aid of any cellular component (Senzel et al., 1998), a process that is common for anthrax toxin as well. Both toxins have this additional capacity to form channels (Hoch et al., 1985), which appears to be indispensable to undergo the lethal effect. Actually, mutants that are defective in pore formation are also defective in killing target cells (Sellman et al., 2001; Silverman et al., 1994). Interestingly enough although diphtheria channels were traditionally

envisioned as multimeric structures, more recent studies suggest that the toxin might indeed be monomeric (Gordon and Finkelstein, 2001).

The diversity in chemical nature and size of molecules that can pass through the channel formed by colicins suggests that this channel is not very selective. However, the channel permeability for proton is 10^4 times greater than for potassium at neutral pH (Kienker, et al., 2002). A recent publication using chimeric proteins constructed from colicins A, E1, and Ia, showed that the structural elements determining proton specificity of colicin A would be located in the last 5 helices (Slatin, et al., 2010). It is difficult to explain how a 10 Å channel can have such a high selectivity for protons over potassium ions. To this paradox is added the low conductance of the channels formed by colicins compared to their rather high diameter. In addition, colicin A has been shown to carry large peptides through the membrane (Slatin, et al., 2002; Slatin and Kienker 2003). Similar results have shown that colicin Ia could transport a protein of 26 Å in diameter across the membrane (Kienker, et al., 2003). The channel formed by the colicins appears to be too small compared to the peptides which can be translocated and too large to display such a high selectivity for protons.

In summary two compatible pathways have been proposed to mediate colicin ionophoric action (i) the pathway for ions, that is, the ion-conducting channel; (ii) the pathway that allows the translocated segment (H2‑5 in colicin Ia) to cross the membrane. This mode of action is also found in diphtheria toxin as discussed above.

1.2.5 Immunity to pore-forming colicins

Irrespective of the cytotoxic mechanism that bacteria use to out-compete neighboring cells, all colicinogenic bacteria have to protect themselves from the lethal effectors they produce. Immunity against pore-forming colicins is conferred by polypeptides of 11 to 18 kDa which are localized in the inner membrane. The narrow specificity of the protection conferred by each immunity protein suggests a direct interaction between colicin and its cognate immunity protein. Based on sequence homology, immunity proteins can be classified into 2 groups, matching the classification of ionophoric colicins (Geli et al., 1989; Schramm et al.,

1988; Song and Cramer, 1991). Group A include: colicins A, B, N, U, Y and S4 and group E1, colicin E1, 5, K, 10, Ia and Ib.

While pore-forming colicins are produced as water-soluble proteins that reach the membrane from the extracellular medium, immunity proteins are integral membrane proteins. The colicin A immunity protein (Cai) has 4 transmembrane helices with the N- and C-termini located in the cytoplasm (Geli et al., 1989a) (Fig. 1.11). On the other hand, E1 immunity proteins (Song and Cramer, 1991) and colicin N immunity protein (Pugsley, 1988) possess 3 transmembrane segments with their N-terminus in the cytoplasm and their C-terminus facing the periplasm.

Various studies have been carried out to determine important regions for the functioning of immunity proteins but the lack of a three-dimensional structure greatly hampers rational design. In the case of Cai, mutagenesis studies have shown that even non-conservative substitutions at the N- or C-terminal regions preserved the activity. Cai and Cbi (colicin B immunity protein) share high sequence similarity (38% sequence identity and 39% conservative substitutions (Geli, et al., 1989a). Cai transmembrane helix 1 can be functionally exchanged with that of Cbi without altering the activity of the modified protein (Geli, et al., 1988). The L2 and L3 loops of Cai are rich in polar residues, the substitution of these residues decreases the activity of the protein. However, the same type of substitution does not alter the function of the immunity protein of colicin E1 (Cei) (Song and Cramer 1991; Zhang and Cramer, 1993). The role of the cytoplasmic loop L2 was glimpsed by Espesset and cols. (1994b). The authors produced the Cai immunity protein in the form of 2 independent segments (H1-H2 and H3-H4) and noticed the lack of functionality of the protein, resulting from an inability of the two segments to interact In the membrane to reform a functional protein (Espesset et al., 1994b). This suggests that the L2 loop plays an important role in the connection between transmembrane helices of Cai. The L2 loop has a significant concentration of positively charged residues which would make it an important topology determinant (von Heijne, 1992; Nilsson and von Heijne, 1990). Periplasmic loops appear to be important for protein activity but do not seem to be determinant for specificity (Espesset et al., 1994b).

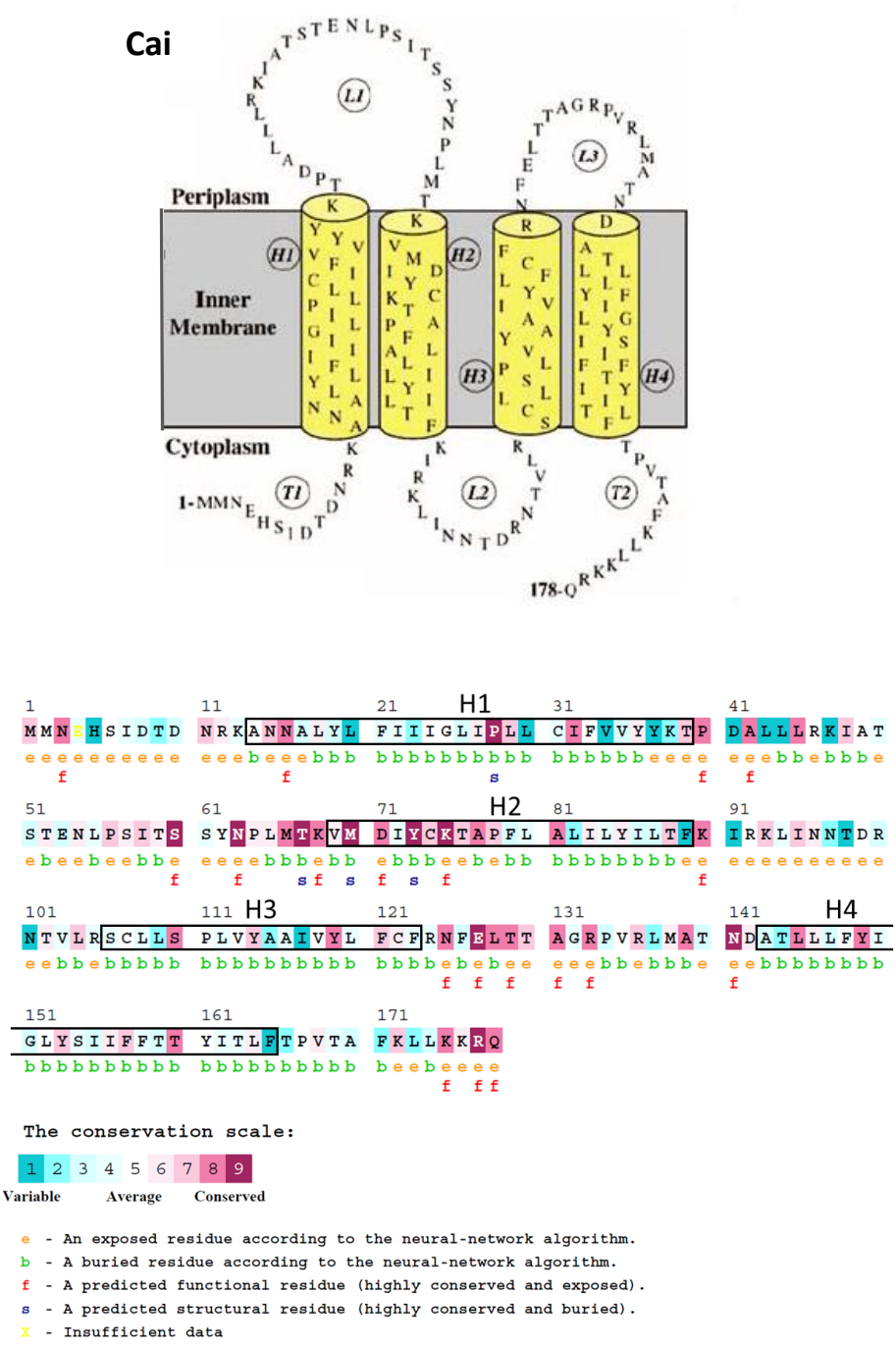

Figure 1.11 Topographical model of immunity protein to colicin A, Cai, in the inner membrane and primary structure of Cai coloured according to conservation scores. Transmembrane helices are indicated as H1-H4 and inter-helical loops are denoted as L1-L3 while the N- and C-terminal ends are indicated as t1 and T2. Topographical model adapted from Cascales and cols. (2007) and multiple sequence alignment performed with ConSeq revealing functionally and structurally important residues (Berezin et al., 2004). Transmembrane segments are indicated inside boxes.

Studies on colicin Ia have shown that the presence of the immunity protein did not prevent the binding of colicin to its receptor on the surface of the bacteria (Konisky and Cowell 1972).

The recognition between the immunity protein and its colicin thus takes place at a latter step in its mode of action (Konisky 1982): during insertion into the membrane or channel opening. The chimeric proteins between colicins Ia and Ib (Mankovich et al., 1984) and colicins A and E1 (Benedetti et al., 1991) identified the C-terminal domain of colicins as the region recognized by immunity proteins. The first biochemical evidence of the interaction between the C-terminal domain of a colicin and its immunity protein came from the work of Espesset et al., in 1996. In that work, the C-terminal domain of colicin A fused to a prokaryotic signal sequence, is targeted to the periplasm of the producing bacteria where it gets inserted into the internal membrane and exert its lethal activity. Bacteria can only survive if they co-express the immunity protein. Under these co-expression conditions, the C-terminal domain of colicin A was shown to co-immunoprecipitate with Cai (Espesset, et al., 1996). Thus, based on these results, the proposed model is that the immunity protein diffuses freely within the inner membrane until it finds the C-terminal domain of its colicin partner and inactivates it. In the case of the immunity protein for ColE1, a high protein diffusion rate constant in the membrane of approximately 10^{-9}–10^{-10} cm^2 s^{-1} was observed, which corresponds to a possible migration length of at least 500 nm within 10 s, which would be sufficient for the toxin-antitoxin association to occur (Song et al., 1991).

In an attempt to determine the specific residues important for protein-protein recognition numerous mutational studies were performed. Different experimental evidence suggest that group A immunity proteins recognize a certain region of their partner colicins while those in group E1 recognize another region. Looking at what is known about the interaction for group A immunity proteins with the pore-forming domain some low resolution models start to arise.

The construction of chimeric colicins between colicin A and colicin B showed that the hydrophobic hairpin formed by helices 8 and 9 was the major determinant recognized by the immunity protein (Geli and Lazdunski, 1992). In fact, pore-forming domains of colicin A and colicin B share 60% identity but differ in specific transmembrane (TM) determinants required for the association with their cognate immunity protein. The sequence that determines the Cai/pfColA interaction is localized between residues L530 and D577 of the pore-forming domain (Geli and Lazdunski, 1992), corresponding to residues L142 and D189 in the truncate pfColA. This result was confirmed a few years later by using a fusion protein

containing helices 8 and 9 of colicin A inserted between a prokaryotic signal sequence and alkaline phosphatase. This fusion protein could indeed be co-immunoprecipitated with Cai even if only the hydrophobic hairpin was present (Nardi, et al., 2001a). All these results made it possible to establish that the smallest region of a group A colicin recognized by its immunity protein consisted of the hydrophobic helices 8 and 9. Results obtained on colicin U made it possible to further reduce the region recognized by the immunity protein. Indeed, deletion of the 9 residues of the loop between Colicin U (Cui) helices 8 and 9 prevents the Cui immunity protein from recognizing the mutated colicin U and hampers inactivation. When the 9 residues of colicin U are replaced by those of colicin B (Cbi), the hybrid protein is partially recognized by Cui but also by Cbi, the immunity protein of colicin B (Pilsl, et al., 1998).

Cysteine crosslinking experiments in bacteria suggest that Cai may form a homodimer in the membrane, in which H3 would be mainly implicated. This study also postulated that interaction with pfColA modifies the dimeric organization, altering intra-helical interactions and the arrangement of the helices in the bilayer (Zhang et al., 2010a).

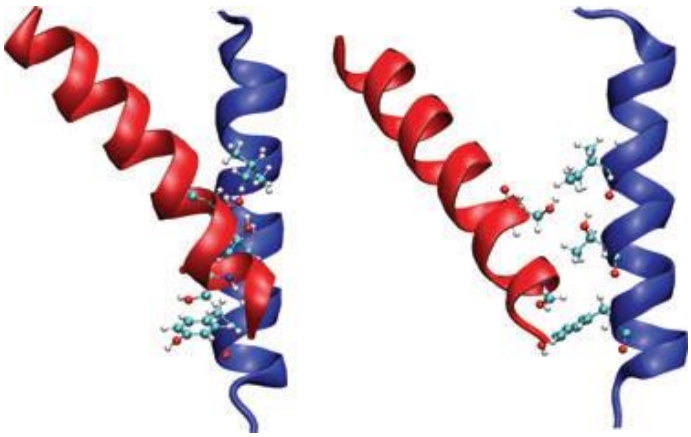

Figure 1.12 A model of the colicin Y, Cya–Cyi intramembrane interaction shown from two perpendicular views (A, B). The blue and red ribbons represent H8 of Cya (from I569 to G590) and TM3 of Cyi (I101 to N121), respectively. Colicin Y residues responsible for the interaction, I578, T582 and Y586, as well as Cyi residues S104 and S107, are shown in a ball-and-stick representation on the ribbons. Both helices form an angle of approximately 20° between the helical axes, which ensures a close contact between the helices (Šmajs et al., 2008).

Additional work was carried out on colicins A and Y in order to identify the key amino acids in the colicin/immunity protein recognition. Colicin Y is an ionophoric colicin (Riley et al.,

2000, et al., 2006) sharing considerable sequence similarity with pfColA (68% identity). Using genetic approaches, Šmajs and cols. (2008) were able to identify residues important for the recognition and interaction between the ionophoric domain of colicin Y and the immunity protein Cyi. These amino acids are located in the two hydrophobic helices of colicin Y and H3 of Cyi (Fig. 1.12) (Šmajs et al., 2008). All these results suggest that the immunity protein interacts with helices 8 and 9 of pfColA in the membrane just before channel opening.

1.3 Objectives

The pore forming fragment of colicin A depolarises bacteria by the formation of voltage dependent channels. Colicinogenic bacteria are provided with an immunity protein that protects the cell against the cognate colicin. The pfColA and Cai toxin-antitoxin pair represents a well behaving system that can be used as a methodological framework to investigate protein-protein interactions in the membrane. A detailed investigation of the behaviour of both proteins in aqueous and membrane environment was approached in this thesis.

Specific objectives can be summarized as follows:

-To optimize the Cai expression and solubilization strategies, in order to achieve a stable monodisperse sample amenable to membrane reconstitution and functional studies.

-To achieve functional reconstitution of the Cai/pfColA complex both in bacterial and model membranes.

- To determine affinity, stoichiometry and stability of the Cai/pfColA complex in micelle solutions

CHAPTER 2

Experimental procedures

2 . EXPERIMENTAL PROCEDURES

2.1 Molecular biology

2.1.1 DNA constructs and cloning

Molecular cloning allows for the isolation, amplification and modification of DNA sequences coding for the proteins of interest. In order to clone the cDNA of interest several steps are necessary: amplification of the DNA fragment by polymerase chain reaction (PCR), digestion by restriction enzymes, isolation of insert and vector by gel purification, ligation of the insert into the vector, transformation in *E. coli* and finally confirmation by DNA sequencing. Inserting the cDNA sequence of the target protein in self-replicating independent plasmids constitutes the first step towards recombinant protein expression in *E. coli* (Green et al., 2012).

In this work, we have applied standard recombinant DNA techniques in order to clone cDNAs of the C-terminal domain of colicin A, pfColA and of the cognate immunity protein, Cai. These two sequences have been fused to histidine tags for purification, to fluorescent proteins (Cherry and GFP) for monitoring and quantification, or to periplasm signal sequences targeting pfColA to the periplasm (PelBss and TorAss). The plasmids used for each of the constructs are summarized in Table 2.1. In addition, site-directed mutagenesis was performed to analyse the effect of selected residues on pfColA conformation and function.

Table 2.1 Vectors used in this work for protein expression, indicating the protein to be expressed, vector name, characteristics and antibiotic resistance.

Protein	Vector	Description	Phenotype
Cai-GFP	pWaldo(d)	TEV protease cleavage site between Cai and GFP, C-terminal 8-histidine tag	Kan^r
CaiH	pWaldo(d)	C-terminal 8-histidine tag	Kan^r
pfColA (WT and mutants)	pBAT4	No tags	Amp^r
PelB-pfColA-Cherry	pET22b(+)	N-terminal signal sequence for Sec-dependent translocation, C-terminal 6-histidine tag	Amp^r
TorA-pfColA-Cherry	pET22b(+)	N-terminal signal sequence for Tac-dependent translocation, C-terminal 6-histidine tag	Amp^r

Different bacterial strains were used, DH5α was used in the cloning steps, BL21 (DE3) for overexpression of pfColA, and Walker strains C41 (DE3) and C4 (DE3) for Cai, Cai-GFP and Cai/pfColA co-expression (Table 2.2).

Table 2.2 Bacterial strains used in this work and their genotype.

Bacterial strain	Genotype
E. coli DH5α	F- *f80dlacZM15 D(lacZYA argF)U169 deoR phoA supE44 hsdr17(rK-, mK+)*
E. coli BL21 (DE3)	*fhuA2 [lon] ompT gal (λ DE3) [dcm] ΔhsdS λ DE3 = λ sBamHIo ΔEcoRI-B int::(lacI::PlacUV5::T7 gene1) i21 Δnin5*
E. coli C41 (DE3)	*F– ompT gal dcm hsdS$_B$(r_{B-} m_{B-})(DE3)*
E. coli C43 (DE3)	*F– ompT gal dcm hsdS$_B$(r_{B-} m_{B-})(DE3)*

The sequences of the two protein targets used in this work are indicated below, for Cai the predicted transmembrane helices are highlighted in grey and positively charged residues that are known to determine the topology in the membrane (von Heijne, 1992; von Heijne, 1989) are highlighted in yellow.

Cai:

MMNEHSIDTDNRKANNALYLFIIIGLIPLLCIFVVYYKTPDALLLRKIATSTENLPSITSSYN PLMTKVMDIYCKTAPFLALILYILTFKIRKLINNTDRNTVLRSCLLSPLVYAAIVYLFCFRN FELTTAGRPVRLMATNDATLLLFYIGLYSIIFFTTYITLFTPVTAFKLLKKRQ

Topological models from fusions with alkaline phosphatase (Geli et al., 1989) confirmed that the N-and C-termini of Cai are directed toward the cytoplasm (Geli et al., 1988).

The last 206 residues of colicin A are indicate below, comprising the pore-forming domain (pfColA) pfColA in its soluble conformation forms a 10-helix helical bundle. Transmembrane helices are highlighted in grey from the crystallographic structure (Parker et al., 1989).

MEVAEKAKDERELLEKTSELIAGMGDKIGEHLGDKYKAIAKDIADNIKNFQGKTIRSFDD AMASLNKITANPAMKINKADRDALVNAWKHVDAQDMANKLGNLSKAFKVADVVMKVE KVREKSIEGYETGNWGPLMLEVESWVLSGIASSVALGIFSATLGAYALSLGVPAIAVGIA GILLAAVVGALIDDKFADALNNEIIRPAH

pfColA was fused to two different signal sequences to target it to the periplasmic space through Sec translocon (PelB) and through Tat machinery (TorA). The sequences of the targeting peptides are the following:

Trimethylamine-N-oxide reductase **TorA signal sequence:**

MNNNDLFQASRRRFLAQLGGLTVAGMLGPSLLTPRRATAAQAA

Erwinia carotova pectate lyase B **PelB signal sequence:**

MKYLLPTAAAGLLLLAAQPAMAM

2.1.2 Protein overexpression and purification

2.1.2.1. Production of Cai

The overexpression and purification of different Cai constructs was performed according to an optimized protocol for membrane protein production (Drew et al., 2006). Following these methodology, *E. coli* C41 (DE3) cells were transformed with pWaldo(d) plasmid and plated in agar-LB plates. A fresh colony of the transformed strain was used to inoculate 50 ml LB containing 50 µg/ml kanamycin grown to saturation. Each liter of LB was inoculated with 50 ml culture supplemented with 50 µg/ml kanamycin and grown at 37 °C. When the OD_{600} reached 0.4 the temperature was lowered to 20 ° C and expression was induced with 0.8 mM IPTG. After 18 h growth cells were harvested by centrifugation in Beckman Coulter AVANTI J-20 XPI (Rotor JLA 9.1) at 3000 g for 15 min. The cell pellet corresponding to 1 L was resuspended in 40 ml 1x PBS, 1 mM $MgCl_2$, 1 mM TCEP and DNase (20–100 U/ml) and subjected to 3 cycles of high pressure homogenization in Emulsiflex-C5 (Avestin, Canada) at 20-25 KPsi. Unbroken cells and cell debris were separated at 14000 g for 10 min on Beckman Coulter AVANTI J-20 XPI (rotor JA 25.50) and broken membranes present in the supernatant were spinned down by ultracentrifugation at 100000 g in ULTRA Beckman Coulter OPTIMA L90k (Rotor TFT-50.38) for 2 h. The pellet corresponding to the membrane fraction was resuspended in a small volume of ice-cold 1x PBS using a syringe, first with a 23-gauge needle then with a 18-gauge needle.

Once an homogeneous solution was obtained membranes were solubilized in 1% detergent (DDM or LDAO in most of the cases), 150 mM NaCl, 1 mM TCEP, 20 mM imidazol, 50 mM sodium phosphate pH 7.5 and one tablet of EDTA-free protease inhibitor cocktail (Roche). Solubilized membranes were separated from non-solubilized material by ultracentrifugation at 100000 g for 1 h in Beckman Coulter OPTIMA L90k (Rotor TFT-50.38) and the supernatant was incubated for 2 h with nickel nitrilotriacetic acid or Ni-NTA (ABT) resin pre-equilibrated in solubilization buffer. The resin was then transferred to a disposable plastic column and subsequent washes with increasing concentrations of imidazol (20-50 mM) were performed by gravity-flow. The protein was eluted with 300 mM imidazol, 0.2% detergent, 150 mM NaCl, 1 mM TCET, 50 mM sodium phosphate pH 7.5.

When Cai without the GFP tail was required, tobacco etch virus (TEV) protease digestion of Cai-GFP was carried out at 4 °C for 10 h or overnight. To this end protein concentration was calculated by absorbance at 280 nm and a 1:10 molar ratio (TEV: Cai-GFP) was added in 0.1% detergent, 200 mM NaCl, 1 mM TCEP, 10% glycerol, 50 mM sodium phosphate pH 7.5. The digestion efficiency was checked by in-gel fluorescence in SDS-PAGE and His-tagged TEV protease as well as the cleaved His-containing GFP tail were removed by reverse-IMAC. The flow-through containing cleaved Cai was concentrated in 50 kDa molecular weight cut of (MWCO) centrifugal concentrator (Amicon) at 3000 g to a final volume of 500 µl. Cleaved Cai, CaiH or Cai-GPF were subjected to an additional purification step using a Superdex 200 10/30 column (GE-Healthcare) in 0.2% detergent, 100 mM NaCl, 1 mM TCEP, 20 mM sodium phosphate pH 7.5. Protein containing fractions were pooled and concentrated in 100 kDa MWCO centrifugal concentrators (Amicon).

In the case of CaiH, when a very pure sample was needed, an ion exchange chromatography step was introduced. Given that Cai has a pI of 9.6 a strong cation exchanger was used to separate contaminants in the sample. The high ionic strength buffer used in previous steps was exchanged to 0.2% LDAO, 1 mM TCEP, 50 mM HEPES pH 7.5 and the sample was loaded onto a HiTrap Capto S 5/5 (GE-Healthcare). Cai eluted at 130 mM NaCl during a linear gradient with 0.2% LDAO, 300 mM NaCl, 1 mM TCEP, 50 mM HEPES pH 7.5 buffer. Eluted fractions were analysed by SDS-PAGE and Cai-containing fractions were pooled and concentrated in 100 kDa MWCO centrifugal concentrators (Amicon).

2.1.2.2 Production of ^{15}N labelled Cai

The expression of isotopically labelled Cai was based on the protocol of Marley et al. in which bacteria are first grown in unlabelled rich media to high cell density followed by exchange into labelled media (Marley et al., 2001). Thus, 1 L cultures were grown in LB at 37 °C up to OD_{600} = 0.2 moment at which cells were pelleted by centrifugation in Beckman Coulter AVANTI J-20 XPI (Rotor JLA 9.1) at 3000 g for 15 min and resuspended in M9 minimal media supplemented with 1 g/l $^{15}NH_4Cl$, 50 µg/ml kanamycin, 1 mg/l D-biotin, 30 mg/l thiamine, 2 g/l D-glucose, 250 µM EDTA and trace elements (Verardi et al., 2012). Following a short period for growth recovery and unlabelled metabolite clearance, cells were induced with

300 mM IPTG and grown for 18 h at 20 °C. Protein purification was carried out as indicated above for unlabelled proteins.

2.1.2.3 Production of pfColA and mutants

The C-terminal domain of colicin A corresponding to the pore-forming domain, pfColA (res 387-592) was cloned in pBAT4 plasmid and transformed into *E. coli* strain BL21 (DE3). A fresh colony of the transformed strain was used to inoculate 5 ml of LB media supplemented with 100 µg/ml ampicillin and it was grown at 37 °C overnight. Cultures of 1 L LB were inoculated and grown at 37 °C up to an OD_{600} = 0.4 and protein expression was induced with 1 mM IPTG. After 3-6 h at 37 °C, cells were harvested at 3000 g for 15 min in Beckman Coulter AVANTI J-20 XPI (Rotor JLA 9.1) and resuspended in 50 mM TRIS-HCl pH 8.0 supplemented with DNase (20–100 U/ml). Cells were disrupted by pulse sonication in a MSE Soniprep 150 (MSE, United Kingdom) for a total of 7 min in an ice bath. The cytoplasm fraction containing pfColA was separated by ultracentrifugation at 100000 g for 1 h in Beckman Coulter OPTIMA L90k (Rotor TFT-50.38). The supernatant was filtered and subsequently applied onto a HiLoad Superdex 200 26/60 column (GE-Healthcare) pre-equilibrated in 50 mM TRIS-HCl pH 8.0. Eluted fractions were analysed by SDS-PAGE and pfColA-containing fractions were further purified by ionic exchange in a strong anion exchanger. The sample was loaded onto a Mono Q HR 5/5 column (GE-Healthcare) in buffer 10 mM TRIS-HCl pH 8.0 and pfColA eluted in a linear gradient up to 0.5 M NaCl, 10 mM TRIS-HCl pH 8.0. After selecting pure pfColA fractions by SDS-PAGE analysis, samples were pooled and concentrated in 10 kDa MWCO centrifugal concentrators (Amicon). Mutants MH6A (E121A, K122A), MH7 (N131A) and M6Y (V119A) were obtained in a similar way.

2.2 Membrane model systems

Many important biological processes occur at the membrane, this means that well-characterized *in vitro* membrane systems are needed if fundamental cell functions are to be assessed. Biological membranes constitute very complex differentially permeable barriers containing lipid molecules organized as bilayer structures in which many different kinds of proteins are embedded. Thus in the path towards a better understanding of these processes at the molecular level, simplified membrane model systems have been developed. Among

the most extensively characterized membrane mimicking systems we find lipid vesicles, lipid monolayers, supported lipid bilayers and micelles.

2.2.1 Detergent micelles

Detergents are important tools to study membrane proteins in solution. They are essential for the extraction of the target membrane proteins from the bilayer and to allow the study of solubilized proteins in solution. They play an important role in membrane protein reconstitution as well.

Detergents are amphipathic molecules with different charge, size and shape, but generally consisting of a polar head group and a hydrophobic tail. They exhibit unique properties in aqueous solutions in which they spontaneously form micelle structures, shielding the aliphatic chain in the interior and exposing the polar moiety. Detergents are usually classified according to their charge into: non-ionic, zwitterionic and ionic detergent.

The chemical structure of detergents and micelle forming lysophospholipids used in this work are summarized in Figure 2.1. and the chemical properties of these molecules are shown in Table 2.1.

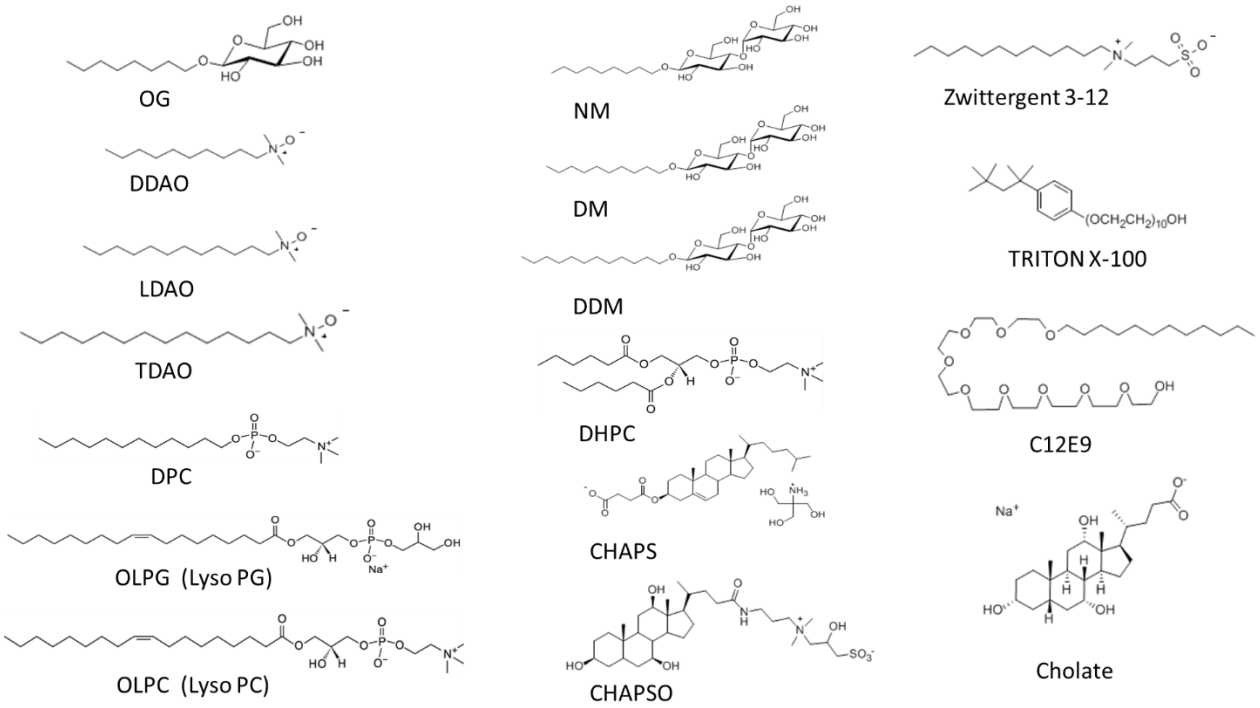

Figure 2.1 Chemical formulas of the detergents and lysophospholipids used for the solubilization of Cai and pfColA. OG, n-octyl-β-D-glucopyranoside; NM, Nonyl-B-D-maltopyranoside DM, Decyl-B-D-maltopyranoside; DDM, Dodecyl-B-D-maltopyranoside; DDAO, Decyl-N,N-Dimethylamine-N-Oxide; LDAO, Dodecyl-N,N-Dimethylamine-N-Oxide; TDAO, n-Tetradecyl-N,N-Dimethylamine-N-Oxide; DPC, n-dodecylphosphocholine; OLPG, 1-oleoyl-2-hydroxy-*sn*-glycero-3-phospho-(1'-*rac*-glycerol); OLPC, lyso-oleoyl-sn-Glycero-3-phosphatidyl-choline; DHPC, 1,2-dihexanoyl-*sn*-glycero- phosphocholine; CHAPS, 3-[(3-cholamidopropyl)-dimethylammonio]-1-propanesulfonate; CHAPSO, 3-[(3-cholamidopropyl)dimethylammonio]-2-hydroxy-1-propanesulfonate; Zwittergent, n-tetradecyl-N, N-dimethyl-3-ammonio-1-propanesulfonate; Triton X-100, *α*- [4-(1,1,3,3-tetramethylbutyl)phenyl]-*w*-hydroxy-poly(oxy-1,2-ethanediyl)]; $C_{12}E_9$, dodecyl nonaethylene glycol ether and cholate. 3α,7α,12α-Trihydroxy-5β-cholan-24-oic acid sodium salt.

Table 2.1. Detergents and their characteristics

Detergent	cmc (mM)	Agg. n.	MW (Da)	MS (kDa)	Chemical character
n-octyl-b-D-glucopyranoside (OG)	19	90	292	26	NI
n-nonyl-b-D-maltoside (NM)	6	55	469	26	NI
n-decyl-b-D-maltoside (DM)	1.8	69	483	50	NI
n-dodecyl-b-D-maltoside (DDM)	0.15	78-149	511	40-76	NI
Decyldimethylamineoxide (DDAO)	10.5	7	201	1.4	NI
Lauryldimethylamineoxide (LDAO)	1-2	76	229	17	ZW
Tetradecyldimethylamineoxide (TDAO)	0.29	n/a	257	n/a	ZW
3-Dodecylamido-N,N'-dimethylpropyl amine oxide (LAPAO)	1.6	126	301	38	ZW
Dodecyl nonaethylene glycol ether ($C_{12}E_9$)	0.05	142	583	83	NI
Sodium dodecyl sulphate (SDS)	8.2	62	288	17	AN
[n-Dodecyl-N,N-dimethyl-3-ammonio-1-propanesulfonate (ZWITTERGENT 3-12)	2	55	335	18.5	ZW
[n-Tetradecyl-N,N-dimethyl-3-ammonio-1-propanesulfonate (ZWITTERGENT 3-14)	0.16	83-130	364	30-47	ZW
3a,7a,12a–Trihydroxy-5b-cholan-24-oic acid, monosodium salt (CHOLATE)	14	2-5	431	0.8-2	AN
3-[(3-cholamidopropyl)-dimethylammonio]-1-propanesulfonate (CHAPS)	8	10	615	6	ZW
3-[(3-cholamidopropyl)dimethylammonio]-2-hydroxy-1-propanesulfonate (CHAPSO)	8	11	631	7	ZW
a–[4-(1,1,3,3-Tetramethylbutyl)phenyl-w-hydroxy-poly(oxy-1-2-ethanediyl) (TX-100)	~ 0.2	75-165	650	50-100	NI
1,2-dihexanoyl-*sn*-glycero-phosphocholine (DH_6PC)	15	19-35	454	9-16	ZW
1,2-diheptanoyl-*sn*-glycero-phosphocholine (DH_7PC)	1.4	25	482	12	ZW
n-dodecylphosphocholine (FC-12) DPC	1.5	54	352	19	ZW
1-oleoyl-2-hydroxy-*sn*-glycero-3-[phospho-rac-(1-glycerol)] (OLPG)	<0.001	n/a	506	n/a	AN
1-oleoyl-2-hydroxy-*sn*-glycero-3-[phosphatidyl choline)] (OLPC)	<0.001	n/a	521	n/a	ZW

Typical values obtained in pure water for detergents used in this study; cmc: critical micellar concentration; aggregation number (Agg. n.): number of monomers per micelle; MW: molecular weight of the monomer (in Da); MS: micelle size (in kDa); Chemical character: NI= non-ionic; ZW = zwitterionic; AN = anionic. Values can vary with ionic strength (e.g., the cmc values of dimethylamine-N-oxide derivatives are 10 times lower in 0.1 M NaCl). Data provided by the manufacturers.

2.2.2 Lipid vesicles

Large Unilamellar Vesicles (LUVs) have only one lamella or bilayer and in contrast to sonicated vesicles have low curvature stress and dimensions ranging from 50 nm to 500 nm in diameter. Due to their stability and homogeneity, LUVs are considered the most appropriate membrane model system for most functional studies. LUVs are prepared from a suspension of MLVs, after a number of freezing-thawing cycles and extrusion through a polycarbonate membrane with the desired pore diameter (Mayer et al., 1986).

Here synthetic lipids or *E. coli* total lipid extracts were purchased (Avanti Polar Lipids, Birmingham, AL) and dissolved in chloroform:methanol 1:1. The desired amount of the lipid stock solution was transferred to a new tube and organic solvent was evaporated under

gentle nitrogen gas flow and left in a high vacuum desiccator for 3 h or overnight to remove traces of organic solvent. The dried lipid film was hydrated with the corresponding amount of an aqueous solution at a temperature above the lipid phase transition midpoint (T_m). The sample was vigorously vortexed and subjected to 10 freeze/thaw cycles. Thereafter, multilamellar vesicles were extruded 10 times through polycarbonate filters (Nuclepore, Cambridge) with the desired pore diameter (in this case 100 nm) at 200 psi nitrogen gas pressure and at temperatures above the main transition. Once liposome preparation was completed the lipid phosphorus final concentration was determined (Fiske and Subbarow, 1925).

2.2.2.1. Assays in LUVs

Leakage assay

This technique measures the ability of a pair of molecules to permeabilise the vesicle lipid bilayer. The fluorescent probe ANTS (8-aminonaphtalene-1, 3,6-trisulfonic acid sodium salt) and its quencher DPX (p-xylene-bis-pyridinium bromide) Molecular Probes (Eugene, OR) are co-encapsulated in the aqueous compartment of the liposome. By entrapping both ANTS and DPX inside the vesicles, their close proximity allows DPX to quench ANTS fluorescence by collision. Upon addition of a membrane-perturbing agent, both molecules leak out and are diluted into the external medium where they hardly interact, which causes an increase in the ANTS fluorescence (λ_{ex}=365nm, λ_{em}=515 nm). Thus vesicle bilayer permeabilization can be followed in time monitoring ANTS fluorescence increase.

LUVs were prepared through extrusion in 12.5 mM ANTS, 45 mM DPX, 40 mM K_2SO_4, 10 mM HEPES pH 7.5 buffer. After extrusion, LUVs containing the probes were separated from the unencapsulated probes by size exclusion chromatography using a PD-10 desalting column. Lipid concentration was assayed with the Fiske method (Fiske and Subbarow, 1925). ANTS/DPX-loaded LUVs were diluted to a final concentration of 100 µM In a 1 cm quartz cuvette with constant stirring. The sample was excited at 365 nm (slits, 4 nm) and the fluorescence emission was monitored at 515 nm in an 8100 Aminco-Bowman luminescence spectrometer. After a stable baseline was observed, pfColA or mutants were added to liposome dispersions the fluorescence signal was recorded for 30 min. To determine 100% release signal, 1% Triton X-100 is added to the sample to ensure complete permeabilization

of the vesicles. The extent of induced release of the probe was then quantified as a percentage according to the equation:

$$\% \text{ Leakage} = [(Ft - F0) / (F100 - F0)] \times 100$$

where F0 is the baseline leakage and corresponds to the fluorescence of the vesicles at time 0, Ft is the fluorescence after a certain period of time and F100 is the maximum leakage that corresponds to the fluorescence value obtained after addition of TX-100.

Flotation experiments in sucrose gradients

A discontinuous sucrose gradient was used to separate proteoliposomes containing Cai. In this experiment, liposomes and liposome-bound proteins float up to the top fraction of the gradient due to their lower density while free protein remains at the bottom of the tube.

Purified Cai-GFP (50 μM in 2% detergent) was mixed with 2 mM *E coli* lipid liposomes (1:50 v/v), lipid/protein molar ratio = 2000, and incubated at room temperature for 1 h. After adding 200 μl of 2.4 M (w/v) sucrose, the mixture was filled into an ultra-centrifuge tube. 200 μl of 1.4, 0.8 and 0.5 M sucrose in 80 mM K_2SO_4, 10 mM Tris-HCl, pH 8.0 solutions were sequentially added onto this layer. The gradient was centrifuged at 500,000 *g* for 3 h in Beckman Optima TLX benchtop ultracentrifuge using a TLA 120.2 Beckman rotor at 4 ºC. Fractions were collected starting from the bottom and assayed for phosphorous by the Fiske method and for GFP fluorescence in a Synergy HT multi- detection Microplate Reader (BIO-TEK, Bad Friedrichshall, Germany) with KC4 software (λ_{ex} = 485 $\pm$ 20 nm, λ_{em} = 528 $\pm$ 20 nm). For the incorporation of CaiH the protein localization was tested by SDS-PAGE and quantified by densitometry of the Coomassie-stained bands.

2.3 Circular dichroism (CD)

Circular dichroism (CD) allows the structural characterization of proteins at low-resolution, both in aqueous solutions and in model membrane systems. Although it cannot provide high resolution information it is an excellent tool for the rapid determination of the secondary structure and folding properties of peptides and proteins in physiological buffers.

Linearly polarized light can be described as a superposition of two circularly polarized light beams of equal phase and amplitude, but opposite directions. If after passage through the sample, the left and right components are not absorbed (or are absorbed to the same extent), combination of the components would regenerate plane-polarized radiation (Fig. 2.2 left). However, when this light passes through a sample containing optically active chiral molecules (such as amino acids) with different absorbance for each of the two circularly polarized components, the amplitude of the component absorbed more strongly will be smaller than that of the other component and in consequence, the resultant radiation would be elliptically polarized.

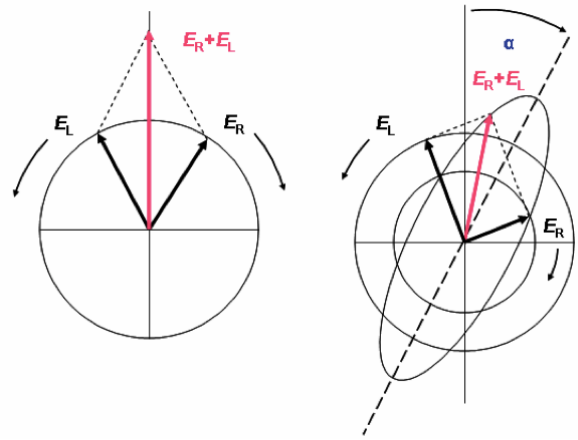

Figure 2.2 Origin of the CD effect. Left, Linear polarized light can be viewed as a superposition of opposite circular polarized light of equal amplitude and phase. Right, different absorption of the left- and right hand polarized components leads to ellipticity (CD) [Taken from Kelly et al., 2005].

CD is measured as the difference of absorbance of left (AL) and right (AR) circularly polarized light: ΔA=AL-AR. It can also be expressed in degrees of ellipticity (θ), defined as the tangent of the ratio of the minor to the major optical axes. It is very easy to inter-convert θ and ΔA using:

$$\theta = 32.982 \times \Delta A \qquad \text{[Eq. 1]}$$

A CD spectrum of a given protein is then obtained measuring θ as a function of wavelength. To be able to compare the circular dichroism spectra in different conditions or for different proteins and to be able to estimate secondary structure content it is usual to normalize to convert the raw measurement in millidegrees to mean residue molar ellipticity in deg·cm^2·$dmol^{-1}$ using the following equation:

$$[\theta] = \frac{100 \times \text{Ellipticity}}{n \times C \times l} \qquad \text{[Eq. 2]}$$

Where ellipticity is the raw measurement, n is the number of peptide bonds, C is the concentration in mole/L and l is the pathlength in cm.

Because chiral molecules are common in biological systems, there are a number of interesting applications for CD spectroscopy in biochemistry. A very common use of this method is the identification and relative quantification of the secondary structure components in a protein or a peptide. This is usually performed at two wavelength ranges (near and far-UV), providing distinct information about protein structure.

In the far-UV range (<240 nm) the peptide bound is the principal absorbing group, and studies in this region can give information on protein secondary structure. In this region, there are two electronic transitions; one corresponding to a weak and broad band centred around 220 nm and a second one of stronger intensity around 190 nm. These transitions are sensitive to the secondary structure of the protein and hence, different secondary structure elements display characteristic CD spectra (Fig. 2.3). The helical content was calculated with equation 1 (Chen and Yang, 1971):

$$\%\ \text{helix} = \frac{(-[\theta]_{222} + 2340)}{30300} \qquad \text{[Eq. 3]}$$

In the near-UV range (250-290 nm), the principal absorbing groups are aromatic amino acid chains (phenylalanine, tyrosine and tryptophan), providing information on the tertiary structure of the polypeptide chain.

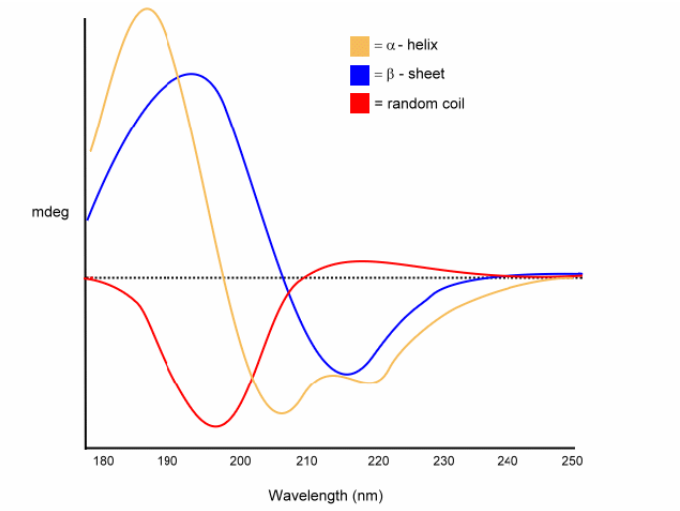

Figure 2.3 Far-UV spectra associated with various types of secondary structure. Different secondary structure elements display characteristic CD spectra: α-helical proteins have negative bands at 222 nm and 208 nm and a positive band at 193 nm. Proteins with well-defined antiparallel β-pleated sheets have negative bands at 218 nm and positive bands at 195 nm. Finally, disordered proteins have very low ellipticity above 210 nm and negative bands near 195 nm. [Taken from http://dornsife.usc.edu/nanobiophysicscore/cd-spectrometer-j-815/].

This technique is also useful to follow protein unfolding as a loss of secondary structure as a function of temperature. Changes in the midpoint of the melting transition ($t_{1/2}$) can be related to changes in the thermal stability of protein under different experimental conditions, and can be used (i) to evaluate the effects of mutations on protein stability or (ii) to analyse changes on the overall tertiary structure of the protein upon binding to lipid vesicles.

In this thesis, far-UV (190–250 nm) and near-UV (250-320 nm) CD spectra were recorded with a Jasco J-810 spectropolarimeter previously calibrated with d-10-camphorsulphonic acid. The device was equipped with a Jasco PTC-423S temperature controller and cuvettes were thermostated at 20 ºC in the wavelength scan mode. Protein concentration was 220 µM in a 0.2 cm cuvette for near-UV, and 22 µM in a 0.01 cm cuvette for far-UV CD spectra, in 1x PBS, 100 mM NaCl, pH 7.5. The samples were centrifuged in an Eppendorf microcentrifuge for 15 min at 14,000 *g* and 4 ºC before measurement. All spectra were corrected by subtracting the appropriate background, and converted to mean residue ellipticity units when required. Thermally induced unfolding was monitored by CD at 222 nm in 0.2 cm pathlength cuvettes in the 10-90 °C temperature range. The temperature was increased at a rate of 1 °C /min, and the ellipticity was recorded every 0.2 °C with a 1 nm bandwidth and 2 s response time.

2.4 Nuclear magnetic resonance (NMR)

Nuclear magnetic resonance (NMR) is a very powerful tool to obtain insight into the chemical environment, dynamics and structure of proteins. Membrane protein studies can benefit from this technique owing to the dynamic character of membrane-related processes (Kim et al., 2009; Nietlispach and Gautier, 2011). Getting good quality spectra amenable to structure determination is however very challenging. The presence of local dynamics in a membrane protein can be both an advantage and a disadvantage. Spectral properties often benefit from the motion of dynamic regions, as for the C-terminus of bovine rhodopsin (Werner et al., 2008) relative to more rigid domains of the protein. These sharp and intense resonances from mobile segments often hinder the observation of underlying broader resonance peaks, corresponding to the transmembrane and micelle-associated segments. A second problem arises from motions that occur at frequencies that result in exchange broadening, a source of peak broadening which is not always improved by TROSY experiments. Optimization of the membrane solubilization agent used in solution NMR as a tool to control internal protein motions has not been sufficiently studied but it is an essential step towards the use of solution NMR in the study of dynamic conformational changes occurring in membrane proteins.

In the NMR experiments performed to compare the effect of different detergents over Cai, three sensitivity optimized versions of the basic 2D $^{1}H,^{15}N$ correlation experiment were tested with a representative sample: (i) SOFAST-HMQC; (ii) fast HSQC; (iii) BEST-TROSY. As expected, the BEST-TROSY yielded the best resolution and narrowest linewidths, yet at dramatic costs in sensitivity.

All NMR data were recorded in an 800 MHz Bruker Avance III spectrometer equipped with a triple resonance cryoprobe (cryo-TCI) with *z* gradient coil. All NMR samples contained [U-15N] isotopically labelled Cai protein (GFP-T-cleaved-Cai or CaiH) in aqueous (90% H2O, 10% D2O) saline buffer (50 mM sodium phosphate pH 7.5, 100 mM NaCl) with different types of detergents added (up to 2% w/v).

The fast HSQC yielded overall stronger and somewhat broader signals than the TROSY experiment, revealing also the underground of weak broad signals presumably from the transmembrane helical regions. The optimized (fast pulsing) SOFAST-HMQC outperformed all

other experiments in terms of sensitivity as it least disturbs the ^{1}H matrix polarization, thus allowing for fastest re-equilibration of the selected ^{1}HN polarization. The sensitivity gains easily outweighed the further increased linewidths inherent to this experiment, and the SOFAST-HMQC was then applied for all further studies.

Line broadening cannot be alleviated by deuteration and/or the TROSY scheme since both strategies only reduce the extent of dipolar relaxation, which defines the natural NMR linewidth depending on fast molecular and local motions. On the contrary, additional transfer delays make the (single quantum) TROSY experiment particularly susceptible to line broadening phenomena.

To analyse the lipids present in the purified CaiH sample, the protein was purified as described above to yield a final sample containing 120 µM CaiH in the buffer 200 mM DPC, 20 mM phosphate, 0.5 mM TCEP, 10% D2O ,0.5 mM EDTA, pH 7.5. Membrane lipids were extracted from *E. coli* cells to be analysed by ^{31}P-NMR. Lipids were purified from bacteria overexpressing CaiH in C41 (DE3) bacterial strain as described previously (Wikström et al., 2009). Shortly, C41 (DE3) cells harbouring the plasmid coding for CaiH were induced with 0.8 mM IPTG and grown at 20 °C for 16 h in LB supplemented with 25 µg/ml kanamycin. Cells were subsequently collected and re-suspended in 20 mM PIPES, 1 mM EDTA, 150 mM NaCl, buffer at pH 7.4. To separate the membrane fraction, cells were lysed and ultracentrifuged at 100.000 g for 1 h. Lipids were extracted with chloroform: methanol 2:1 (v/v) and extensively washed in the same buffer to remove divalent ions. The chloroform phase was then collected, concentrated to about 50 mg/ml and kept at −20 °C in a 2:1 (v/v) chloroform: methanol solution.

To solubilize the total lipid extract for solution ^{31}P NMR, the chloroform: methanol solvent was evaporated from the lipid stock under a stream of N_2 gas and the lipid film was rehydrated in 50 mM DPC, 20 mM MES, 1 mM EDTA, 10% D2O, pH 6.5 to obtain a final lipid concentration of 20 mM.

^{31}P NMR spectra were recorded on a Bruker Avance spectrometer operating at 14.1 T (152.7 MHz ^{31}P frequency), equipped with a 5 mm TXI triple resonance probe. NMR measurements were conducted at 25 °C. The spectra were processed with 0.5 Hz line broadening and referenced externally to phosphoric acid.

2.5 Protein stability by equilibrium unfolding

Equilibrium unfolding can be investigated by protein denaturation experiments to study protein folding and determine the conformational stability. Proteins can be denatured by changing the physical or chemical environment most commonly by changing the temperature, the pH or the pressure, adding chemical denaturants like urea or guanidinium chloride, or applying force. When proteins regain their folded conformation after returning to native conditions, the unfolding process can be treated as a two-state reaction for which thermodynamics of chemical equilibria apply.

In this work urea was used to denature pfColA alone and in complex with Cai by monitoring the changes in intrinsic fluorescence of pfColA. The intrinsic fluorescence of proteins comes from the natural fluorophores: tryptophan, tyrosine and phenylalanine with tryptophan being responsible for the 90% of the fluorescence signal. Although Cai contains a large number of tyrosines it does not contain any tryptophan, whereas pfColA has three tryptophans (W88, W132, W142). The fluorescence of tryptophans is very sensitive to the polarity of the medium (this is not the case for tyrosines and phenylalanines), thus exposure of tryptophans to the polar medium as a result of denaturation induced a decrease in fluorescence intensity which can serve to determine the fraction of denatured protein at each concentration of denaturant.

Fluorescence measurements were performed in 100 mM NaCl, 20 mM HEPES pH 7.5 and 0.05% DDM when thus specified. Individual samples with increasing concentration of urea where prepared and 5 µl of concentrated protein were added to a final concentration of 2.5 µM before measuring in a QuantaMaster 40 spectrofluorometer (Photon Technology International, Lawrenceville, NJ) with an excitation wavelength of 290 nm and at a constant temperature of 20 °C using a 1 cm path length quartz cuvette.

Empirically, the free energy of unfolding can be estimated from denaturation experiments due to the linear dependence between the concentration of urea and the free energy of transferring the protein backbone and side chains from water to urea (Tanford, 1968). Therefore, the free energy of denaturation at each particular concentration of urea is given by:

$$\Delta G_{N-D} = \Delta G_{N-D}^{H_2O} - m_{N-D}\,[denaturant] \qquad \text{[Eq. 4]}$$

Where $\Delta G_{N-D}^{H_2O}$ is the free energy value in water and $m_{N\text{-}D}$ is a constant of proportionality ($m_{N\text{-}D}$ = -∂($\Delta G_{D\text{-}N}$)/∂[denaturant]) with the dimensions of cal/mol/M, and it represents the increase in solvent accessible surface area between the denatured and native states. A typical denaturation curve is illustrated in Figure 2.4.

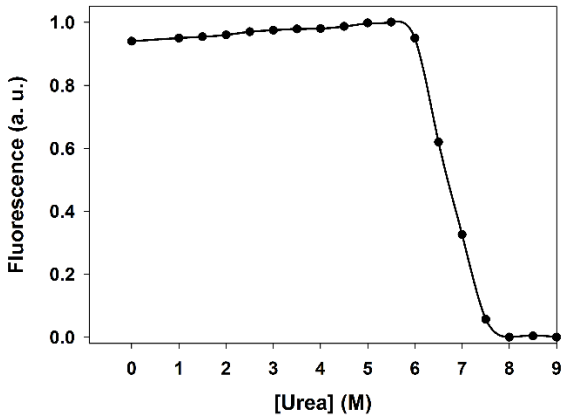

Figure 2.4 Protein denaturation curve monitored by fluorescence decrease (λex = 290 nm, λem = 315 nm) induced by increasing concentrations of urea. (Theoretical example)

Fluorescence data often displays sloping baselines because the fluorescence signal of both the native and denatured state are linearly affected by the urea concentration and these factors must be considered when fitting the data (Santoro and Bolen, 1988). Therefore, the fluorescence data obtained with this experimental methodology is fitted by non-linear least squares analysis to the equation:

$$F = \frac{F_N + m_N[urea] + (F_D + m_D[urea])\, e^{\frac{-\Delta G_{N-D}^{H_2 0} + m_{N-D}\,[urea]}{RT}}}{1 + e^{\frac{-\Delta G_{N-D}^{H_2 O} + m_{N-D}\,[urea]}{RT}}} \qquad \text{[Eq. 5]}$$

where F_N and F_D represent the different fluorescence intensities for native and denatured protein, respectively, as a function of denaturant concentration with the slopes m_N and m_D corresponding to the pre- and post-unfolding regimes, respectively.

The $\Delta G^{\circ}{}_{N-D}$ values obtained in the transition can then be plotted against urea concentration and the linear fit of these points can then be extrapolated to zero denaturant, which gives the free energy of unfolding in the absence of denaturant.

This methodology has been extensively applied to study small globular proteins that exhibit reversible denaturation. It is worth noting that the application of this model for membrane proteins is often limited by several factors. Many membrane proteins denature irreversibly leading to aggregation and/or precipitation. Moreover there is no consensus regarding the criteria to define the denatured state of a membrane protein. While the two-state model assumes that the denatured state is largely unfolded, membrane proteins retain a high helical content upon exposure to denaturing conditions.

2.6 Ion conductance assay in liposomes

In order to measure the channel forming activity of pfColA and the capacity of Cai to inhibit its activity, a functional assay in lipid vesicles was set up. Unilamellar vesicles were prepared from synthetic lipids and *E. coli* total extract by extrusion through 100 nm filters in a buffer containing 10 mM phenol red, 80 mM K_2SO_4, pH 8.0 (internal buffer: IB). Vesicles were incubated at 50 °C for 10-15 min after a 1:60 dilution to 0.1 mM lipid in external buffer with the desired amount of pfColA to induce partial incorporation of the protein. Initially, the external buffer contained 66 mM Na_2SO_4, 24 mM Tris phosphate pH 7.5 (EB_{Na}), but buffers with $NMDG^+$ or Li^+ were also tested , EB_{NMDG} (66 mM $NMDG_2SO_4$ 24 mM Tris phosphate, pH 7.5) and EB_{Li} (66 mM Li_2SO_4, 24 mM Tris phosphate, pH 7.5). Iso-osmolarity (0.205 osmol/kg) of the internal and external buffers was monitored for each experiment, measurements were performed in an Osmomat 030 Cryoscopic osmometer (Gonotec, Germany).

Later extrusion (internal) buffer was exchanged for storage buffer using a PD-10 column (GE Healthcare) to eliminate non-encapsulated probes. Fractions containing the liposomes were collected and lipid concentration was measured by the Fiske reaction (Böttcher et al., 1961; Fiske and Subbarow, 1925). Measurements were performed at 0.1 mM lipid concentration, unless otherwise stated.

Phenol-red absorbance, which has been shown to provide a reliable measure of internal pH in liposomes, was used to measure hydrogen ion influx into phospholipid vesicles. Induced pH change was calibrated by titration of a phenol red preparation in the presence of 0.1 mM empty liposomes.
In a plastic cuvette, 1.2 ml liposome dispersion (at 0.1 mM lipid) was monitored for phenol red basic form absorbance (559 nm) with a Cary 300 BIO Spectrophotometer (Varian, Australia).

After baseline recording, 1 µl of 1 µM valinomycin dissolved in ethanol was added to the cuvette (final 0.83 nM). Valinomycin provides a pathway for K^+ ion movement, so a K^+ diffusion potential develops that would inhibit further K^+ flux. Basal membrane permeability to protons is observed as a linear decrease in A559 signal, even in the absence of protein. Finally, 2 µl of 4 µM CCCP in ethanol (final 6.45 nM) was added at 1000 s to destroy any remaining K^+ gradient. The pH typically fell by ~1 unit after valinomycin/CCCP combined action. The internal to external volume ratio (V_i/V_o) was determined by measuring the absorbance of a known dilution of liposomes. Possible leakage of phenol red outside liposomes was discarded. The amount of external phenol red was shown to be negligible according to an additional gel filtration step. The liposomes were used immediately after preparation but the external probe did not increase to > 10% after 24 h.

2.7 Cai/pfColA binding assays

Binding of Cai to pfColA was studied by a combination of techniques including native-PAGE, crosslinking or both equilibrium and kinetic optical assays.

Experimental data from equilibrium binding assays was fitted to a quadratic function (Cooper, 2004). When the free ligand cannot be approximated to the added concentration of ligand, most often because the protein concentration used is above the K_D, it is necessary to derive an equation in which the dissociation constant can be obtained from the concentrations of added ligand and protein as well as the concentration of protein-ligand complex at equilibrium. Thus the data is fitted to the following quadratic equation:

$$S = S_0 + \frac{(S_{max} - S_0)}{2 \cdot C_P} \cdot \left[(C_L + C_P + k_D) - \sqrt{(C_L + C_P + k_D)^2 - (4C_L \cdot C_P)} \right] \quad \text{[Eq. 6]}$$

where S is the observed signal (e. g. fluorescence, fluorescence anisotropy, band intensity) S_0 is the initial signal in the absence of ligand, S_{max} is the signal at which saturation is reached, C_L is the total concentration of protein ligand added (which varies over a wide range), C_P is the fixed concentration of protein and K_D is the dissociation constant.

2.7.1 Binding assays by fluorescence anisotropy

Developing an optical assay to study protein-protein association is often a requisite to extract affinity and thermodynamic information of a given binding reaction. The simplest approach is to design an assay in which the product of the reaction exhibits a distinct spectroscopic signal compared with the reactants. When the optical assay is able to report the concentration changes of one of the components in equilibrium with other components of the reaction, both equilibrium and kinetic measurements can be performed. Fluorescence anisotropy measurements are extensively used to measure protein-protein interactions since the formation of the complex almost always causes an increase on rotational diffusion. The fact that the anisotropy is independent from fluorophore concentration simplifies experiments considerably. Fluorescence anisotropy experiments often require that one of the reactants is tagged with a fluorescent dye.

Fluorescence anisotropy takes advantage of the fact that when randomly oriented fluorophores are excited by vertically polarized light, a partial orientation of the excited-state population is induced. Those fluorophores whose absorption transition moments are oriented along the electric vector of the incident light are preferentially excited and the subsequent emission will be also polarized to some extent. The extent of polarization depends on the average angular displacement of the fluorophore that takes place between absorption and emission (Lakowicz, 2006). The emission can become depolarized by different processes, e. g. energy transfer or rotational diffusion. The rotational diffusion rate depends on the size of the rotating molecule as well as the viscosity of the solvent. In a binding assay, association of the fluorescently labelled protein with its ligand will slow down the rotational diffusion

which results in an increase in anisotropy. Anisotropy measurements become relevant for protein binding studies when the timescale of rotational diffusion of the protein is in the same range as the fluorescence lifetime of the fluorophore.

The experimental arrangement for the fluorescence anisotropy experiment is illustrated in Figure 2.5. The sample is excited with vertically polarized light and the emission intensity is measured through a polarizer. When the emission polarizer is oriented parallel to the direction of the polarized excitation beam $I_{\parallel}$ intensity is measured, and when the orientation is perpendicular, the $I_{\perp}$ intensity is obtained. The anisotropy is then calculated using these two intensities according to:

$$r = \frac{(I_{\parallel} - I_{\perp})}{(I_{\parallel} + 2I_{\perp})} \qquad \text{[Eq. 7]}$$

In the case of isotropic protein samples the fluorescence anisotropy values lay in the 0-0.4 range. When the emission is completely depolarized, then $I_{\parallel} = I_{\perp}$ and r = 0. Alternatively if the absorption and emission dipoles are colinear and in the absence of depolarization-causing processes, the value of $I_{\perp}$ is one-third $I_{\parallel}$, so the maximum anisotropy that can be measured is 0.4. Anisotropy values of 1 can only be observed for completely oriented samples or scattered light.

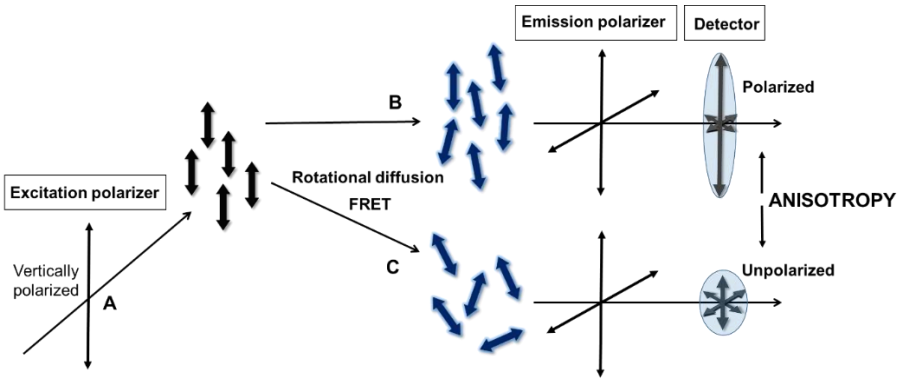

Figure 2.5 Fluorescence polarization and anisotropy. (A) Upon polarized excitation those fluorophores whose absorption transition moments are oriented along the electric vector of the incident light are preferentially excited (B) Fluorophores bound diffuse or rotate more slowly, resulting in highly polarized emission and high anisotropy. (C) The emission can become depolarized by different processes, like energy transfer or rotational diffusion, resulting in lower anisotropy.

The spectrofluorometer used here was equipped with polarizers in the excitation and emission channels, thereby the two polarized components of the fluorescence emission were detected sequentially (L-format), at 90° to the excitation beam. After the emission beam is

polarized it passes through a monochromator before reaching the detector. Because the transmission efficiency of the optical elements, as the monochromator, can be very different for vertically and horizontally polarized light, a correction value or G-factor needs to be determined for each emission wavelength. The G-factor represents the ratio of sensitivity of the detection system for vertically and horizontally polarized light. In order to determine the detection efficient on the parallel and perpendicular detectors horizontal excitation is used. When measuring with horizontal excitations both detectors are perpendicular to the excitation polarized light enabling the calculation of the G-factor (eq. 8) The intensity measured in this way corresponds to $I_{\perp}$ and any difference that can be detected in this arrangement must come from the detection system.

$$G = \frac{I_{HV}}{I_{HH}} = \frac{S_V}{S_H}\frac{I_{\perp}}{I_{\perp}} = \frac{S_V}{S_H} \qquad \text{[Eq. 8]}$$

Measurements of fluorescence spectra of labelled proteins were performed under continuous stirring and at a constant temperature of 20 °C using a 1 cm path length quartz cuvette in a QuantaMaster 40 spectrofluorometer (Photon Technology International, Lawrenceville, NJ).

2.6.1.1. Protein labelling for fluorescence anisotropy experiments

Fluorescein isothiocyanate (FITC) is an amine-reactive probe and was used to label pfColA. After purification by SEC and ion exchange in Mono Q, pure pfColA is obtained in TRIS buffer. In the case of amine-reactive reagents like isothiocyanate, primary amines like TRIS compete for conjugation so a buffer exchange step was introduced. 0.1 M sodium bicarbonate pH 9.0 buffer was used to maintain the ε-amino groups in a non-protonated state. 1 mg FITC was dissolved in DMSO and 15 µl were added to 100 µl of pfColA at 800 µM. The reaction mixture was incubated at 25 °C for 1 h and stopped by the addition of 100 µl of 1.5 M hydroxylamine pH 8.5. To remove any excess of dye a gel filtration column was used. pfColA labelled with FITC was applied onto a Superdex 200 column equilibrated in 50 mM NaCl, 10 mM sodium phosphate, pH 7.5 (Fig. 2.6).

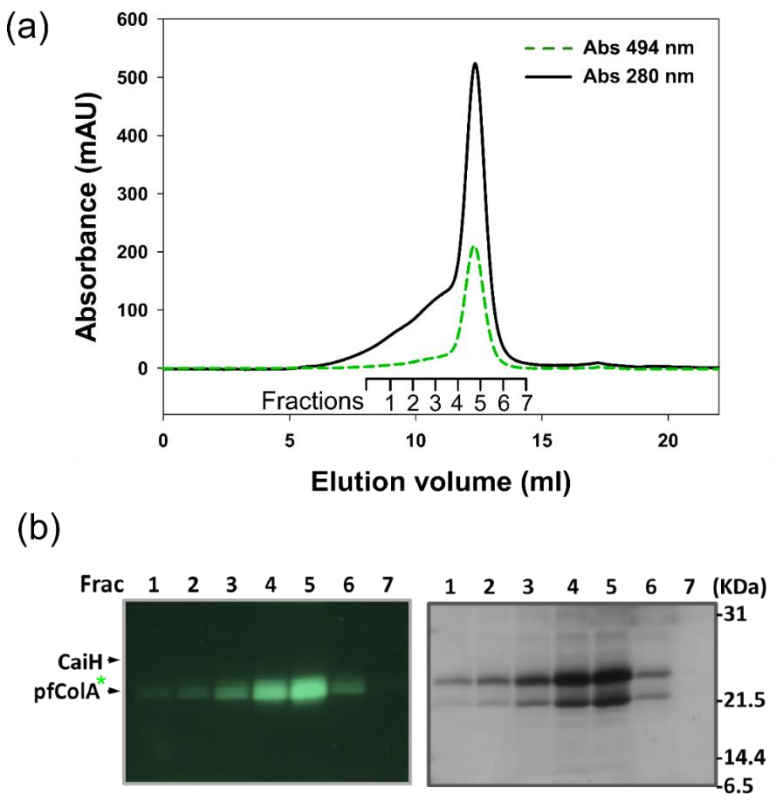

Figure 2.6 Fluorescein labelling of pfColA in complex with Cai. (a) Chromatogram of the complex by SEC in Superdex 200, monitored by protein absorbance at 280 nm and fluorescein absorbance at 494 nm. (b) SDS-PAGE analysis of fractions eluted from SEC by in-gel fluorescence (left) and Coomassie staining (right).

The concentration of bound fluorescein was measured spectrophotometrically assuming a molar absorption coefficient of 8×10^4 $M^{-1}cm^{-1}$ at 496 nm for the fluorescein bound to the protein (Mitchinson et al., 1982)

The following formula was used to calculate the degree of labelling (D.O.L.):

$$\text{Degree of labelling} = \frac{\text{Abs} \times \text{MW}}{[\text{protein}] \times \varepsilon_{496}} \qquad \text{[Eq. 9]}$$

Where MW = the molecular weight of the protein, ε = the extinction coefficient of the dye at its absorbance maximum, and the protein concentration is in mg/ml.

The thiol-reactive coumarin (7-diethylamino-3-(4'-maleimidylphenyl)-4-methylcoumarin) CPM was used for maleimide labelling of folded protein. It is very weakly fluorescent until it reacts with thiols producing a conjugate with excitation/emission maxima of 384/470 nm.

Both Cai and Cai in complex with pfColA were subjected to CPM (Molecular Probes, Eugene, OR) labelling. To optimize the labelling specificity at thiol groups, the reaction must be performed at pH 7.0–7.5. Cysteines present in the protein were reduced by several concentration and dilution steps in Eppendorf concentrators of 30.000 MWCO in 0.2 mM TCEP, 0.1 mM EDTA, PBS pH 7.4 buffer. The dye was resuspended in DMSO and a 3-fold molar excess of dye was added to the protein while vortexing gently. The labelling reaction was allowed to happen for 2 h at room temperature and the reaction was quenched by adding 10 mM DTT. The excess CPM was removed by several rounds of dilution and concentration and loaded onto a Superdex 200 (GE, Healthcare) size exclusion column. The column was previously equilibrated in 0.05% DDM, 150 mM NaCl, 0.5 mM TCEP, 50 mM sodium phosphate pH 7.5. After removal of the dye that might be unspecifically bound to the protein, eluted fractions were run in a SDS-PAGE gel and analysed by in-gel fluorescence. Fractions containing CPM-labelled Cai were pulled and concentrated up to the required concentration. In the case of CPM labelled Cai/pfColA complex, the integrity of the complex upon conjugation was checked by native-PAGE. The degree of labelling was calculated according to Equation 9, Cai in complex with pfColA rendered a 38% labelling while Cai alone exhibited a higher CPM conjugation, up to 65%.

RESULTS

CHAPTER 3

Characterization of Cai in detergent micelles

3. Characterization of Cai in detergent micelles

Unlike soluble proteins, integral membrane proteins have hydrophobic domains exposed to the solvent, which are stabilized by the lipidic environment within the membrane. These domains must be protected by amphipathic agents when extracted *in vitro*. As for the case of most membrane proteins, the purification and characterization of Cai undertaken here implies the isolation of the polypeptide from its native lipid environment. Detergent micelles are commonly used to solubilize membrane proteins and stabilize them in aqueous solution for subsequent analysis. There are important properties to be considered when choosing detergents for membrane protein extraction and stabilization ranging from the purity of the detergent, the ability to protect against subunit dissociation, the ability to protect against unfolding, the minimization of transmembrane helix exposure, and practical aspects like a low cmc to minimize the cost and exchangeability. Exhaustive trials are indispensable for finding an appropriate detergent or mixture where the membrane protein maintains its native structure and function. The most widely accepted indicator for nativeness is the retention of protein activity, whenever possible. Additionally, many membrane proteins have several functional states with varying relative stability in different media.

Here we have applied a variety of biochemical and biophysical methods to study Cai in solution and characterize its behaviour in different protein-detergent complexes employing a representative group of detergents. First we describe how to extract and solubilize the protein from the membrane with the aim of improving its yield and purity. We subsequently analysed the polymerization behaviour by chemical crosslinking and SEC, and the conformational properties by CD and NMR. Finally, the capacity of Cai to bind its partner toxin pfColA was assayed *in vitro*.

3.1 Expression and purification of Cai

The immunity protein of colicin A Cai, is a 178 residue polypeptide (around 20 kDa) with four predicted transmembrane helices. The purification of Cai was performed according to the expression and purification protocol implemented by Drew and cols. (2006). Cai was produced as a GFP fusion product with a C-terminal histidine tag cloned in the pWaldo(d) vector. The Cai-GFP fusion is advantageous for initial purification trials because the intense GFP fluorescence can be used to monitor expression at the cell level and to follow purification by in-gel fluorescence of SDS-PAGE gels (Drew et al., 2006).

For the past decade, the fluorescence properties of the green fluorescent protein GFP have been successfully modified by mutagenesis (Heim and Tsien, 1996). Enhanced GFP (eGFP) is one of the most widely used mutants with increased brightness, improved photostability, and a single excitation peak at 488–490 nm (Heim and Tsien, 1996). It contains the mutations F64L (to improve folding at 37ºC), S65T (for 5-fold increase in amplitude and red shift), and Q80R. Cycle 3 mutations are F99S, M153T and V163A (Crameri et al., 1996; Fukuda et al., 2000) to reduce the tendency for aggregation. All six mutations are present in the GFP encoded in the pWaldo(d) plasmid used here, while further monomer stabilizing mutations like A206K are absent.

Cai was cloned into a cleavable GFP fusion vector pWaldo(d) and expressed in *E. coli* C41 (DE3) cells. GFP fluorescence intensity was used to find best Cai-GFP expression conditions. Best results were obtained when C41 (DE3) cell cultures bearing pWaldo-Cai-GFP vector were induced with 0.8 mM isopropil-β-D-1-tiogalactopiranósido (IPTG) at OD_{600} = 0.4 and left at 20 °C overnight. After cell rupture and fractionation, Cai-GFP was found in the membrane cell pellet. The purification details for Cai-GFP are further described under Experimental Procedures. The purification was first tried using the mild detergent DDM as it is a good initial choice for solubilization (Privé, 2007). DDM is one of the most broadly used detergents for integral membrane protein purification and crystallization (Newstead et al., 2008). DDM-solubilized cell membranes were bound to Ni-NTA and eluted with increasing concentrations of imidazol (Fig.3.1b first lane). Cai-GFP was further purified by size exclusion chromatography

in Superdex 200 equilibrated in 0.2% DDM, 100 mM NaCl, 1 mM TCEP, 50 mM sodium phosphate pH 7.5. When untagged Cai was needed cleavage by TEV protease was performed (Fig.3.1b second lane). TEV protease and cleaved His-tagged GFP were separated by reverse Ni affinity chromatography and Cai was further purified by size exclusion chromatography (Fig.3.1c). Another Cai version named CaiH, was engineered with a C-terminal histidine tag. CaiH was purified by essentially the same protocol as Cai-GFP. Typical yields were 1.7 mg (Cai-GFP) and 2 mg (CaiH) per culture litre. Once we were able to obtain enough protein quantities for further characterization of the protein detergent complex (PDC) other solubilization conditions could be tested.

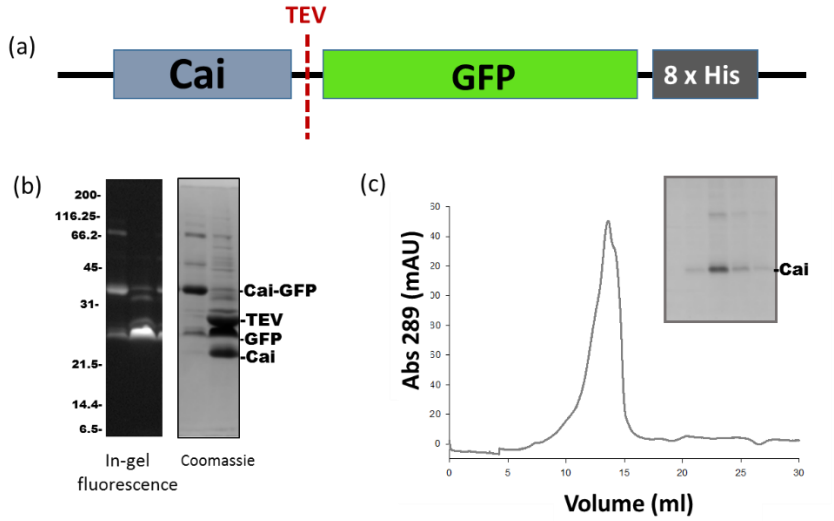

Figure 3.1 Purification of Cai from Cai-GFP after TEV digestion. (a) Schematic diagram of the primary structure of Cai-GFP indicating the cleavage site for TEV. (b) SDS-PAGE visualized by in-gel fluorescence and after coomassie staining of Cai-GFP before and after TEV cleavage (c) Size exclusion chromatography in Superdex 200 of Cai, the eluted samples were analysed by SDS-PAGE (inset).

3.2 Solubility and stability of Cai under different solubilization conditions

The stability of membrane proteins in solution depends on factors like the physicochemical properties of the detergent and the buffer, the ability of the detergent to fully mask the transmembrane regions, the extent of induced delipidation, and the ionic strength of the solution. Protein aggregation is in a permanent competition with protein folding. This is particularly true for membrane proteins that have been extracted from the native membrane. When a certain detergent at a given concentration is unable of efficiently shielding hydrophobic surfaces, the lack of stability would be revealed as protein insolubility.

We analysed the solubility of Cai-GFP by fluorescence imaging in 96-well plates. Buffers of different composition and several detergents were assayed. Purified Cai-GFP was incubated in the conditions indicated in Figure 3.2. Multiple parameters could be tested simultaneously by detecting GFP fluorescence in a 96-well plate. Maximum solubility was obtained in the lysophospholipid OLPG and in DPC regardless of whether phosphate or NaCl were added. Lysophospholipids, unlike diacylphospholipids which naturally form bilayers, organize as micelles and are frequently used to solubilize membrane proteins (Kang et al., 2008; Koehler et al., 2010). Non-ionic detergents in the presence of 50 mM Tris-HCl pH 8 resulted in lower protein solubility and precipitation could be observed in the case of OG, while protein solubility was improved in 50 mM sodium phosphate. Samples to which 150 mM NaCl was added also contained more soluble protein. Zwitterionic detergents showed an intermediate behaviour. Remarkably, sodium phosphate prevented protein precipitation in all conditions tested. This was more apparent for bad solubilizers (e.g. OG, Fig. 3.2).

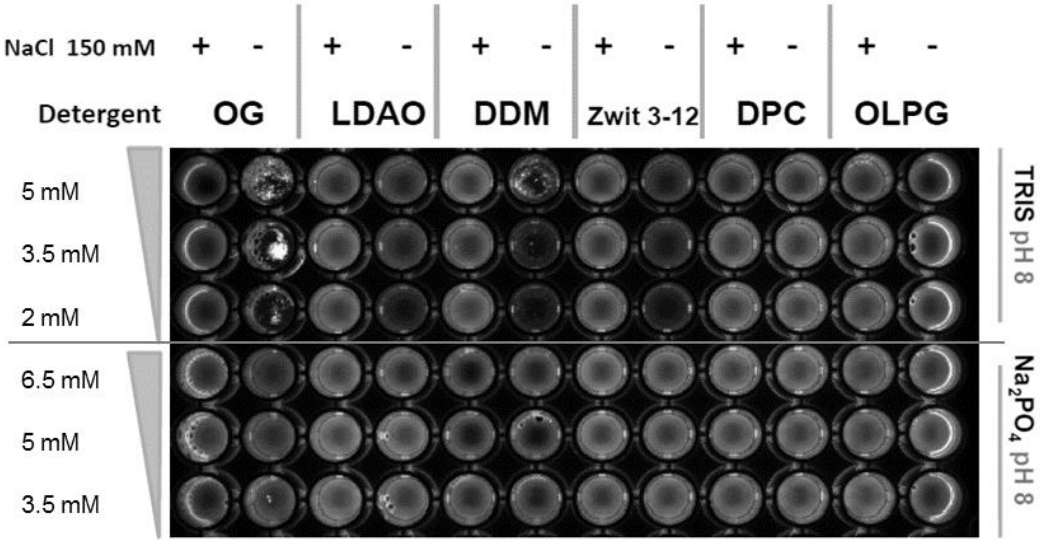

Figure 3.2 Fluorescence image of a 96-well plate where solubility of Cai-GFP was tested in the presence of TRIS and phosphate buffers. The ionic strength of the solution was also analysed comparing the fluorescence intensity in 0 and 150 mM NaCl for all 6 different detergents.

The effect of ionic strength, phosphate concentration and phosphate containing detergents on Cai stability and solubility was then investigated in more detail. We used GFP fluorescence as Cai solubility reporter in buffer and salt titration assays in different detergents. Cai-GFP purified in DDM as previously described, was concentrated to 800 µM and 5 µl of the protein

sample was diluted into 400 µl of the condition to be tested. After centrifugation, precipitated protein was discarded and GFP fluorescence of the supernatant was measured (λ_{ex} = 490 nm, λ_{em}= 520-540 nm) in a 96 well plate reader. Samples were also analysed by SDS-PAGE observing that in-gel GFP-fluorescence correlated reasonably well with data in solution. No substantial cleavage of Cai-GFP was observed under the experimental conditions used (Fig 3.3c). Soluble GFP alone was also exposed to the various conditions tested resulting in no detectable change in fluorescence intensity (data not shown).

Optimal Cai solubility was obtained in the pH range 7 to 8.5 while highest fluorescence values were found at pH 7.5 (data not shown). Subsequently, different buffers were assayed at pH 7.5 in the presence and absence of 150 mM NaCl (Fig 3.3a and b). Among all buffers tested phosphate buffer, even at low concentrations, induced a dramatic increase in Cai-GFP solubility. Raising the ionic strength of the solution by NaCl supplementation caused an additional linear increase in solubility for all conditions as higher ionic strength favours hydrophobic interactions in general. To elucidate if the stabilizing effect induced by phosphate ion could be specific and reminiscent of some role of lipidic phosphate in the natural environment, we compared it with that of sulphate, a chemically similar anion. 10 mM TRIS pH 7.5 was added in these samples to compensate the low buffering capacity of sulphate. The results shown in Figure 3.3d indicate that sulphate can stabilize Cai-GFP/DDM mixed micelles to the same extent of phosphate.

This led us to confirm that the effect kosmotropic sulphate and phosphate have over proteins in general stays true for this integral membrane protein as well. In fact phosphate and sulphate are the anions having the most favourable effects on protein stability according to the well-known Hofmeister series (Baldwin, 1996). A deep understanding of the underlying molecular mechanism that drives this invariable phenomenon is still elusive. It seems to emerge from a combination of general effects involving the stabilization of the folded conformation by changes in surface tension and specific interactions between the anions and the protein (Jungwirth and Cremer, 2014; Kramer et al., 2012). This becomes especially relevant in the solvation of a hydrophobic protein with a high content in positively charged residues (Cai has a 10% of positive residues and pI= 9). The effect that anions may have over the affinity between a mild detergent like DDM and the membrane protein has to be considered as well. As a matter of fact, the cmc of many detergents is known to decrease as

the ionic strength of the solution increases (Chattopadhyay and Harikumar, 1996; Maeda et al., 1997). Although, both sulphate and phosphate seem to increase the solubility of Cai, integral membrane proteins are exposed to a phospholipidic environment where sulphate is not present. The reason why nature chose phosphate esters and anhydrides as crucial molecules in living systems has been discussed before (Westheimer, 1987).

To further determine if the preferential stabilization of Cai by phosphate can be attributed to direct binding, not necessarily strong or specific, but involving the immediate environment or first hydration shell of the protein, we tested the effect of phosphate using detergents with varying chemical properties. The phosphate titration of Cai in the phosphate containing detergent DPC, at different protein to detergent ratios demonstrated that DPC can totally compensate for the effect of inorganic phosphate (Fig. 3.3e). A similar effect was observed in the case of the lysophospholipid OLPG as depicted in Figure 3.3f. We proved also that the effect of phosphate on Cai-GFP in DDM or LDAO micelles cannot be compensated by adding more detergent.

The improved solubility obtained for some detergents in the previous experiment (e.g. DPC, OLPG) are only reporting on protein solubility. PDCs were obtained from a Cai-GFP sample originally extracted and purified in DDM. Yet different detergents play distinct roles at the step of protein extraction from the natural membrane. Lipid-protein and lipid-detergent interaction will also determine the protein solubilization yields and the properties of resulting PDCs. We tested the ability to extract the overexpressed protein from membranes in six different detergents and lysophospholipids: DDM, Triton X-100, LDAO, OLPG, DH_7PC and DPC. CaiH was used in this assay to test the effect of detergents on CaiH, in the absence of GFP. Membrane fractions were solubilized in buffers containing 1% detergent and were subsequently subjected to a single Ni-NTA purification step in the same solubilizing buffer. SDS-PAGE results of the eluted samples are shown in Figure 3.4. All detergents assayed improved the extent of solubilization attained in DDM. Highest solubilization yields were obtained with phosphate containing detergents including OLPG, DH_7PC and DPC. These detergents are known to behave as high solubilizing harsh agents, that may induce denaturation in some cases (Banerjee et al., 1995; Zoonens et al., 2013).

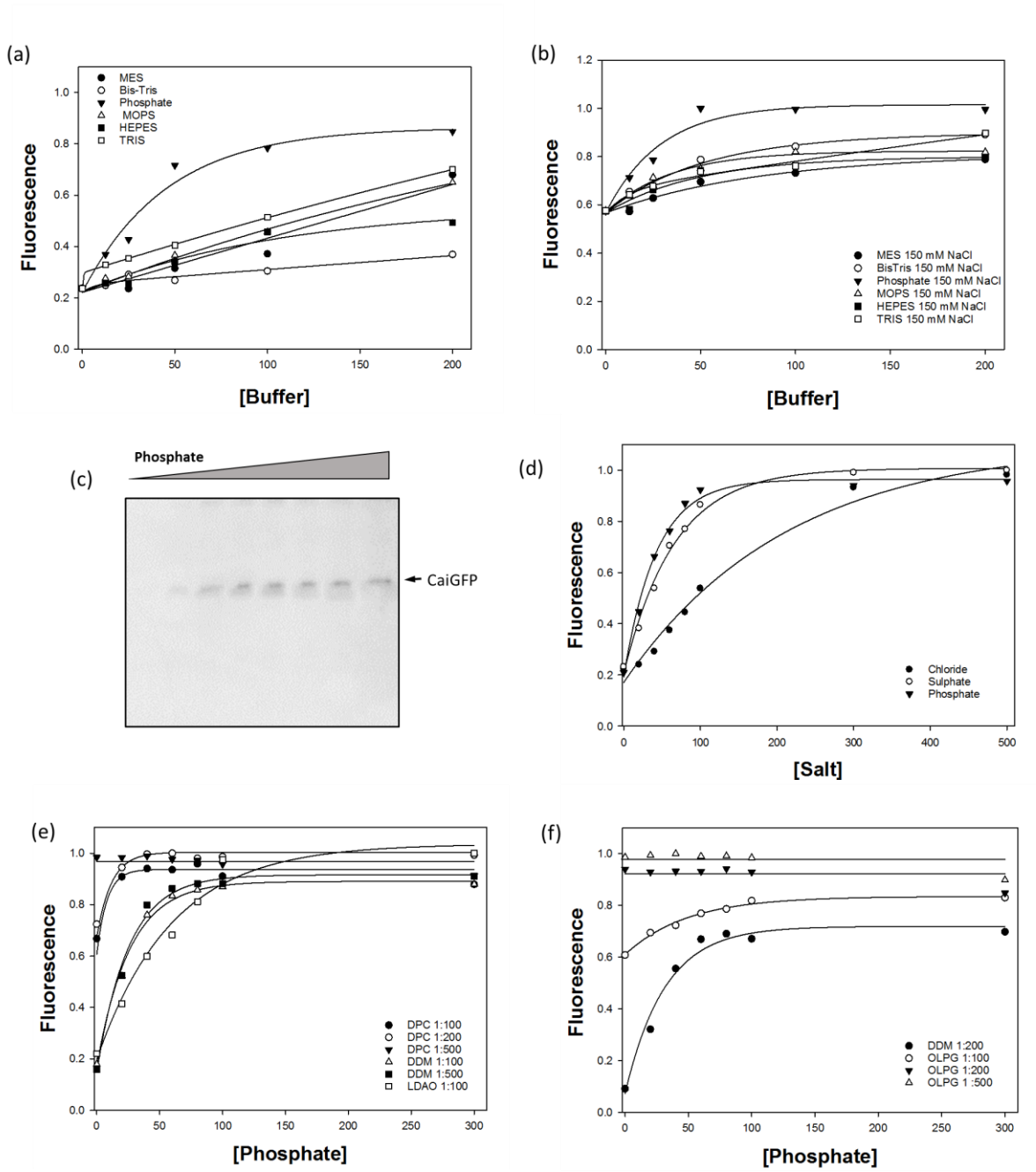

Figure 3.3 Effect of different buffers at pH 7.5 in the solubility of Cai-GFP in the presence and absence of 150 mM NaCl. 10 µM Cai-GFP in 3 mM DDM (Ri 1:300) were incubated with 6 buffers at pH 7.5, after centrifugation the fluorescence emission at 508 nm was recorded. (a) No NaCl (b) In the presence of 150 mM NaCl. (c) SDS-PAGE of the samples used in the phosphate titration. (d) Comparison of sulphate, phosphate and chloride anions over the stabilization of Cai-GFP. (e) and (f) Effect of phosphate on the stability of Cai-GFP in different detergent micelles at different protein to lipid ratios (Ri).

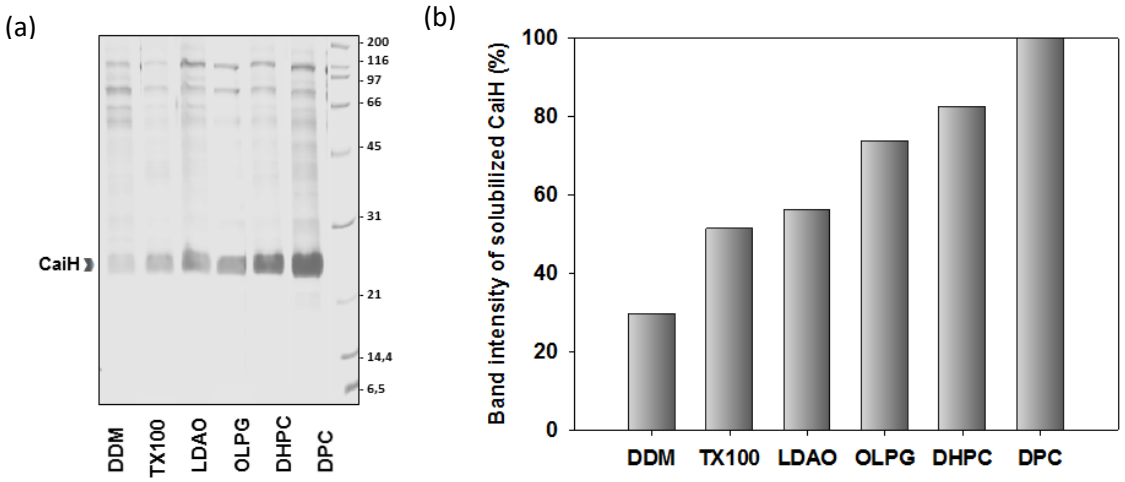

Figure 3.4 Relative yields of CaiH membrane extraction in different detergents after nickel affinity purification. (a) After membrane extraction and purification in NI-NTA resin eluted samples were run on a 12% SDS-PAGE. (b) Relative intensities of each protein band were quantified by densitometry and represented as percentage for each detergent (100% assigned to DPC).

The fact that inorganic phosphate, DPC and OLPG increase Cai solubility and/or stability might be interpreted as a reminiscence of a particular role of the phosphate moiety in the physiological environment. This motivated us to examine the involvement of *E. coli* inner membrane lipids in Cai folding and stability. For some proteins it has been shown that total delipidation results in loss of activity (Garavito and Ferguson-Miller, 2001). For lactose permease the addition of lipids is essential to preserve the function (Newman et al., 1981) and improve crystallization (Guan et al., 2006). Quality control assays (by thin layer chromatography and phosphorous quantification) on CaiH purified in DDM micelles indicated that phospholipids co-purify with the protein even after three chromatographic purification steps. Therefore we aimed to evaluate the putative stabilization capacity of *E. coli* lipids using a cysteine accessibility assay. To do so we used a fluorescent-based test in which the dye N-[4-(7-diethylamino-4-methyl-3-coumarinyl)phenyl]-maleimide (CPM) is able to emit fluorescence upon reacting with accessible sulfhydryl groups of the protein (Alexandrov et al., 2008). Cai contains 4 cysteine residues that are predicted to be located in the transmembrane region of the protein. Cysteine reactivity to CPM was measured over time at 30 °C for a CaiH sample purified in DDM with or without externally added *E. coli* lipids. One microliter of purified protein at 600 µM (10 mg/ml) was diluted 150 fold in assay buffer containing 20 mM TRIS pH 7.5, 0.1 mM NaCl and 3 times cmc of DDM (0,03%) and measured in a 96-well plate spectrofluorimeter. *E. coli* lipid extract suspension (4 µl) was added to one of the wells to a

final concentration of 0.3 mg/ml. The lipid extract was prepared according to (Bligh and Dyer, 1959) from the original C41 bacterial culture where CaiH was expressed. As shown in Figure 3.5, the addition of lipids hinders CPM access to cysteine residues and the trace of the sample with added lipids gets saturated at a lower fluorescence intensity than that of Cai in DDM micelles, the gel inset shows that intensity differences can be ascribed to Cai-bound CPM.

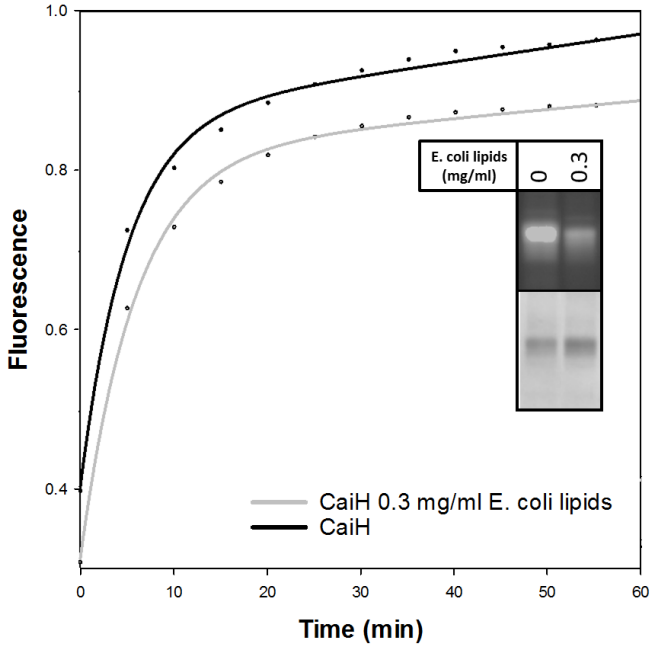

Figure 3.5 Stabilization of CaiH by addition of *E. coli* lipids followed by CPM incorporation. CPM incorporation to CaiH was followed by fluorescence for 1 h at 30 °C. 4 µM CaiH in DDM (black) and 4 µM CaiH in DDM to which 0.3 mg/ ml *E. coli* lipid extract has been added (grey). Both samples contain 0.03% DDM, 100 mM NaCl, 20 mM TRIS pH 7.5. Inset, SDS-PAGE gel of the same samples after CPM modification (upper) Fluorescence image; (lower) image after coomassie-staining.

^{31}P NMR represents a powerful method to detect phosphorous containing lipids in solution. In this kind of experiment phospholipid head groups can be discriminated by their chemical shifts. We recorded the ^{31}P-NMR spectra of purified CaiH and that of the chloroform lipid extract of the bacterial culture where Cai was originally expressed, both samples solubilized in DPC. Peaks corresponding to different phospholipid head groups were identified based on previously published analysis (Liebau et al., 2016; Meneses and Glonek, 1988). The lipid composition of bacteria overexpressing CaiH (Fig. 3.6b) showed the standard *E. coli* lipid composition consisting of three main types of phospholipids, PE (60–80 mol%), PG (15–30 mol%), and CL (5–10 mol%) (Andersson, 1996; Shokri and Larsson, 2004). Comparison of both ^{31}P NMR spectra indicates that lipids co-purify with CaiH. A significant amount of

phospholipids are detected in the sample as a major peak around 0.2 ppm. Although correct assignment of the peaks needs further investigation this experiment further supports the notion that Cai drags membrane lipids even after solubilization at high detergent concentrations.

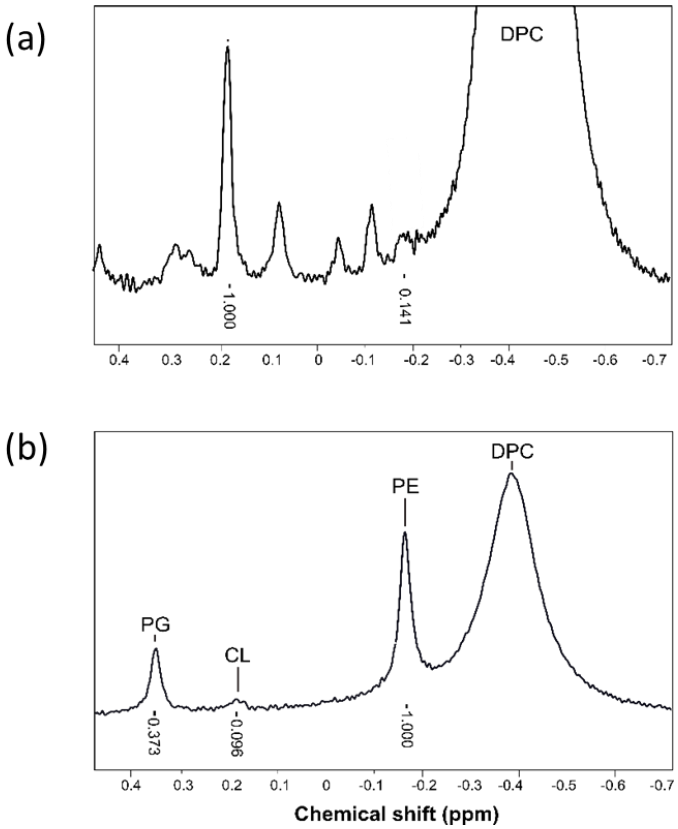

Figure 3.6. ^{31}P NMR spectra of CaiH purified in DPC compared with total lipid extract of membranes containing CaiH (a) Purified CaiH in 200 mM DPC, 20 mM phosphate, 0.5 mM TCEP, 10% D_2O, 0.5 mM EDTA, pH 7.5 in the upper panel. The phosphate buffer peak is located at 1.8 ppm, not shown in the figure. (b) the total lipid extract of bacteria expressing CaiH solubilized in 50 mM DPC, 20 mM MES, 1 mM EDTA, 10% D_2O, pH 6.5 (the upper spectrum has been scaled up 5 times compared with the one below to show the lipid peaks).

3.3 Oligomerization state of Cai

Previous experiments might only report differences in Cai solubility and provide no information about conformational heterogeneity. Consequently, size exclusion chromatography (SEC) was used to study monodispersity of different PDCs. Homogeneous and folded proteins generally give rise to single symmetrical Gaussian peaks while unstable,

polydisperse samples typically exhibit multiple asymmetric peaks (Ricker and Sandoval, 1996). Purified Cai in DDM was exchanged to LDAO, CHAPS, DPC and OLPG by dilution to yield a 500 µl sample with a protein-detergent ratio of 1:500 which was loaded onto a Superdex 200 column. Elution profiles shown in Figure 3.7 suggest that the bile salt derived CHAPS has a deleterious effect over Cai. The amount of eluted protein was lowest in this detergent, most probably because of aggregation and sedimentation of the protein in the centrifugation step prior to chromatography. In contrast, DDM, LDAO and DPC show a unique peak of varying sharpness that can be attributed to different oligomerization states of the samples. Following this hypothesis polymerization state of Cai in different detergents was studied more in depth by chemical crosslinking.

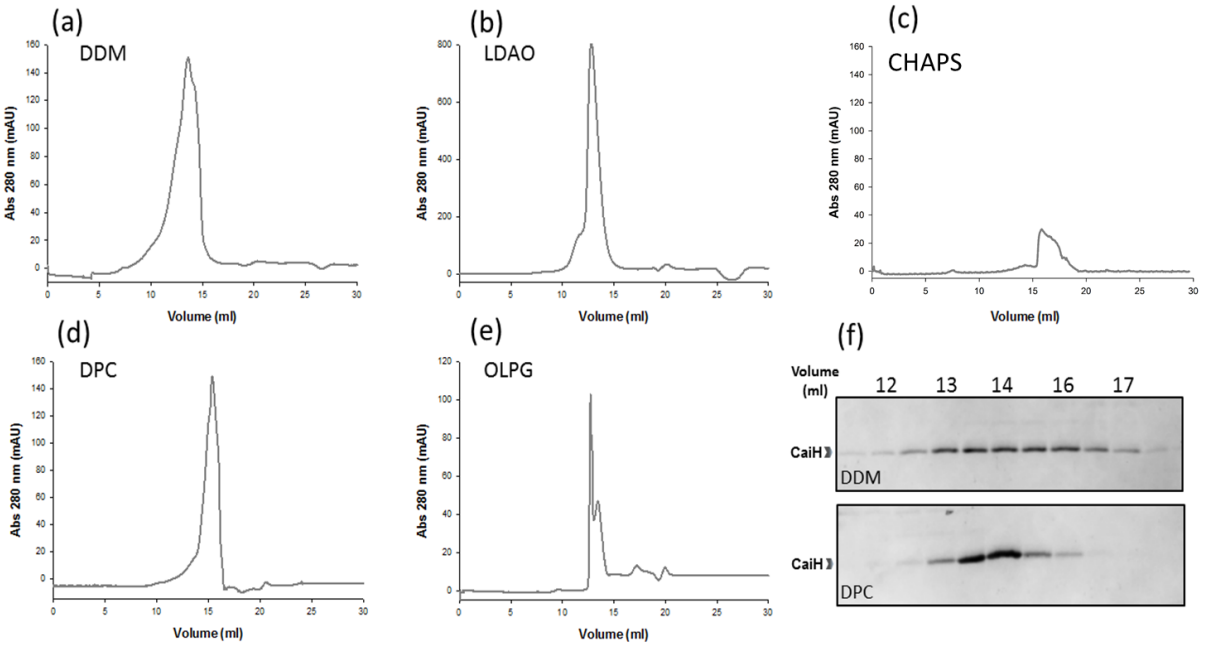

Figure 3.7 Monodispersity of Cai in different detergents analysed by size exclusion chromatography in Superdex 200 10/30. (a) to (e) chromatography elution profiles of Cai in 0.2% detergent, 100 mM NaCl, 1 mM TCEP, 20 mM sodium phosphate pH 7.5. (f) SDS-PAGE analysis of collected fractions for DDM and DPC.

Optimal detergents should extract the protein from the membrane to produce stable and homogenous PDCs while preventing irreversible dissociation of functional oligomers as well as detergent induced non-specific aggregation.

The effect of different detergents on protein-protein interactions was analysed by bis(sulfosuccinimidyl)suberate (BS^3) crosslinking. This bifunctional reagent introduces linkages between lysine residues. The detergent in purified samples of Cai-GFP in DDM

micelles was exchanged to 11 different detergents by means of Ni affinity chromatography. After extensive washing of immobilized protein with 50 mM sodium phosphate pH 7.5, 150 mM NaCl, 1mM TCEP and 2% detergent, CaiH was eluted from the Ni-NTA column with the same buffer supplemented with 150 mM imidazol and quantified by fluorescence. Protein aliquots (6.5 μM) were subjected to BS^3 crosslinking (400 μM) for 15 minutes at room temperature (Fig. 3.8a). Anionic lysophospholipid OLPG and zwitterionic DPC showed a striking ability to solubilize Cai-GFP oligomers from the original DDM sample. By contrast, the bile salt derived detergents, CHAPS, CHAPSO and cholate, yielded the highest amount of high molecular weight oligomers. Together with previously described SEC experiments this indicates that bile salt derived amphiphilic agents induce dead-end non-native protein-detergent aggregates.

In Figure 3.8c the relative intensities of the gel bands corresponding to multimers have been plotted and the detergents reorganized attending to their chemical properties. It can be appreciated that the effect detergents have over the oligomerization tendency of Cai-GFP can be differentiated in three groups: (i) bile salt like detergents causing massive aggregation, (ii) phosphate containing detergents with a high monomerizing capacity, and (iii) non-ionic and zwitterionic detergents with intermediate oligomerization effect. Interestingly, the tendency for protein polymerization increased with the alkyl chain length within the maltoside detergent series: DDM (C12) > DM (C10) > NM (C9), suggesting that shorter alkyl chains might not be able to shield the transmembrane segment.

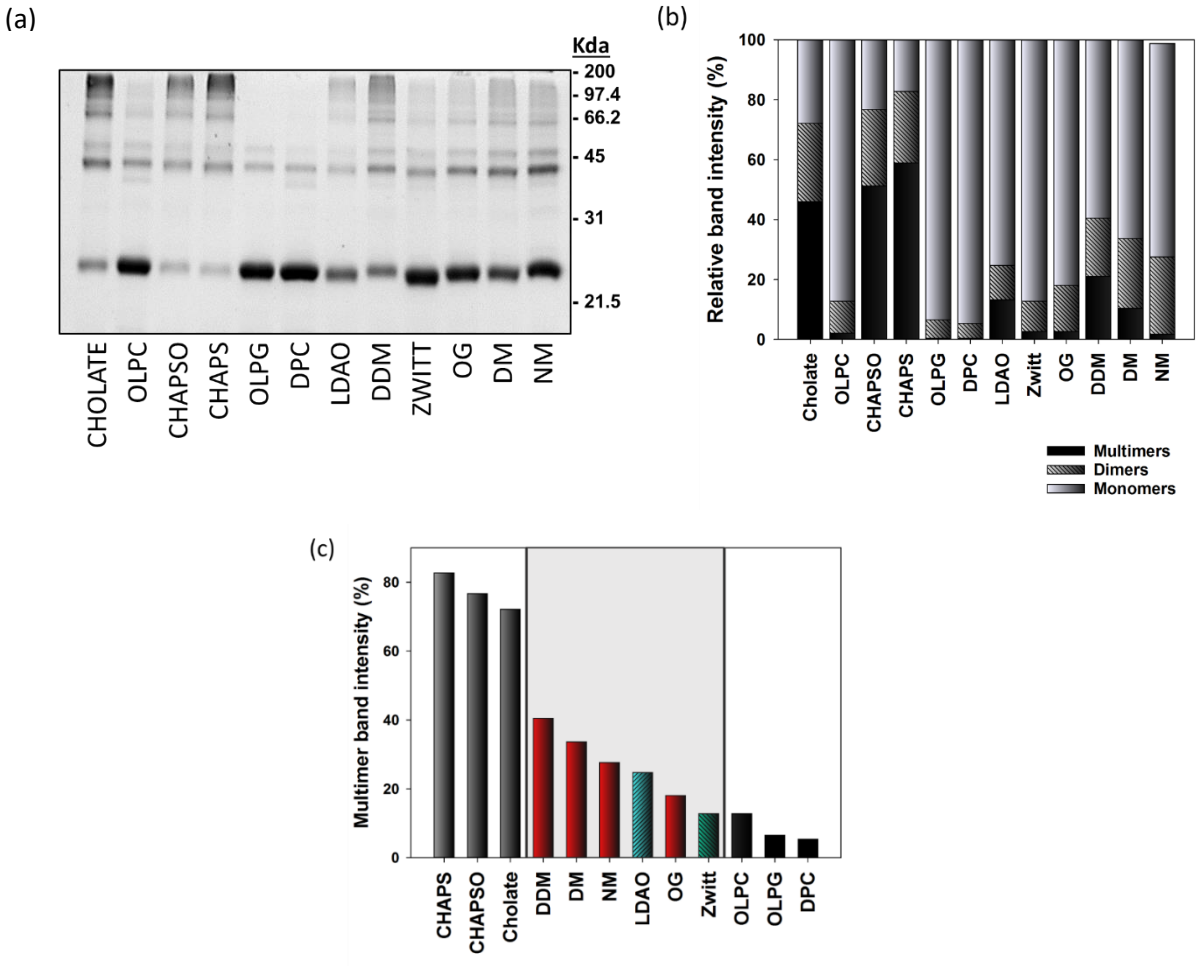

Figure 3.8 Polymerization state of Cai-GFP in different detergents analysed by BS^3 crosslinking. (a) SDS-PAGE of the crosslinked samples (b) Relative amounts of different types of oligomers normalized with respect to total protein in each line. (c) Quantification of Cai-GFP multimers (including dimmers), sorted by polymerization extent and detergent type. Bile-salt derived detergents in dark grey, glycosides in red, zwitterionic LDAO and Zwirttergent 3-12 in blue and phosphate containing lysophospholipids and DPC in black.

3.4 Conformational stability of Cai

A considerable work remains to be done to establish high-throughput and robust methodologies to discriminate when the conformation of an integral membrane protein that has been subjected to detergent solubilization is still physiologically relevant, or, in other words, when its native structure has being irreversibly altered. In the absence of straightforward structure quality controls we explored a series of different spectroscopic techniques to get more insights into the secondary and tertiary structure of detergent-solubilized Cai. Different detergents used throughout this chapter were chosen with the aim

of correlating their effects with what was already observed by complementary methodologies above.

Analysing the secondary structure content of soluble proteins by circular dichroism has become the standard protocol to assess correct folding of proteins or mutant variants. In the case of integral membrane proteins, however, as long as the protein is kept in an apolar environment, the disruption of the hydrogen-bonded secondary structure is very unfavourable. Hence, detergent-induced non-native conformations with weak or absent tertiary interactions can exist whose total secondary structure content has not been altered (J. Miles and A. Wallace, 2016).

The far ultraviolet CD spectrum of 3 µM Cai in DDM shown in Figure 3.9a displays two strong minima at 222 nm and 208 nm as expected for a highly α-helical protein. The predicted ratio of Cai residues within transmembrane helical regions is about 54%, which is in good agreement with the experimental 42% calculated here (according to equation 3 under Experimental Procedures). Regarding the shape of the far CD spectra, when the ratio of ellipticities at 222 and 208 nm are compared, Cai in DDM micelles shows a ratio $\theta_{222}/\theta_{208}$ = 1.25. Similar spectral distortions ($\theta_{222}/\theta_{208} > 1$) have been observed in coiled-coils (Burkhard et al., 2001) and frequently in proteins embedded in bilayers (Langosch and Heringa, 1998). Helical bundles with left-handed low crossing angles and extended contacts along considerable surfaces of the helices frequently show mixtures of knobs-into-holes and ridges-into-grooves packing which are believed to be important in transmembrane helix-helix recognition (Bowie, 1997; Dunker and Jones, 1978; MacKenzie et al., 1997).Therefore a ratio greater than 1 for Cai in DDM suggests tight helical packing presumably involving inter-molecular helical contacts, in agreement with previous oligomerization results.

Far CD spectra were also recorded at increasing phosphate concentrations and the $\theta_{222}/\theta_{208}$ ratio calculated for each concentration. As seen in Figure 3.9b, phosphate induces a reduction of the $\theta_{222}/\theta_{208}$ ratio at similar phosphate concentrations as those used in solubility experiments (Fig. 3.3a). Temperature induced changes in ellipticity at 222 nm was monitored in 5 mM and 50 mM phosphate (Fig. 3.9c). At low phosphate concentration the protein undergoes irreversible aggregation with a midpoint ~ 45 °C, while a typical small, reversible and non-cooperative loss of helicity characteristic of integral membrane proteins (J. Miles and A. Wallace, 2016) is obtained in 50 mM phosphate.

In order to assess the effect of different detergents over the secondary and tertiary structure of CaiH, the protein was purified in LDAO and exchanged to DM, OLPG and DH_6PC by dilution. All samples were quantified by absorbance at 280 nm and adjusted to 22 μM in 50 mM detergent, 50 mM NaCl, 20 mM sodium phosphate pH 7.5. Most intense spectrum was obtained in LDAO (Fig. 3.10a). Differences in total intensity might be attributed to the extent of protein solubility after exchange but the ability of some detergents to induce α-helicity at flexible loops should also be considered. Regarding the $\theta_{222}/\theta_{208}$ ratio, LDAO yielded the lowest value while DM and OLPG gave $\theta_{222}/\theta_{208} \sim 1$, and DH_6PC $\theta_{222}/\theta_{208} = 1.3$. As seen in oligomerization and protein extraction experiments presented above, differences in intensities at 222 nm and $\theta_{222}/\theta_{208}$ ratios may arise from differences in the extent of oligomerization and solubilization.

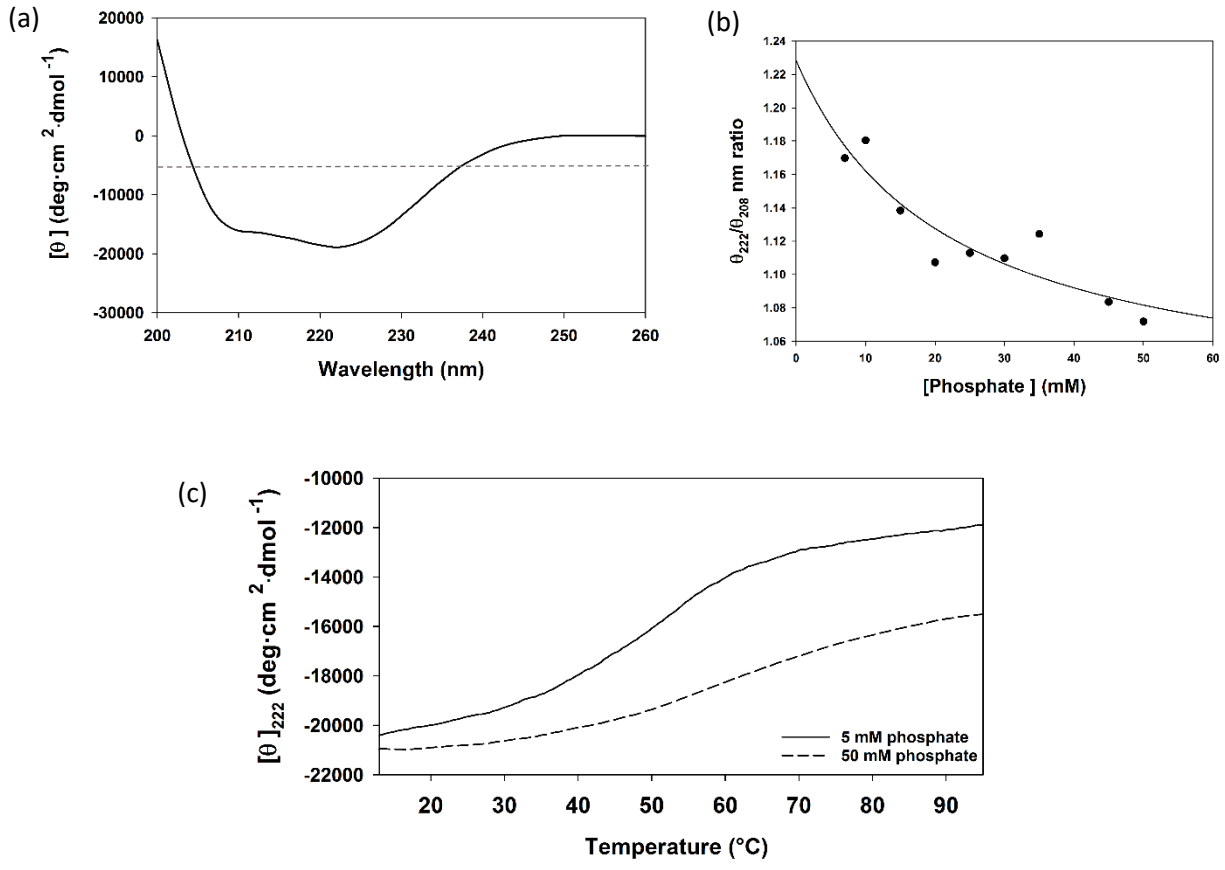

Figure 3.9 Circular dichroism analysis of Cai in different conditions. (a) Far CD spectra of 3 μM Cai in 2 mM DDM at 20 ºC (b) Correlation between phosphate concentration and 222/208 ratio of Cai in 2 mM DDM. (c) Cai thermal denaturation traces at 222 mM in 5 mM phosphate (green) and 50 mM.

CD spectroscopy in the near ultraviolet region provides information about the conformation and orientation of aromatic residues and is used as a sensitive probe of protein tertiary

structure (J. Miles and A. Wallace, 2016). Thus, near-UV CD profiles vary from one protein to another because the contribution of each aromatic residue may be positive or negative, or can cancel out. Yet, sharp and intense CD spectra are indicative of well folded proteins with defined tertiary structure. As seen in Figure 3.11b the overall shape of the traces remains unaffected by the detergent at use but the intensity appears to reflect the differential solubilization capacity previously identified for these detergents in particular (DH_6PC > OLPG > DPC > DM > LDAO) with phosphate-containing detergents showing more intense near-UV CD bands. The fact that DH_6PC gave the highest absolute intensity at 278 nm and highest $\theta_{222}/\theta_{208}$ ratio suggests an improved helical packing for Cai in DH_6PC micelles.

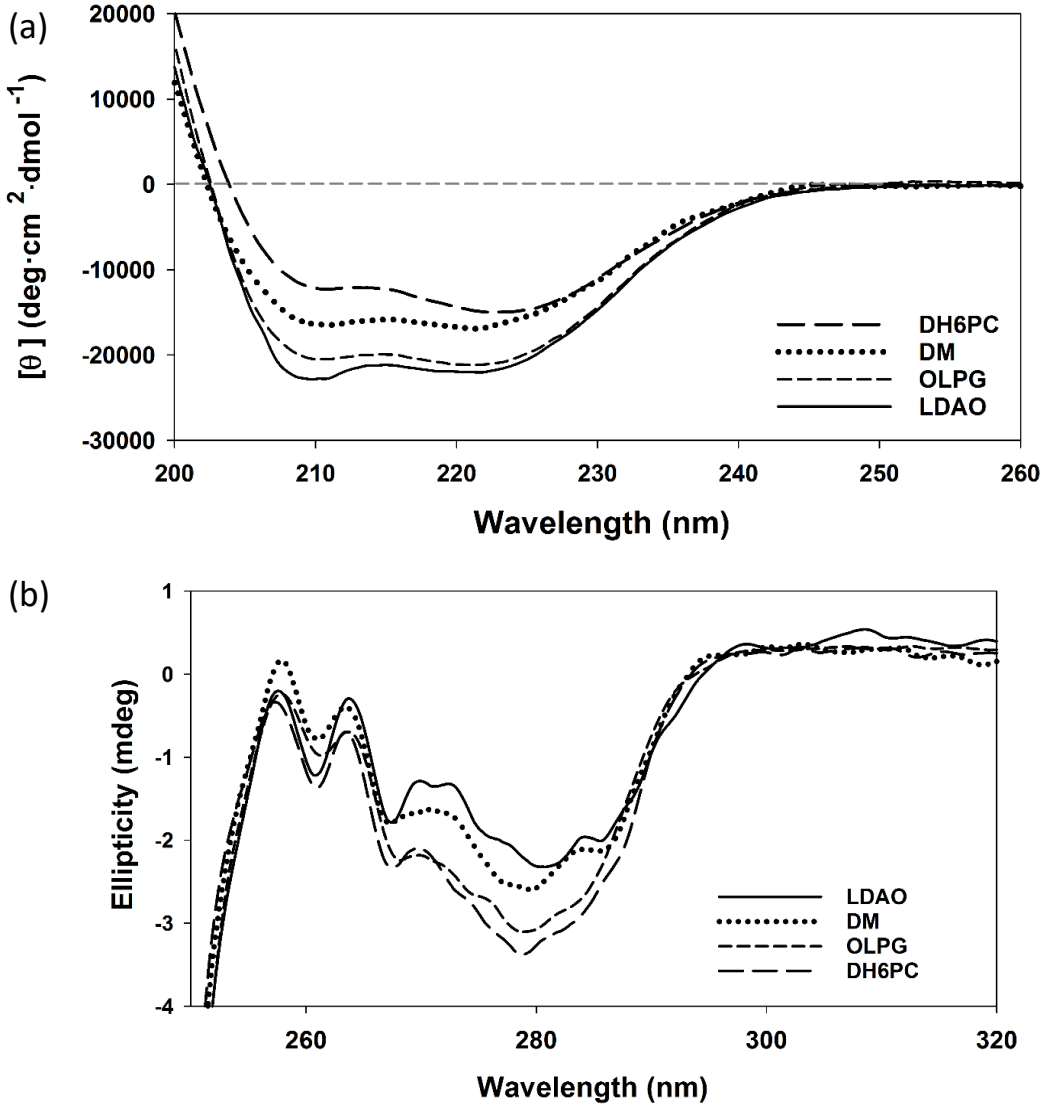

Figure3.10 Secondary and tertiary structure of Cai in different detergent solutions studied by far and near CD. (a) Far UV CD spectra of CaiH (22 µM) in 50 mM NaCl, 20 mM sodium phosphate pH 7.5, and 50 mM detergent. (b) Near UV CD spectra of 220 µM CaiH in the same buffer.

Due to the lack of cooperativity in unfolding transitions for helical membrane proteins, CD experiments of temperature induced denaturation could not yield much information. The CPM thermostability assay was used instead to evaluate the efficiency with which detergents of different chemical structure mask the transmembrane hydrophobic regions. Cysteine accessibility for CaiH in OLPG, DHPC and DPC yielded significantly faster CPM incorporating rates (Fig. 3.11) suggesting a possible exposure of transmembrane regions that ought to be masked in the lipid environment. This observation could be revealing differential detergent behaviour in terms of interactions that distort the native protein conformation by means of occupancy of cavities or interactions with soluble exposed loops (Zoonens et al., 2013).

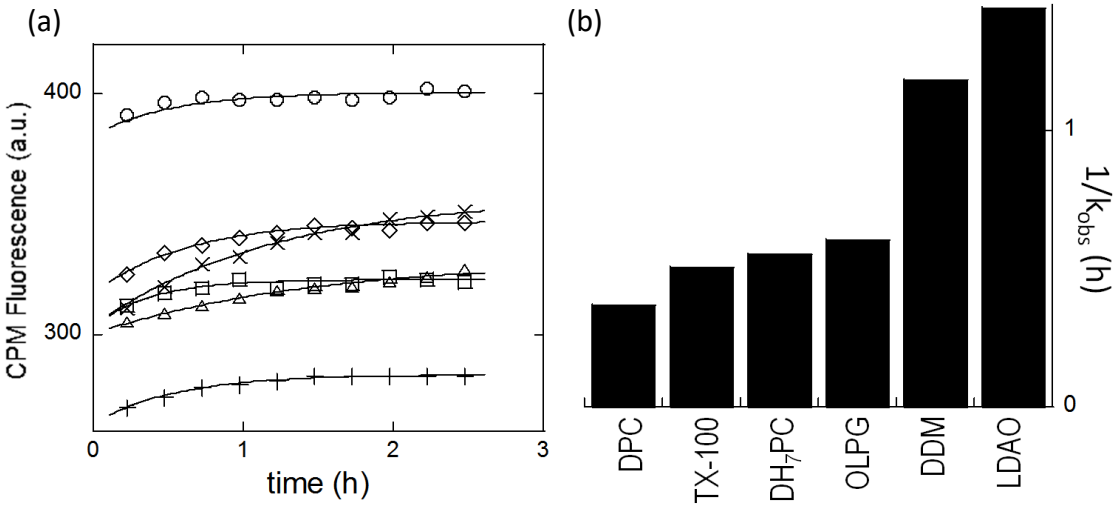

Figure 3.11 CaiH modification by CPM. (a) CPM fluorescence after incubation with CaiH in different detergents (1% w/v), 100 mM NaCl, 20 mM sodium phosphate pH 7.5 at 30 °C. CPM fluorescence was measured in a plate reader for 3 h. Detergents: TX-100 (○), DPC (□), OLPG (◊), DDM (×) DH_7PC (+), LDAO (Δ). (b). Kinetic time constants for CPM incorporation to CaiH in different detergents.

^{15}N-NMR spectroscopy represents another valuable tool to study the tertiary folding of membrane proteins (Kim et al., 2009; Krueger-Koplin et al., 2004; Murail et al., 2008). Cai was uniformelly ^{15}N-labelled and purified in DDM, LDAO, DDAO, TDAO and DPC. Samples in DH_7PC, OLPG and $C_{12}E_9$ were obtained by exchange from pure Cai in DDM by size exclusion chromatography in a Superdex 200 column. As seen in Figure 3.12, none of the 2D ^{1}H, ^{15}N fingerprint spectra (recorded with the most sensitive SOFAST-HMQC experiment) of CaiH reached a high-resolution which precludes further detailed analysis. Significant detergent-dependent effects and spectral improvements were still observable. In a first round we

tested the known good solubilizing detergents DH_7PC (Fig. 3.12A), OLPG (Fig. 3.12B) or $C_{12}E_9$ (Fig. 3.12C) which yielded very incomplete spectra with only a few sharp and intense signals characteristic for highly flexible protein regions, typically the loops and C- and N-termini. The entire helical transmembrane region remains essentially invisible with these detergents, suggesting that they are unable to restrict the conformational heterogeneity and dynamics, causing signal dispersion and line broadening beyond observability. Remarkably, only the spectrum in OLPG (Fig. 3.12B) showed some weak negative signals (around ^{1}H= 7.2 and ^{15}N = 124 ppm) indicating single folding in F1 (^{15}N) by one sweep width = 40 ppm. These signals can be unambiguously assigned to arginine side chain NE-HE moieties (around ^{15}N = 83 to 85 ppm), and their visibility indicates some specific interaction with this detergent leading to increased immobilization and protection from HE/H_2O exchange. The most plausible explanation is electrostatic interaction between the positively-charged arginine guanidinium and the negatively-charged phosphate group in OLPG. Although DH_7PC (but not $C_{12}E_9$) also contains such phosphate groups, the corresponding spectrum shows no trace of arginine NE-HE signals suggesting that electrostatic attraction alone is not sufficient for a stable interaction. Rather, additional hydrophobic interactions appear necessary to properly position the charged groups, for which the side chains of DH_7PC (C7) seem too short as opposed to OLPG (C18).

We next tested detergents with fixed long alkyl side chains (C12), but different polar headgroups. Again, arginine NE-HE signals are only observed with the phosphocholine-bearing DPC (Fig. 3.12D), but not with maltoside-bearing DDM (Fig. 3.12E) or even the zwitterionic amine oxide-bearing LDAO (Fig. 3.12F). For all these C12 detergents, however, the fingerprint spectrum not only showed the sparse set of intense sharp signals from the loop regions, but a background of weak, broad signals deriving most likely from the helical transmembrane regions of the protein. Thus, detergents with long alkyl chains (about C12) in combination with a polar headgroup (particularly LDAO) appear capable of significantly reducing the conformational heterogeneity and dynamics of the transmembrane helices, thus stabilizing them much better than the first set of solubilizing detergents. To further analyse their impact, we finally tested a set of detergents with variable alkyl chain length and fixed polar head group (amine-N-oxides). Upon decreasing the chain length from C14 (TDAO, Fig. 3.12G) *via* C12 (LDAO, Fig. 3.12H) to C10 (DDAO, Fig. 3.12I), the background of weak, broad signals from the helical transmembrane region increases while the overall

distribution of signal intensities, including the sharp signals from the loop regions, becomes more homogeneous (see the ^{1}H rows shown below in Fig. 3.12G-I).

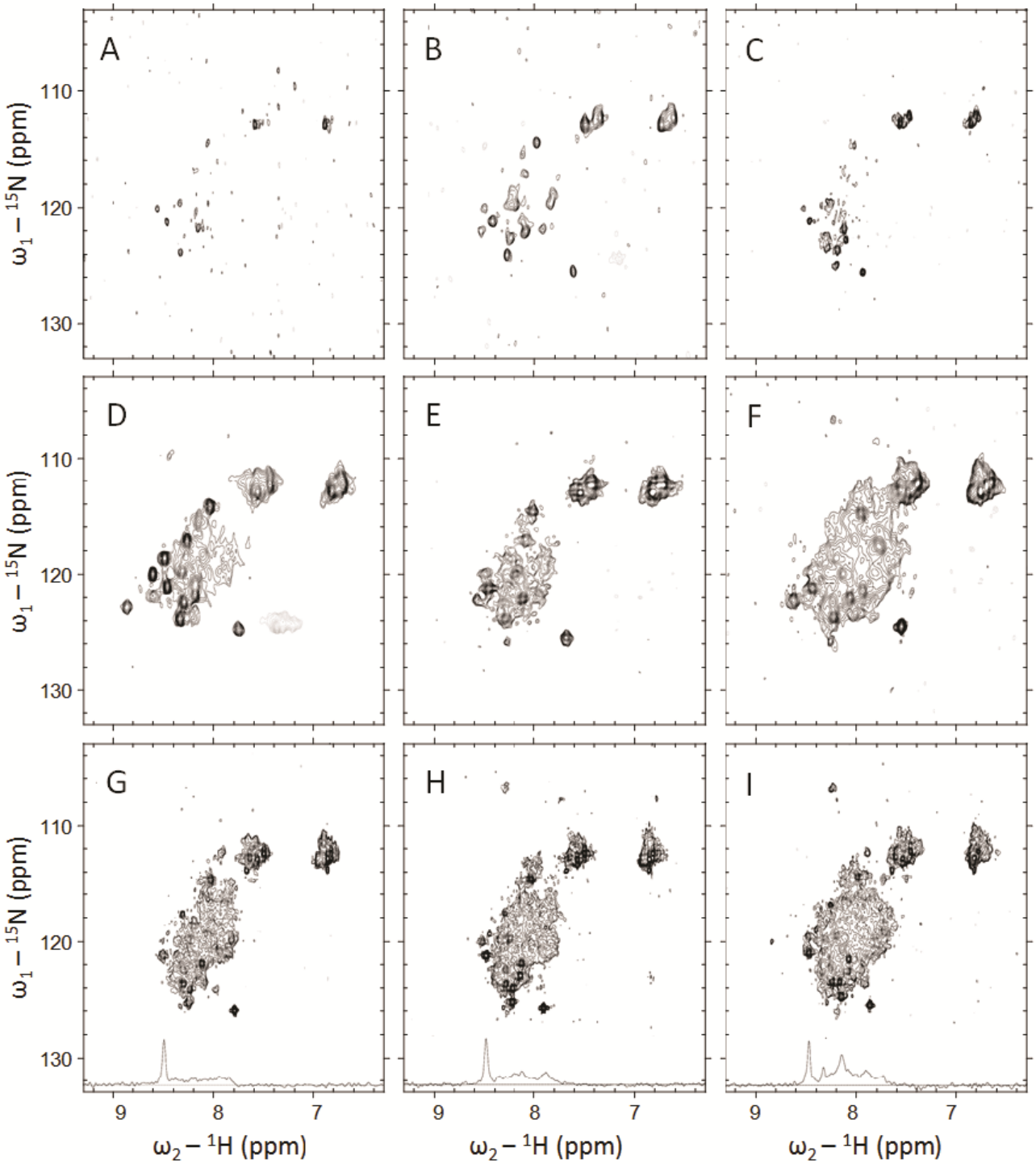

Figure 3.12 2D 15N, 1H-HMQC spectra of CaiH in aqueous buffered solution (50 mM sodium phosphate pH 7.5, 100 mM NaCl) with different detergents. A) DH_7PC (298 K), B) OLPG (290 K), C) $C_{12}E_9$ (298 K), D) DPC (290 K), E) DDM (290 K), F) LDAO (290 K), G) TDAO (298 K),H) LDAO and I) DDAO (298 K). The horizontal 1D 1H rows shown in the lower spectra (G–I) were taken at a ^{15}N shift of 121.5 ppm. The protein and detergent concentrations ranged between 50-100 µM and 20-40 mM, respectively.

Thus we may summarize that, from the point of view of NMR the most appropriate detergent appears to be that with intermediate alkyl chain length (around C_{10}) and an amino-N-oxide head group (DDAO).

3.5 Functional analysis of Cai in micelles

One of the main hurdles limiting the biochemical study of membrane proteins is that it requires the protein to preserve its biological activity even when extracted from its native lipid environment by detergents. Considerable efforts have been devoted over the last decades to develop high-throughput detergent screenings that would speed up initial experiments leading to membrane protein structure function investigations (Alexandro et al., 2008; Hattori et al., 2012; Sonora et al., 2011). In the absence of a general and solid methodological ground to assess membrane protein tertiary and quaternary structure in micelles, functionality is stipulated to be a good criterion to guide the choice of detergent. Nevertheless, the diversity of methodologies used to demonstrate the functional integrity of different membrane proteins, is as broad as their physiological roles (Geertsma et al., 2008; Lee et al., 2013; Marin et al., 2007; Moffat et al., 2008; Murray et al., 2014; Read and Duncan, 2011). In the case of pore forming toxins, ion channels, or transporters, the capacity to bind ligands or partner proteins is often used as a functionality trait that can be also applied to the solubilized proteins prior to setting up more elaborated functional assays in lipid vesicles.

The chemical nature of detergents strongly determine the solubility, conformational stability, and polymerization state of Cai. We intended to correlate these observations with differences in Cai functionality. We investigated how a suite of different kinds of detergents and detergent like phospholipids affect the capacity of Cai to bind to its cognate toxin. While Cai is a four TM integral membrane protein, colicin A and its pore forming domain, adopts both soluble and membrane bound conformations according to its role as secreted soluble toxin that inserts into the inner membrane of target cells. The pore forming domain (pfColA), responsible of channel formation (Martínez *et al.,* 1983) and binding to Cai (Geli *et al.,* 1992*)*, was studied here. It is important to emphasise, that the effect that different detergents may have over the stability of the multiple conformations of pfColA will also influence its ability to bind to Cai. These initial binding experiments were not only aimed to test which detergents

keep Cai in a native conformation but also which of them enable pfColA to undergo the necessary conformational changes to interact with Cai.

For the first binding assay, equimolar quantities of Cai-GFP and pfColA were subjected to crosslinking by BS^3. The NHS ester groups react with exposed primary amines in Cai-GFP and pfColA to form intermolecular amide bonds when these two proteins are found in close proximity. The crosslinking experiment was carried out at 0.7% detergent concentration except OG, for which 2% was used to ensure that it was well above its cmc. Of the 12 detergents tested, only five gave rise to a detectable band corresponding to the crosslinked pfColA/Cai-GFP complex, precisely DDM, DM, NM, OG and Zwittergent 3-12 (Fig. 3.13). It is remarkable that all detergents, except one, are sugar-based molecules, suggesting a distinct effect for glycosides over Cai, pfColA and/or their binding interface. Alkyl-maltosides accounted for the highest complex yields, even if the amount of complex did not represent more than 10% of total protein in any case.

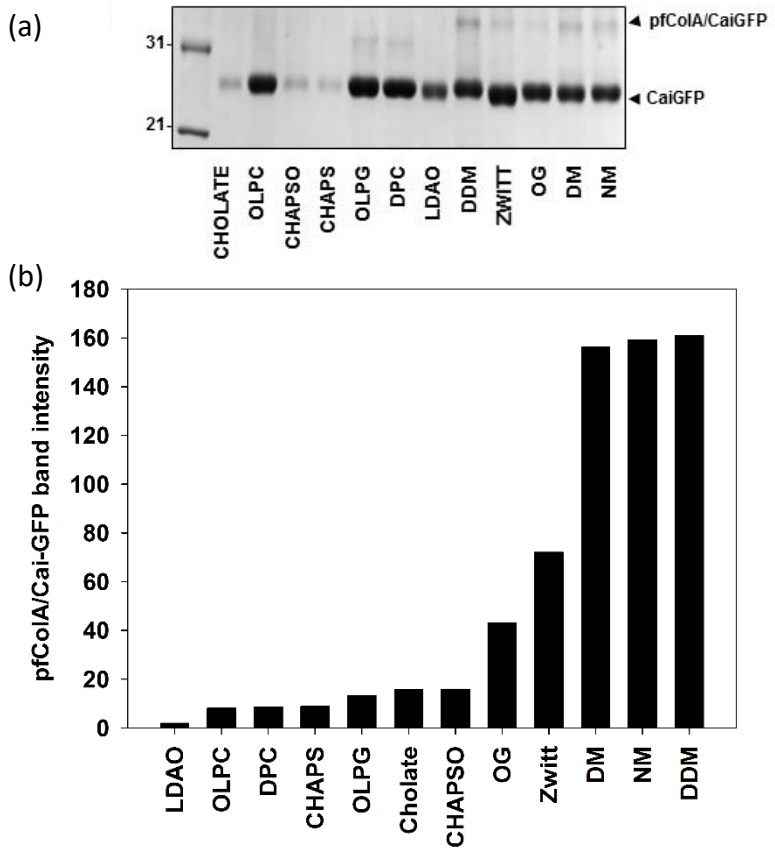

Figure 3.13 Detergent screening for pfColA/Cai-GFP complex formation analysed by BS^3 crosslinking. (a) 6 µM of Cai-GFP was incubated with 6 µM of pfColA in the presence of 625 µM of BS^3 for 25 min in 0.7% detergent, except for OG at 2% (to ensure being above cmc), samples were loaded into a 12.5% SDS-PAGE gel. (b) Quantification of the gel band corresponding to crosslinked pfColA and Cai-GFP.

The second method by which we screened for detergents compatible with complex formation, was co-elution from Ni-NTA. We examined the ability of detergents to co-purify pfColA bound to His-labelled Cai-GFP by means of Ni affinity chromatography. A three-fold molar excess of pfColA was added to 10 µM of Cai-GFP in 0.2% of each detergent and incubated with Ni-NTA resin. After extensive washing of the unbound pfColA with buffer containing 0.2% detergent, eluted samples were analysed by SDS-PAGE and the band corresponding to pfColA was quantified. The results obtained are consistent with the crosslinking assay depicted in Figure 3.13, being DDM, DM, NM, OG and Zwittergent 3-12 the only detergents in which binding is detected (Fig. 3.14).

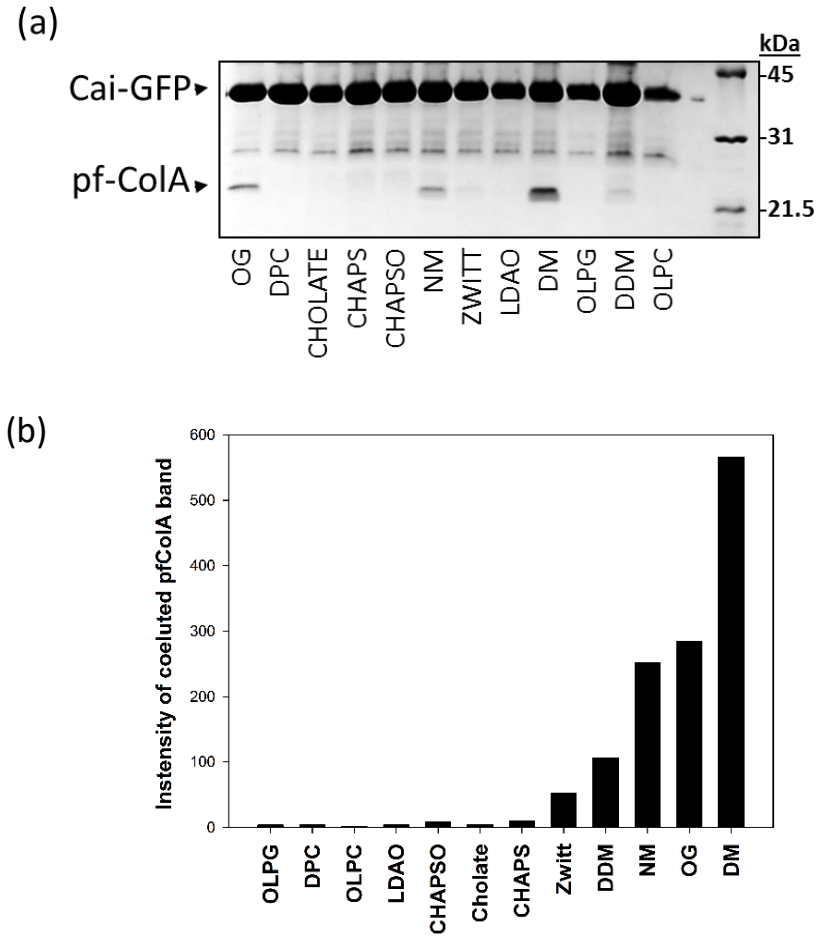

Figure 3.14 Co-purification of pfColA and His tagged Cai-GFP by Ni affinity chromatography in the presence of different detergents. (a) 10 µM of Cai-GFP was incubated with 3 molar excess of pfColA in 0.2% of each kind of detergent, subjected to Ni affinity chromatography by gravity flow and the eluted sample loaded onto a 12.5% SDS-PAGE gel. (b) Detergents have been organized according to detergent chemical character and extent of polymerization.

Interestingly, the yields obtained for the three maltosides tested show some differences with respect to the previous crosslinking results. This can be due to various factors like the use of lower concentrations of detergents and the presence of phosphate in the co-purification experiment. The crosslinking experiments, on the contrary, were carried out in HEPES buffer. It is also important to mention that the crosslinked band is the result of the accessibility of lysine residues from both proteins and the partition of BS^3 in the protein-detergent mixed micelles, where the acyl chain length might not have a strong influence.

Overall the results indicate that the most solubilizing detergents, OLPC, OPLG and DPC are detrimental for Cai/pfColA association. Glucosides and maltosides, on the other hand, having a lower solubilization capacity and promoting protein polymerization, turn out to be suitable for complex formation. The bile-salt derived CHAPS, CHAPSO and cholate are aggregation prone, unable to produce a stable Cai sample, and consequently incompatible with complex formation.

Regarding the zwitterionic detergent LDAO, it is interesting to note that, although it is optimal for Cai solubility and monodispersity, it did not allow binding. We hypothesized that may be due to a deleterious effect of LDAO over pfColA. To further explore this possibility and understand how complex formation is influenced by the effect of detergents on pfColA, we then analysed the conformational behaviour of pfColA in micelles of varying chemical character.

3.6 pfColA conformations in micelles

The C-terminal fragment of colicin A pfColA, has an intrinsic capacity to undergo multiple conformational transitions required for its biological function. In the absence of additional high resolution structures, the majority of models proposed for membrane insertion and pore formation mechanisms are based on the atomic structure of the closed soluble conformation of the pfColA obtained in 1989 (Parker et al., 1989). Therefore, structural studies providing further insights into the membrane associated closed or open channel conformations are of great interest. Previous work has suggested that a conformational change has to be induced to trigger the insertion-competent state of pfColA. Traditionally, a chemical destabilization by means of acidic pH, has been used to maximize the insertion in vesicles composed of anionic

lipids (van der Goot et al., 1991). Protein destabilization, that presumably induces the exposure of the hydrophobic hairpin, can also be caused by shortly heating the sample (chapter 4) or by the addition of detergents. Characterizing the behaviour pfColA in detergent micelles will contribute to understand the modulation of the conformational flexibility of the toxin.

CD spectroscopy allows rapid identification of global conformational changes at low resolution and was used here to follow conformational changes induced by detergents on pfColA. Near CD spectra of pfColA was recorded in three different detergents at a detergent to protein molar ratio of 300 to inspect their effect on the tertiary structure of the protein. As representatives of different chemical characters, we chose OLPG (low cmc, anionic lysophospholipid), LDAO (zwitterionic) and DDM (non-ionic sugar-based detergent). The spectra of pfColA in these detergents were compared with the spectrum of pfColA in aqueous buffer which exhibits characteristic minima around 268 nm and 292 nm, conventionally associated with the rigidity of aromatic residues. A cluster composed of aromatic residues, W88 stacked with Y163 and W132 and perpendicularly located with respect to Y127, is detected in the crystallographic structure of the soluble form (Parker et al., 1989). Near-CD spectra of pfColA in detergent micelles showed two strikingly different trends, the spectrum in 9 mM DDM was well structured and displayed a minimum at 272 nm implying fixed orientation of aromatic residues. In contrast, spectra obtained in 9 mM OLPG and 9 mM LDAO indicate lack of a defined tertiary structure. The overall shape of these last spectra resembles the ones obtained in DOPG vesicles at acidic pH (Muga et al., 1993) conditions at which colicin E1 was shown to be inactive (Lindeberg et al., 2000).

The interaction between detergent monomers and the soluble form of pfColA has previously been studied in our lab. The experiment consisted in titrating ^{15}N-pfColA with seven different detergents and measuring chemical shift perturbations in ^{15}N-^{1}H-HSQC spectra (Ibañez de Opakua, A., 2011, PhD Thesis). The results of these experiments showed that detergents induced chemical shift changes in residues located at three different hydrophobic patches present in the protein, mainly the loop between H3 and H4, a small region in H10 and several residues in the partially buried regions of the hydrophobic hairpin (H8 and H9). Peaks move smoothly towards the bound form, pointing at fast exchange generally related to weak

interactions. At higher detergent concentrations, around the cmc, more drastic changes were detected to the point that no signals remained.

Similarly, we sought to study the conformational change of pfColA upon addition of alkyl-maltosides, and so detergent titration experiments were performed followed by near CD. The maltosides DDM and DM were used because they exhibit highest complex formation yields. Ellipticity at 294 nm was plotted against detergent concentration as depicted in Figure 3.15b. The initial additions of DDM provoked a slight decrease in ellipticity but the pronounced minimum was still visible. Around 1 mM DDM, however, the overall shape of the spectrum changed and the minimum became undetectable (Fig. 3.15a). Further addition of detergent did not induce further changes. In the case of DM, this general conformational change occurs at around 2 mM detergent, most probably because of its cmc being one order of magnitude higher than for DDM.

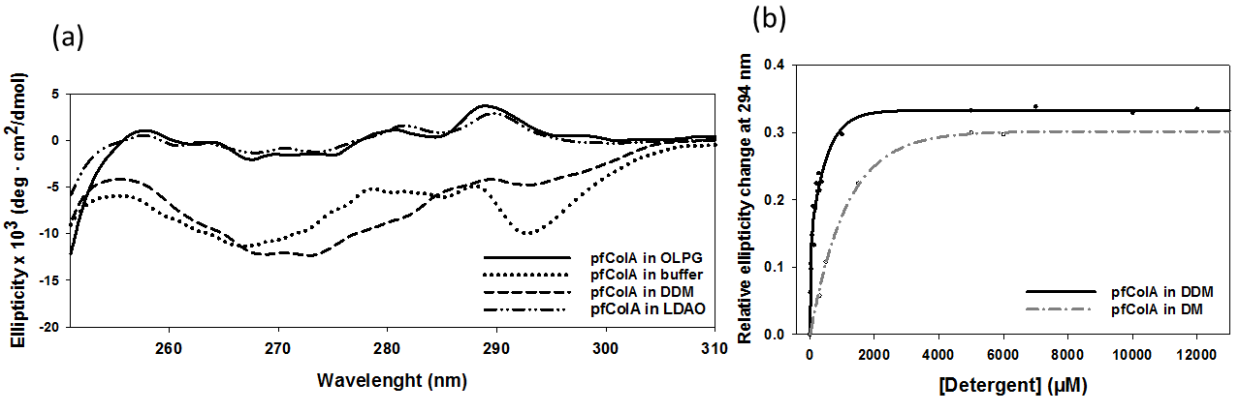

Figure 3.15 Tertiary structure of pfColA in detergents studied by near CD spectroscopy. (a) Near CD spectra of 30 µM of pfColA in 9 mM of anionic lysophospholipid OLPG and non-ionic DDM. (b) Detergent titration of pfColA followed by ellipticity changes at 294 nm.

These two distinct behaviours at two different detergent concentration regimes have been observed before by thermal denaturation monitored by ellipticity at 222 nm. In the presence of submicellar detergent concentration, the melting temperature and cooperativity of the transition are significantly lowered whereas above the cmc a reversible loss of ellipticity occurs, without any cooperative transition (A. Ibañez de Opakua, PhD thesis). All this results suggest that alkyl-glycosides are able to bind to exposed hydrophobic regions of pfColA and eventually trigger a detergent solvated conformation with a very stable secondary structure and considerable tertiary interactions.

Chemical crosslinking was used to understand the effect of different detergent conditions over the oligomerization state of pfColA. Even if the structure of membrane inserted ColA is still missing, it is accepted that the hydrophobic hairpin inserts perpendicularly into the bilayer (Padmavathi and Steinhoff, 2008) and that additional helices are reversibly translocated upon pore opening (Slatin et al., 1994, 2002). Moreover, there is no agreement around the stoichiometry of the pore. Despite some studies suggesting that a single ColA molecule is able to kill a bacteria, the formation of an ion conducting pore points towards the requirement of a bigger oligomeric configuration (Cascales et al., 2007). Recent EPR data indicate that the full-length colicin A can form dimers both *in vivo* and in liposomes of *E. coli* lipids (Dunkel et al., 2015). Thus, to reconcile these multiple scenarios with the *in vitro* detergent-protein system, we performed BS^3 crosslinking of pfColA in 12 detergent solutions (Fig. 3.16).The samples were analysed in two SDS-PAGE gels, for the one in the left in Figure 3.16a, 10 µM pfColA were incubated with 625 µM BS^3 and detergent concentrations were 2% for DPC and OG, due to their high cmc, and 0.7% detergent for the rest, in 10 mM HEPES pH 7.5. For the gel depicted in the right, 10 µM of pfColA were incubated with 625 µM BS^3 in 0.1% detergent, PBS, 50 mM NaCl, 1 mM TCEP. All the alkyl-glycosides gave rise to oligomers (DDM, DM, NM and OG), together with DH_7PC and Triton X-100. Only dimers and no higher oligomers were detected in all cases.

Dimerization results obtained in the case of DDM, LDAO and OLPG can be related to the near CD results obtained for these detergents. It would be very interesting to obtain the near-CD spectra of a broader set of detergents to be able to relate dimerization results with the induction of stable tertiary structure. Nevertheless, taking together all the data collected for pfColA in DDM micelles a correlation between functionality, tertiary structure and dimerization seems to emerge.

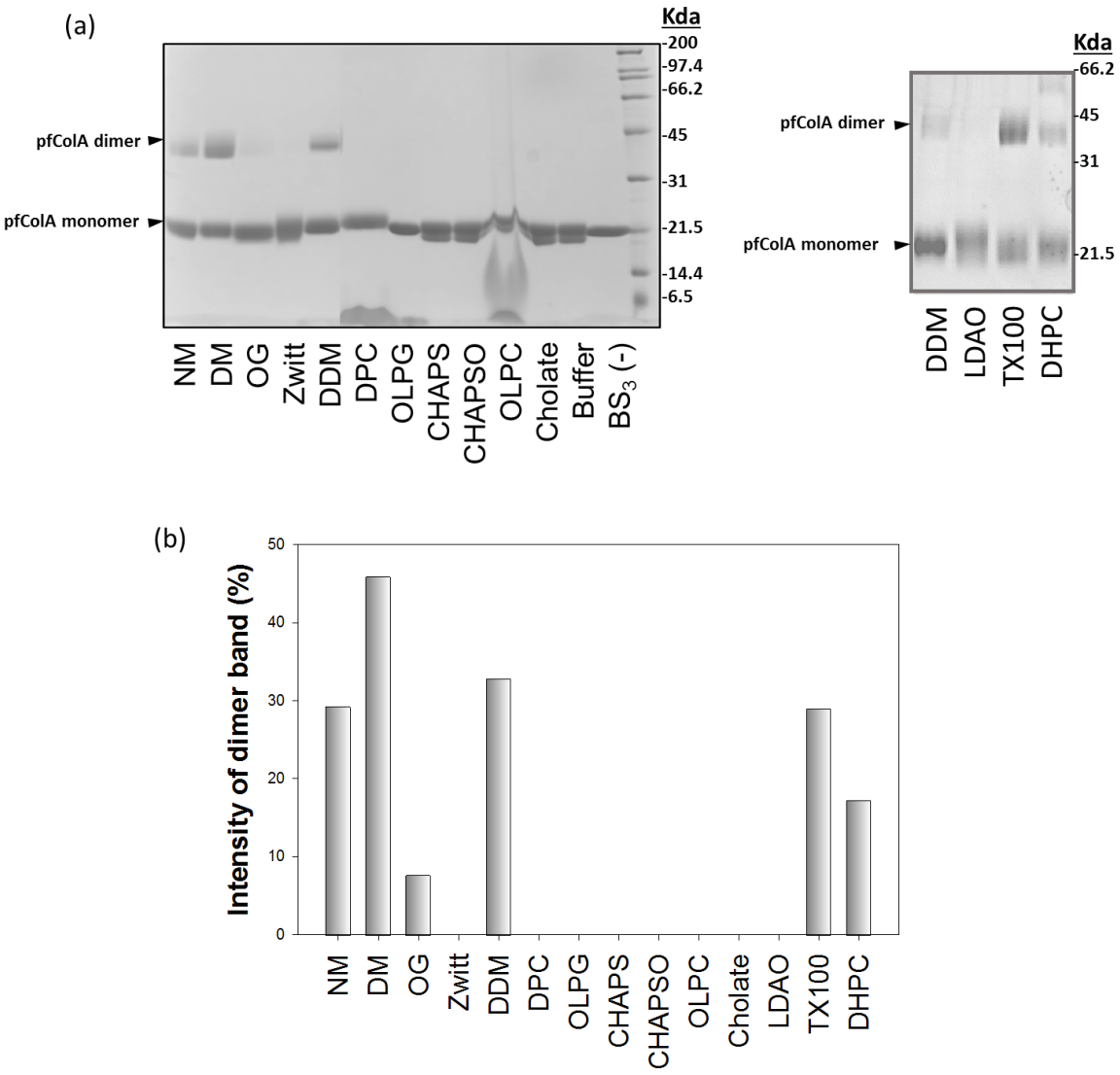

Figure 3.16 pfColA dimerization by BS^3 crosslinking in different detergents. 10 µM of pfColA were incubated with 625 µM BS^3 for 20 min at room temperature. The reaction was stopped by adding 10 mM Tris-HCl. (a) SDS-PAGE gels of the crosslinked samples in the 14 detergents tested. In the left: 0.7% detergent (2% for OG and DPC) in 10 mM HEPES pH 7.5. In the right: 0.1% detergent and PBS, 50 mM NaCl, 1 mM TCEP. (b) Quantification of the band corresponding to the pfColA dimer in the gels by gel densitometry.

3.7 Discussion

The different physico-chemical properties of monomeric and aggregate states of detergents make difficult the interpretation of their effects on protein structure, stability and dynamics of the PDCs formed. Attempts to categorize detergents, e.g., in terms of hydrophilic-lipophilic balance (Davies, 1957; Umbreit and Strominger, 1973; Griffin, 1954), do not consider molecular diversity. Conversely, the behaviour of a specific detergent depends on the

character and stereochemistry of both its head group and hydrophobic tail (Garavito and Ferguson-Miller, 2001), and differential effects can more easily be interpreted when only one of these moieties is changed at a time. A comparison of detergent performance is more pertinent for chemically similar detergents where (i) either a given alkyl chain is combined with different polar head groups, or (ii) a polar headgroup is attached to alkyl chains of different lengths. Thus, some general tendencies have been proposed to rank detergents according to their ability to maintain membrane proteins in their native conformation, where (i) neutral polar headgroups are preferable over zwitterionic and charged headgroups, and (ii) detergents with large polar headgroups (maltoside *versus* glucoside) and long alkyl chains (C12 *versus* C8) are milder solubilizers (Privé, 2007). Here we have analysed several detergents according to these series where, on one hand, alkyl chains of different length are attached to maltopyranoside within the series NM (C9), DM (C10) and DDM (C12), or to dimethylyamineoxide within the series DDAO (C10), LDAO (C12) and TDAO (C14); and, on the other hand, the C12 alkyl group is common to various detergents: LDAO (aminoxide), DDM (maltoside), Zwittergent 3-12 (sultaine), C12E8 (glycolether) or DPC (phosphocholine). Some tendencies have emerged from our studies with the integral membrane protein Cai:

(i) Cai solubilization/extraction from the membrane was higher for zwitterionic, especially phosphate-containing, *versus* neutral detergents with invariant C12 alkyl chain: DPC > LDAO > DDM (Fig. 3.4).

(ii) The same order was found for the capacity of these detergents with variable headgroup to maintain the protein in a monomeric state: DPC > LDAO > DDM (Fig. 3.8).

(iii) The tendency for protein polymerization increased with the alkyl chain length within the maltoside detergent series: DDM (C12) > DM (C10) > NM (C9) (Fig. 3.8)

(iv) Overall NMR spectral quality for CaiH in PDCs formed with C12 detergents improves in the order LDAO > DPC > DDM, i.e. small zwitterionic headgroups appear to be preferable (Fig. 13). For an invariant amine-N-oxide headgroup, shorter alkyl chains yield higher NMR spectral quality: DDAO (C10) > LDAO (C12) > TDAO (C14). Of note, the chain length determines both CMC and size of the micelles, the latter being smallest for DDAO.

Mixed detergent/Cai micelles were characterized by circular dichroism, size exclusion chromatography, chemical crosslinking, NMR spectroscopy, cysteine accessibility, and binding to pfColA. Bile-salt derivatives induced extensive protein polymerization that precluded further investigation. The physical characterization of detergent-solubilized protein indicates that phosphate-containing detergents are more efficient in extracting, solubilizing and maintaining Cai in a monomeric state. Yet, their capacity to ensure protein activity, helix shielding, and high quality NMR spectra was inferior to that of milder detergents. Most importantly, binding to pfColA occurred almost exclusively in sugar-derived detergents. In this case detergents that allow for protein-protein interactions may be optimal for Cai if these interactions are to be studied *in vitro*. In fact, Zhang and cols. reported in 2010 the formation of Cai homodimers through interaction of the transmembrane H3 monitored by *in vivo* cysteine crosslinking (Zhang et al., 2010a). They proposed that the Cai dimer is disrupted upon interaction with pfColA indicating a putative functional implication of Cai oligomerization.

The relative performance of the different detergents in each experiment depends on their impact not only on Cai structure, solubility and oligomerization state, but also on other reaction components and technical aspects. NMR spectra were greatly affected by the solubility, monodispersity, fold and dynamics of the protein-detergent complexes, and none of those tested here provided NMR spectra of sufficient quality to allow for peak assignment. Homogeneity of signal intensities is a commonly accepted criterion for good NMR spectral quality. According to this feature, the best performing detergent in our study was DDAO which also yielded the smallest micelle size with an average MW of 1.4 kDa (see Table 2.1). This result is in line with the general conclusion drawn from previous structural studies of membrane proteins by solution-state NMR where small monodisperse PDCs are preferable as they still allow for rather fast isotropic tumbling thus good relaxation behaviour (Fernández and Wüthrich, 2003); it is essential, however, that these PDCs also stabilize a homogeneous protein conformation to suppress size-independent line broadening.

Detergents with phosphate-containing head groups positively affect Cai solubility and PDC monodispersity. If aligned properly, these negatively charged moieties can provide further stabilization (apart from the dominant hydrophobic contacts) via electrostatic interaction with positively-charged amino acid side chains from Arg and Lys that are commonly located

near the ends of transmembrane elements. This likewise neutralizes electrostatic repulsion within such clusters of positive charges, which also accounts for the stabilizing effect of salts, particularly of multivalent anions like phosphate (Weckström, 1985). Indeed, our Cai fingerprint spectra reveal HE,NE correlation signals from the arginine side chains only in OLPG (Fig. 3.12B) and, most prominently, in DPC (Fig. 3.12D). Both detergents carry phosphate-containing headgroups on long alkyl chains (OLPG: C18, DPC: C12) that apparently allow for suitable alignment and electrostatic interaction with Arg side chains since their NMR observability indicates conformational fixation and protection from fast HN/H_2O exchange.

Functional studies may also be responding to distinct particular requirements. The known biomolecular function of Cai is the capture of exogenous colicin molecules reaching the bacterial inner membrane after internalization from the medium, by forming an inactive binary complex within the membrane. Our Cai/pfColA binding studies suggest that Cai is functional in sugar-derived detergents. These detergents, however, were not optimal in terms of solubility, monodispersity, and NMR spectral quality (alkyl-glycosides appear especially unsuitable for NMR studies). Negative functional results, however, should be considered with caution. For instance, LDAO as well as all other amine-N-oxides in our tests provided the best quality NMR spectra, and the observed failure to promote Cai/pfColA binding could be due to a destabilizing effect on pfColA only. Positive functional results can only be expected with detergents that stabilize the native, complex-forming conformation of both proteins. A similar preference for alkyl-glycosides was also observed in functional studies of other integral membrane proteins. For instance, LPPG was the detergent yielding the best NMR spectral quality and sample lifetime for staphylococcal multidrug resistance transporter (Krueger-Koplin et al., 2004), but the stabilized conformation did not fully correspond to the protein native tertiary structure. Only DDM (and, to a lesser extent, DM) allowed for reproducible ligand binding (Poget and Girvin, 2007). Furthermore, a low-resolution solution-state NMR structure of mitochondrial uncoupling protein 2 (UCP2) was only obtained in DPC (Berardi et al., 2011) although functional studies suggested that the protein was inactive when purified in this detergent (Zoonens et al., 2013). It remains to be established whether the common suitability of alkyl glycosides for functional and crystallographic studies (Newstead et al., 2008) is only due to their mild (i.e. less denaturing) solubilization properties, or whether it is also related to the rather loose binding of these

detergents to the protein surface. Such reversible solubilization would allow for easier dissociation of the unstable protein-detergent complex thus facilitating the association of proteins from different mixed micelles to give rise to homo-oligomers or hetero-dimers, ligand binding (Poget and Girvin, 2007), or protein crystals (Newstead et al., 2008); although, on the other hand, undesired aggregation would also be favoured.

The thermodynamic stability of membrane proteins in complexes with amphiphiles has consequences on protein tertiary structure, solubility, polymerization state, rate of transient exposure of transmembrane segments, and function. This study emphasises the importance of screening a variety of detergents and characterizing protein-detergent complexes by a combination of biophysical techniques in order to obtain a more detailed picture of an integral membrane protein (including its conformational ensemble, oligomerization state and functional features) and guide the rational handling of protein samples. With regard to the Cai protein studied here, we found that there is no single detergent that can be generally applied and would satisfy the requirements for different methodologies used to further study this particular membrane protein.

CHAPTER 4

Functional reconstitution of Cai/pfColA in lipid vesicles

4. Functional reconstitution of Cai/pfColA in lipid vesicles

The reconstitution of the integral membrane protein Cai in model membranes was addressed once the membrane protein had been extracted and purified in detergent micelles. As concluded from experiments described in Chapter 3, the suitability of a given detergent must be assessed from a combination of experimental evidence including stability, tertiary structure, functional integrity and others. The capacity of the solubilized membrane protein to be reconstituted in an artificial membrane would further complement previous data by discarding irreversible detergent denaturation effects. Moreover, the reconstituted protein can be subjected to additional functional studies including binding to, and functional inhibition of pfColA.

In order to address the membrane functionality of Cai, an experimental set-up to monitor pfColA channel activity and its inhibition had to be implemented. Artificial membranes such as those in lipid vesicles are commonly used to elucidate the mechanism of action of membrane proteins with a vectorial transport function. These systems entail the optimization of reconstitution of overexpressed and purified membrane proteins to yield active membrane-embedded proteins in an artificial system. In an effort to meet these requirements, both Cai reconstitution as well as pfColA incorporation strategies were assessed.

4.1 Reconstitution of Cai in proteoliposomes

The correct reconstitution of Cai in the lipid bilayer is required in order to test its ability to inhibit pfColA activity. Reconstitution yield and protein orientation in the bilayer are parameters that have to be tuned prior to attempting activity measurements. Buffers and detergents used to purify the protein, vesicle lipidic composition and specific protocol details are variables that can affect the overall yield and specificity of the reconstitution experiment. Reconstitution of Cai was tested by incorporating the protein to pre-formed liposomes since this generally produces a more homogeneous proteoliposome population (Rigaud and Lévy,

2003). Cai-GFP was purified in a number of different detergents and diluted (1:50) in a detergent-free solution of liposomes. Lowering the initial detergent concentration by dilution allows spontaneous proteoliposome formation (Rigaud and Lévy, 2003). Protein incorporation to liposomes was analysed by fluorescence detection of the C-terminal GFP protein after vesicle float-up centrifugation of protein-liposome mixtures. During ultracentrifugation, liposomes and liposome-bound protein float up to the top of the sucrose gradient owing to their lower density, while free protein and aggregates remain at the bottom of the tube.

All reconstitution assays were performed in 80 mM K_2SO_4, 10 mM TRIS pH 8. Fractions extracted from the bottom to the top of the gradient after ultracentrifugation were assayed for GFP fluorescence intensity and lipidic phosphorous content. Only the detergents LDAO, DDM, Zwittergent 3-12a and to a lesser extent also OLPC, gave rise to protein containing vesicles in the top fraction (Fig. 4.1a). Among all detergent tested, Cai-GFP gave the best reconstitution results in LDAO micelles. Further details of the co-flotation for Cai in LDAO are shown in Figure 4.1S (Supplementary Information).

Different strategies can be followed to favour a certain orientation during membrane protein reconstitution. As a general rule, adding Cai-GFP to the external medium of preformed liposomes will most probably lead to the N-out C-out orientation due to the presence of the GFP domain. This hypothesis was tested by cleavage with TEV protease. A TEV specific recognition site is present in the linker region between the two proteins of the Cai-GFP construct. Cai-GFP in LDAO was incubated with increasing concentrations of DOPG liposomes and equimolar amounts of TEV endoprotease (in a 1:1 molar ratio to Cai-GFP) were added. It is noticeable that complete proteolysis occurs much faster than in detergent preparations, due to the inactivation of the protease in the latter and possibly by co-localization of the positively charged proteins in the negative bilayer surface. The reaction was completed in 2 h at lipid-to-protein ratios of 500 or higher (Fig. 4.2S). These observations suggest that the GFP moiety is not able to cross the bilayer to the vesicle lumen when added to preformed vesicles, although mere superficial association cannot be discarded.

-Cai

The lipid composition of vesicles employed for reconstituted systems can greatly influence the activity of the membrane proteins under study. Phospholipids derived from the native organism are more and more frequently used for functional membrane protein experimental

set-ups (Vitrac et al., 2013; White et al., 2000). The *E. coli* lipid extract contains three main phospholipid classes, phosphatidylethanolamine (PE), phosphatidylglycerol (PG) and cardiolipin (CL) carrying predominantly C16:0, cyc17:0 and C18:1 acyl chains (Andersson, 1996; Raetz, 1978).Thus we sought to compare Cai reconstitution yields in different lipids. For these experiments Cai was used instead of Cai-GFP, in an attempt to avoid obtaining a unique protein orientation conditioned by the C-terminal protein fusion. Float-up experiments were carried out with LUVs of pure DMPC and pure DMPG as well as LUVs of 30:70 mixtures of DMPG/DMPC and LUVs of *E. coli* lipid extract. The protein content of bottom and top fractions of the sucrose gradients after centrifugation were analysed by SDS-PAGE and the lipid content quantified by phosphorous detection. The results obtained for each fraction are plotted in Figure 4.1b. Liposomes composed of the natural *E. coli* lipids gave the highest reconstitution yields. Most of the protein and the liposomes made with *E. coli* lipids were detected at the top of the gradient.

Further proteolysis experiments were then carried out on Cai reconstituted in liposomes made of *E. coli* lipids to gain a better insight into the conformational variations with respect to Cai in LDAO micelles. The specific glutamyl endopeptidase, V8 and the broad specificity protease elastase were used. While after 10 and 40 min digestion with V8 and elastase respectively Cai is completely digested in micelles, protease accessibility is more limited in liposomes (Fig 4.3S). Results obtained with the less specific elastase, cutting at C-end of small hydrophobic residues (Schoomburg et al. 2013) indicate a substantial protection of Cai incorporated into liposomes *versus* the detergent-solubilized protein.

The Cai sequence contains three potential cleavage sites for V8 (after residues 4, 52 and 127) (Fig. 4.3Se). Both E52 and E127 sites are predicted to lie in the periplasmic loops of the protein. As observed in Figure 4.3S three fragments of ~16 kDa, 14.6 kDa and 7 kDa are populated after V8 protease addition to Cai proteoliposomes. The biggest fragment (~16 kDa) is subsequently digested suggesting that although both periplasmic loops are accessible from the liposome exterior, E52 is more exposed. Apparently, incorporation into liposomes shows a preferred orientation with a cytoplasmic loop and N- and C-termini oriented to the liposome interior. This orientation corresponds to the topology Cai adopts in the inner membrane when colicin A reaches it from outside.

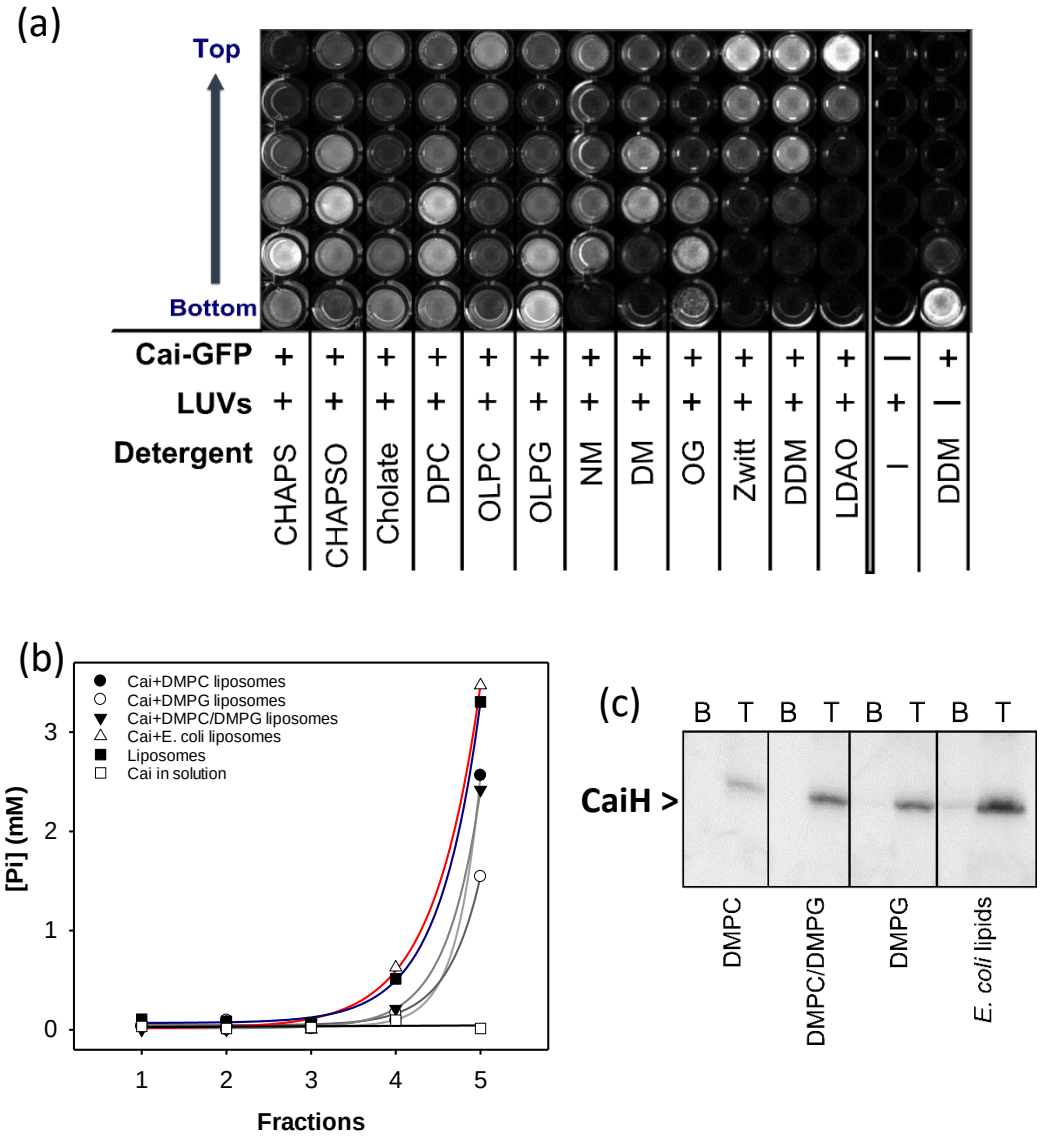

Figure 4.1 Cai reconstitution into liposomes analysed by equilibrium sucrose gradient centrifugation. (a) Detergent screening for Cai-GFP reconstitution. Cai-GFP in 2 % detergent, 150 mM NaCl, PBS pH 7.4 was diluted in a solution of 5 mM liposomes of *E. coli* lipids (protein-lipid ratio of 1:1000) in 80 mM K_2SO_4, 10 mM TRIS pH 8. After separation by isopicnic centrifugation in a discontinuous sucrose gradient, fractions were collected from the bottom to the top, transferred to 96-well plates and analysed by GFP fluorescence imaging. (b), (c) Incorporation of Cai into liposomes of varying lipid composition**.** Liposomes of 100% DMPC, 70:30 DMPC: DMPG, 100% DMPG and *E. coli* lipids were tested. (b) Quantification of phospholipid content of different fractions of the sucrose gradient as measured by Pi content (c) Coomassie-stained SDS-PAGE of bottom (B) and top gradient fractions (T).

Then the effect of protein-to-lipid ratio on the maintenance of liposome integrity was addressed. In the best scenario, proteins should be evenly distributed in the liposome dispersion and the permeability of proteoliposomes minimized, giving them the ability to maintain an ion gradient. To this end the liposome float-up assay was used which allowed us

to detect when the liposomes break because of an excess of added protein-detergent mixed micelles (Fig. 4.4S). The results established that the maximum ratio that can be used before liposomes break down is 1:300, even if subsequent functional experiments were tried at much lower protein concentrations. At least 2000 lipids per protein molecule were used in subsequent flux measurements.

4.2 pfColA incorporation to liposomes

The membrane insertion of pore-forming colicins is thought to depend on two main factors: electrostatic interactions between the protein and phospholipid headgroups (Lakey et al., 1994) and hydrophobic interactions of the apolar core of the protein with the hydrocarbon core of the membrane (Lakey et al., 1991). The hydrophobic hairpin of pfColA is protected by surrounding amphipathic helices in the water-soluble conformation, hence the acquisition of an unstable insertion-competent state has been proposed as intermediate in the membrane insertion pathway (van der Goot et al., 1991). In order to trigger such destabilization of the water-soluble conformation, different methodologies have been described in the literature, ranging from the use of acidic pH, anionic lipids, detergents or urea (Dunkel et al., 2015; Pulagam and Steinhoff, 2013; Wu et al., 1999). It is becoming more and more apparent that the discrepancies between different topological models proposed for the membrane inserted form of pfColA, may arise from the experimental conditions used to trigger its insertion (Padmavathi and Steinhoff, 2008). Because not all the membrane-associated colicin conformations seem to be active (Zakharov and Cramer, 2002b), some effort had to be directed to screen for an appropriate pfColA incorporation method.

With the final objective of setting-up a functional test for the ion channel activity of pfColA and its inhibition by Cai, it was important to determine how different membrane insertion conditions affect pfColA incorporation yields. More specifically, we aimed at exploring different ways of inducing pfColA incorporation into liposomes, in such a way that the protein inserts quantitatively into the membrane while maintaining the structural and activity features close to the physiological membrane scenario.

To estimate the extent of pfColA partitioning into vesicles we performed fluorescence resonance energy transfer (FRET) measurements between the tryptophans of the protein and dansylated lipids present in liposomes of different lipid compositions (Fig. 4.5S). The results show pfColA incorporation into DOPG liposomes at pH 4.0, but not at pH 7.0, suggesting that even when using anionic liposomes the protein must be destabilized to induce insertion into the bilayer hydrophobic core.

The use of a moderately low pH (pH 4-5) to trigger the membrane insertion of colicin A presents several drawbacks. Although lowering the pH to 5 enhances the electrostatic interaction with membrane phospholipids as pfColA gets positively charged (pI 5.8), the protein is more likely to get adsorbed rather than inserted into the membrane (Padmavathi and Steinhoff, 2008). Most of the experiments that speak in favour of the penknife model for membrane-inserted pfColA, were carried out with liposomes of 100% DOPG at pH 5.0. Lower pH values (pH 3.0 or below) are thought to be necessary to obtain the insertion-competent state (van der Goot et al., 1991). Following this premise, Pulagam and cols. pre-incubated the protein at pH 2.0 before adding it to liposomes at neutral pH (Pulagam and Steinhoff, 2013). Therefore, we tested this and other denaturation treatments to trigger the physiological membrane-inserted pfColA state, including pre-incubating in 9.5 M urea, incubation in the detergent DDM, incubation with the anionic lysophospholipid OLPG or thermal denaturation. Table 4.1 summarizes the typical yields of incorporation after dilution (1:500) of the protein from different denaturing conditions into liposomes of *E. coli* lipids prepared at pH 7.0. After dilution, a competition is established between renaturation and lipid partitioning; hence, the relative rates of both reactions in the different media will determine the final yields quantified by FRET. Differences in the extent of incorporation revealed the implication of both electrostatic and hydrophobic interactions governing the membrane insertion process. Extensive unfolding in 9 M urea caused the highest incorporation yields while the acidic pH jump (pH 2) in low and high ionic strength conditions, reflects the interplay of electrostatic and hydrophobic interactions (Lakey et al., 1994). The non-ionic detergent DDM triggered a moderate level of binding (22%) while the negatively charged OLPG allowed an even lower insertion (11%).

The use of thermal denaturation to trigger pfColA incorporation constitutes an alternative means of destabilization and incorporation which would presumably favour a more homogeneous population of protein containing liposomes. Vesicles of *E. coli* lipids were mixed at the desired proportions and heated for 10 min at 50 °C, this way protein destabilization occurs when lipid and protein solutions are already fully mixed. The incorporation yields by thermal treatment however did not exceed 10%. Thus the heat denaturation was combined with destabilization by mutation to increase protein partitioning into liposomes. Mutant V119A, with a denaturation T_m of 61 °C, increased the incorporation yield from 10% for WT pfColA (T_m=72 °C) to 48% (Table 4.1).

Tabla 4.1 pfColA and V119A incorporation into liposomes of *E. coli* lipids, at a lipid concentration of 0.1 mM (Ri 500) and pH 7.0, data derived from FRET measurements of tryptophan to dansyl-doped vesicles.

	Percentage of incorporation
pfColA	0
pfColA in 9M urea	82
pfColA in pH 2.0	65
pfColA in pH 2.0, 150 mM NaCl	46
pfColA in 1% DDM	22
pfColA in 1% OLPG	11
pfColA after 50 °C for 10 min	10
V119A after 50 °C for 10 min	48

The effectivity of thermal denaturation to trigger pfColA incorporation into vesicles was further validated by separation and quantification of the free and liposome-bound protein by size exclusion chromatography. 14 µM pfColA or V119A were incubated with liposomes of DOPG or *E. coli* lipids at 7 mM (molar ratio 1:500) pre-heated at 50 °C and separated in Superose 6 column in 160 mM NMDG-SO_4 and 20 mM HEPES pH 7.0 buffer. Figure 4.2a corresponds to a representative chromatogram comparing WT pfColA and V119A binding capacity, the liposome fraction eluted at 7 ml and the free protein at 17.3 ml. Free protein recovered after the 50 °C incubation was fully native as judged by the elution profile and no traces of aggregation were observed. Quantification of the liposome-bound and free protein was performed by densitometry of the protein bands corresponding to the liposome and free protein fractions separated in the chromatography and analysed by Coomassie stained SDS-PAGE gel (Fig. 4.2b). Higher binding yields were detected for V119A (90%) as compared to WT pfColA (20 %) while using liposomes of 100% DOPG did not improve protein incorporation to a considerable extent as demonstrated previously (Fig. 4.5Sc). Thereby the amount of anionic

lipids present in *E. coli* lipid extract (20%) is sufficient to ensure maximum insertion of the protein as previously suggested (Géli et al., 1992).

It is worth noting that at the same protein to lipid ratio (1:500) higher concentrations of both components gave a two-fold increment in incorporation yields (FRET experiments were done at 0.1 mM lipid while SEC was done at 7 mM). Liposomes of *E. coli* lipids were employed in functional assays considering not only that similar incorporation yields can be attained but also previous evidence showing that colicins are not active in liposomes of 100% negatively-charged lipids (Lindeberg et al., 2000; Zakharov et al., 2002). Indeed, the trypsin digestion profile of pfColA in DOPG liposomes at pH 4.0 turned out to be different from the protein bound to liposomes of native lipids at neutral pH (Fig. 4.2c). To perform the limited proteolysis assay free protein was separated from liposome-bound protein after temperature-induced incorporation. It is tempting to speculate whether this membrane-adsorbed conformation gave rise to the postulation of the penknife model for the membrane inserted conformation of pfColA, while the umbrella model is the physiologically relevant conformation.

To ensure that liposomes remain tight after pfColA incorporation by heat treatment, a permeability assay was carried out at different protein-to-lipid ratios. The release of liposome content from vesicles of *E. coli* lipids was monitored by the fluorescence increase of released ANTS previously encapsulated together with DPX. When both molecules are inside the vesicle DPX acts as ANTS quencher. Fluorescence measurements were performed at the same lipid concentration as the FRET assay used to quantify pfColA incorporation yields (0.1 mM). ANTS fluorescence was shown to be negligible for pfColA concentrations up to 1 µM (Ri 1:200) (Fig. 4.2d). Considering that pfColA incorporation yields do not outreach 10% of the added protein, a nominal 1:200 ratio corresponds to an effective 1:2000 ratio of bound protein. The same experiment was performed with the destabilized V119A mutant for which protein concentrations of 0.1 µM (Ri 1: 1000) induced moderate release of ANTS that became massive at 0.5 µM (Ri 1:200). Thus, taking into account that the incorporation efficiency of V119A to 0.1 mM lipid is around 50%, liposomes became leaky over an effective protein-to-lipid ratio of 1:2000. In subsequent ion conductivity assays, molar ratios of 1:10000 and higher were used, well above the leakage threshold.

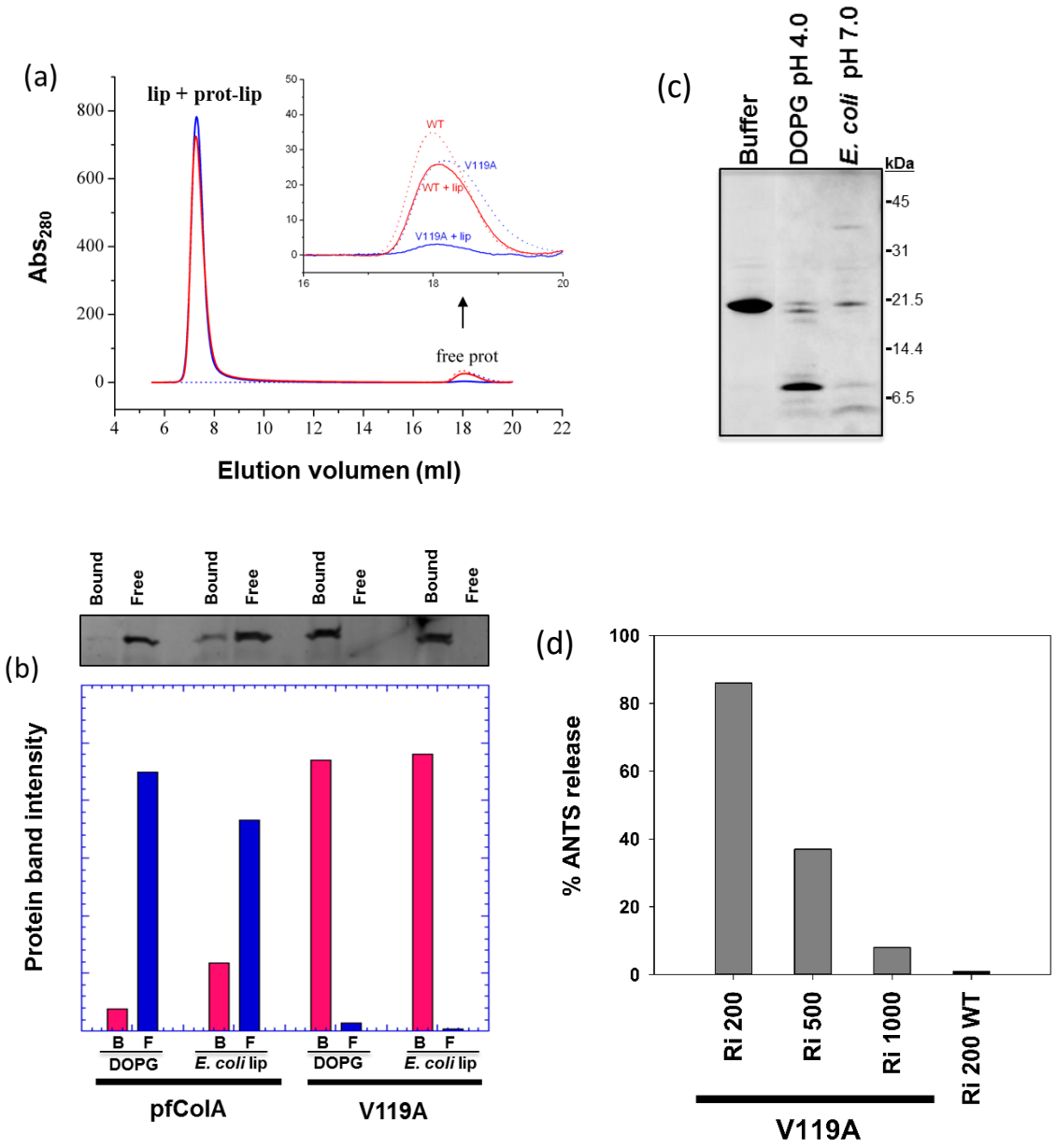

Figure 4.2 Incorporation of pfColA and V119A into liposomes of *E. coli* lipids, separation and quantification of free protein and protein incorporated to liposomes by size exclusion chromatography. (a) Size exclusion chromatography traces (absorbance 280 nm) of lipid-protein mixtures at Ri 1:500 (7 mM lipid) incubated for 10 min at 50ºC, for wild-type pfColA (red) and V119A mutant (blue). Liposomes eluted at 7 ml and free protein at 17.30 ml. (b) Protein quantification of the liposome bound and free protein fractions from SEC. Coomassie-stained gel and quantification of protein bands by densitometry. Bound protein in magenta (B) and free protein in blue (F). (c) Limited proteolysis profile of membrane bound pfColA (d) Effect of increasing concentrations of pfColA and V119A added to liposomes of *E. coli* lipids on dequenching of encapsulated ANTS/DPX. Content leakage measured by fluorescence of released ANTS (λ_{ex} = 365 nm and λ_{em} = 515 nm). The extent of leakage was calculated from the equation % ANTS release= $[(F_t-F_0) / (F_{100} - F_0)]$ x 100 where the baseline fluorescence is subtracted and the 100% of released assigned to the fluorescence value obtained after Triton X-100 addition. Ri values indicated correspond to added protein; protein incorporation was estimated to be 50% for V119A and 10% for WT pfColA (Table 4.1).

4.3 pfColA activity in liposomes of *E. coli* lipids

Once Cai reconstitution and quantitative pfColA incorporation into *E.coli* model membranes were achieved, efforts were aimed at arranging an experimental set-up in which the activity of pfColA, as well as its inhibition by the immunity protein, could be assessed. In such a vesicular system, a more careful control of the level and mode of protein incorporation were feasible.

The precise mechanism by which colicin A exerts its cytotoxic activity is not well understood, however a remarkably high proton conductance has been reported for the colicin A channel (Slatin et al., 2008). Thus we aimed at measuring the pfColA mediated proton influx using the pH probe phenol-red encapsulated in liposomes of *E. coli* lipids. Absorbance of the basic form of phenol-red (λ_{max} = 559 nm) was monitored upon pfColA insertion after heat treatment. This methodology allows to detect the acidification of an otherwise unbuffered internal solution. Given that pfColA activity has been shown to be voltage-dependent (Bourdineaud et al., 1990), the potassium ionophore valinomycin was used to induce a potassium diffusion potential of approximately 100 mV (Andreoli et al., 1967). Liposomes were loaded with K_2SO_4 and dispersed in an iso-osmolar Na_2SO_4 buffer. Upon addition of valinomicyn, potassium diffuses down its concentration gradient building up an electrical potential across the membrane. Figure 4.3a shows the time-course absorbance decay upon valinomycin addition for increasing amounts of pfColA. After approximately 1000 s, the protonophore carbonyl cyanide m-chlorophenyl hydrazine (CCCP) was added, inducing further internal acidification by K^+/H^+ exchange. Under these conditions, a chemical H^+ gradient is created at the expense of the K^+ gradient due to the facilitated diffusion of both ions. Absorbance (A_{599}) values obtained in equilibrium after CCCP addition indicate the extent of the K^+ gradient remaining after the previous step of pfColA and valynomycin combined effect.

Increasing amounts of pfColA produced progressively steeper decreases in internal pH (Fig. 4.3a). The initial slope and amplitude of the induced pH jump are linearly dependent on the added protein concentration up to 50 nM (Fig. 4.3d). Above this threshold the amplitude of the pH drop becomes saturated, as most liposomes contain more than one pfColA channel and thus the membrane potential rapidly decreases. This is consistent with the proposed

mechanism of colicins in which channel opening requires an energized membrane, around 110 mV, that produces a single channel conductance in the order of 10^6 ions·channel^{-1}·sec^{-1} (Bourdineaud et al., 1990; Gouaux, 1997). Once the potential drops below 80 mV the channel closes, subsequently the cell manages to restore its transmembrane potential and the colicin channel opens again (Bourdineaud et al., 1990). Obviously the lipid vesicles used here do not allow channel reopening as mechanisms for membrane potential rebuilding are absent.

Differences in final absorbance measurement after CCCP addition are indicative of the total H+/K+ exchange under facilitated diffusion conditions. Interestingly, addition of higher pfColA concentrations produced lower pH jumps after valinomycin and CCCP addition (Fig. 4.3a). This smaller internal pH drop suggested that pfColA-mediated H^+ entry, happening in the first part of the trace, was not the only effector counter-balancing the valinomycin-induced electrical potential. Thus the fact that the remaining K^+ gradient was lower for increasing pfColA concentration would reveal the passage of other ions (most probably Na^+, while $SO_4^=$ concentration is symmetrical in both compartments). A putative discontinuity in the membrane permeability barrier was ruled out at an effective protein-to-lipid ratio of 1: 10000, as previously assessed by content leakage assay (Fig. 4.2d). Note that phenol-red could not report the conduction of ions other than protons.

To explore the participation of ions other than protons in pfColA functionality, equivalent experiments were performed placing cations of different sizes in the external solution. Inside the liposomes, K_2SO_4 was encapsulated as it is required to induce the membrane potential, while Li_2SO_4 or $NMDG_2SO_4$ were added to the external buffer. N-methyl-D-glucamine (NMDG) was chosen as it is a membrane-impermeable organic cation commonly used to block K^+ channels owing to its larger size (Wang et al., 2009). As depicted in Figure 4.10c, pfColA-mediated proton influx was more prominent in the case of $NMDG_{out}$ as protein concentration increased (Fig. 4.3c), while the total pH jump after CCCP addition remained equal for all the pfColA concentrations tested (Fig. 4.3e). This evidence supports the hypothesis that when Na+ is substituted by an impermeable ion, pfColA activity is detected only as the conduction of protons. An intermediate behaviour was observed for liposomes with Li^+_{out} and K_{in}^+ (Fig. 4.3b) suggesting that upon membrane energization both protons and lithium ions are conducted. This is reflected in Figure 4.3e where the net change in absorbance for Li^+_{out} is

higher than the CCCP induced pH jump in Na^+_{out}. The absence of an initial lag phase in the protein concentration-dependence of activity measurements argues in favour of the monomer as the proton-permeable species (Fig. 4.3d). The same conclusion can be deduced from the calculated protein-per-vesicle ratio. Considering that the estimated incorporation yield of pfColA by heat treatment is about 10%, and that vesicles with a diameter of 100 nm contain approximately 10^5 lipid molecules (Butko et al., 1996), at most a single protein monomer could have been incorporated into each vesicle at the lowest pfColA concentration tested.

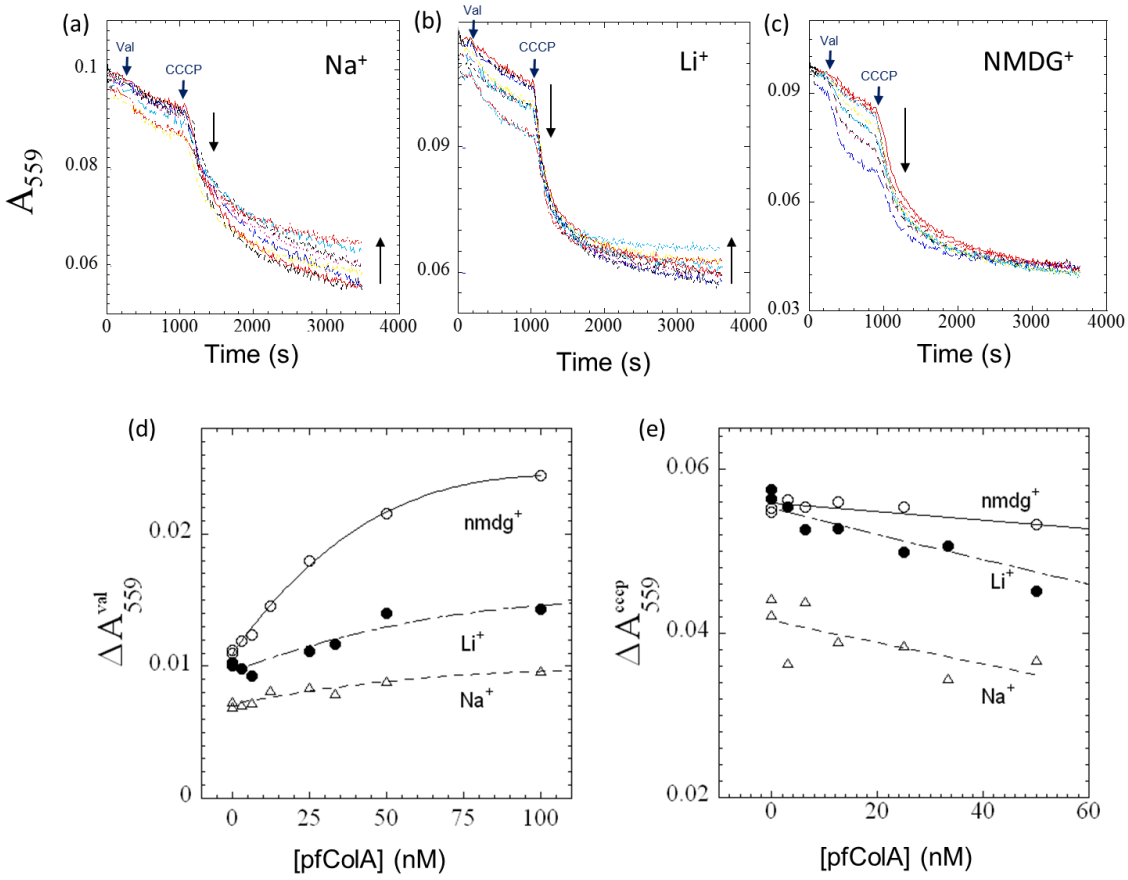

Figure 4.3 Cation conductance through pfColA ion channel. Time course of the decrease in absorbance at 559 nm of the basic form of phenol red (10 mM) encapsulated in 0.1 mM total *E. coli* lipid LUVs. Internal buffer also contained 75 mM K_2SO_4 and was initially equilibrated at pH 7.8. 0.83 nM valinomycin was added after 200 s and 6.45 nM CCCP at 1000 s. Arrows indicate increasing concentrations of pfColA from 0 to 100 nM. Different cations were placed outside the liposomes: (a) Na_2SO_4 (b) Li_2SO_4 (c) $NMDG_2SO_4$. (d) Net absorbance decrease upon valinomicyn addition plotted against pfColA concentration (e) Net absorbance decrease upon CCCP addition plotted against pfColA concentration.

This data provide some insight into pfColA ion selectivity. We estimated that in the absence of a pH gradient, the external Na^+ concentration (132 mM) was $4 \cdot 10^6$ times higher than that

of protons at pH 7.5. Considering that the pH jump induced by pfColA in the presence of valinomycin was approximately 1/5 of that observed for $NMDG^{+}_{out}$, the permeability of the pfColA channel to protons, relative to that of Na^{+}, was approximately six orders of magnitude larger. Overall, our results were consistent with the idea that pfColA preferentially transports protons but also other small cations, such as sodium and lithium, dissipating the valinomycin-induced trans-negative potential.

More importantly, the ability to monitor the dose-dependent voltage-dependent activity of pfColA in *E. coli* liposomes provided a valuable experimental set-up in which Cai activity could be addressed. Thus phenol-red acidification was used as a reporter of valinomicyn-induced pfColA activity in the presence or absence of its cognate immunity protein Cai.

4.4 Inhibition of pfColA activity by Cai in liposomes of *E. coli* lipids

Both Cai and Cai-GFP were tested against the proton-conducting activity of pfColA. A first inhibition experiment was designed in which 25 and 50 nM of pfColA were added to liposomes of *E. coli* with or without the reconstituted immunity protein. The results for the addition of pfColA to control liposomes in the absence of Cai are shown in Figure 4.4a. For Cai-containing liposomes, significant inhibition could only be observed when Cai (but not Cai-GFP) was used to form proteoliposomes at Ri 2000 (Fig. 4.4b). The GFP fusion protein incorporated to preformed vesicles was unable to inhibit the H^{+} efflux induced by pfColA (Fig. 4.4c). The reason why Cai-GFP failed at blocking pfColA is not clear, but most probably the non-functional orientation is predominant as demonstrated above (Fig 4.2S).

Considering that 10% of the added pfColA is actually incorporated to liposomes by the heating method the actual Ri values for pfColA were higher than 20000 in these experiments, what represents a Cai:pfColA ratio of more than ~10. This limitation motivated us to design an experiment in which the number of incorporated pfColA molecules could range below and above the equimolecular relation to Cai. Thus, studying the behaviour of pfColA channels when their concentration exceeded that of reconstituted Cai molecules seemed to be a good approach to address the mechanism of Cai inhibition.

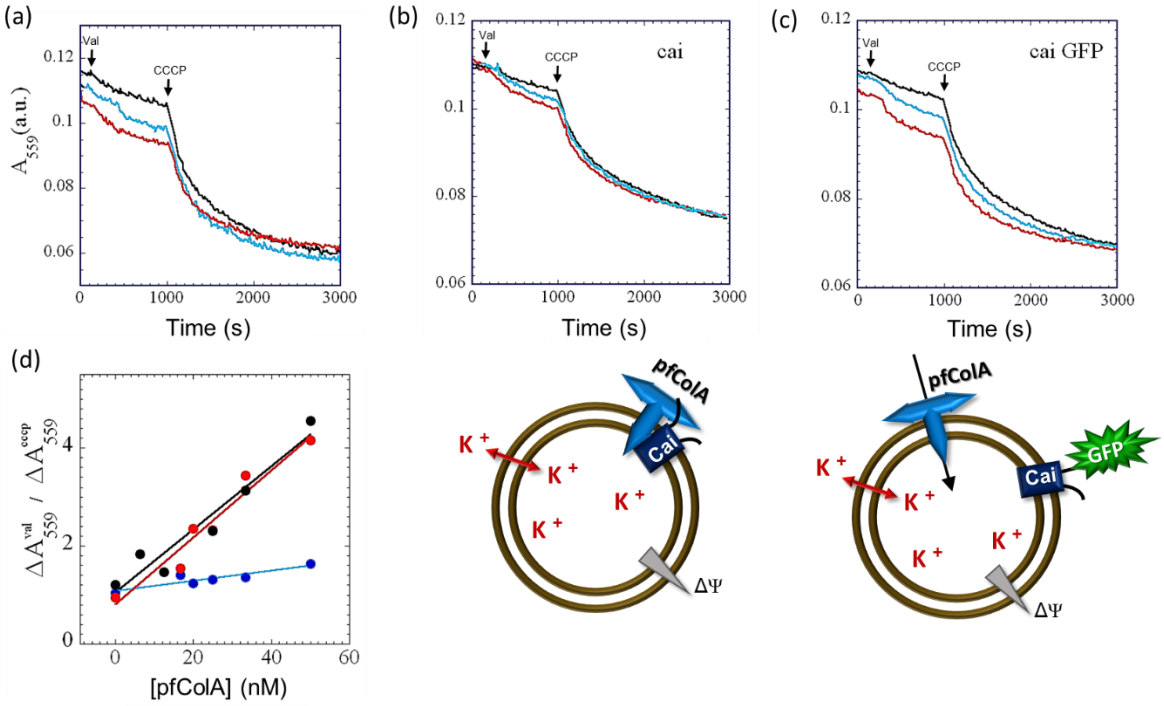

Figure 4.4 Experimental setup for analysis of pfColA inhibition by Cai and representative A559 traces. LUVs of *E. coli* lipids at 0.1 mM were heated for 10 min at 50 °C in the absence (black) or in the presence of 25 nM (blue) or 50 nM (red) pfColA. Valinomycin (0.83 nM) was added at 200 s and CCCP (6.45 nM) at 1000 s. (b) Activity of pfColA is only inhibited by cleaved Cai reconstituted during liposome formation at Ri 2000. (c) Results obtained with Cai-GFP under similar conditions are undistinguishable from those in control experiments without Cai (a). (d) Plot summarizing the relative changes in A_{559} after valinomycin and CCCP addition as a function of added pfColA for control liposomes (black), proteoliposomes with Cai-GFP (red), and proteoliposomes formed with cleaved Cai (blue).

In order to gain more insight into the inhibition mechanism, liposomes with lower Cai content were prepared (9 nM Cai in 0.04 mM lipid, 1:4500) and pfColA was added over a range of 0-25 nM. Incorporation of pfColA into liposomes of *E. coli* lipids was triggered by pre-incubating the protein in denaturing conditions (9.5 M Urea, 0.1 M H_2SO_4). Incorporation to liposomes was expected to be highly efficient under these conditions (yield ~ 80%) and effective Ri values were closer to those estimated from the amount of added protein. As concluded from section 4.3, phenol-red absorbance is a better reporter of pfColA activity when only protons are allowed to go through, for this reason $NMDG^+$ was placed in the external buffer.

We started by analysing pfColA-mediated liposome acidification upon valinomycin addition in the absence of Cai to understand the dose-dependent effect in detail. The results on proton influx (A_{559} decay) induced by increasing amounts pfColA on 0.04 mM liposomes are shown in

Figure 4.5a. Net absorbance change values (ΔA_{559}) showed a linear dependence with respect to added protein up to 8.5 nM (Ri ~ 3500), which approximately represents 20 pfColA protein molecules per liposome (4.5a). The fact that the time-course absorbance measurements are rapidly stabilized after the exponential decay, is consistent with the reported activity of colicin A *in vivo* (Bourdineaud et al., 1990). As a consequence of pfColA activity, K^+ concentration inside the liposomes rapidly decreases. This in turn will produce dissipation of the electrical potential below a threshold, the pfColA-mediated proton diffusion rate will decrease and no further acidification will be measured. If there is enough pfColA to induce the acidification of virtually all liposomes, adding more channel forming proteins (more than 20 molecules per liposome on average) would not change the ΔA_{559} value at which pfColA activity saturates. We speculate that below this threshold not all the liposomes are affected by pfColA activity and therefore, adding more pfColA molecules still has an additive effect on ΔA_{559}.

Despite ΔA_{559} being constant above a certain Ri, the initial slope ($\Delta A_{559}/\Delta t$) was linear up to higher protein concentrations (Fig. 4.5b, filled circles). In fact, higher pfColA/lipid molecularities induced higher initial ion fluxes even if the same saturation value was reached.

Then the initial proton efflux rate was used to study the inhibitory effect of Cai over pfColA. Increasing amounts of pfColA (0-25 mM) were added to Cai (9 nM) containing proteoliposomes. Comparing the net absorbance change per second ($\Delta A_{559}/\Delta t$) for liposomes with or without Cai revealed that below 3 nM similar amounts of pfColA did not induce a dose-dependent proton efflux in the presence of Cai (Fig. 4.5b, open circles). This threshold value (Fig. 4.5b dashed line) was calculated by extrapolation of the linear region to null activity. Considering that not all reconstituted Cai adopts the correct topological orientation required to neutralize unidirectionally inserted pfColA molecules, the effective Ri value for Cai lays far above 1:4500. Given that the effective incorporation of pfColA corresponds to an approximate Ri of 8000, the pfColA concentration at which pfColA activity is recovered is in good agreement with a 1:1 complex. This result suggests that a stable inactive complex is formed between pfColA and Cai in the bilayer and that pfColA monomers exceeding accessible Cai sites retained almost full activity. Each Cai could only inhibit the pfColA molecule to which it is bound, which implies that upon formation the Cai/pfColA complex is highly stable.

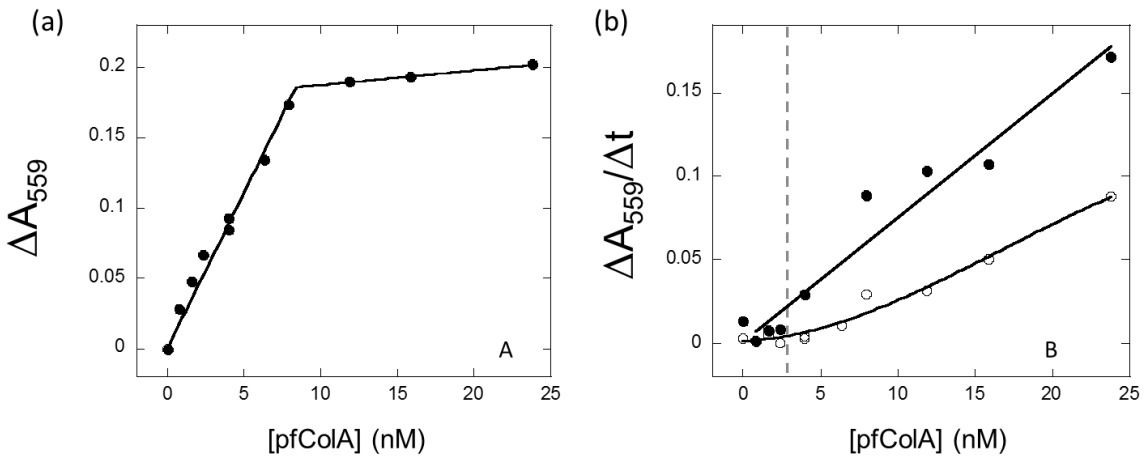

Figure 4.5 Acidification of the liposome lumen after valinomycin addition as a function of added pfColA concentration. Incorporation of pfColA was triggered by urea denaturation (9.5 M urea) to liposomes of *E. coli* lipids at 0.04 mM (incorporation yield ~ 80%) (a) Net absorbance change plotted against pfColA concentration (b) The initial velocity, or net absorbance change per second plotted against pfColA concentration for proteoliposomes containing pfColA (●) or pfColA and previously reconstituted Cai (1:4500) (○). Dashed line indicates the intersection between the initial trend and the subsequent linear increment after the number of pfColA molecules exceeds that of reconstituted Cai molecules.

4.5 Discussion

Taken together, this data indicate that the Cai/pfColA toxin/antitoxin pair can be functionally reconstituted in artificial membranes *in vitro*. Both Cai and pfColA can be incorporated into model membranes mimicking the native lipid composition found in the bacterial inner membrane. As compared to simple lipid mixtures made from a few synthetic lipids, higher Cai reconstitution yields could be obtained in biomimetic bilayers composed of the *E. coli* total lipid extract.

The cytotoxic activity of pfColA was addressed using different ion gradients revealing that pfColA exhibits measurable permeability to Na^+ and Li^+, but the channel selects for H^+ over Na^+ by a factor of approximately 10^5-10^6. This is in good agreement with previously reported high proton conductivity of colicin A (Slatin et al., 2008, 2010). Time-course absorbance was measured to follow the pH changes inside the liposome yielding three main conclusions: (i) pfColA proton efflux is a voltage-dependent transport, (ii) it causes partial depletion of membrane potential in a dose dependent manner, and (iii) this activity is inhibited to a great extent by the interaction with the immunity protein Cai.

It is believed that the lateral diffusion of immunity proteins in the membrane would ensure the rapid recognition of the imported colicin (Geli and Lazdunski, 1992; Zhang and Cramer, 1993). Interestingly, according to the results presented, a saturation of the reconstituted Cai at high pfColA concentration gave rise to a subsequent recovery of the channel function. This observation is consistent with a very stable and permanent complex within the membrane, but could apparently represent a rather ineffective inhibition mechanism. Putative scenarios in which the multiplicity of colicin molecules exceeds that of immunity proteins in the bacterial inner membrane would end in cell death. Estimates of the number of immunity proteins per cell, around 10^2-10^3 (Song and Cramer, 1991), seem sufficient to protect the cell against colicin action. Colicinogenic bacteria withstand cognate colicin concentrations 10^4-10^7 times higher than those required to kill non-immunized bacteria (Pugsley, 1988; Cramer et al., 1995). The most commonly accepted explanation for this high resistance is that a small number of exogenous colicin molecules does actually reach the inner membrane due to saturation of the entry sites. It has been estimated that each bacteria contain about 400 colicin A receptors and 1000 translocation sites (Duché et al., 1995) located at the contact sites between the outer and inner membranes (Guihard et al., 1994). Thus, immunization will be effective as long as the number of immunity protein molecules per cell surpass those of functional BtuB and OmpF receptors or Tol translocation sites.

4.6 Supplementary information

Figure 4.1S

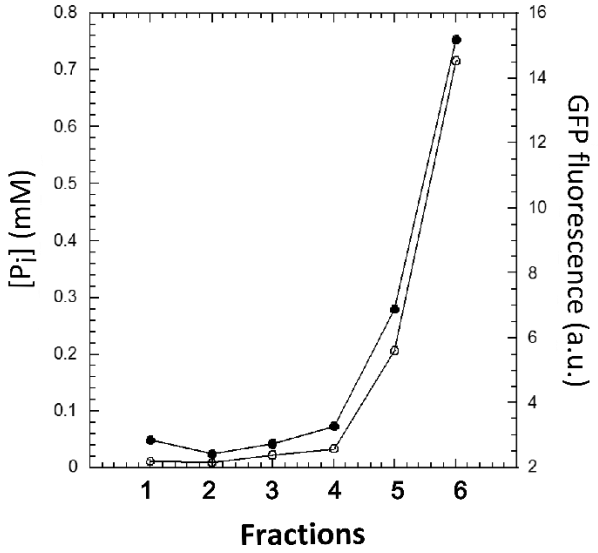

Co-flotation of Cai-GFP with liposomes of *E. coli* lipids. Cai-GFP in LDAO was pre-incubated with liposomes and separated by isopicnic ultracentrifugation in sucrose gradient. Gradient fractions were collected starting from the bottom and assayed for protein and lipid content by GFP fluorescence (●) and phosphate quantification (○), respectively.

Figure 4.2S

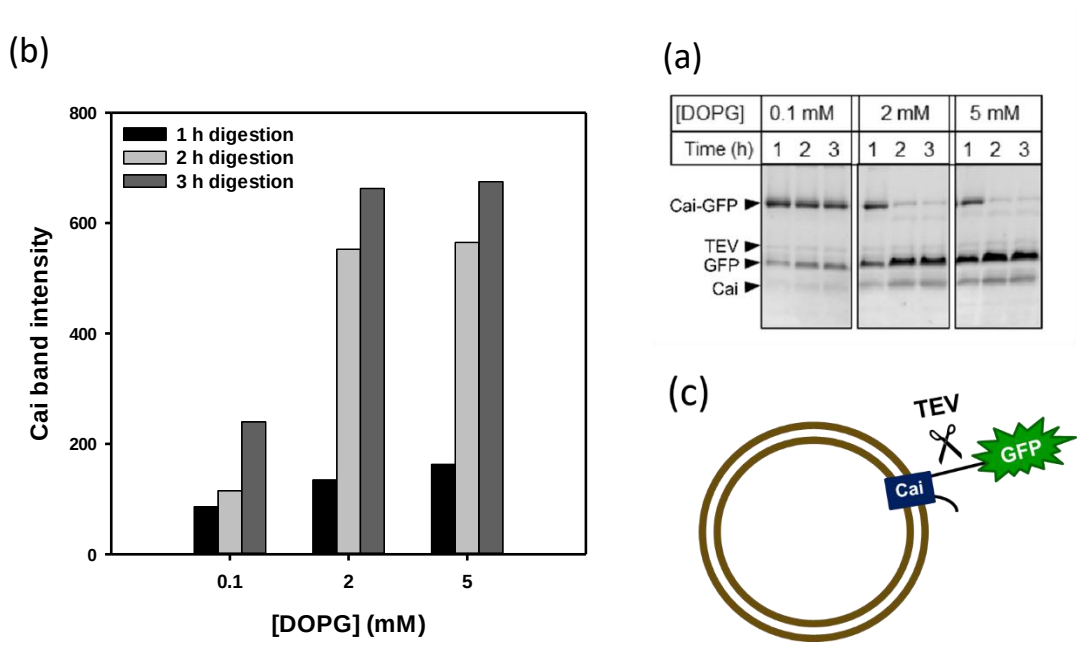

Cai-GFP digestion by TEV protease in lipid vesicles composed of DOPG. Protein samples in 0.2% DDM, 150 mM NaCl and PBS pH 7.4 were incubated with LUVs at lipid concentrations of 0.1 mM, 2 mM and 5 mM, corresponding to protein-lipid ratios of 1:25, 1:500 and 1:1250 respectively. The reaction was stopped after 1, 2 and 3 h and loaded on a SDS-PAGE gel (a) and the band corresponding to Cai quantified and plotted against lipid concentration (b). Considering the bulkiness of the fused GFP moiety, the most probable orientation is illustrated in (c). Liposomes of DOPG were used in this experiment after observing surprisingly high cleavage yields when Cai-GFP was incorporated into them. There are several possible explanations for low proteolysis yields for the protein-detergent complex. The detergent could block the accessibility of the protease to the cleavage site. Previously reported detrimental effects of detergents over TEV proteolytic activity should also be taken into account (Lundbäck et al., 2008).

Figure 4.3S

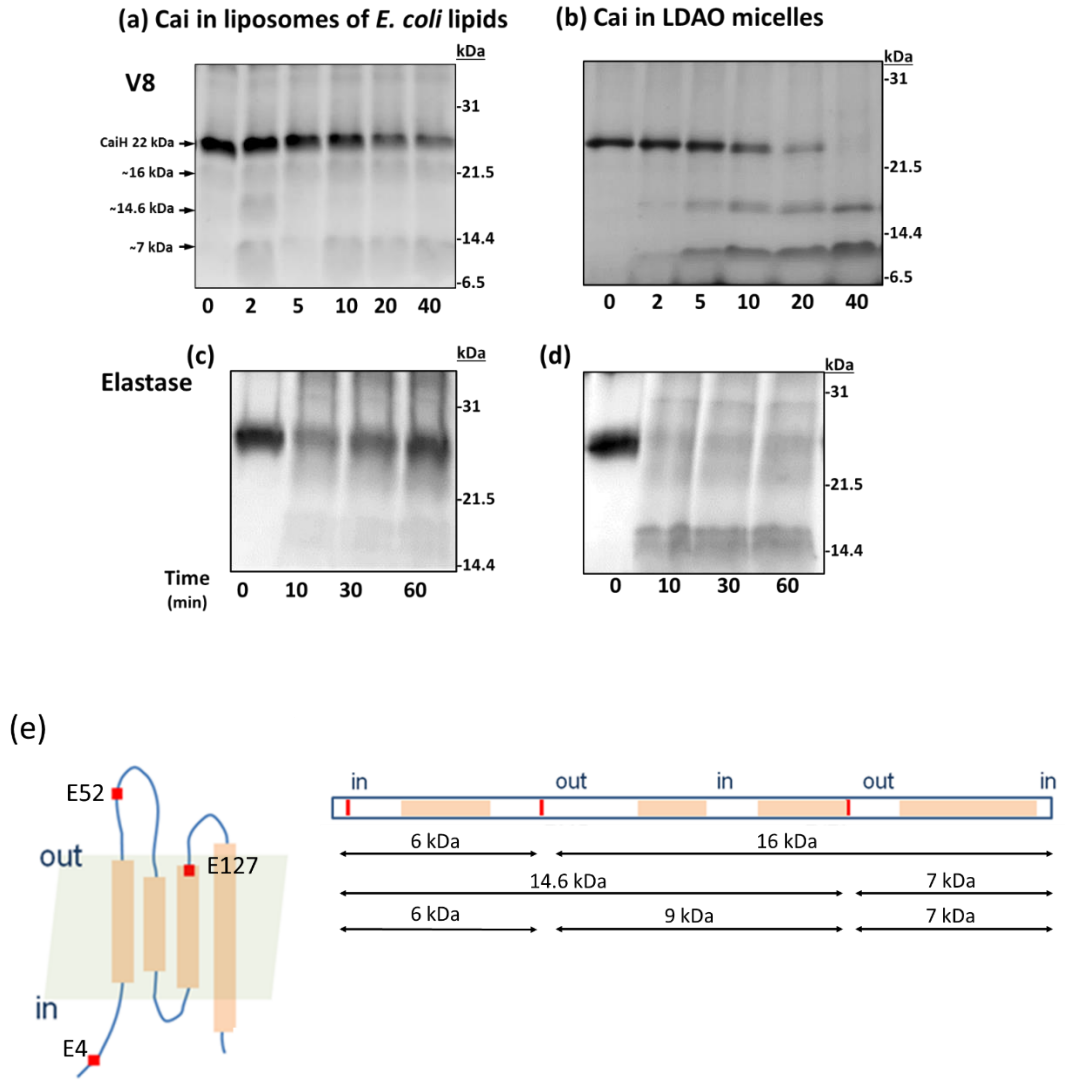

Limited proteolysis of CaiH in liposomes of *E. coli* lipids compared with micelles of LDAO by glutamyl endopeptidase V8 and elastase. For the proteolysis in liposomes CaiH was reconstituted and proteoliposomes were separated by sucrose gradient. For V8 digestion 25 µM CaiH was incubated at 37 °C with 4 µg of V8 protease in 50 mM NaCl, 1 mM TCEP, 50 mM TRIS pH 7.5, in the presence of liposomes at 12.5 mM (a), or 0.05% LDAO (b). For elastase digestión 50 µM CaiH was incubated at 37 °C with 0.5 µg of elastase protease in 50 mM NaCl, 1 mM TCEP, 1 mM EDTA, 50 mM TRIS pH 7.5, in the presence of liposomes at 20 mM (c) or 0.1% LDAO (d).(e) Locations of cleavage sites of V8 proteasa in Cai sequence and topology model, molecular mass of putative fragments.

The glutamyl endopeptidase V8 could cleave Cai at its 3 putative cleavage sites: E4, E52 and E127, while pancreatic elastase cleaves protein at the carboxyl side of small hydrophobic amino acids such as Ile, Gly, Ala, Ser, Val, and Leu (Schomburg and Salzmann, 2013). In some cases, orientation of membrane proteins after reconstitution can be determined by the

proteolytic band patterns before and after proteolytic treatment of the reconstituted sample (Rigaud et al., 1983). The experiment of V8 can provide interesting information about the orientation of the reconstituted protein as E52 and E127 residues happen to be located at the two periplasmic loops of Cai. Results for the proteolysis with V8 indicate that glutamate residues are more exposed in the micellar system compared with the proteoliposomes, as the protein is fully digested after 40 min. Looking at the band pattern for Cai in LDAO micelles, we can speculate that cleavage at E127 is more likely than after E52. In the case of the proteliposomes, a considerable amount of protein remains intact, although a preference for cleavage at E52 is detected.

Figure 4.4S

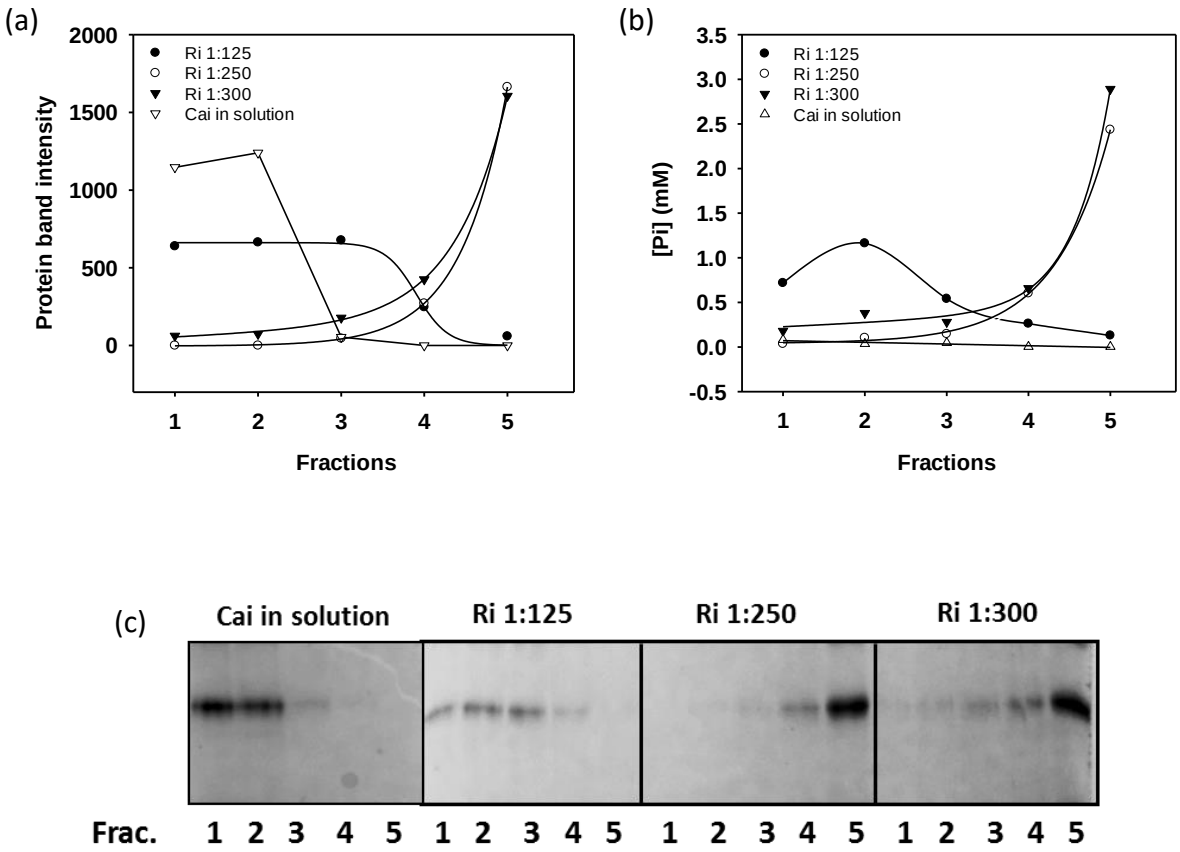

Establishing the highest protein-to-lipid ratio that can be used before liposomes start to break down. Liposomes of *E. coli* lipids were preincubated with 35 µM Cai, purified in 0.2% LDAO, 150 mM NaCl, 50 mM sodium phosphate pH 7.5 buffer. Four different conditions were tested, with increasing concentrations of Cai at protein-to-lipid ratios of 1: 300, 1:250 and 1:125. The protein added was previously subjected to purification in LDAO detergent and incubated with liposomes of *E. coli* lipids prior to sucrose gradient ultracentrifugation. Five fractions were collected starting from the bottom and assayed for phosphorous content and protein localization was tested by SDS-PAGE protein band quantification. Cai in micelles of LDAO was also analysed in the absence of lipid vesicles, which remained at the bottom of the ultracentrifuge tube as expected.

Figure 4.5S

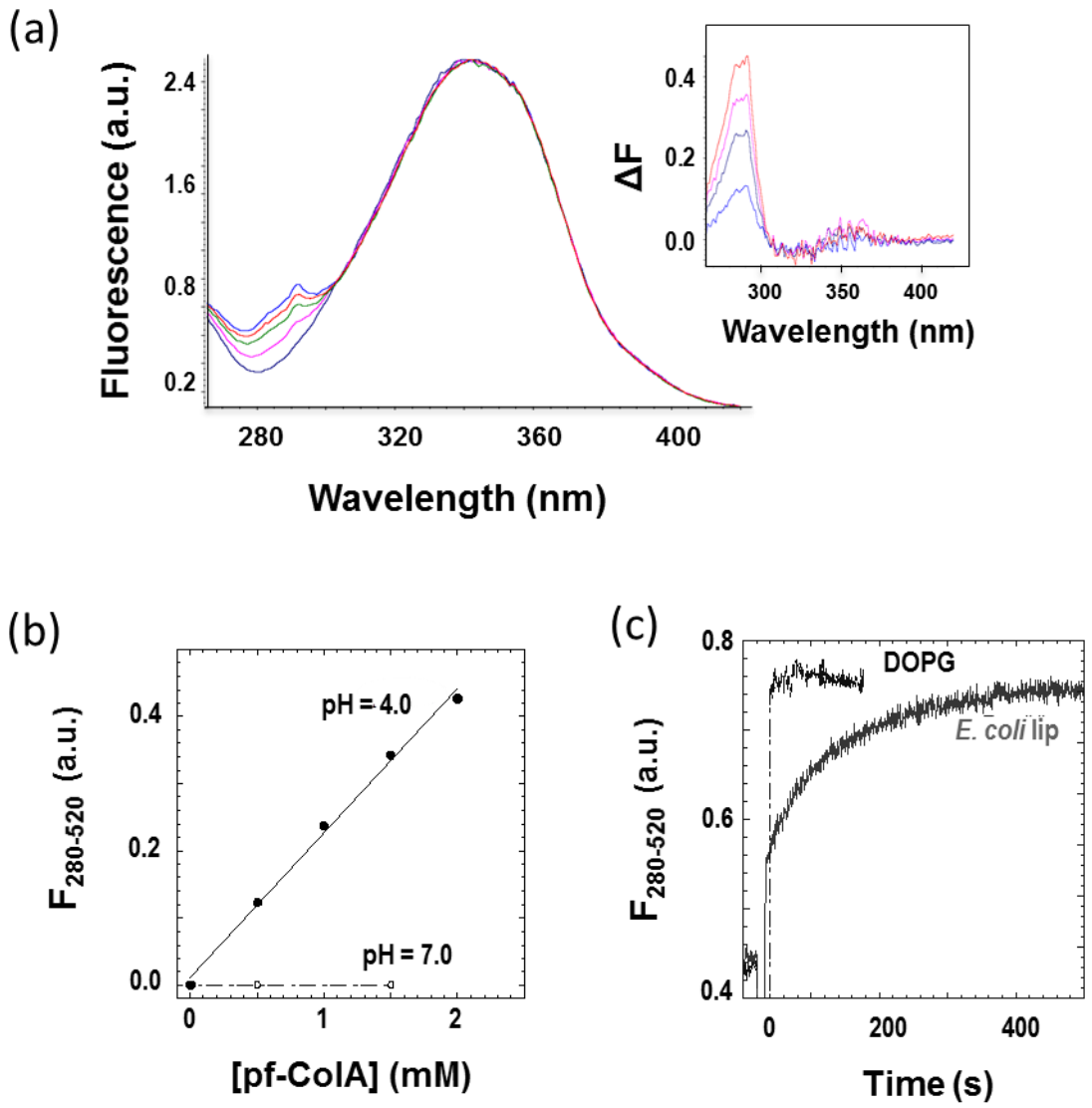

Incorporation of pfColA into liposomes assayed by tryptophan-dansyl fluorescence energy transfer. (a) Excitation spectra (λ_{em}=520 nm) of 3% dansyl-DOPE in 0.6 mM liposomes of *E. coli* lipids in the presence of 0.5 to 2 µM pfColA at pH 4.0. Difference spectra obtained by subtraction of curves minus control spectrum without protein (inset). (b) Fluorescence Intensities obtained in previous difference spectra (λ_{ex}=280 nm, λ_{em}=520 nm) at varying concentrations of pfColA at pH 7.0 or pH 4.0. (c) Time course of fluorescence transfer (λ_{ex}=280 nm, λ_{em}=520 nm) after mixing 2 µM pfColA with 0.60 mM liposomes of *E. coli* lipids or DOPG with 3% dansyl-DOPE at 25º C.

The figure shows a representative titration experiment in which 0.5 to 2 µM pfColA have been added to LUVs containing 3.3 mol% dansylated 1,2-dioleoyl-sn-glycero-3-phosphoethanolamine (DOPE) and the excitation spectra of the probe (λem = 520 nm) was recorded. The spectrum component of the lipid-bound protein could be observed at 280 nm

and quantified after subtraction of the reference spectrum without protein (inset) and plotted against protein concentration. The comparison of acidic or neutral bulk pH in the incorporation of pfColA to DOPG liposomes, which showed no incorporation at pH 7. Based on previous results indicating that pfColA can be successfully incorporated to liposomes prepared with the native lipid composition of *E. coli* (Pulagam and Steinhoff, 2013), we compared the binding kinetics of pfColA to liposomes of pure DOPG with liposomes of *E. coli* lipids at pH 4. Interestingly, even if the reaction was slowed down for liposomes of *E. coli* lipids (containing around 20% of anionic lipids) the extent of binding at equilibrium was equal in both cases (c). Hence the use of liposomes of 100% anionic lipids is not a requisite to obtain high incorporation yields.

CHAPTER 5

The Cai/pfColA complex *in vivo*: co-expression and isolation

5. The Cai/pfColA complex *in vivo:* co-expression and isolation

In nature, Cai and pfColA encounter within the planar matrix of the bilayer. The lipidic environment limits the conformational space of the proteins and warrants the correct relative orientation. It also provides any additional biological component that could be needed such as cofactors or chaperones. In this chapter we approach pfColA/Cai complex formation in the native biological membrane. Protein-protein interactions in the membrane are very difficult to quantify, but the toxin-antitoxin pairs are singular in this sense since complex formation can indirectly be assured by cell survival or rescue (Espesset et al., 1996).

As described in Chapter 3 Cai and pfColA interact with each other by crosslinking and co-elution experiments but only to a moderate extent and in a limited set of detergent. The same group of detergents also induced the formation of pfColA dimers and a higher degree of Cai oligomerization compared to other amphiphilic agents. These observations raised some questions: (i) on one hand, the apparent interaction detected could be the result of the agglutinating effect that alkyl-glycosides have over proteins in general. Our observations could be due to unspecific detergent-induced artifacts and not really respond to specific true binding. (ii) On the other hand, it is interesting to explore the stability of the complex analyzing the phenomena starting from the preformed complex instead of from the components. In simple reactions in equilibrium, the same ratio of populations should be reached at given experimental conditions independently of the starting point or the reaction pathway. In the case of a complex formed from membrane proteins in detergents, a negative result in the association semi-reaction could have many explanations, among them side-reactions that inactivate proteins (conformational changes, unfolding, misfolding and aggregation). It is still possible that a different relative product/reactants ratio could be obtained under the same conditions (detergents) in the dissociation semi-reaction starting from the pre-formed complex. For a given detergent, the association reaction could be greatly impeded, and at the same time, it could maintain the complex stable out of the membrane once it is formed; meaning that the reaction is under kinetic control. If reactants or products

are subjected to parallel irreversible reactions (i.e. Cai aggregation) the result obtained starting from reactants or from the complex could be different. It is not unthinkable that the very hydrophobic Cai may be denatured in aqueous solution far more easily than in complex with pfColA. In other words, there may be detergents that produced negative results in chapter 3 but are able to solubilize and maintain a pre-formed complex from the membrane. Similarly, different results could also be obtained for detergents for which a positive result was obtained.

Each of the three different domains of colicins performs a specific function (Cramer, 1995; Pattus, 1990). The central regions form unique structures that bind to outer membrane receptor proteins (Brunden et al., 1984; el Kouhen et al., 1993) and the N-termini acts in unknown ways during the transport of the toxin through the outer membrane. Group A colicins are Tol-system dependent (Davies and Reeves, 1975a)**.** The C-termini contain the toxic activities of colicins (Baty et al., 1988). In parallel, the spectrum of mechanisms developed by bacterial organisms to fight colicin cytotoxicity range from resistance, to tolerance or immunity. Bacteria are said to be resistant when the cell surface receptor (BtuB in the case of pfColA) is mutated rendering the mutant strain insensitive to the action of a particular colicin. Thus the colicin is not able to initiate the internalization, a prerequisite to exert its toxic action. Another type of insensitivity to colicins resides in the inhibition of signal transmission after binding of the colicin to its receptor or its internalization. In this case mutations are localized in the tol or tonB genes and these strains are said to be tolerant or refractory (Rodriguez-Lemoine, 1999). Finally, strains containing the colicinogenic plasmid pCol are immune to the action of the corresponding colicin, due to the constitutive expression of the immunity protein Cai (Zhang et al., 2010a), which forms an inactive complex with the exogenous colicin.

The simplest way to generate the Cai/pfColA complex by means of the natural machinery, would imply adding purified Colicin A to bacteria overexpressing Cai. This plan suffers two main drawbacks. On one hand, Colicin A is a much larger multidomain protein (592 aa) compared with pfColA (206 aa) and this would complicate protein purification and manipulation. On the other hand, very few colicin A molecules reach the inner membrane when added exogenously; this is in part because there are a limited number of translocation sites, 400 colicin A receptors and 1000 translocation sites per cell (Duché et al., 1995). Another

approach was used previously by Espesset and cols. (1994a) that overcame these inconveniencies. These authors fused pfColA to mitochondrial presequences of cytochromes c1 and b2. This signal peptides could effectively direct the pfColA to the periplasm of *E. coli* where upon it was inserted into the inner membrane yielding a functionally active channel (Espesset et al., 1994a). In the absence of Cai the plasmid encoding exportable pfColA could not be maintained. Later the same authors used a specific prokaryotic signal peptide (pelB) with similar targeting efficiency and cytotoxic effect in non-immunized bacterial strains (Duché et al., 1999; Espesset et al., 1996; Nardi et al., 2001).

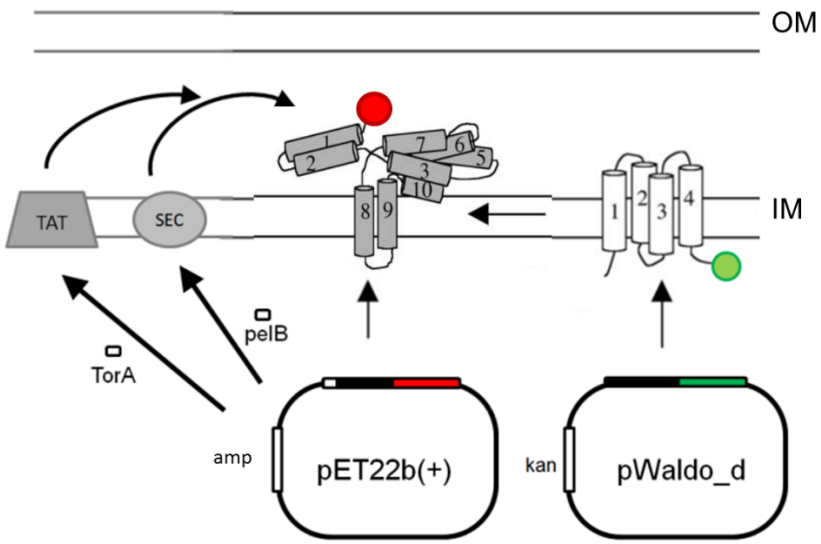

Figure 5.1 Diagram of the engineered system to overexpress and lead Cai and pfColA to the inner membrane of bacteria. pfColA-Cherry bearing PelB or TorA signal sequences was expressed from pET22b(+) plasmid while Cai-GFP was encoded in the pWaldo(d) vector.

Here we used two different N-terminal signal sequences to target colicin A pore-forming domain to the periplasm by means of the type II secretory pathway (Fig. 5.1). Of the six secretory pathways described in Gram negative bacteria, type II involves the translocation of cytoplasmic proteins across the inner membrane mainly through the Sec or Tat pathways. The translocation of partially unfolded proteins occurs through the Sec pathway while the Tat machinery transports folded cargos. The Tat secretion pathway consists of 2–3 components (TatA, TatB, and TatC). In Gram-negative bacteria, TatB and TatC bind a specific N-terminal signal peptide containing a twin-arginine motif on folded Tat secretion substrates. TatB and

TatC then recruit TatA to the cytoplasmic membrane, where it forms a channel. Folded proteins are then translocated across the channel and into the periplasm where the signal sequence is cleaved by signal peptidases. This system is well known for the transport of redox proteins that require co-factors to fold properly, such as cytochrome C.

In the Sec translocation pathway, proteins destined for transport to the periplasm or external media contain a removable signal sequence recognized by the SecB protein (Fig. 5.2). This protein serves as a chaperone, binding to pre-secretory proteins and preventing them from folding. SecB then delivers its substrates to SecA, a multi-functional protein that guides proteins to the SecYEG channel, and also serves as the ATPase that provides the energy for protein translocation. Prior to transport through the channel, a protease protein cleaves off the SecB signal sequence from the protein.

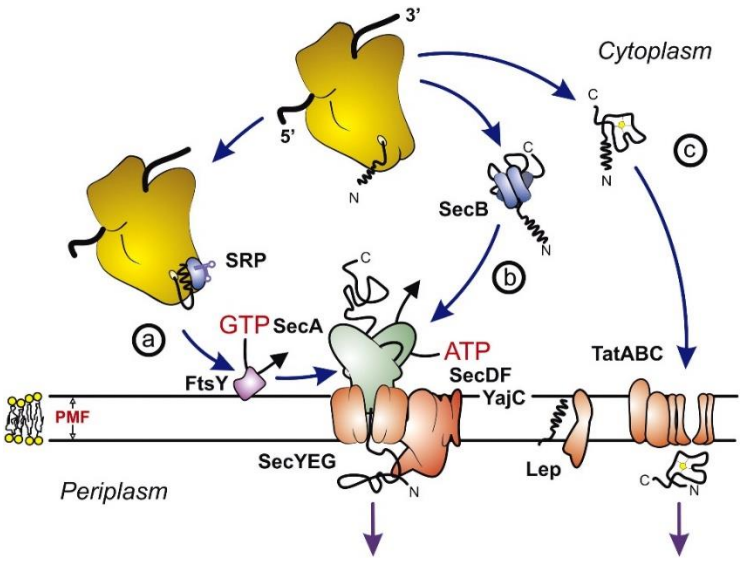

Figure 5.2 Schematic overview of the *Escherichia coli* Sec- and Tat translocases. (a) Co-translational and (b) post-translational targeting routes and translocation of unfolded proteins by the Sec-translocase. (c) Translocation of folded precursor proteins by the Tat translocase. Adapted from Natale and cols (2008).

The signal sequence from *Erwinia carotova* pectate lyase B (PelB) was used here to target pfColA to the bacterial periplasm through the Sec system and the signal peptide of trimethylamine-N-oxide reductase (TorA) directed to the Tat pathway. Additionally the red fluorescent protein mCherry (Shu et al., 2006) was fused to both constructions at the C-terminal end of pfColA. These sequences were subcloned into the vector pET22b(+) which confers resistance to ampicillin. Previously described pWaldo(d) plasmid (conferring

kanamycin resistance) was used to overexpress Cai-GFP. GFP and mCherry protein reporters were used due to their spectral properties since the excitation is centered at 488 nm and 587 nm, and the maximal light emission is centered at 530 nm and 620 nm respectively.

5.1 Optimization of ColA pore-forming domain and immunity protein co-expression

The first step towards the production of pfColA in association with its immunity protein in the bacterial plasma membrane was to choose a bacterial strain in which both proteins could be expressed. Cytosolic pfColA has routinely been overexpressed in our laboratory in *E. coli* BL21 (DE3) with high yields. Heterologous expression of the integral membrane proteins, on the contrary, poses a harder challenge to the cell often resulting in toxicity or formation of inclusion bodies (Drew et al., 2003; Wagner et al., 2006). This led us to use the so-called Walker strains, which allow for improved membrane protein overexpression yielding considerable amounts of membrane-inserted Cai when overexpressed in bacterial strain C41 (DE3), as shown above (Chapter 3). We first tested the overexpression of pfColA in C41 (DE3) as a prerequisite for co-expression. The expression of pfColA in C41 (DE3) was compared with that of BL21 (DE3) in cultures induced at OD 0.2 with 0.5 mM IPTG grown at 37 °C. After 7 h induction, yields of pfColA expression in BL21 (DE3) and C41 (DE3) were similar, the contaminant proteins co-expressed together with pfColA being more abundant in the case of C41 (DE3) (Figure 5.3a). Then Cai-GFP expression in both BL21 (DE3) and C41 (DE3) was tested under the same conditions. The Cai-GFP expression in BL21 (DE3) was strongly hampered (Figure 5.3b). As already seen in chapter 3, overexpression of Cai-GFP in C41 (DE3) was considerably better although hardly detected by Coomassie staining, while the Cai-GFP band was clearly distinguishable by in-gel fluorescence.

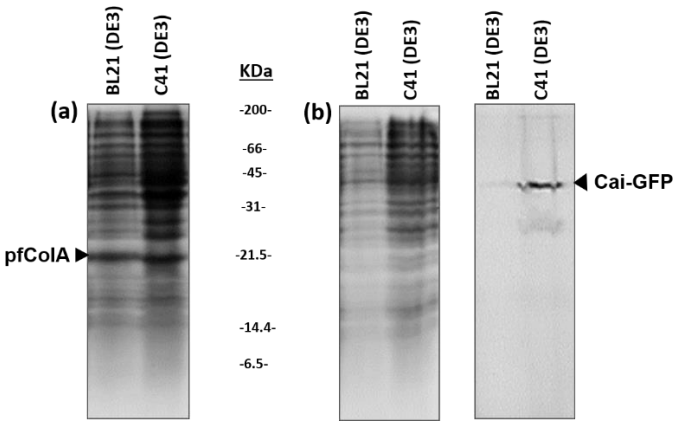

Figure 5.3 Separate expression test of cytosolic pfColA and Cai-GFP in both BL21 (DE3) and C41 (DE3). *E. coli* strains BL21 (DE3) and C41 (DE3) were independently transformed with pHAT plasmid harbouring pfColA (a) and pWaldo plasmid containing Cai-GFP (b). Bacteria were harvested 7 h after IPTG induction and analysed by SDS-PAGE. pfColA was detected by Coomassie staining and Cai-GFP could be detected by in-gel fluorescence (right panel).

To explore the effect of co-transformation of the exportable forms of pfColA with or without simultaneous expression of the immunity protein in equal conditions, all cultures where co-transformed with two plasmids. The empty expression vector pWaldo(d) was used as the reference for non-immunized bacteria. Hence, all bacterial cultures were supplemented with both ampicillin and kanamycin. To monitor both the pfColA and Cai expression kinetics, we cultured cells in a 96-well plate under agitation at 25 °C and 37 °C. Absorbance and green and red fluorescence records were taken at given time intervals in a plate reader.

When bacteria were co-transformed with empty pWaldo(d) and either TorA-pfColA-Cherry or PelB-pfColA-Cherry no expression of the red pfColA variants was detected (Figure 5.4). Cell growth was neither altered with respect to the non-induced cultures. All the different conditions of induction tested: induction at culture OD_{600}= 0.2, OD_{600}= 0.45; with 0.1 mM IPTG or 0.5 mM IPTG; in strains C41 (DE3) and C43 (DE3) resulted in no pfColA expression in the absence of the immunity protein.

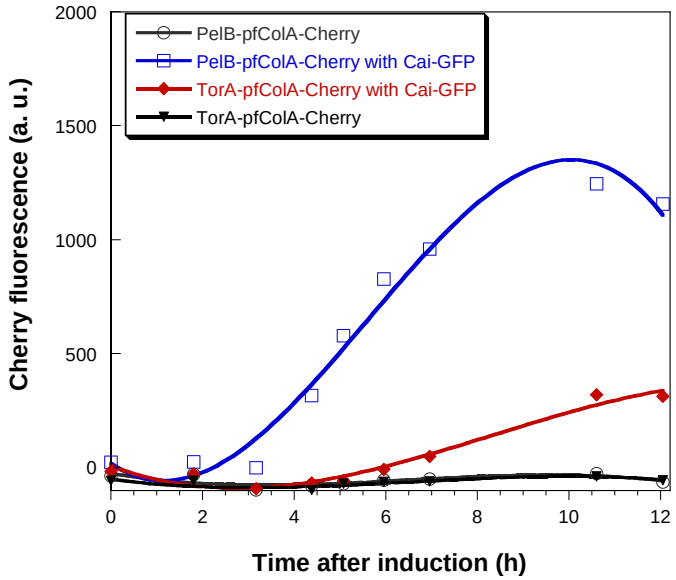

Figure 5.4 Overexpression of the toxin in the absence or presence of the immunity protein. Cells containing the toxin plasmid and both the toxin plasmid alone, or with the antitoxin plasmid. C41 (DE3) cells co-transformed with pWaldo(d) empty vector where Induced with 0.1 mM IPTG at OD 0.45.

Then, we co-transformed the exportable forms of pfColA with pWaldo(d) plasmid harbouring Cai-GFP in C41 (DE3) cells. Two hours after cell induction with IPTG, the expression of PelB-pfColA was visible as an increment in Cherry fluorescence and reached a maximum after 10 hours (Figure 5.4). The expression level of TorA-pfColA-Cherry was significantly lower under the same conditions.

The expression test was also performed in C43 (DE3), another Walker strain, after transformation with the same plasmid combinations. In previous Cai-GFP expression tests, best yields were obtained in C41 (DE3) strain grown at 20 °C for 16 h after induction with 0.8 mM IPTG at OD_{600} = 0.4. In contrast, Figure 5.5 illustrates that expression yields of PelB-pfColA-Cherry or TorA-pfColA-Cherry are superior in C43 (DE3) as compared to those in C41 (DE3) in bacteria expressing Cai-GFP also.

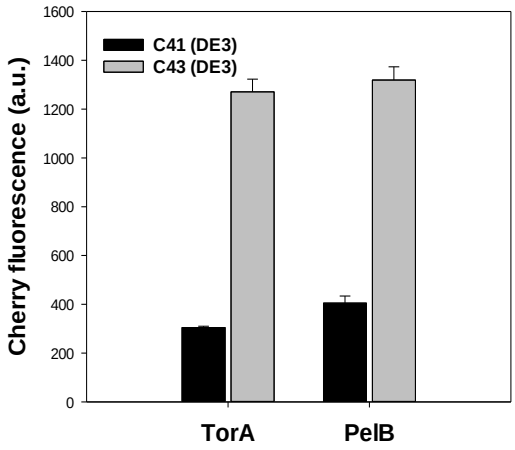

Figure 5.5 Overexpression of pfColA-Cherry fused to TorA or PelB targeting peptides in C41 (DE3) and C43 (DE3) bacterial strains. The fluorescence of cherry at 620 nm was used to monitor the expression of the toxin pore-forming domain in cells overexpressing Cai-GFP at 12 hours after induction. Bacterial cultures were induced with 0.1 mM IPTG at OD 0.45.

Cai-GFP expression was also measured in the same strains in combination with the exportable red pfColA constructions as well as not exportable pfColA. In the later, there is no interference of Cherry fluorescence and the GFP signal is more reliably related to Cai-GFP expression. Figure 5.6 shows fluorescence intensity of GFP over time for bacterial cultures induced with 0.5 mM IPTG at OD 0.2 or 0.45, or non-induced. Cai-GFP expression showed low sensitivity to the OD_{600} at which cells were induced, however the most notable observation was that in the C43 (DE3) strain (but not in C41 (DE3)) the highest protein expression occurred in the absence of IPTG. Protein expression in the absence of inducer can be encountered in T7 promoter-based expression vectors such as pWaldo(d), in C43 (DE3). Insufficient amounts of transcription repressors lead to basal T7 RNA polymerase production that ultimately cause leaky expression of the target gene (Mertens et al., 1995). This observation might provide an explanation for the higher expression of the toxic forms of pfColA in C43 (DE3). Bacteria of this strain are protected by the leaky expression of Cai before induction of pfColA expression, which in turn, was not shown to occur in the absence of IPTG.

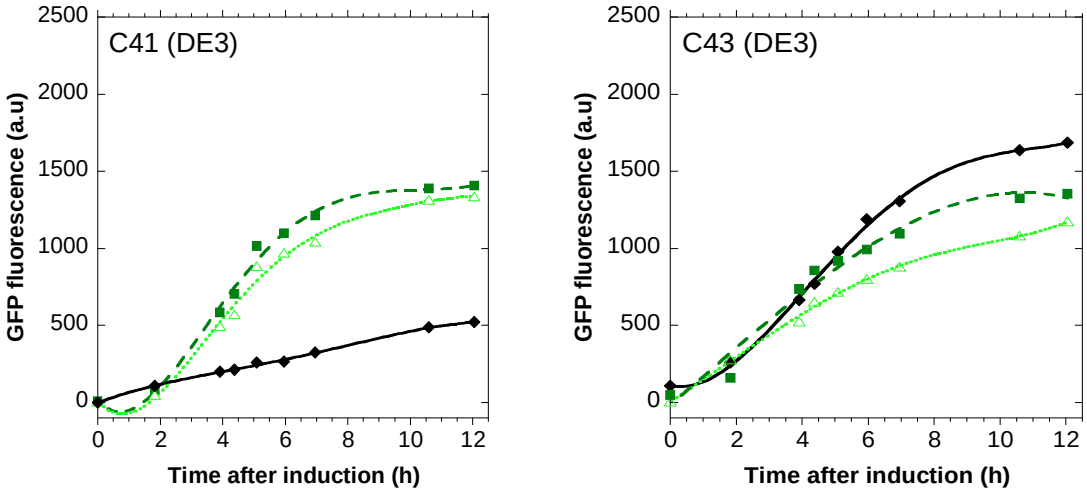

Figure 5.6 GFP fluorescence over time in bacteria co-expressing cytoplasmic pfColA and Cai-GFP in Walker strains C41 and C43. Uninduced (black diamonds) induced at OD 0.2 (light green triangles) and induced at OD 0.45 (dark green squares).

Once co-expression in C43 (DE3) proved to be superior to that of C41 (DE3), the effect of PelB and TorA on expression yields of pfColA was measured in that bacterial strain. No major differences were found when PelB or TorA targeting sequences were compared (Figure 5.7), PelB expression being slightly higher.

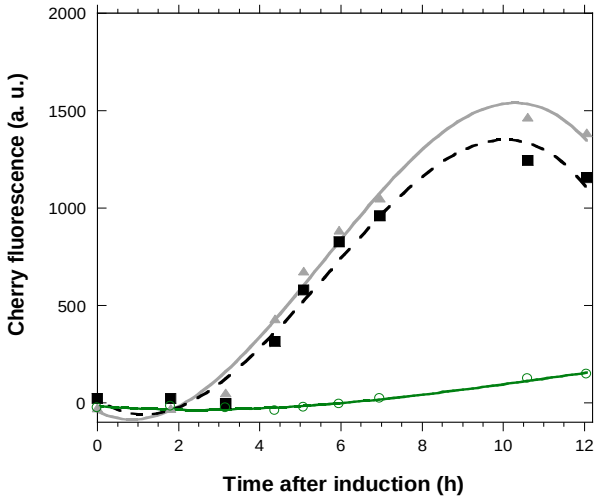

Figure 5.7 Effect of TorA and PelB targeting signals over the expression of pfColA-Cherry in cells carrying Cai-GFP. Toxin overexpression was detected by Cherry fluorescence at 620 nm in C43 (DE3) cells induced at OD 0.45 with 0.1 mM IPTG. PelB-pfColA-Cherry is depicted as grey triangles and TorA-pfColA-Cherry as black squares, green open circles correspond to uninduced cells.

Even though overall total protein expression did not seem to be altered by OD of induction, differences in cell growth over time upon induction at OD 0.2 or OD 0.45 were observed. Early induction caused a constant increase in biomass formation as determined by A_{600}

measurements, while a late induction resulted in arrest of growth followed by a small increase in growth rate after 8 h. Consequently, higher expression per cell was attained in cultures induced earlier, at (OD_{600} 0.2 *versus* OD_{600} 0.5) (Fig. 5.8).

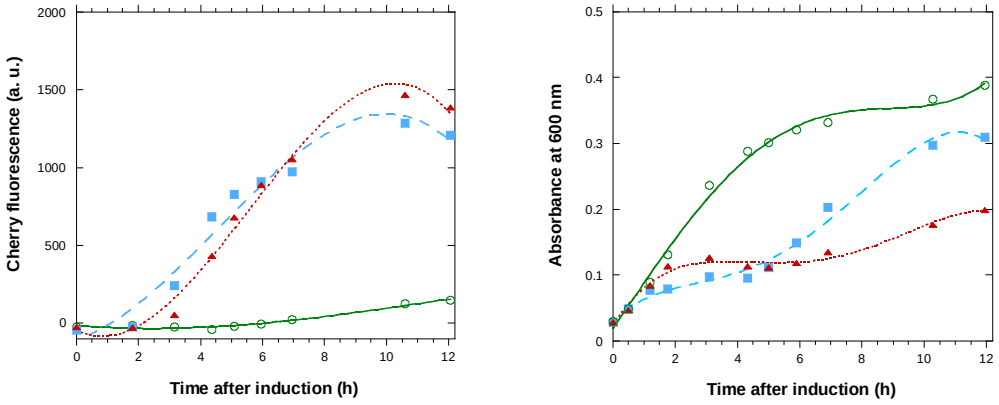

Figure 5.8 Co-expression of Cai-GFP and PelB-pfColA-Cherry in C43 (DE3) induced by IPTG at different growth phases. (a) Protein expression in cells overexpressing PelB-pfColA-Cherry and Cai-GFP monitored by measuring Cherry fluorescence at 620 nm every hour. (b) Cell growth measured by absorbance at 600 nm every hour. Traces correspond to uninduced cells (green open circles), cells induced at OD 0.2 (blue squares) and cells induced at OD 0.45 (red triangles).

The effect of the GFP moiety on immunization of toxic pfColA was analysed by comparing the red fluorescence of PelB-pfColA-Cherry in cells co-expressing Cai-GFP or Cai-His overtime at different induction conditions. No mayor difference on the expression of the exportable pfColA was detected for any of the Cai versions (Figure 5.9).

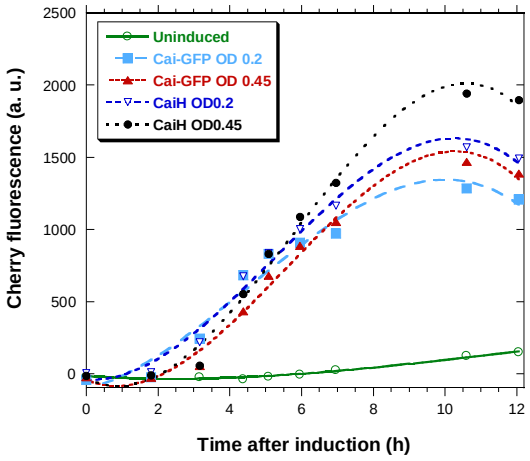

Figure 5.9 PelB-pfColA-Cherry overexpression in cells expressing Cai-GFP or CaiH induced at two different growth phases. The fluorescence of Cherry was measured at 620 nm every hour in C43 (DE3) cells induced with 0.1 mM IPTG at OD 0.2 and OD 0.45.

Taken together, optimal co-expression of exportable pfColA and Cai was obtained after early IPTG induction (OD_{600} 0.2) in C43 (DE3) bacterial strain with any of the targeting peptides. This

result indicates that the production of immunity protein is essential for the expression of the exportable-pore forming domain to occur.

As exposed above, exportable toxic forms of pfColA can only be overexpressed when the bacterium is immunized by the simultaneous or previous expression of Cai. This evidence suggests that the inactive complex is being effectively produced at the plasma membrane. In order to determine the degree of export and insertion efficiency, culture fractionation was carried out. Shortly, C43 (DE3) cultures were co-transformed with Cai-GFP and PelB-pfColA-Cherry or TorA-pfColA-Cherry, induced at OD 0.2 with 0.5 mM IPTG and grown for 12 h at 30 °C. After cultures were harvested, periplasm and spheroblasts were isolated by washing the cells with fractionation buffer (20% sucrose, 10 mM TRIS pH 8, 0.1 mM EDTA), subsequent addition of 5 mM $MgSO_4$ and centrifugation. Lysis of spheroblasts was facilitated by sonication and, upon ultracentrifugation, the cytoplasmic fraction and the inner membrane fraction were obtained. Samples were analysed in 7.5% SDS-polyacrylamide gels and bands corresponding to Cherry and GFP reporter-fusions comprehensively detected by in-gel fluorescence. Figure 4.10 shows how the integral membrane protein Cai was only localized in the inner membrane while the exportable forms of pfColA are found in both the cytoplasm and the inner membrane fractions.

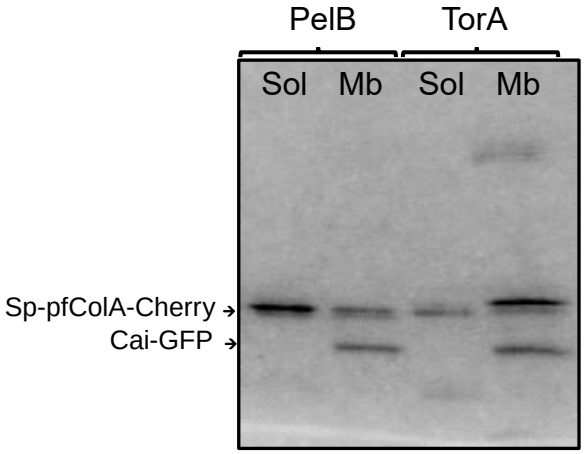

Figure 5.10 Subcellular fractionation of C43 (DE3) cells co-transformed with Cai-GFP and PelB-pfColA-Cherry or TorA-pfColA-Cherry. In-gel fluorescence of 7.5% SDS-PAGE (Sol: cytoplasmic fraction, Mb: inner membrane fraction).

The main differences between PelB and TorA fusions reside in the relative amounts of cytosolic precursors and secreted mature forms detected in both compartments. In the case of TorA-pfColA-Cherry, virtually all the protein in the cytoplasm corresponds to the processed

form. This is more likely due to partial degradation of the precursor form in the cytoplasm as observed earlier (Thomas et al., 2001). In the membrane fraction, the unprocessed form tends to accumulate, coexisting with smaller quantities of the mature form, most likely as a result of signal peptidase impairment. For PelB-pfColA-Cherry however, the precursor carrying the signal peptide presumably accumulates in the cytoplasm because of the saturation of the Sec-translocon capacity. A considerable amount of protein is however also inserted in the membrane.

Overall, despite small differences in targeting efficiency, both TorA and PelB protein fusions were able to correctly direct the pore-forming domain to the inner membrane, where they are meant to bind to the immunity protein. These findings corroborate that periplasmic targeting is an efficient method to study colicin activity *in vivo* and suggest that the inhibition of expression reported earlier for the non-immunized bacteria, could arise in the cell as a mechanism to elude cytotoxicity.

5.2 Membrane extraction of the ColA pore-forming domain/immunity protein complex

Obtaining a stable, intact membrane protein complex, in which the native structure and protein–protein interactions are preserved, represents a unique purification challenge largely due to the requirement for detergent solubilization (Walian et al., 2004). Experience has shown that preservation of an intact membrane protein complex is sensitive to the method of solubilization and isolation. The use of an unsuitable detergent or detergent-to-protein ratio can lead to the disruption of complexes or the formation of non-native protein oligomers. Here we report on the results obtained from membrane extraction of Cai-GFP/pfColA-Cherry complex from membrane preparations by the use of detergent solutions of varying chemical nature.

Upon expression of PelB-pfColA-Cherry with Cai-GFP-H and TorA-pfColA-Cherry with Cai-GFP in 1 L *E. coli* C43 (DE3) cultures for 12 h at 25 °C, the fraction containing the bacterial membrane was isolated and solubilized in 1% LDAO, a detergent that proved suitable for the purification of Cai (Chapter 3). To test the capacity of the detergent to preserve the association, LDAO solubilized membranes were subjected to ion affinity chromatography.

Figure 5.11 shows that the elution profiles of GFP and Cherry fluorescent proteins do not overlap, indicating that the complex is not stable in this detergent. The same result is obtained for both TorA and PelB variants.

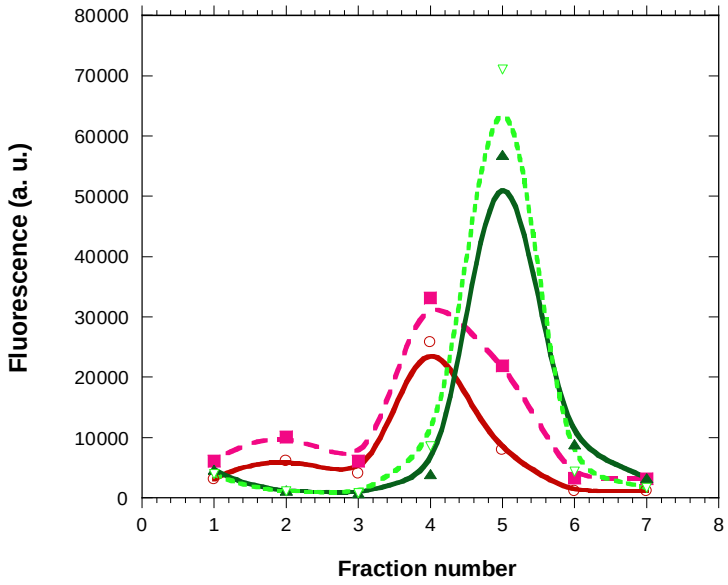

Figure 5.11 Elution profiles from Ni affinity chromatography of His tagged TorA or PelB fused to pfColA-Cherry and Cai-GFP in 1% LDAO. Elution from Ni-NTA resin was performed in PBS pH 7.5 with a step gradient of 20-400 mM imidazol and 1% LDAO. PelB-pfColA-Cherry (pink dashed line) co-expressed with Cai-GFP (green dashed line) and TorA-pfColA-Cherry (solid red line) co-expressed with Cai-GFP (green solid line).

A selected group of detergents was then tested in similar co-elution experiments. Considering the efforts necessary to overexpress and purify the complex, only TorA-pfColA-Cherry co-expressed with Cai-GFP was used for detergent screening. Membrane fractions were solubilized with SDS, DPC, Triton X-100 and DDM and the complex was bound to Ni-NTA agarose resin. Co-elution from the column and native gel electrophoresis of the eluted samples were considered to identify the detergents capable of maintaining the complex integrity.

The elution profiles for the four detergents tested are depicted in Figure 5.12. Cai-GFP and TorA-pfColA-Cherry fusions were eluted as two distinct peaks in DPC, indicating dissociation of the complex. In SDS, the fluorescence of the proteins decreased over time and although signals could be recorded after elution from the column, no fluorescence was visible in the

native gels. In the case of Triton X-100 and DDM the chromatography resulted in reasonable overlap of the fluorescence peaks.

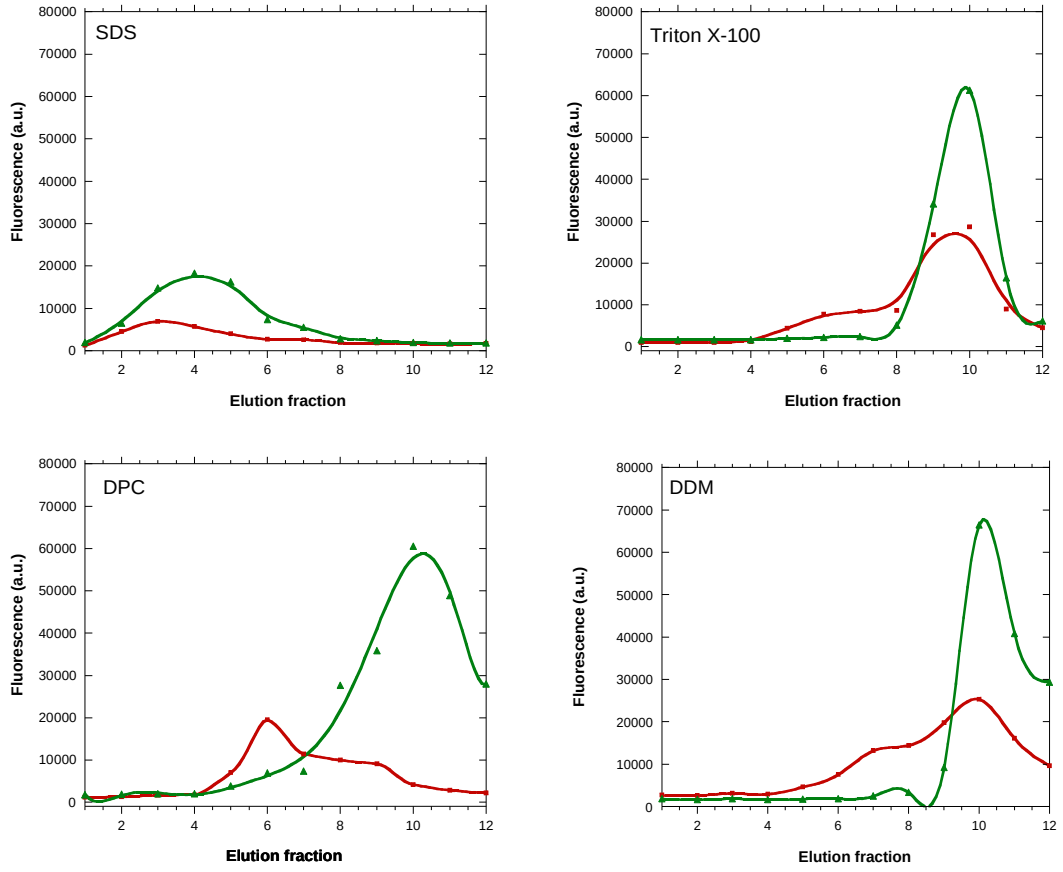

Figure 5.12 Co-elution of pfColA-Cherry and Cai-GFP in Ni affinity chromatography after extraction by different detergent solutions. pfColA-Cherry targeted to the inner membrane of cells co-expressing Cai-GFP were subjected to co-purification. SDS, Triton X-100, DDM and DPC detergents were tested for their capacity to preserve the intact complex formed *in vivo*.

Nevertheless, native-PAGE analysis of eluted samples in Triton X-100 showed Cai-GFP and pfColA-Cherry running as separate bands, Cai-GFP at the top of the gel owing to its high positive charge and pfColA-Cherry at the bottom (Figure 5.13). Most remarkably, the sample solubilized and purified in 1 % DDM yielded a single band in native-PAGE after being co-eluted from Ni-NTA. Some of the TorA-pfColA-Cherry protein eluted earlier than the complex, but the major second band was shown to contain the intact Cai-GFP/pfColA-Cherry complex. Taking into account that native electrophoresis is able to separate native-complexes based on both charge and size, the band corresponding to this complex ends up very close to the upper part of the gel.

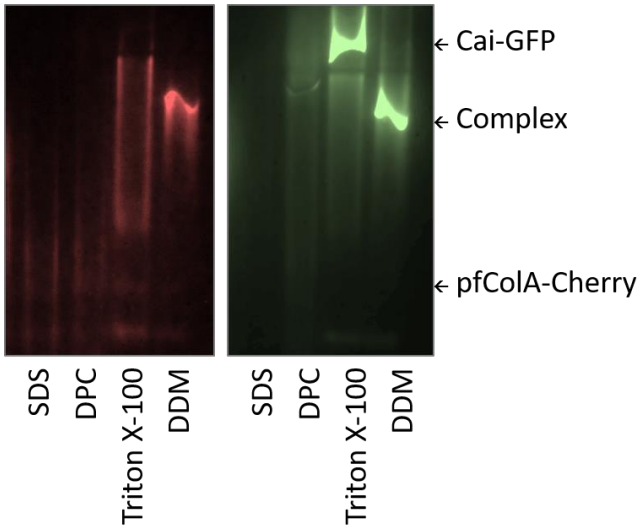

Figure 5.13 Native-PAGE of the complex after solubilization and Ni affinity chromatography in four different detergents. Fluorescence of Cherry was detected in the left panel and GFP fluorescence in the right.

Since DDM proved to be a suitable detergent for complex isolation, complex co-purification was further studied for both PelB-pfColA-Cherry or TorA-pfColA-Cherry together with Cai-GFP. Fractions eluted from nickel affinity chromatography were simultaneously subjected to denaturing and native electrophoresis as depicted in Figure 5.14.

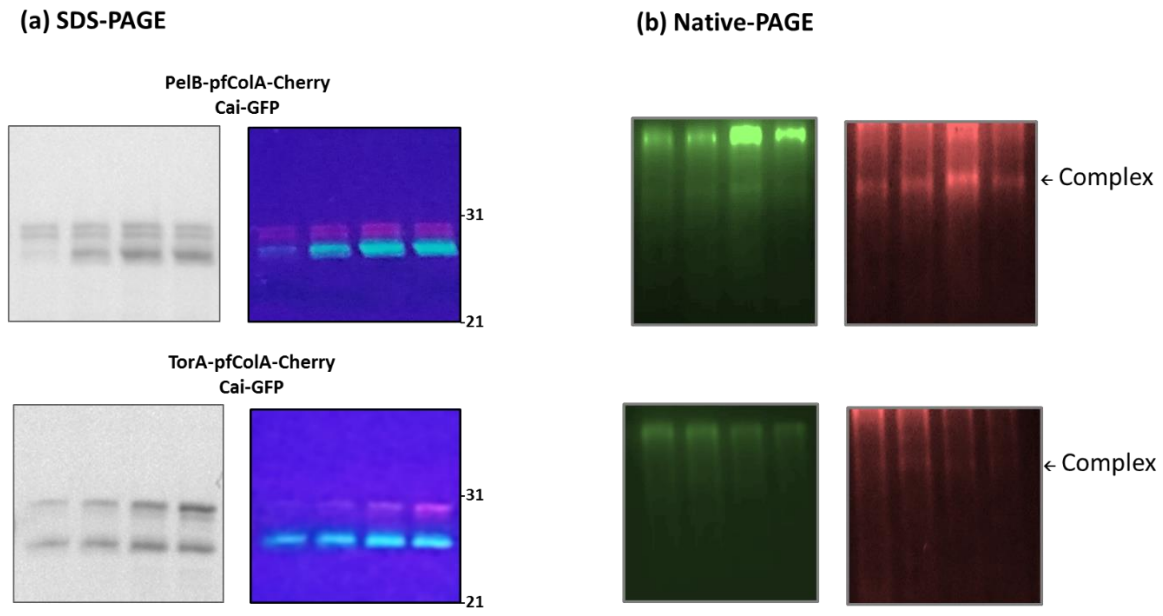

Figure 5.14 Co-elution of ColA pore-forming domain and immunity protein by Ni affinity chromatography from DDM solubilized C43 (DE3) membranes. Protein fractions eluted in 0.5% DDM, 50 mM NaCl, 1 mM TCEP 100 mM phosphate pH 7.5 and 50-250 mM imidazol step gradient. (a) Eluted fractions were loaded onto a SDS-PAGE. Coomassie and in-gel fluorescence by UV transillumination. (b) Same fractions were loaded on Native-PAGE to check for preservation of intact pfColA-Cherry and Cai-GFP complex.

UV transilumination of SDS-PAGE gels shows real colors of protein bands and turned out to be very helpful to rapidly identify components of the complex by means of the fluorescent reporter moieties. To detect the fluorescent bands the unstained gel was exposed to UV light in a transiluminator (λ ~ 312 nm) and images were captured with a digital camera. Alternatively, fluorescence of GFP or Cherry could be independently detected in a VersaDoc Imager by means of specific excitation leds and detection through band-pass filters. Both the precursor and mature forms of PelB-pfColA-Cherry were observed to co-elute with Cai-GFP, whereas the unprocessed form predominates in TorA-pfColA-Cherry. It is interesting to point out that the complex was eluted at a lower imidazol concentration than that required to detach Cai from the column. Regarding the native-PAGE of the chromatographic fractions, the complex appeared to involve a small amount of the total Cai-GFP expressed at the membrane. This, on the other hand, seems to be very reasonable, especially because it is the excess of pfColA which compromises cell viability. As a matter of fact, no pfColA-Cherry is found in membrane preparations apart from that engaged in complex formation.

5.3 Discussion

The colicin A toxin enters the target bacteria by the initial binding of the central domain to the outer membrane receptors (BtuB and OmpF) and subsequent translocation of its N-terminal domain through the Tol machinery. Finally the pore-forming C-terminal domain inserts into the inner membrane and forms voltage-dependent channels. How the pore-forming domain reaches the inner membrane and how the immunity protein can inhibit the opening of the channel is not well understood. The inhibition is believed to occur through direct helix-helix interaction between the exogenous pore-forming domain and the immunity protein that is constitutively produced in the host cell. Studies of colicin A pore-forming activity *in vivo* have been very difficult to carry out mainly because the number of molecules reaching the inner membrane is very low (Duché et al., 1995). The approach described here however, involves the co-expression of both Cai and pfColA in the same cell allowing the formation of a functional complex in the inner membrane. In order to preserve the physiological orientation of the interacting pair, pfColA was exported to the periplasm by fusing it to two periplasm targeting signals. The significance of the use of targeting peptides

is that the number of colicin A channels inserted into the inner membrane can be increased by a factor higher than ten (Espesset et al., 1996).

According to our results, non-immunized bacteria did not express exportable forms of pfColA, while co-expression with Cai gave rise to considerable amounts of protein, as monitored by both GFP and Cherry fluorescence. From this observation, we can deduce that the targeting peptide is able to direct the protein to the periplasm where it inserts probably as a consequence of translocation-induced partial unfolding (Sec) or partial destabilization in the periplasm (Tat). Non-immune bacteria defend themselves against the toxicity of exported pfColA by inhibiting its expression, whereas the formation of the inactive complex allows protein overproduction. It is worth noting that higher cell growth is observed in the absence of the immunity protein, which indicates that the inhibition of expression is so effective that no toxicity is detected. Lower cell growth is observed in those bacteria that are co-expressing the inactive complex. A possible explanation can come from the higher energy cost of co-expressing both proteins, although the maintenance of the immunized state in the presence of high amounts of toxin may also be responsible for this observation.

Even if pfColA co-localizes with Cai in the inner membrane, the efficiency of expression, export and/or insertion steps is not that high, as mature forms of the pre-protein are found in both the cytoplasm and the periplasm as been previously reported (Linton et al., 2012; Thomas et al., 2001). The proportion of pfColA that is inserted in the inner membrane associated with Cai does not exceed a 30% of produced protein.

Subsequent extraction of the complex is performed only from the inner membrane fraction containing the mature form of pfColA in complex with Cai. The choice of the optimal detergent has been made based on two criteria, the co-elution of both proteins by Ni affinity chromatography and co-migration in native-PAGE. The detergent DDM turned to be the only one in which the purification of the Cai-GFP/pfColA-Cherry complex was possible after membrane solubilization of *E. coli* C43 (DE3) bacteria overexpressing both components.

Previous attempts to co-solubilize the immunity protein together with the pore-forming domain showed that both proteins were able to co-immunoprecipitate after membrane extraction using 2% Triton X-100 and suggested that both proteins must be membrane-inserted as a prerequisite for the interaction to occur (Espesset et al., 1996). Here we show for the first time that the preservation of an intact complex is mainly dependent on the

chemical character of the detergent used in solubilization. Chapter 3 together with this result indicate that the complex can be formed both *in vitro* and *in vivo* in the presence of alkyl-glycosides. Therefore, additional cellular components do not seem to be essential for the interaction to occur. As previously indicated, pfColA insertion in the inner membrane does not appear to be dependent on the translocation machinery. The contrary could have been anticipated considering the notion that pfColA should unfold to interact with the membrane (van der Goot et al., 1992). The Sec machinery is known to induce unfolding of the cargo while TAT system transports folded proteins, but this difference does not seem to critically influence toxicity nor immunization.

Most importantly, the same kind of detergent is selected here when analyzing the reaction in the dissociation direction and in chapter 3 where the association direction was analysed. For example, detergents like LDAO that did not favour complex assembly *in* vitro, was now shown to destroy an *in vivo* pre-assembled complex. It seems obvious that complex formation is more efficient *in vivo* than *in vitro* and that the relatively low yields obtained in chapter 3 in DDM are not revealing equilibrium populations, but are possibly conditioned by irreversible processes in direct competition. It can be expected that inhibition or a tighter control over these side reactions would help increasing the complex yields obtained *in vitro*.

CHAPTER 6

Studying the Cai/pfColA complex *in vitro*: stability, stoichiometry, binding affinity and sequence dependence.

6. Studying the Cai/pfColA complex *in vitro*: stability, stoichiometry, binding affinity and sequence dependence

Previous results suggested the functional *in vivo* association of Cai with pfColA within the bacterial membrane (Espesset et al., 1996). Results obtained in this thesis, described in Chapter 5, corroborate that Cai efficiently inhibits toxicity of exportable forms of pfColA when co-expressed in bacteria, while allowing their expression to detectable levels. Furthermore, we showed that the purification of the intact complex from the membrane was possible in DDM but not in other detergents also tested. Alkyl-glycosides were also identified as the detergents that allowed the optimal association of the free proteins in aqueous solution (Chapter 3). Still the subsequent study of the Cai/pfColA complex at the structural and thermodynamic levels require large amounts of purified complex. Protein yields obtained for the complex by the co-expression strategy described in chapter 5 are not high, probably due to the tight control of the bacteria on protein expression to maintain free toxin amounts at a tolerable level. For the following *in vitro* analysis, complex-constituent proteins were expressed and purified independently -pfColA in non-exportable form- and co-incubated in buffers supplemented with the detergent DDM. DDM was chosen as representative of the few detergents that solubilized the complex from the membrane and preserved it in mixed micelles (Chapter 5) and also allowed complex formation from free proteins (Chapter 3).

6.1 Formation and co-purification of Cai/pfColA complex

Experiments that allow the detection of complexes and individual proteins provide a starting point to identify biomolecular associations. Thereafter, quantitative binding experiments are required to extract affinity, kinetic and thermodynamic data. Performing accurate association measurements requires active homogeneous protein samples, yet the inherent restraints in the assessment of the influence of solubilizing detergents, concentration and fractional activity determination of integral membrane proteins often challenges the interpretation of binding experiments. Frequently, the experimental design of membrane protein interaction

studies requires additional control assays and careful protein quantification. We intended to establish different methodological approaches to measure and quantify the Cai/pfColA interaction *in vitro*. Apart from the fluorescent Cai and pfColA obtained by fusion with GFP and Cherry proteins respectively, other derivatives were obtained by protein chemical modifications.

Initially, fluorescent fusion proteins Cai-GFP and pfColA-Cherry mixtures were incubated in the presence of DDM micelles and the extent of complex formation was detected by clear-native polyacrylamide gel electrophoresis (native-PAGE). In clear-native-PAGE in which no protein dye is used, proteins migrate according to their mass and intrinsic pI (Wagstaff et al., 2005) and the different bands can be directly assigned by in-gel fluorescence. In native-PAGE, complexes can be separated from free proteins provided that the complex is stable enough and does not dissociate during the electrophoresis. The electrophoretic separation by native-PAGE of mixtures of equimolar (10 μM) amounts of purified Cai-GFP and pfColA-Cherry incubated for 2 h at 4 °C is shown in Figure 6.1. Three bands could be distinguished: an upper band corresponding to Cai-GFP exhibiting green fluorescence, a red fluorescence band corresponding to pfColA-Cherry in the bottom of the gel and the complex, with an intermediate mobility, displaying both green and red fluorescence. The migration rate of molecules through the matrix, that determines the final positions of the bands, depends on molecular weight, charge and shape of the different protein species. Considering that Cai-GFP and pfColA-Cherry have rather similar molecular weights (49 and 50 kDa respectively) the position of the bands is mostly influenced by intrinsic pI values. pfColA-Cherry with a pI of 5.9 and -9 net charge at neutral pH penetrated the gel readily while migration was severely retarded for Cai-GFP, owing to its high pI, 8.32 (net charge +3 at neutral pH) and accumulated on top of the gel resolving region (Fig. 6.1). The complex is estimated to have a molecular weight of 100 kDa and an excess negative charge of -6, and it advanced to an intermediate position in the gel.

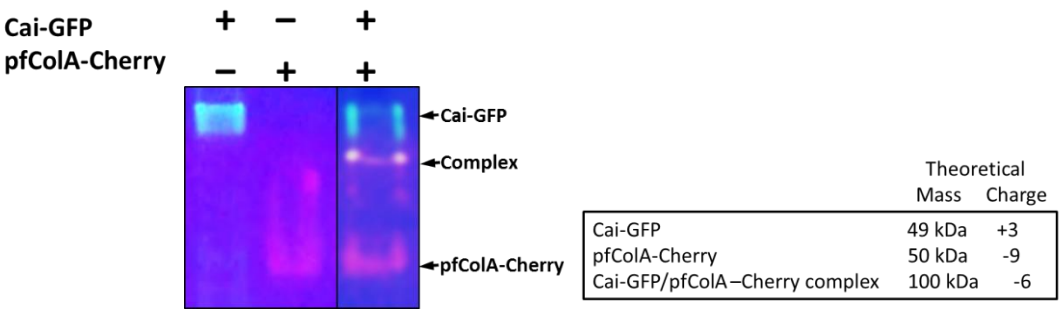

	Theoretical Mass	Charge
Cai-GFP	49 kDa	+3
pfColA-Cherry	50 kDa	-9
Cai-GFP/pfColA–Cherry complex	100 kDa	-6

Figure 6.1 Cai-GFP/pfColA-Cherry complex formation *in vitro* detected by electrophoretic mobility shift assay in native-PAGE. 10 µM of Cai-GFP (lane 1), 10 µM pfColA-Cherry (lane 2), 10 µM Cai-GFP and 10 µM pfColA-Cherry (lane 3). All samples were incubated in 0.1% DDM, 150 mM NaCl and 50 mM sodium phosphate pH 7.5. In gel-fluorescence was monitored by UV transilumination.

In-gel fluorescence provides only semi-quantitative information due to the different efficiencies of leads and filters used for detection of green and red fluorescence, and an accurate quantification is not pertinent in this case. Anyhow, it can be estimated that the distinct band with intermediate mobility showing red/green fluorescence (pfColA-Cherry/Cai-GFP complex) in Figure 6.1 does not account for more than 20-30% of the fluorescence of free proteins (pfColA-Cherry, red and Cai-GFP, green). As stated above, electrophoresis through acrylamide gels does not provide a static view of the initial equilibrium. In general, dissociation is favoured along the progress of the electrophoresis, and this effect is more dramatic for complexes with larger K_D values. Band smearing or even lack of detection of complexes is obtained in extreme cases. A moderately high K_D value could explain the results of Figure 6.1, and the amount of complex in the original loaded sample could be somewhat higher than that finally visualized in the gel. Alternatively, the apparent low yield could be explained by conformational or chemical heterogeneity in pure Cai-GFP or pfColA-Cherry samples, i.e., only a fraction of detergent-solubilized protein is native or functional. Detergent-induced denaturation and/or strong oligomerization could significantly reduce the amount of free proteins available for heterodimer formation. If the considerable amounts of free proteins coexisting in the reaction mixture were in real equilibrium in the binding reaction, this free/bound proportion should be re-established after isolation of the complex. To corroborate if this was the case the complex was purified by Ni-NTA affinity chromatography and subjected to native-PAGE (Fig. 6.2a).

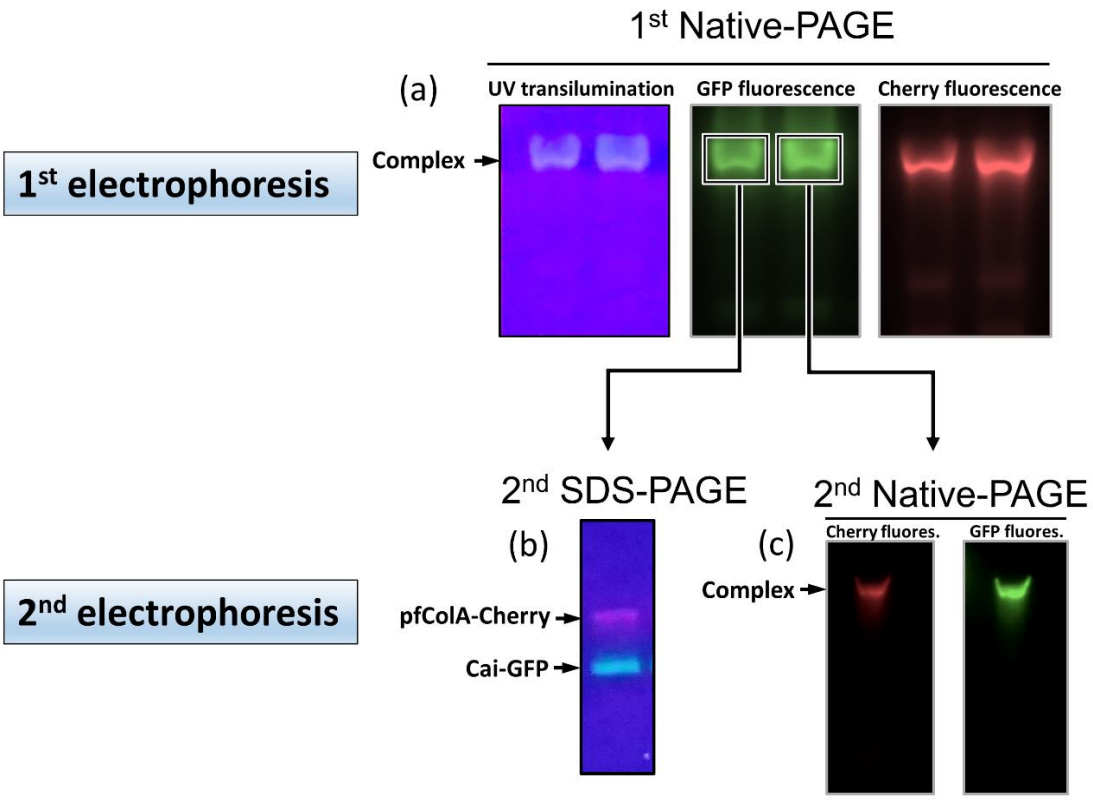

Figure 6.2 Electrophoretic analysis of the purified Cai-GFP/pfColA-Cherry complex. (a) In the first electrophoretic step the purified complex was applied into a native-PAGE gel from where the bands corresponding to the complex were cut. The gel was analysed by in-gel UV transilumination, GFP and Cherry fluorescence. (b) One of the bands from the first electrophoretic step was subjected to denaturing SDS-PAGE and the complex components could be resolved and identified owing to red and green fluorescence. (c) The other band was analysed by a second native-PAGE for which green and red fluorescence was measured. (Considering that fluorescence it is not strictly quantitative, GFP gives a higher fluorescence signal as compared to Cherry).

Each duplicate fluorescent slice of the native gel in Figure 6.2a was further analysed in a second electrophoresis, by either native-PAGE (Fig. 6.2c) or denaturing SDS-PAGE (Fig. 6.2b) (Burré et al., 2009). Interestingly, no dissociation is detected in native electrophoresis shown in Figure 6.2c, suggesting that previous partial binding (Fig. 6.1) should be explained either by parallel reactions or traps that inactivate one or both free proteins. A very slow binding reaction could also explain that result, if reaching equilibrium takes more than 2 h. Kinetics of complex formation will be further analysed below. Denaturing SDS-PAGE induced complete dissociation, further revealing that both proteins were present in the sliced band from the first native gel (Fig 6.2b).

It is important to note that GFP and Cherry tags could distort the results on homo- and hetero-complex formation, as these proteins have some tendency to dimerize. GFP used in the Cai-GFP fusion contains mutations F99S, M153T and V163A (Crameri et al., 1996; Fukuda et al., 2000) that reduce the tendency for aggregation, although further monomer stabilizing mutations like A206K are absent (Drew et al., 2008). In this sense, CaiH/pfColA complex formation was also analysed from derivatives without the fluorescent GFP or Cherry after independent expression and purification.

The His-tag tail at the C-terminus of Cai was used to purify CaiH as well as the complex after incubation with un-tagged pfColA. A two-fold excess of the latter was used to maximize the occupancy of CaiH sites, as unbound pfColA would not be retained in the Ni^{2+} affinity step. CaiH saturation was not observed under these conditions. Initial 2:1 pfColA:CaiH incubation gave rise to pfColA/CaiH complex, free pfColA and free CaiH as detected by native-PAGE (Fig. 6.3a). Relative band intensities of limiting CaiH in monomer and complex forms in the Coomassie stained gel indicate a reaction yield of ~ 40%. The sample was then mixed with pre-equilibrated Ni-NTA resin where the CaiH/pfColA was retained through the C-terminal His tagged Cai. Excess pfColA was washed away and the complex specifically eluted with buffer containing 150 mM imidazol. Eluted fractions were analysed by SDS-PAGE, where two distinct bands were detected corresponding to CaiH with an apparent mass of approximately 25 kDa and untagged pfColA with 22 kDa (Fig. 6.3b). The sample was then applied into a Superdex 200 size-exclusion column to further purify the complex and evaluate the conformational homogeneity and resilience. The CaiH/pfColA complex was detected in the major sharp elution peak as analysed by SDS-PAGE (Fig. 6.3c).

The fact that the extent of complex dissociation after two purification steps is very small, almost undetectable, speaks in favour of a stable association of non-fluorescent forms of Cai and pfColA.

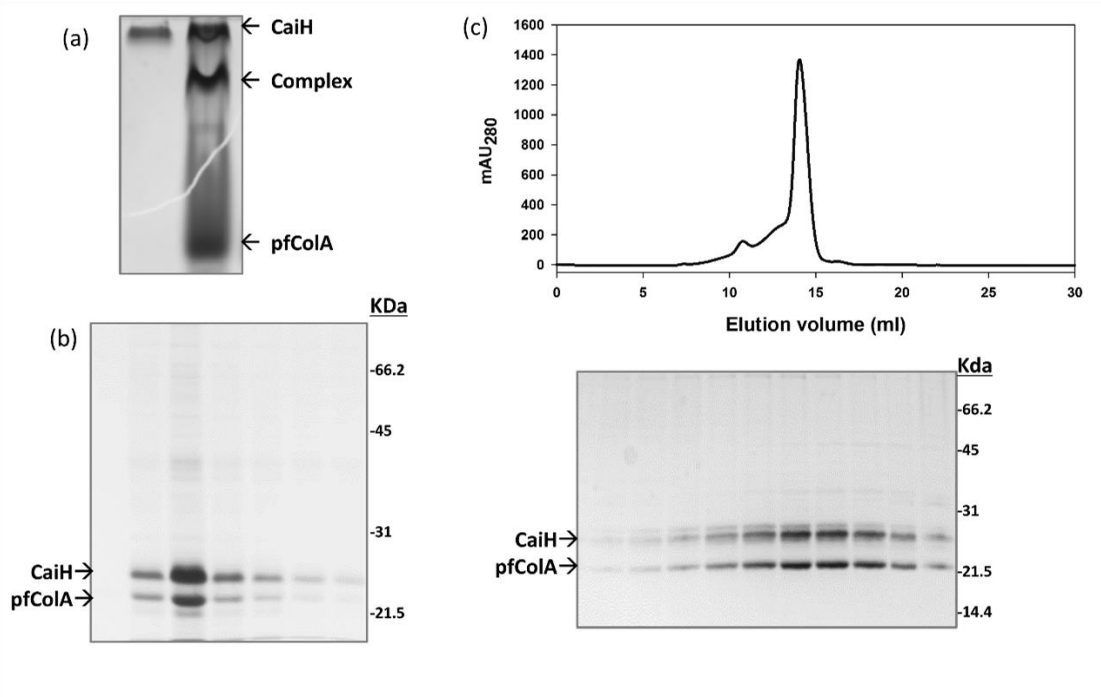

Figure 6.3 CaiH/pfColA *in vitro* complex formation and co-purification. (a) Native-PAGE of CaiH/pfColA complex formation, a 2-fold molar excess of pfColA was incubated with 160 µM CaiH in 0.2% DDM, 150 mM NaCl, 1 mM TCEP and 20 mM sodium phosphate pH 7.5 and loaded onto a 7.5% polyacrilamide gel. The gel was subjected to Coomassie staining. First lane corresponds to CaiH sample before addition of pfColA and the second lane is the CaiH/pfColA sample after 2 h incubation in which the reaction yield can be estimated. (b) SDS-PAGE of eluted fractions of the complex in Ni affinity chromatography carried out to remove the pfColA excess, the upper band represents C-terminal His-tagged CaiH and the lower band untagged pfColA. (c) Size exclusion chromatography of pfColA/CaiH complex in 0.1% DDM, 150 mM NaCl, 1 mM TCEP and 20 mM sodium phosphate pH 7.5 in a Superdex 200 column. The chromatogram is depicted in the upper part with the corresponding SDS-PAGE below, containing different fractions of the eluted protein peak.

6.2 Stoichiometry of ColA pore forming domain/immunity protein complex

Oligomerization states of pore-forming colicins (Cavard et al., 1988; Greig et al., 2009), Cai and their functional implications (Zhang et al., 2010a) have long been a matter of debate. As a first approximation similar relative intensities of pfColA and Cai protein bands in Coomassie-stained SDS-PAGE gels throughout pfColA/Cai co-purification, suggested an equimolar association. To further evaluate the molecularity of the complex, two different approaches based on bifunctional crosslinking reagents were applied. In the first procedure purified CaiH/pfColA or Cai-GFP/pfColA were crosslinked in solution by BS^3, a homobifunctional ester reactive to lysine primary amines. The second protocol involved affinity immobilization of the

His-tagged protein, Cai-GFP, incubated with the interacting partner, pfColA-Cherry, followed by glutaraldehyde crosslinking at a critically low protein density.

In the first approach, CaiH/pfColA complex purified as indicated in section 6.1 by Ni-NTA and SEC chromatography was subjected to BS^3 crosslinking. The CaiH/pfColA complex was incubated with increasing concentrations of BS^3 for 15 min at room temperature in the presence of 0.02% DDM, 100 mM NaCl and 20 mM sodium phosphate pH 7.5. All the protein in the sample was crosslinked at any BS^3 concentrations tested, yielding a crosslinked band of approximately 40 kDa, in good agreement with a theoretical molecular weight of 42.6 kDa (Fig. 6.4a).

Alternatively, glutaraldehyde crosslinking of NI-NTA resin-bound substrates was applied to purified Cai-GFP/pfColA complex. In this experiment no oligomers apart from Cai-GFP/pfColA were detected, indicating that the GFP moiety does not induce complex oligomerizations. The 1:1 stoichiometry was also confirmed here by an apparent molecular weight of ~ 70 kDa for the crosslinked band (theoretical molecular weight of Cai-GFP/pfColA complex: 72KDa) (Fig. 6.4b).

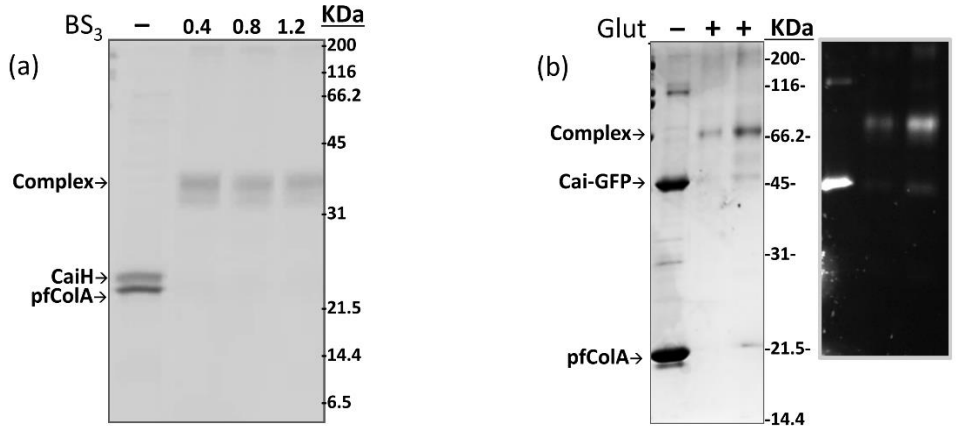

Figure 6.4 pfColA binds to CaiH and Cai-GFP in 1:1 complexes. Determination of 1:1 stoichiometry for the ColA pore forming domain/immunity protein complex. (a) BS^3 crosslinking of purified CaiH/pfColA complex in 0.02% DDM, 100 NaCl and 20 mM sodium phosphate pH 7.5 (theoretical molecular weight CaiH/pfColA complex: 42.6 KDa). The reaction was stopped after 15 min by addition of 10 mM TrisH.Cl (b) Glutaraldehyde crosslinking of purified Cai-GFP/pfColA complex in 0.1% DDM, 100 mM NaCl and 50 mM sodium phosphate pH 7.5 (theoretical molecular weight of Cai-GFP/pfColA complex: 72kDa). The crosslinked samples contain ten times (lane 2) and five times (lane 3) less total protein compared with the control sample to which no glutaraldehyde was added (lane 1) Coomassie staining (left) GFP fluorescence (right).

Crosslinking by glutaraldehyde was also performed by adding equimolar amounts of pfColA-Cherry to immobilized Cai-GFP. Although a relatively large amount of Ni-NTA resin was used for crosslinking experiments of immobilized protein with glutaraldehyde to avoid unspecific reactions, Cai-GFP oligomers are observed in the denaturing gels of the Cai-GFP/pfColA-Cherry reaction after elution from the resin (high MW green bands in Fig. 6.5). This suggests that Cai association might be in competition with complex formation. Regarding the co-migration of Cai-GFP bound to pfColA-Cherry however, a single band was detected which emits both red and green fluorescence and an apparent molecular weight of ~100 kDa corresponding to a 1:1 complex. Extensive dimerization is observed however in control experiments in which individual proteins were subjected to the same protocol.

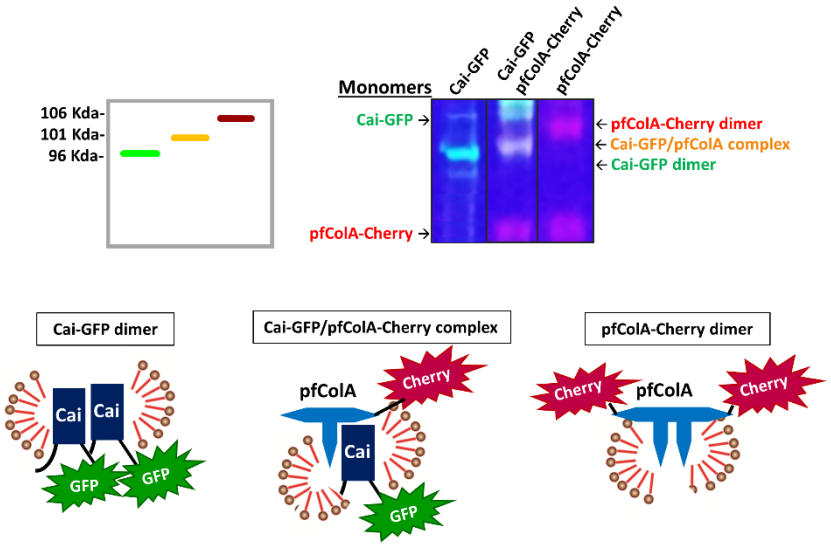

Figure 6.5 Protein oligomerization state based on the combination of Ni affinity chromatography and glutaraldehyde crosslinking. 200 µg Cai-GFP, 200 µg Cai-GFP plus 200 µg pfColA-Cherry and 200 µg pfColA-Cherry were immobilized in Ni-NTA resin, crosslinked with glutaraldehyde and subjected to SDS-PAGE analysed by UV transilumination of the gel. At the left hand of the gel, a diagram indicating the theoretical molecular weight of the crosslinked bands. Below the gel: schematic representations of the hypothetical homo and hetero-dimers present in the samples.

6.3 Stability and conformational analysis of Cai/pfColA complex

The accumulated experience dealing with the stability of soluble proteins has established a solid methodological and theoretical framework to study protein folding and dynamics. Thus, conformational dynamics and stability of soluble globular proteins *in vitro* has provided a better understanding of protein structure-function principles. In comparison, the advances in the thermodynamic characterization of membrane protein stability lags far behind. Despite

the potential biological and biomedical significance of membrane proteins, the number of studies dealing with their stability, conformational dynamics or high resolution mechanistic models are very scarce. Even considering the high complexity of the thermodynamics governing the folding process of soluble proteins, a simple methodology is available to measure their stability by means of the free energy of folding, $\Delta G_{D\text{-}N}$ (Fersht, 1999). Helical membrane proteins, on the contrary, appear to be resistant to chaotropic agents and total thermal denaturation (Roman and González Flecha, 2014). Taking into account these limitations, we attempted to explore the biophysical and spectroscopic techniques available to characterize the conformational stability of the Cai/pfColA complex. Once verified that it was possible to isolate and purify the Cai/pfColA complex in relatively high amounts (Fig. 6.6b inset), the complex was subjected to CD analysis, thermal unfolding, urea denaturation, cysteine accessibility, and NMR spectroscopy.

The effect of binding on the CD spectra of individual pfColA or Cai was investigated to detect any change in secondary or tertiary structure. Far and near-UV CD spectra of the pure CaiH/pfColA complex compared with spectra of individual free proteins revealed that while binding did not significantly affect per-residue α-helical content (not shown), near-UV signal was significantly affected (Fig. 6.6b). Near CD spectra of pfColA in 0.1% DDM shows a more intense negative ellipticity (with a minimum at 272 nm) than CaiH (minimum at 278 nm). Simple addition of both spectra does not account for the signal recorded for CaiH/pfColA complex, with an intensity similar to pfColA but shifted to longer wavelengths (minimum 277 nm). Overall, the differences in the conformation of aromatic residues suggested that the Cai/pfColA complex represents a distinct tertiary fold that cannot be explained by the simple arithmetic sum of near-CD spectra of protein components alone.

Our first hypothesis implied that binding of pfColA to CaiH would stabilize the structure of one or both of the proteins, and that this could be monitored either by chemical or physical denaturation. Thermal unfolding can be followed by measuring ellipticity at 222 nm over a T range of 20 °C to 90 °C. Figure 6.6a depicts the θ_{222} temperature scans of Cai, pfColA and Cai/pfColA complex. The loss on secondary structure of Cai occurred with an apparent Tm of 55 °C, showing considerable cooperativity. However, protein aggregation due to deficient solubilization by DDM might account for part of the signal loss. At 90 °C Cai retained a

considerable helical content as expected for helical membrane proteins for which the unfolding of α-helices in an hydrophobic environment is very unfavourable (Cymer et al., 2015). Alternatively, pfColA showed a gradual loss of secondary structure with very poor cooperativity. This is consistent with previous results reporting the absence of an unfolding transition for the membrane-inserted form of pfColA in DOPG vesicles (Muga et al., 1993). A very similar trend is observed for Cai/pfColA complex although shifted to slightly lower temperatures, what refutes the idea of a pfColA secondary structure stabilization induced by CaiH binding.

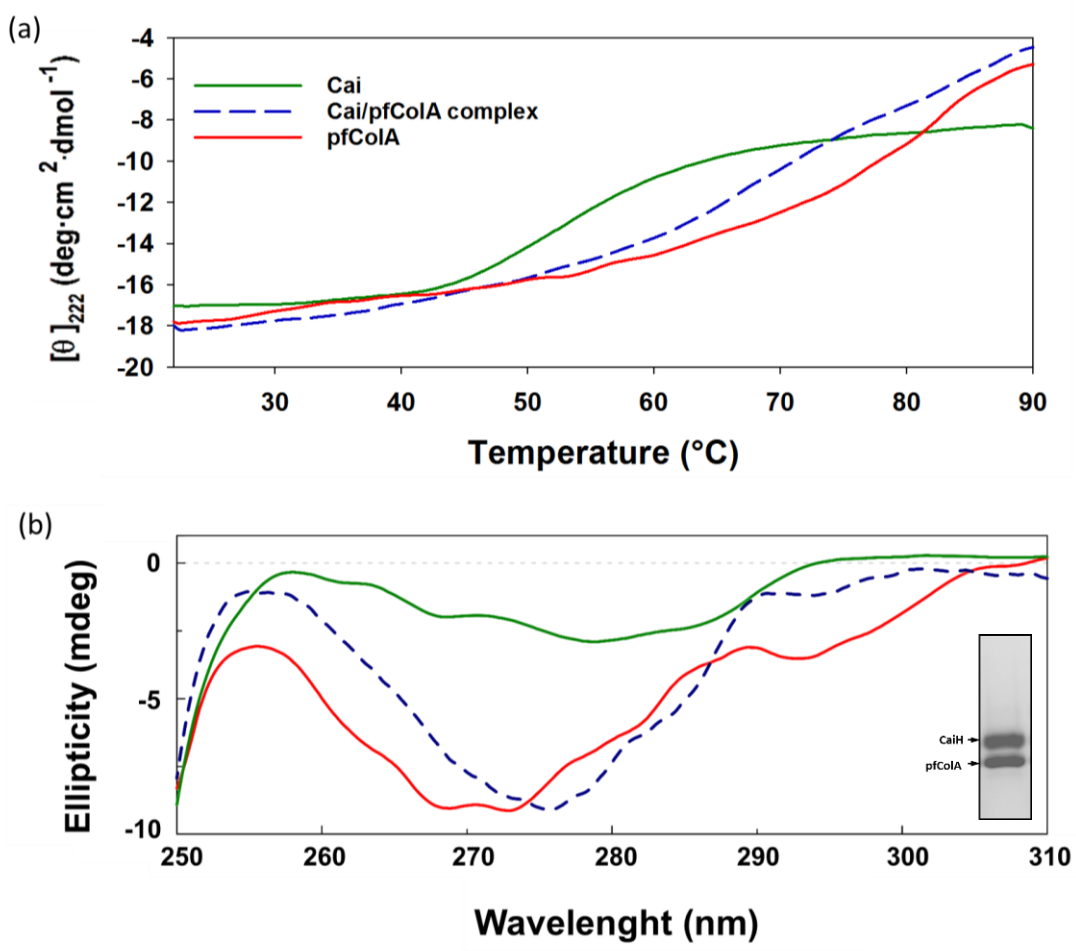

Figure 6.6 CD analysis of Cai/pfColA complex. (a) Temperature scans monitored by ellipticity at 222 nm of 5 μM Cai/pfColA (blue), Cai (green) and pfColA (red) in 20 mM sodium phosphate, 150 mM NaCl, 0.1% DDM pH 7.5**.** (b) Tertiary structure of 50 μM Cai/pfColA (blue), Cai (green) and pfColA (red) in 20 mM sodium phosphate, 150mM NaCl, 0.1% DDM pH 7.5 (c). (SDS-PAGE of purified CaiH/pfColA complex; inset).

To further complement the data obtained by thermal denaturation, the CPM fluorescent assay was used to study the relative stability of Cai/pfColA complex with respect to that of isolated Cai. Since Cai contains four cysteines in the transmembrane segments, while pfColA contains no cysteine residue, the chemical reactivity of cysteines served as a measure of overall integrity of the protein complex. At the same time, despite a low occurrence in α-helices (around 2%), cysteines have a high propensity to take part in membrane protein helix-helix interfaces due to their high packing value (Eilers et al., 2002). Following this approach Cai, pfColA and Cai/pfColA were exposed to CPM dye which became fluorescent upon reacting with free sulfhydryl groups yielding isothermal denaturation profiles presented in Figure 6.7. This assay provides a measure of relative stability expressed as unfolding half-life values of 12 min for Cai and 22 min for the Cai/pfColA complex. Half-lifes were obtained after fitting the data to a single exponential function by non-linear regression analysis. Therefore, the slightly greater half-life of the Cai/pfColA complex indicates a more stable conformation of Cai, with a lower degree of solvent exposure of transmembrane regions.

The raw fluorescence intensity plots are shown in Figure 6.7 to illustrate the different intensities at which traces saturate, reflecting differences in the number of derivatized cysteines at 30 °C for the different molecular species tested. CPM incorporation has been used previously to quantify the extent of cysteine labelling or CPM accessibility to different sites of both soluble and membrane proteins (Branigan et al., 2013). In the case of Cai, the highest fluorescent signal was achieved while the Cai/pfColA complex reached half the fluorescence of Cai alone. This seems to indicate that additional cysteine residues protected in the interior of Cai are no longer accessible to the CPM dye upon pfColA binding. The pfColA sample in DDM corresponds to the baseline fluorescence signal as it contains no cysteine residues. This data suggests that part of the cysteine residues are engaged in the CaiH/pfColA binding interface. This result was also observed when attempting to label the complex and individual proteins for kinetic binding experiments presented below.

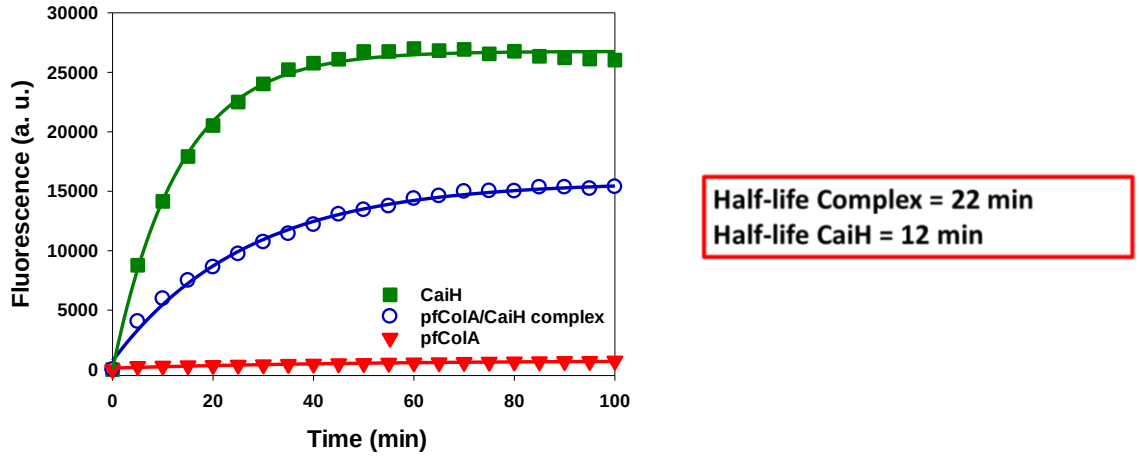

Figure 6.7 Cysteine accessibility for Cai, pfColA and Cai/pfColA complex as seen by isothermal incorporation of CPM over time. CPM incorporation to 4 µM CaiH (green), pfColA/CaiH complex (blue) or pfColA (red) was followed by fluorescence at 463 nm at 30 °C in 0.03% DDM, 100 mM NaCl, 20 mM TRIS pH 7.5. Unfolding half-lifes were calculated by fitting the data to a single exponential function.

As mentioned above chemical destabilization together with thermal unfolding are commonly used to characterize the effect of molecular binding in terms of conformational stability. Chaotropic agents like urea or guanidinium chloride cause protein denaturation through solubilization of the protein polypeptide backbone and hydrophobic side chains (Tanford, 1968). The denatured state is more exposed to the solvent and becomes more populated as the denaturant concentration increases. This is true for the destabilization of intra-molecular interactions, occurring at a single polypeptide chain, as well as inter-molecular interactions between two molecular partners. Thus, we were interested in testing the capacity of urea to disrupt the three dimensional structure configuring the Cai/pfColA binding interface. It is important to consider that the unavoidable requirement of detergents and other membrane mimetic systems in membrane protein samples creates highly anisotropic environments making spectroscopic analysis more challenging. On top of that, the differences between the folded and unfolded states for transmembrane helices are often very small (Schlebach et al., 2011).

The first approach to evaluate whether urea could destabilize the Cai/pfColA complex in DDM micelles, involved analysing stability changes by far-UV CD, native-PAGE and Trp fluorescence intensity upon addition of 6 M urea (Fig. 6.8). Figure 6.8a indicates a substantial loss in secondary structure of the complex in urea, equivalent to half of the total ellipticity observed in native conditions. The native-PAGE of the pure Cai/pfColA complex in native *versus* denaturing conditions revealed the loss of the complex integrity in 6 M urea as the CaiH and pfColA protein components migrated separately towards their corresponding electrophoretic

positions. Urea-induced aggregation artefacts cannot be discarded and could be responsible for the intense band detected at the top of the gel. The fluorescence emission spectrum of Cai/pfColA is mainly determined by the polarity of the environment around the three tryptophan residues present in helix four and seven of pfColA (W88, W132 and W142). While Cai contains no tryptophan residues, the accumulation of small fluorescence contributions owing to the high number of tyrosine residues present in Cai might not be negligible (Cai contains 11 tyrosine residues). The emission spectra of 4 µM Cai/pfColA displayed both a change in the maximum emission wavelength, showing a shift from 235 nm in native conditions to 245 nm in denaturing conditions, as well as a minor increase in fluorescence intensity after adding 6 M urea (Fig. 6.8c).

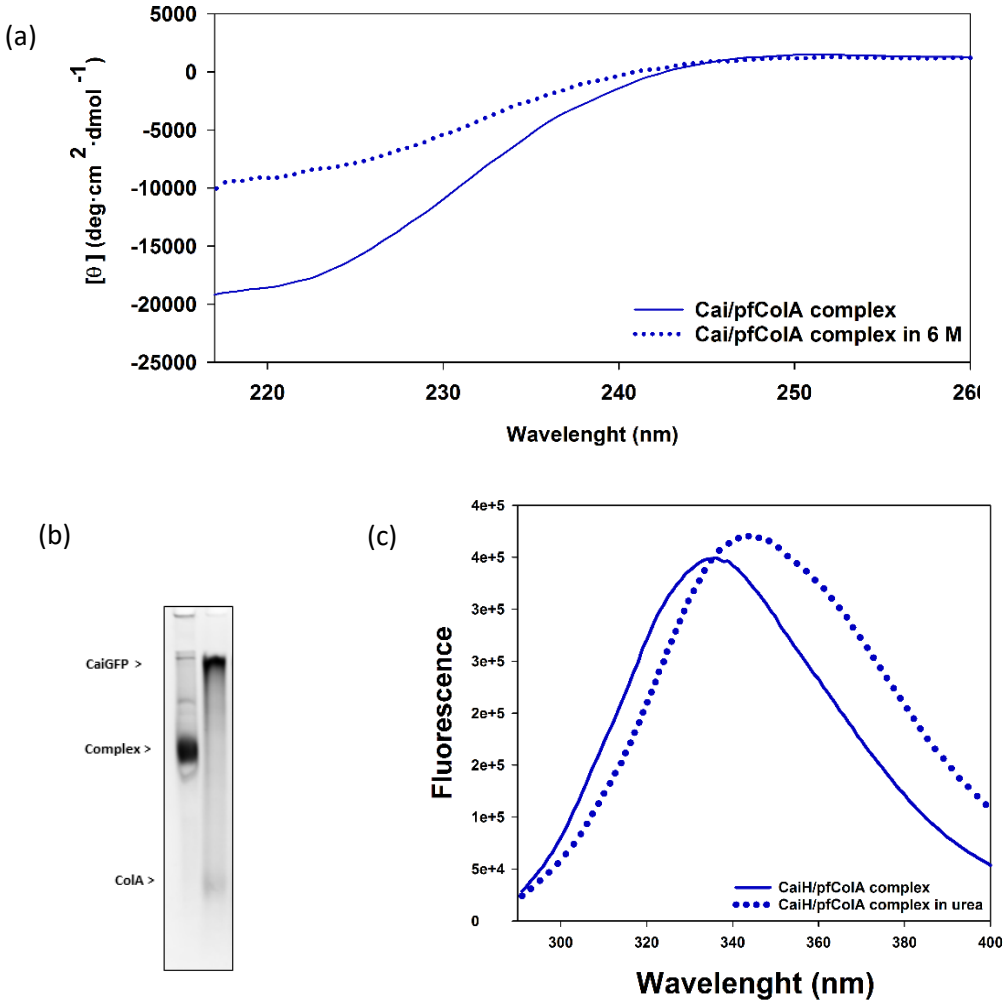

Figure 6.8 Chemical destabilization of Cai/pfColA complex by 6 M urea. (a) Far-UV CD spectra of 4 µM of Cai/pfColA complex (solid line) and 4 µM of Cai/pfColA complex in 6 M urea (b) Native-PAGE analysis of Cai/pfColA complex in the absence (lane 1) and the presence of 6 M urea (lane 2) (c) Fluorescence emission spectra of 2.5 µM Cai/pfColA complex (solid line) and Cai/pfColA complex in 6 M urea (dashed line) in 0.05% DDM 100 mM NaCl, 20 mM HEPES pH 7.5.

Experiments on urea-induced protein denaturation can be used to extract valuable thermodynamic information when certain physical-chemical conditions are fulfilled. Thus the free energy of unfolding of the soluble form of pfColA can be readily estimated measuring the changes in intrinsic fluorescence as a function of urea concentration. $\Delta G_{N\text{-}D}$ can be extrapolated to native conditions in the absence of denaturant, since the free energy of transferring the protein from water to denaturant is linearly proportional to the concentration of denaturant. But in order to extract $\Delta G_{N-D}^{H_2O}$, the unfolding transition must be fully reversible. This is an empirical model that does not hold for the majority of integral membrane proteins. As a consequence, urea denaturation must be tested on a case-to-case basis. Thus, once observed that 6 M urea can indeed destabilize the Cai/pfColA complex, and given that at least pfColA denaturation is reversible, we sought to investigate the effect of titrating pfColA with denaturant with or without bound CaiH. Denaturation curves for pfColA and Cai/pfColA in DDM micelles are depicted in Figure 6.9a together with the denaturation curve for soluble pfColA used as a reference. The urea-induced transition of the three molecular species displays sigmoidal profiles. Strikingly the denaturation curve for pfColA is almost indistinguishable from that of the Cai/pfColA complex. Because this experiment is sensitive to stabilizing effects over pfColA, different scenarios could explain this data: (i) the surrounding environment of tryptophan residues is not able to sense the interaction with Cai (there should be unconnected folding units, at least one with the three tryptophans and another one with the binding site for Cai), or (ii) most probably, that the complex is dissociated at a lower urea concentration than that required to unfold pfColA. In fact, previous results demonstrated that Cai/pfColA complex dissociates at urea concentrations lower than 6 M (Fig. 6.7) at which pfColA is folded. Interestingly, the total variation in fluorescent intensity was two-fold lower for the proteins in detergent micelles as compared with soluble pfColA (raw data, not shown).

Estimated thermodynamic parameters obtained by fitting the fluorescence transition observed in Figure 6.9a to a two-state unfolding model (Eq. 5 under Experimental Procedures) are shown in table 6.1. pfColA and the CaiH/pfColA complex, both in DDM (red and blue traces in Figure 6.9a) show a much lower unfolding cooperativity, exemplified by the $m_{N\text{-}D}$ parameter (1.4 and 1.6 kcal mol^{-1} M^{-1}, respectively) as compared with soluble pfColA without detergent ($m_{N\text{-}D}$ 2.9 kcal mol^{-1} M^{-1}). The conformation that pfColA adopts in detergent is also less stable

in 0 M urea ($\Delta G_{N-D}^{H_2O}$ =-10 or -11 kcal mol^{-1}) compared with the soluble free form ($\Delta G_{N-D}^{H_2O}$ = -17 kcal mol^{-1}), although the mid-point of denaturation occurs at higher urea concentration (7.1 M *versus* 5.9 M urea respectively) due to the lower cooperativity. The calculated parameters for the three species were used to create the model curves of Gibbs energy dependence with urea concentration shown in Figure 6.9b according to the equation: $\Delta G_{N-D} = \Delta G_{N-D}^{H_2O} + m_{N-D}$ [urea] (Eq. 4), where slopes represent m_{N-D} values; lines cross the ordinate at $\Delta G_{N-D}^{H_2O}$ and the abscissa at the midpoint of denaturation, where ΔG_{N-D}=0.

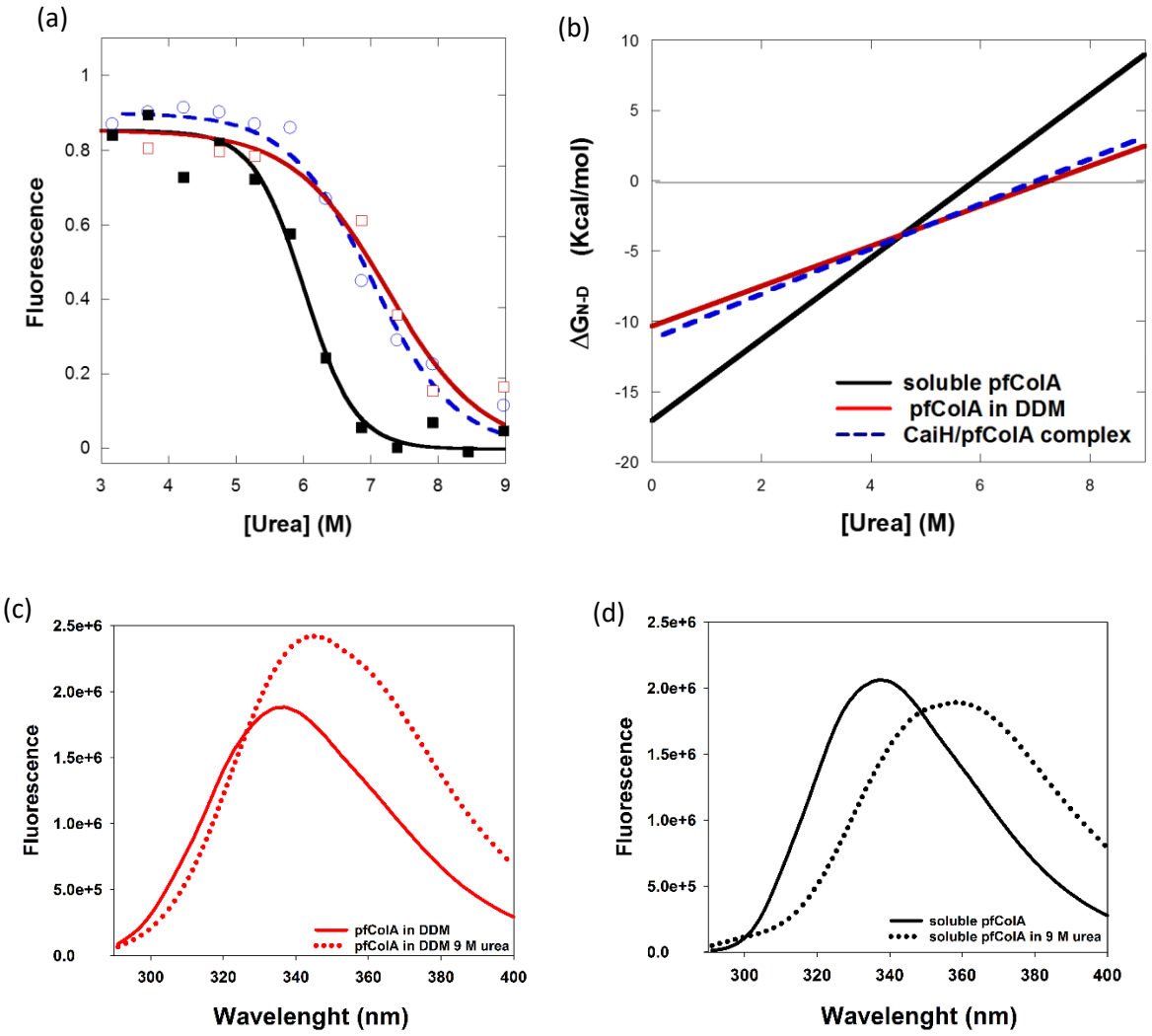

Figure 6.9 Chemical unfolding studies of CaiH/pfColA complex and pfColA. (a) Unfolding as a function of urea concentration monitored by tryptophan fluorescence intensity at 315 nm for CaiH/pfColA complex (blue open circles), soluble pfColA (black squares) and pfColA in DDM (red open squares). Samples were incubated in urea for 30 min before measurement. (b) Linear extrapolation of the dependence on free energy change as a function of urea concentration. (c) Fluorescence emission spectra of 2.5 µM pfColA (solid line) and pfColA in 9 M urea (dashed line) in 0.05% DDM 100 mM NaCl, 20 mM HEPES pH 7.5. (d) Fluorescence emission spectra of 2.5 µM pfColA (solid line) and pfColA in 9 M urea (dashed line) in 100 mM NaCl, 20 mM HEPES pH 7.5.

The $m_{D\text{-}N}$ value, or unfolding cooperativity, measured as slope of $\Delta G_{N\text{-}D}$ dependence with urea concentration is generally interpreted as a measure of the change in buried surface area during unfolding. A high $m_{D\text{-}N}$ value implies a compact folded state that buries a large hydrophobic region and that unfolds completely with urea to a highly unfolded state in which this area becomes exposed. Small hydrophobic cores in folded states or incomplete denaturation to partially structured conformations can both explain low $m_{D\text{-}N}$ values.

Table 6.1 Thermodynamic parameters for soluble pfColA, pfColA in DDM detergent micelles and Cai/pfColA in DDM detergent micelles.

	$\Delta G_{N-D}^{H_2O}$ (kcal ·mol^{-1})	$m_{D\text{-}N}$ (kcal ·mol^{-1}·M^{-1})
Soluble pfColA	-17 ± 1.	2.9 ± 0.7
pfColA in DDM	-10. ± 1.	1.4 ± 0.3
Cai/pfColA complex	-11 ± 1.	1.6 ± 0.2

Since $\Delta G_{N\text{-}D}$ and $m_{D\text{-}N}$ are differential quantities, their interpretation could be made on the basis of the native and/or denatured states. This is especially pertinent when considering denaturation of detergent-solubilized membrane proteins. The hydrophobic environment imposed within micelles bias the conformational ensemble to species with high secondary structure content and thus the reference state still preserves some native features. The lower stability and cooperativity induced by detergent solvation of pfColA agrees with this expectation. Also the relatively high content in α-helix (Fig. 6.8a) and the less exposed environment of tryptophans (more intense blue-shifted fluorescence, Fig. 6.9c, d) in high urea concentration suggest important differences regarding the exposure to solvent and remnant structure of the urea-induced states in the presence and absence of detergent. Additionally, substantial differences can be envisioned between detergent-protein complexes and soluble free protein in the absence of urea, but techniques such as CD and fluorescence are less sensitive to detect them, because both protein components have high secondary structure content and buried tryptophan residues.

6.4 Equilibrium binding of Cai with pfColA

To our knowledge, there is no previous information in the literature about the affinity or interaction dynamics of any pore-forming colicin with its cognate immunity protein. Our previous results indicated that formation of Cai/pfColA complex as a conformationally stable form was achievable and a moderately high affinity could be anticipated as the two proteins co-purify after bacterial membrane solubilization and can only be separated under denaturing conditions (urea or harsh detergents). We then addressed *in vitro* equilibrium binding experiments to obtain parameters like affinity, kinetic stability or association rates. Since one possible reason for the apparent low efficiency in complex formation described in section 6.1 was that a 2 h incubation was insufficient to complete the reaction, an initial estimation of the reaction rate was made by native gel electrophoresis of mixtures of the fluorescent proteins. It was observed that several hours were needed to reach equilibrium. For the following series of experiments, reagents were left to react overnight, unless otherwise stated.

Titration experiments were conducted using several combinations of the different available versions of both Cai and pfColA. Results shown in Figure 6.10 were obtained by native-PAGE of mixtures of 6 μM pfColA-Cherry with increasing concentrations of Cai-GFP, kept at room temperature overnight in 0.02% DDM, 50 mM NaCl and 10 mM sodium phosphate pH 7.5. A first estimate of K_D ~ 8 μM was calculated by fitting the intensity of the Coomassie-stained band corresponding to the Cai-GFP/pfColA-Cherry complex to equation 6 (under experimental procedures). The plot of the intensity of the complex *versus* added Cai-GFP is depicted in Figure 6.10d. Interestingly, all the red pfColA-Cherry is converted into the orange complex at saturating concentrations of Cai-GFP. The same is not true if Cai-GFP is kept constant in mixtures with increasing concentrations of pfColA (Fig. 6.11). Higher pfColA concentrations do not induce changes in the intensities in any of the two green fluorescent bands corresponding to the free and bound Cai-GFP. This explains our initial observation in Section 6.1 of partial binding with equimolar mixtures of Cai-GFP and pfColA-Cherry under conditions where the complex does not re-equilibrate to the same dissociation degree when separated from reactants. The coexistence of unreactive – active populations (undistinguishable by native-PAGE when free) of any of the complex components would justify partial binding even if concentrations are well above K_D. Since equimolar amounts were

used in section 6.1, some Cai-GFP would be unavailable because of inactivation and the corresponding fraction of pfColA would remain free because of the absence of partner Cai-GFP. The fact that Cai-GFP is partially inactivated is not surprising due to its highly hydrophobic character. DDM is not one of the most solubilizing detergents (see Chapter 3) and the low concentration used in these experiments (0.02% w/v) may be insufficient to keep the protein in solution in the long run. Our observations are consistent with DDM induced Cai-GFP aggregation as the main source of inactivation and apparent low yield in complex formation.

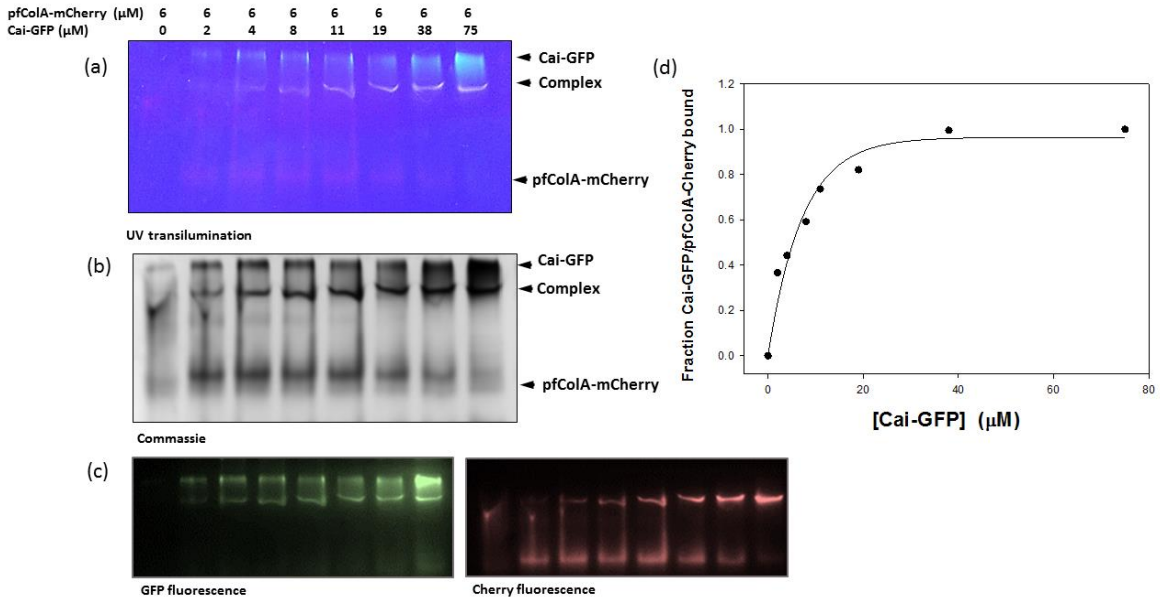

Figure 6.10 Equilibrium binding isotherm between Cai-GFP and pfColA-Cherry. 6 μM pfColA-Cherry was incubated with increasing concentrations of Cai-GFP (0, 2, 4, 8, 11, 19, 38, and 75 μM) overnight, in the buffer: 0.02% DDM, 50 mM NaCl and 10 mM sodium phosphate, pH 7.5. (a) Native-PAGE of the separation of the complex and the reacting proteins, band identified by UV-transillumination. Numbers above each lane indicate total Cai-GFP and pfColA-Cherry concentrations added. (b) Coomassie-staining of Native-PAGE gel. (c) Native-PAGE gel analysed separately for GFP fluorescence (left) and Cherry fluorescence (right). (d) Quantification of the Coomassie-stained band corresponding to the complex and plotted against added Cai-GFP concentration.

Since Cai-GFP does not enter into the native gel even as a monomer, the extent of inactivation cannot be distinguished at low pfColA concentrations (Fig. 6.11). At saturating concentrations, however, inactive Cai-GFP remains in low-mobility positions while pfColA-bound Cai-GFP migrates to the expected mobility for the complex. A ~30% inactive Cai-GFP fraction can be estimated under these experimental conditions. At low pfColA concentrations, experimental

data deviates significantly from the model. Only above 5 µM pfColA can the complex be visualized, initially with intermediate mobilities. This raised the idea that pfColA could bind to Cai-GFP oligomers at low pfColA:Cai-GFP ratios and that stoichiometries other than 1:1 can be coexisting under conditions where there is not enough pfColA to extract Cai-GFP from higher oligomers and reach the final 1:1 complex.

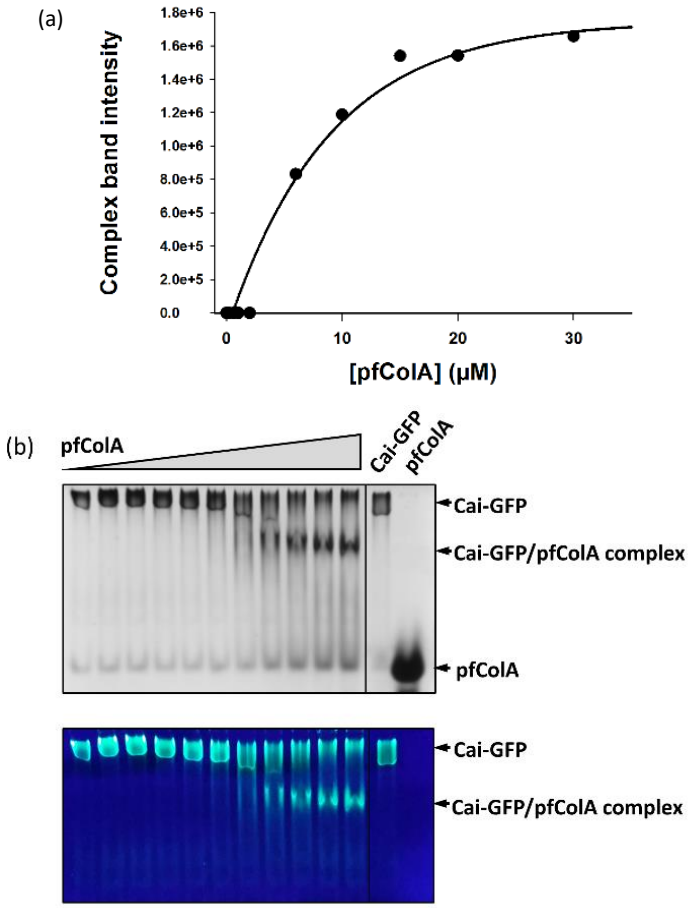

Figure 6.11 Equilibrium binding of pfColA to Cai-GFP measured by increased fluorescence anisotropy and native-PAGE. (a) Quantification of the native-PAGE band corresponding to Cai-GFP/pfColA complex by gel densitometry of the Coomassie stained gel. (b) Native-page analysis of the samples used for anisotropy measurements.

This effect was corroborated by titrating non-fluorescent CaiH with a fluorescein-labelled pfColA derivative. Lanes 2, 3 and 4 of the native gel shown in Figure 6.12 contain 10 µM CaiH and 2, 6, 10 µM FITC-pfColA concentration. For ratios below 1:1 pfColA does not fractionate into a free high-mobility form and a complexed intermediate-mobility band, as expected. For mixing ratios with excess Cai-GFP, pfColA seems to incorporate to the very low mobility, probably oligomeric, Cai-GFP. A monomerizing effect of pfColA on an otherwise dimeric Cai

was also proposed *in vivo* by Zhang and cols. (2010). Although we can be confident about the final 1:1 stoichiometry, we should be cautious while analyzing titration data in which complexes or different ratios could coexist.

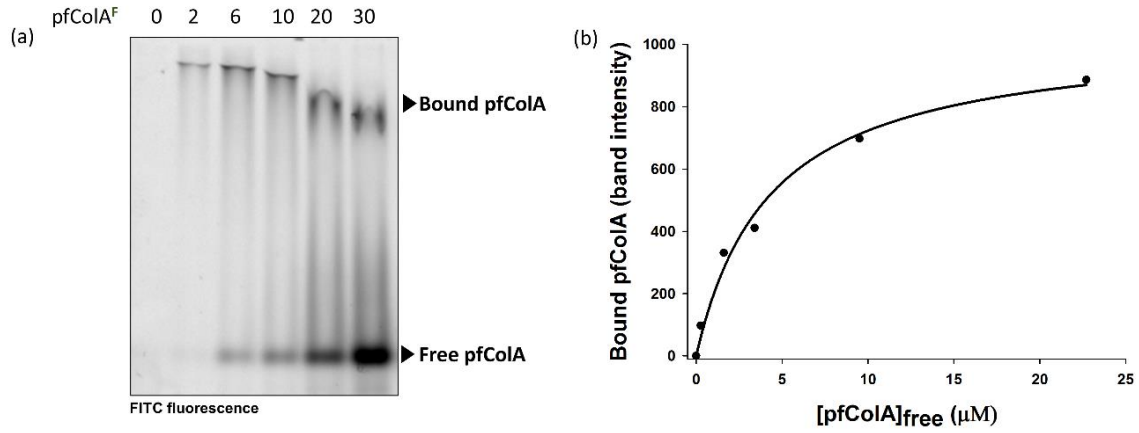

Figure 6.12 Equilibrium binding of FITC-labelled pfColA to CaiH measured by quantification of the complex band against the free ligand fluorescence intensity. (a) In-gel fluorescence of FITC labelled pfColA in native-PAGE gel. Loaded samples contained 10 μM CaiH and increasing concentrations of FITC-labelled pfColA. (b) Equilibrium binding isotherm of CaiH/pfColA complex against free pfColA concentration as quantified from native-PAGE gel.

As indicated previously, only qualitative information can be expected from native-PAGE data, since the experiment does not proceed under equilibrium conditions. As soon as the different species start progressing through the gel, reactants and products are separated and new equilibria are established. The whole process acts in favour of dissociation and approximate affinities are underestimated. Spectroscopic features of samples in equilibrium are more appropriate to derive quantitative binding data. The chosen spectroscopic signal should be differentially sensitive to free and bound species. Fluorescence of the GFP and Cherry fusion derivatives was insensitive to binding because fluorophores are very distant from the Cai/pfColA interaction interface. Intrinsic pfColA fluorescence was neither useful, because the apolar environment around pfColA tryptophans is common to both free and bound species in detergent. Additionally, tryptophan residues are absent in Cai sequence. Fluorescence anisotropy was finally chosen to obtain affinity as well as kinetic information of Cai/pfColA interaction.

Fluorescence anisotropy can be related to the rotational diffusion of the molecules, hence when the fluorescently labelled molecule binds its partner, the complex results in a lower rotational diffusion coefficient and a higher fluorescence anisotropy (James and Jameson,

2014; Jameson and Mocz, 2005; Lakowicz, 2006). Three different fluorophores were used for different steady-state and time-resolved anisotropy measurements: to label Cai, GFP and the small thiol-reactive fluorophore coumarin (CPM) were used while the amine-reactive fluorescein (FITC) was added to pfColA.

Results on Cai-GFP titration experiments with pfColA are shown in Figure 6.13 4 μM Cai-GFP aliquots were mixed with increasing concentrations of pfColA up to 30 μM and incubated overnight in 0.01% DDM, 50 mM NaCl and 10 mM sodium phosphate pH 7.5. As expected, the K_D = 0.48 μM calculated by fitting the anisotropy data (Fig. 6.13) is lower than qualitative values obtained earlier by native-PAGE. A simple hyperbolic binding equation without direct information on actual [pfColA] for each point, would be inadequate in this scenario, in which the concentration of substrate being titrated is of the same order as the K_D value. Although we considered the partition of the added ligand in free and bound forms (Eq. 6, under Experimental procedures) calculated K_D can be underestimated in this experiment. Much lower [Cai-GFP] would be more adequate for the determination of a K_D ~ 1 μM (Pollard, 2010), but the anisotropy signal would be insufficient and too noisy.

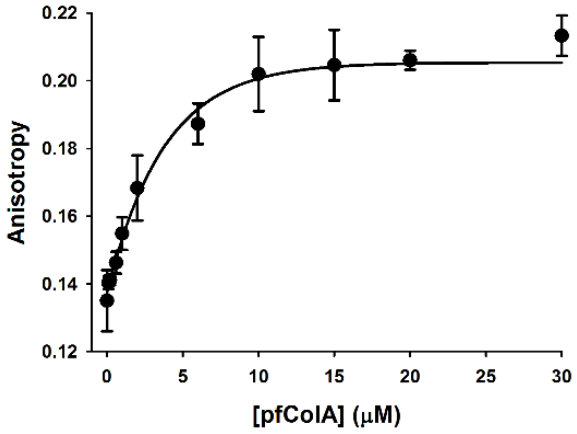

Figure 6.13 Fluorescence anisotropy changes upon pfColA addition to 4 μM Cai-GFP. Fluorescence anisotropy measurements monitored by excitation at 470 nm and emission at 530 nm at 20 °C in 0.05% DDM, 50 mM NaCl, 10 mM sodium phosphate pH 7.5.

6.5 Cai - pfColA binding kinetics

The Cai/pfColA association kinetic constants that could be calculated in a micellar aqueous media should greatly differ from those within the membrane, however their sensitivity to different factors could help extracting some mechanistic information. We report here dissociation experiments by subunit exchange and association reactions under pseudo-first order conditions to measure the kinetic constants of the pfColA /Cai complex.

Obtaining the k_{off} appeared relatively straightforward once the CaiH/pfColA complex could be isolated. The dissociation reaction would, in principle, be less influenced by side reactions, detergent concentration effects, or errors in protein concentration measurements. As a matter of fact, k_{off} is concentration-independent and reflects the probability that the complex will spontaneously fall apart in a unit of time. Studying the association reaction *in vitro*, on the other hand, seemed more challenging *a priori*, as conditions would greatly differ from those in the physiological scenario.

The dissociation rate reaction was studied by subunit exchange. The simplest way to observe the dissociation was to chase the anisotropy of labelled bound CaiH once exposed to a large excess of an unlabeled CaiH competitor, thereby minimizing the contributions of rebinding to the observed rate. Thus a 15-fold excess of unlabeled CaiH (36 µM) was incubated with the purified, stoichiometric complex between pfColA and CPM labelled CaiH (2.5 µM complex). The dissociation rate was followed by monitoring the decrease in fluorescence anisotropy of CPM-labelled CaiH as it separates from the complex over time (Fig. 6.14b). The fluorescence emission of CPM bound to CaiH was recorded using an excitation wavelength of 387 nm and monitoring the fluorescence emission at 450 nm with excitation and emission slits of 5 nm. Reactions were carried out in 0.02% DDM, 50 mM NaCl and 10 mM sodium phosphate pH 7.5 buffer at 20 °C. The data were fitted to a single exponential decay function yielding a k_{off} = 0.004 ± 0.0003 s^{-1}. The time course was repeated and a higher concentration of CaiH was also tested (45 µM) to ensure that the conditions used did not substantially affect the rate constant being measured.

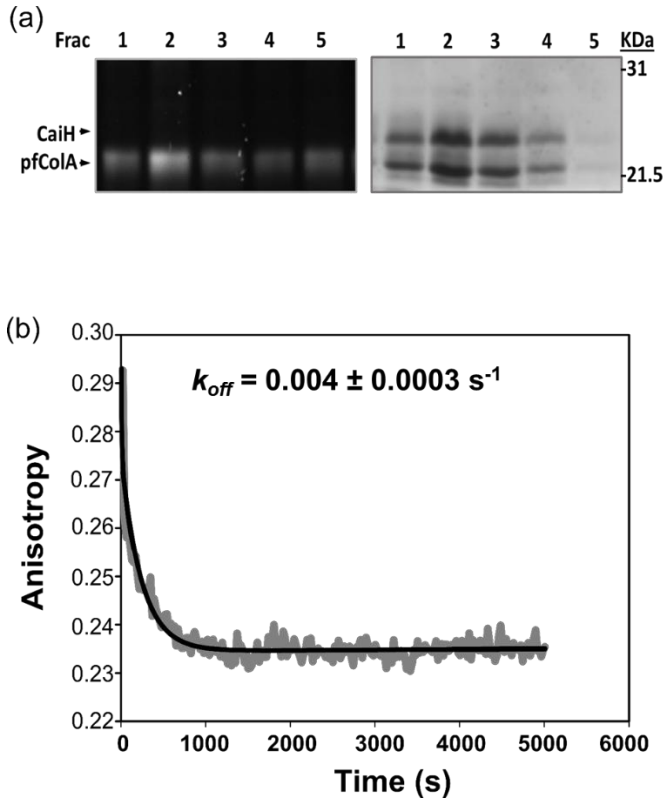

Figure 6.14 Time course of the dissociation of CaiH from CPM labelled CaiH/pfColA complex followed by fluorescence anisotropy. (a) SDS-PAGE of the eluted fractions from Superdex 200 of the complex, CPM labelled CaiH in association with unlabelled pfColA. In-gel fluorescence (left) Coomassie staining (right) (b) Dissociation followed by fluorescence anisotropy. A 15-fold molar excess of unlabelled CaiH (36 µM) was incubated with the purified, stoichiometric complex between pfColA and CPM labelled CaiH (2.5 µM of complex).

The FITC-modified pfColA (prepared as indicated under experimental procedures) was used to estimate an association kinetic constant (k_{on}). Compared with other fluorophores (GFP and coumarine), FITC has a relatively longer fluorescence lifetime which could be more advantageous for fluorescence anisotropy measurements. Interestingly, when binding of pfColA to CPM labelled CaiH was tested no anisotropy increase was detected, which suggest that some of the cysteines might be located at the binding interface.

The polarization increase induced by complex formation of FITC-labelled pfColA was measured upon addition of increasing amounts of CaiH. As a second-order reaction the association of pfColA with CaiH was studied under pseudo-first order conditions with a low concentration of labelled pfColA and a great excess of CaiH, assuring that most CaiH was free and did not change during the reaction. Association between FITC-labelled pfColA and Cai was monitored by fluorescence anisotropy using at least a four-fold excess of Cai and reaching a

40-fold excess (10 µM, 45 µM and 100 µM). The fluorescence anisotropy of FITC bound to pfColA was recorded using an excitation wavelength at 494 nm and monitoring the fluorescence emission at 512 nm with excitation and emission slits of 5 nm.

The plot of k_{obs} *versus* [CaiH] is linear; the slope and y intercept yield apparent on- and off-rate constants of 256 M^{-1} s^{-1} and 0.0036 s^{-1}, respectively (Fig. 6.15b). This latter value agrees, within the experimental error, with the value of k_{off} determined from the direct dissociation experiment (k_{off} = 0.004 ± 0.0003 s^{-1}).

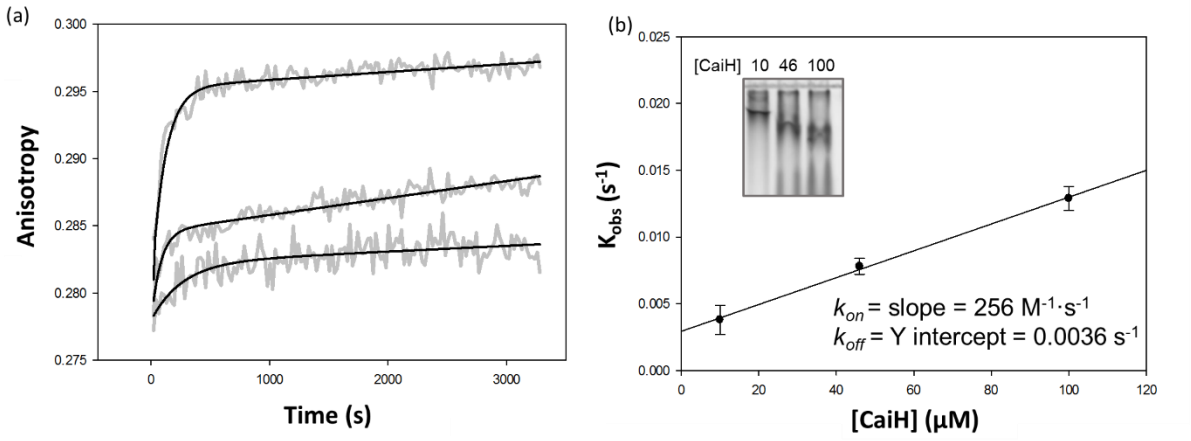

Figure 6.15 Kinetic analysis of CaiH pfColA association. Fluorescence anisotropy was used to monitor the binding of CaiH at different concentrations to FITC-labelled pfColA. A selection of anisotropy traces against time is shown for CaiH concentrations of 10 µM, 45 µM and 100 µM. (b) The observed rates (k_{obs}) from association experiments were plotted against the different CaiH concentrations, the data were linearly fitted to obtain the association rate constant (k_{on}).

The apparent K_D of 14 ± 2 µM deduced from the apparent kinetic constants k_{on} and k_{off}, is substantially larger that the previously determined in equilibrium experiments (0.48 µM). This should be further investigated in future studies.

6.6 pfColA mutants in complex formation

Little is known about the structural mechanism of colicin A association with Cai. Cross-immunization experiments had been used in the past to derive sequence determinants of the interaction of colicins with their cognate immunity proteins. Bacterial cross-immunization experiments with chimeric colicins of varying sequences derived from those of pfColA and pfColB, suggested that the specific recognition involves at least the intramembrane helix-helix

association between the hydrophobic hairpin of pfColA and the transmembrane segments of Cai. Additionally, the second periplasmic loop of Cai might also be important (Geli and Lazdunski, 1992). In vivo experiment, however do not allow the dissection of effects of a mutation on stability, activity, binding and inhibition. Binding of Cai and pfColA has not been addressed before *in vitro*. pfColA mutants were used here to draw some mechanistic information about complex formation.

We designed a competition experiment in which several mutants of pfColA were allowed to react with Cai-GFP in the presence of pfColA-Cherry. Displacement of the equilibrium of formation of Cai-GFP/pfColA-Cherry complex was used to extract mutant K_D values relative to that of wild-type pfColA. Mutant design strategy was described elsewhere (Ibañez de Opakua, PhD thesis). In summary: (i) in the MH series polar residues located at helix-helix interfaces were mutated to disrupt inter-helical salt bridges while maintaining the net charge of the domain, (ii) hydrophobic residues were truncated to shorter ones in the MY series, and (iii) in an additional group of mutants, apolar Val167 and Leu169 residues within the H8-H9 loop were exchanged by charged Lys or Glu (Table 6.1).

Table 6.1. pfColA mutants used in this study

Name	Mutation
MH1	E12A/K16A
MH3	N66K/K67A
MH6A	E121A/K122A
MH6C	E117K/K118E
MH7	N131A
MH10	D191K/K192D
M2Y	I43A
M10Y	L197A
M6Y	V119A
M7Y	V139A
E	V169E
EE	V169E/L167E
K	V169K
KK	V169K/L167K

Mixtures of pfColA-Cherry, Cai-GFP, and each unlabelled mutant were incubated overnight in ratios 1: 1,7 : 3,4 respectively and were loaded in native-PAGE gels. In-gel red and green fluorescence is shown in Figure 6.15a, b and the amount of free and bound pfColA-Cherry was quantified by in-gel fluorescence (Fig. 6.16c).

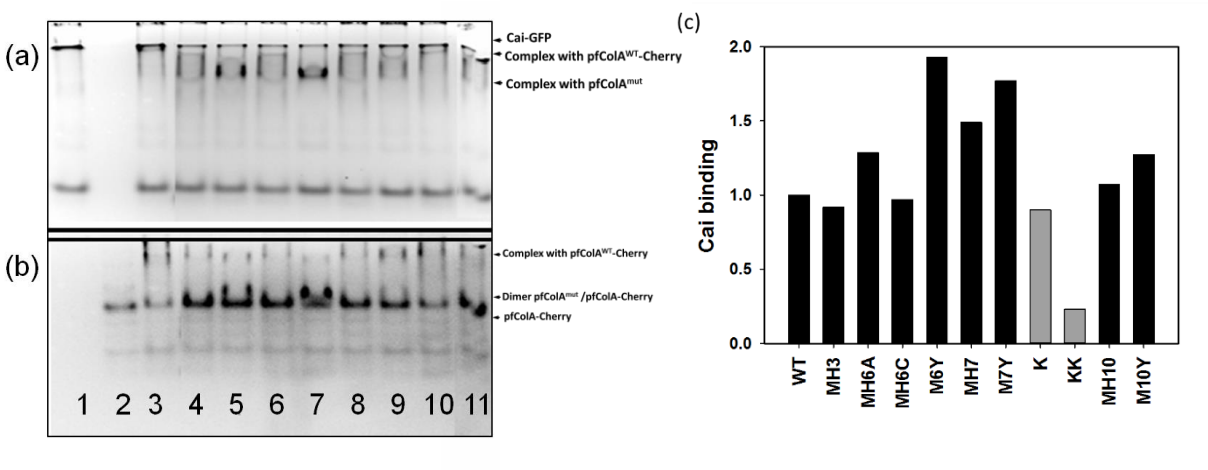

Figure 6.16 In-gel green (A) and red (B) fluorescence of native-PAGE gels of Cai-GFP / pfColA-Cherry incubated with unlabelled pfColA mutants. Lanes: 1, Cai-GPF control; 2, pfColA-Cherry control; 3, pfColA / Cai-GFP; 4, pfColA / Cai-GFP / MH3; 5, pfColA / Cai-GFP / MH6A; 6, pfColA / Cai-GFP / MH6C; 7, pfColA / Cai-GFP / MH7; 8, pfColA / Cai-GFP / MH10; 9, pfColA / Cai-GFP / K; 10, pfColA / Cai-GFP / KK; 11 pfColA / Cai-GFP / WT. All samples were incubated overnight at room temperature Incubation in PBS, 50 mM NaCl, 1mM TCEP, 0.4% DDM pH 7.5.(C) In-gel red fluorescence of the band corresponding to free pfColA-Cherry of the gel shown in 6.15 corresponding to competition experiments with pfColA mutants.

As expected and in agreement with previous data (Geli et al., 1992) mutations within the loop between helices 8 and 9 resulted in lower binding. The same region came up in the co-evolution analysis performed with pfColA and Cai sequences in the web server EV-complex (http://evfold.org) summarized in Figure 6.17. Within the pfColA higher scores concentrate in the loop H8-H9 and H8 region (A152-A171), while key sites spread along a larger region for Cai (T40 to R137). Highest score localizes in Cai helix 3 that has been suggested to be critical for colicin binding.

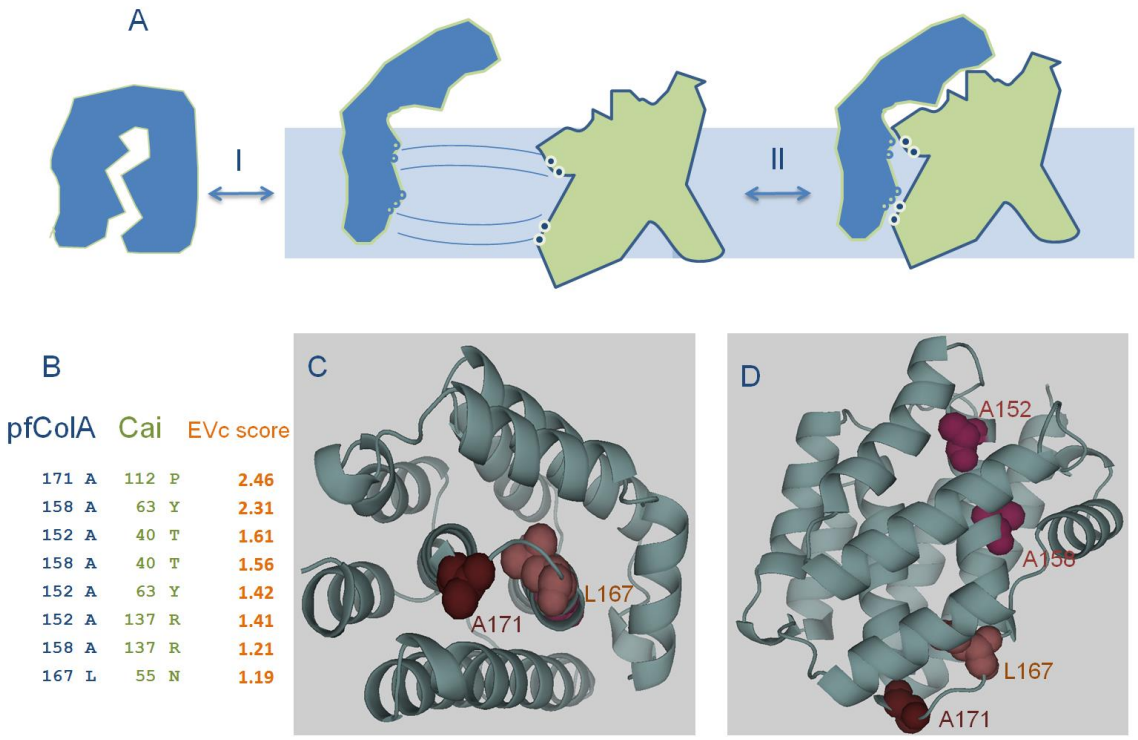

Figure 6.17. Proposed model for Cai-pfColA interaction. (A) Schematic representation of binding reaction (step II) with previous pfColA conformational changes (step I) (B) Residues with higher EV sores (C) Side and (D) front views of pfColA X-ray structure (Parker et al., 1992).

Unexpectedly some mutants showed better binding to Cai-GFP than the wild-type protein (Fig. 6.16c). Mutations that destabilized helices 6 and 7 and their mutual interactions, competed effectively for Cai-GFP with pfColA-Cherry. The effect of mutations in H6 and H7 are interpreted less straightforwardly. These mutants are also those showing a major distortion in free pfColA-Cherry migration in native gels. We tentatively assigned the upper band in the gel region corresponding to free pfColA-Cherry, to mutant/pfColA-Cherry dimers. Mutants were then subjected to BS^3 crosslinking in the same buffer conditions to test this hypothesis and results shown in Figure 6.18 corroborated the higher dimerization tendency of mutants in the H6, H7 region.

It is also worth noting that detergents which allow complex formation are also those in which pfColA dimerizes more readily formed. Gels shown in figures 3.16 and 3.13 in chapter 3 showed that alkyl-glycosides allowed pfColA homodimerization as well as pfColA/Cai heterodimer formation as revealed by BS^3 crosslinking.

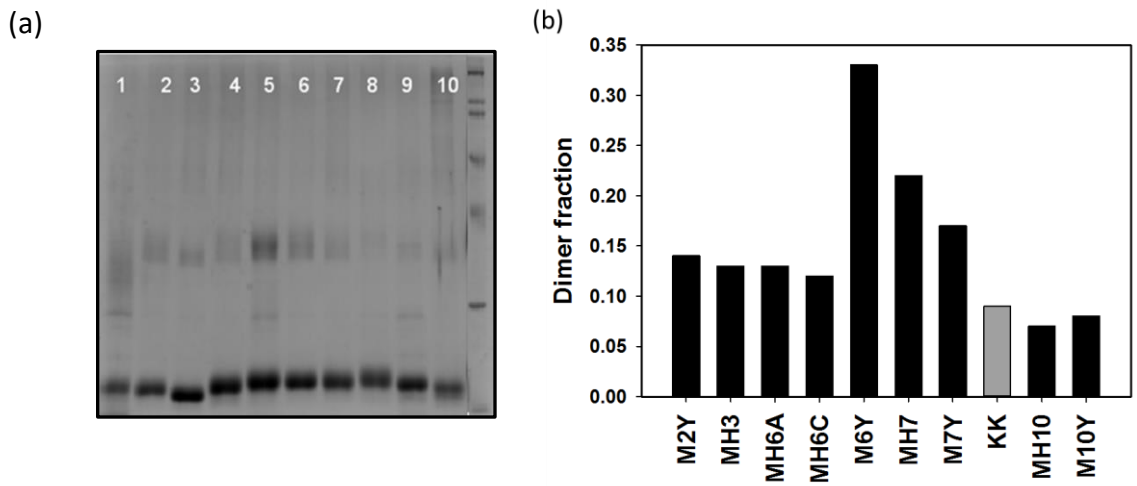

Figure 6.18. SDS-PAGE of BS^3 crosslinked pfColA mutants. (a) Each mutant (20 µM) was incubated with 12 mM BS^3 for 15 minutes in PBS, 50 mM NaCl, 1mM TCEP, 0.4% DDM pH 7.5. Reaction was stopped by adding 10 mM Tris-HCl. Lanes:1, M2Y; 2, MH3; 3, MH6A; 4, MH6C; 5, M6Y; 6, MH7; 7, M7Y; 8, M10Y; 9; MH10; 10, KK. (b) Fraction of BS^3-crosslinked-dimer calculated by the program ImageJ.

The functional assay designed to measure pfColA-induced H^+ flux in liposomes, described in chapter 4, was also performed with some of the pfColA mutants. Typical traces are shown in Figure 6.19a and relative activities are summarized in figure 6.19b. Most relevant is the loss of activity of mutants K and KK (shown in grey in Fig. 6.19b). Of the mutants shown, K and KK are the only ones for which the global protein charge increases, since mutations introduce one or two positive charges (L167K and L167K/V169K). Mutants in which these residues are mutated to Glu (E and EE) show identical negative results (Fig. 6.19b and c), suggesting that net charge does not justify inactivation. As occurs with many other functional aspects of pfColA (e.g. incorporation to bilayers), destabilizing mutants induced larger effects also in H^+ conductivity in liposomes. Major effects are also observed when the H6-H7 region is destabilized. We hipothesize that this enhancing effects in activity as well as the increased tendency to dimerize are related to step I (in which we consider all the protein structural transformation that pfColA must suffer to be converted from a soluble domain to a voltage-gated membrane channel, also including those involved in the transition from the closed- to the open-channel, Fig. 6.17A), while mutations within H8-H9 region are involved in direct Cai binding (step II). Activity measurement shown in Figure 6.19 are conducted under conditions where protein incorporations yields are identical among all the species (destabilization by urea and pH). When milder incorporation protocols are used (10 min treatment at 50 ºC), all

destabilizing mutations in pfColA induce higher membrane incorporation yields independently of the mutation site. However upon incorporation, and looking at H^+ influx, only mutations within the H6-H7 region are activity enhancers, suggesting a particular role of this hairpin in the close- to open-channel transition or in voltage gating. This is also the region whose mutation induces increased tendency to form pfColA homodimers (Fig. 6.18) as well as heterodimers with Cai (Fig. 3.13). It sounds reasonable that similar protein opening or local unfolding transitions are involved in all these processes.

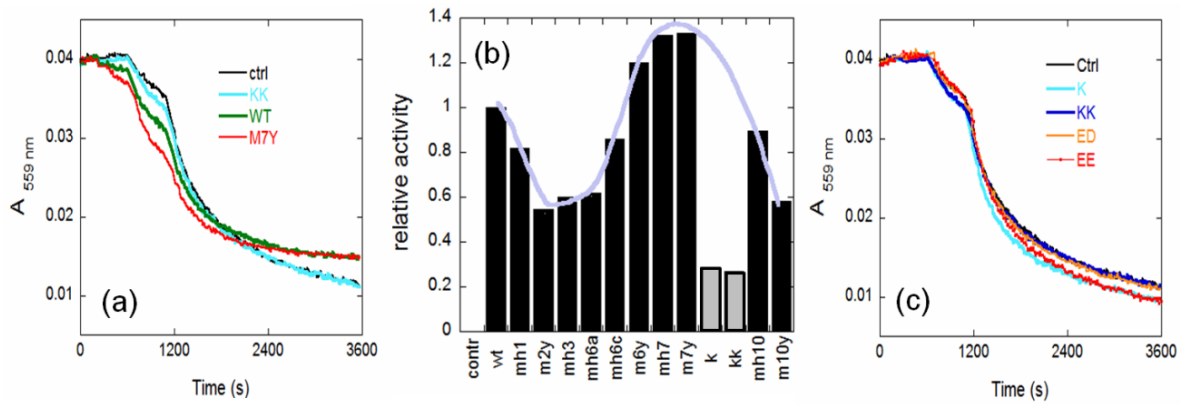

Fig 6.19 Proton transport in liposomes induced by some mutants. (A,C) A_{559} records of liposomes after successive addition of protein (wild-type or mutants), valinomycin and CCCP . Baseline signal of 1.2 ml of 60 μM phenol-red loaded liposomes was recorded for 200 s. Then 1.2 μl of 12.5 μM protein were added. Wild-type and mutant proteins had been pre-incubated in 9.5 M urea 1 mM H_2SO_4. In control experiments 1.2 μl of the incucation buffer was used. pfColA:lipid ratio was 4720. Valinomycin was added to 0.6 nM concentration at 700 s. and 2 nM CCCP at 1200 s. Internal buffer: 75 mM K_2SO_4 10 mM phenol-red pH 8.0. External buffer: 80 mM $(NMDG)_2SO_4$, 10 mM Tris pH 8.0. Experiments were conducted at 23ºC.

6.7 Discussion

Many membrane proteins are functional as stable or transient complexes (Daley, 2008). An understanding of the conditions and sequences that elicit and enhance protein-protein interactions within the membrane is important in several research areas. Studying complex assembly within the membrane however remains a challenge, considering that the methodology and mathematical models to standardize binding reactions have been mostly developed to monitor the association of soluble proteins. Due to the hydrophobic nature of membrane proteins application of classical approaches is not always possible and

methodological adaptations or implementation of new approaches to measure associations between integral membrane proteins are of particular interest. The information derived from these experiments could help building mechanistic models on membrane proteins function in living cells. During recent years new methods have emerged that offer new opportunities to determine membrane protein-protein interactions (Benke et al., 2015; Hong et al., 2010; Subburaj et al., 2015; Yu et al., 2013), although the measurement of kinetic and thermodynamic data is still quite limited.

Cai - pfColA recognition is a dynamic process which occurs once the toxin is inserted in the membrane and before it exerts its lethal activity (Espesset et al., 1996). Previous results have suggested that the lateral diffusion of immunity proteins in the membrane would ensure the rapid recognition of the pore-forming domain (Zhang and Cramer, 1993). Confinement of the two intervening proteins within the plane of the membrane would condition kinetic and affinity parameters. Other aspects, such as co-localization in specific membrane regions could also be important. These circumstances cannot be mimicked in solution, and kinetic parameters calculated for the detergent-solubilized proteins should be very different from physiological ones. Effective collisions between both proteins (k_{on}) will diminish in the three-dimensional space also due to orientation and conformational variability. Similarly the different lateral pressure experienced by the heterodimer in these two environments will make dissociation relatively less probable within the membrane (k_{off}). K_D values obtained in DDM micelles are all in the micromolar range which might not reflect the affinity of both proteins in the natural scenario that should be much larger. The fact that complex formation can also occur in the very unfavourable 3D solution speaks in favour of an extremely stable complex within the bilayer.

The major problem we have met when trying to reproduce the association of Cai and pfColA in DDM micelles has been the relative instability of the integral membrane protein Cai as a monomer. Alkyl-glycosides are mild detergents that have shown to be more efficient in preserving protein activity, although at the expense of a better solubility. In our binding measurements, Cai was partly inactivated by oligomerization. Interestingly, our results suggest that binding sites for pfColA are still accessible in these Cai oligomers suggesting that Cai-Cai contacts do not occur though the surface of Cai-pfColA interaction. In contrast, pfColA homodimers and heterodimers are stabilized by the same agents, detergents and mutations. We have neither found any evidence of 2:1 (pfColA:Cai) complexes. This may indicate that

there are populations of conformations of pfColA that are prone to dimerization (either homo- or hetero-), and that both dimers use the same protein interface and exclude each other.

Complex formation improves the global behaviour of Cai in solution, Cai/pfColA complex is shown to be more monodisperse than isolated Cai or Cai-GFP and the complex remains 1:1 even at high concentrations. pfColA is shown to incorporate into Cai polymers and extract Cai in the form of 1:1 complexes. In this sense, complexation represents some stabilization of the Cai moiety. On the other hand, urea titration experiments sensitive to the environment pfColA tryptophan residues, did not revealed any stabilization of the pfColA moiety within the complex. It became apparent that the contact interface between the two proteins is more labile than the interactions within pfColA and that the complex is destroyed at lower urea concentrations than those required to unfold pfColA. We have not more deeply investigated the concentration dependence of urea denaturation experiments, partly because they would require a high amount of protein, but it is envisioned that a different balance could be obtained between the second-order (complex formation) and first-order (unfolding) reactions at different protein concentrations. pfColA stabilization could possibly be demonstrated in experiments performed at much higher protein concentrations.

Computation approaches can address the knowledge gap of protein interactions. The analysis of correlated evolutionary sequence records represents a rich source of information (Hopf et al., 2014) and has been used here to predict “hot-spots” in Cai/pfColA complex assembly (http://evfold.org). High EV-complex scores converge around pfColA helix 8, while a more disperse pattern is obtained along the sequence of Cai. Previous work by other authors (Geli, 1992) and our mutational analysis indicated that mutations in helix 8 and subsequent loop greatly inhibit the interaction with Cai. Mutants K and KK within this protein region were those showing a significant inhibition, and we were unable to purify complex Cai/KK due to its instability. A similar behaviour was not obtained for any other mutant and most probably the binding site is only compromized in K, KK, E and EE mutants. Our results show that binding can even be easily reinforced by mutation. This observation is not unusual in other pfColA functional features due to its peculiarities. Colicin A acquires multiple conformations along its translocation, insertion and channel formation pathway. Once the pore-forming domain is inserted into the membrane, the voltage-dependent gating of the channel is believed to

involve a considerable structural rearrangement that results in the translocation of several helices across the membrane giving rise to the open-state (Slatin et al., 1994, 2002). It is generally accepted that pfColA must be destabilized to trigger the opening of the protein leading to the membrane insertion-competent state. In the cell, colicin A undergoes partial unfolding during its translocation through the bacterial envelope (Bénédetti et al., 1992; Duché et al., 1994b; London, 1992; Zakharov et al., 2008). Results in our laboratory have shown that the rate of incorporation of pfCoA mutants to model membranes is directly proportional to their unfolding rate (Ibañez de Opakua, PhD thesis). Mutations that improved Cai binding, however, seem to cluster in helix 6 and helix 7 of pfColA. Destabilizing mutations in other protein regions do neither reinforce nor hinder Cai binding.

Membrane bound pfColA adopts at least two conformations known as the closed- and open-states. The closed-state occurs when the mobile protein segment is located in the *cis* side of the membrane, and the open state, when it is translocated to the *trans* side. This voltage-dependent behavior has been proposed to be localized in the first four helices of pfColA (Nardi et al., 2001), although these helices are not directly involved in the formation of the toxic channel which, in turns, comprises at most 4 transmembrane segments (presumably helices H6-H9) (Slatin et al., 2002). Mutational studies conducted *in vivo* by other authors indicated that the interaction with Cai requires pfColA to be inserted into the membrane, although not necessarily as an active channel (Espesset et al., 1996). In the colicin homolog E1, however, interaction with the immunity protein is presumably mediated by one amphiphilic and one hydrophobic helix of the colicin channel, implying that the immunity protein can react with the open state (Zhang and Cramer, 1993). Our results also agree with this later finding. Most active pfColA mutants are also those with higher affinity for Cai, and the reverse is also true, KK mutant is unable to bind to Cai or to facilitate proton conductance in liposomes. The fact that the particular pattern of effects of the different mutations is observed in Cai binding as well as in proton conductivity measurements suggests that both processes share the same limiting steps. Our results are compatible with the idea that Cai associates with the pfColA open channel.

CHAPTER 7

Overview and conclusions

7. OVERVIEW AND CONCLUSIONS

The immunity protein Cai is an integral membrane protein residing in the inner membrane of some colicinogenic bacteria which prevents the lethal activity of the exogenous colicin A toxin by the inhibition of its pore-forming activity. It has been proposed that Cai diffuses in the inner membrane to interact with the pore-forming domain of colicin A through helix-helix association preventing channel opening by a yet unknown mechanism.

This thesis covers different approaches to study Cai pfColA helix-helix interaction using overexpressed proteins in detergent micelles, artificial membranes or in the bacterial inner membrane through co-expression. The process involves the interaction of an integral membrane protein with an amphitropic protein that undergoes a considerable conformational change from a soluble protein to a membrane inserted form. Despite the complexity of the system, it provided a series of advantages. The often difficult task of finding optimal solubilization and stability conditions for the integral membrane protein Cai could be assessed by its capacity to bind to pfColA (chapter 3). While for pfColA, as it is readily produced in its soluble form, the effect of different detergents could be studied by simple incubation of the purified protein in the detergent to be tested (section 3.6). Cai could be reconstituted into lipid vesicles from its detergent solubilized form and its concentration dependent inhibitory function tested by adding increasing amounts of pfColA in a controlled manner (chapter 4). Moreover, pfColA could be fused to various signal peptides targeting it to the periplasm where it inserts into the inner membrane. The functional interaction with Cai could then be tested by correlating it to cell viability, as non-immunized bacterial strains inhibit pfColA expression to avoid cytotoxicity. The optimal solubilization conditions to isolate the complex formed in the inner membrane was then addressed, revealing that alkyl-glycoside detergents allow for the extraction of the intact complex from the membrane. This result is consistent with the conditions in which the complex can be formed *in vitro* from the proteins purified independently.

Finally, once we knew the complex could be formed *in vitro* in the alkyl-glycosides like DDM, the binding reaction could be further characterized in DDM micelles in terms of affinity and

stoichiometry. Traditional binding assays are difficult to apply in the case of integral membrane proteins, membrane protein samples can vary a lot from preparation to preparation and the detergent concentration in the final sample is difficult to control. Nevertheless, the fact that pfColA is a soluble protein and that it can be incubated in DDM to drive a conformational change with a distinct tertiary arrangement implies that at least we have some control over one of the interacting partners.

Thus, the data presented in this work provides more insights into the association of Cai with pfColA which can contribute in the elucidation of the mechanism of inhibition. The stoichiometry of the complex was determined to be 1:1 by all the methodologies used. The complex formed in a solution of DDM micelles revealed a 1:1 association by different crosslinking approaches. The concentration dependent proton conductance activity of pfColA in artificial membranes indicated that the channel formed is monomeric in agreement with previous evidence (Lakey and Slatin, 2001). This activity could be inhibited in the case of Cai containing proteoliposomes at an equimolar relation between the two proteins. Equilibrium binding studies by fluorescence anisotropy or native-PAGE were also consistent with a 1:1 interaction. Both the co-expression and *in vitro* formation of the complex indicate that the complex is stable in the absence of other cellular components even if additional proteins or characteristic of the native membrane environment might modulate the interaction. Previous experiments targeting pfColA to the periplasm demonstrated that the functional insertion of pfColA is independent of the translocation machinery suggesting that the partial unfolding of pfColA necessary to trigger membrane insertion could be mimicked in our experiments by Sec or Tat mediated translocation.

Much of our initial efforts were devoted to the screening of detergents and conditions in which this protein behaves properly in terms of solubility, conformational stability, monodispersity and function. We applied a variety of biochemical and biophysical methods to study Cai in detergent micelles in an attempt to understand if any particular detergent or group of detergents, could favour the native conformation of the protein once extracted from the membrane. We found however, that there is no single detergent that can be generally applied and would satisfy all requirements of the different methodologies to study Cai structure and function. For instance, the final yield of CaiH varied significantly with the detergent used, where the best solubilizing detergents (lipid-like, e.g DPC) failed to produce

good NMR spectra and preserve protein function. Mild zwitterionic detergents like LDAO still ensured acceptable protein extraction levels while yielding the best NMR spectral quality and reconstitution efficiency. Yet, only non-ionic sugar-derived detergents (e.g. DDM) supported functional complex formation with pfColA. This indicates that with the tools available today to evaluate conformational stability of membrane proteins, the detergent of choice is still very conditioned by the methodology itself which makes it more difficult to draw conclusions about the molecular model of action of a certain membrane protein when different evidence come from differing experimental conditions.

Activity preservation is a commonly accepted criterion for protein integrity and is used to identify native environments (e.g. best bilayer lipid composition, best reconstitution methods, best detergent performance in aqueous solution, etc). In nature, Cai activity involves direct interaction with the channel-forming domain of its cognate toxin. This fundamental aspect has been studied here from different perspectives:

(i) The simplest although incomplete functional test would be bare complexation. Any environment would be in principle amenable to binding detection and this is the only functional feature that can be assessed in aqueous environment. This functional checkpoint has been used to rank and classify detergent suitability in chapter 3. Only alkyl-glycosides produced positive results.

(ii) Complete functionality can only be proven under conditions where pfColA-induced membrane permeability can be inhibited by Cai. Reconstitution of Cai in liposomes has been described in Chapter 4. Liposome lumen acidification induced by pfColA was reduced in Cai-proteoliposomes, especially at low pfColA:Cai ratios.

(iii) The formation of an inactive complex was also tested *in vivo* by co-expressing both proteins in C43 *E. coli* strain. Exportable pfColA variants could only be expressed in combination with Cai. The complex thus produced *in vivo* was also only stable in DDM, while other detergents induced its disruption to the monomers, probably indicating that they interfere with the protein-protein interface.

Implementing an experimental set up to test protein functionality using a reconstitution approach served to understand which detergents established a reversible non deleterious

association with Cai which does not denature or hinder the conformational flexibility of the protein. Alternatively, the composition of the artificial membrane appeared to be important and the highest reconstitution yields were obtained in the more physiological vesicles made of *E.coli* total lipid extract. Concerning the controlled incorporation of pfColA into lipid vesicles a novel strategy involving a partial thermal denaturation was implemented which allowed to obtain the first evidence for Cai/pfColA functional association in lipid vesicles reported to date. Furthermore it further confirmed that the pfColA channel exerts a high selectivity for protons, which is dose-dependent, voltage-dependent and which is inhibited by Cai. Finally the fact that Cai can bind to pfColA out of the membrane in detergent micelles opened the door for equilibrium and kinetic binding studies. Being a toxin/antitoxin pair the association of Cai with pfColA showed high stability once formed. Native-PAGE of fluorescently labelled proteins and pfColA mutants provided further insight into oligomerization processes involving Cai, pfColA and Cai/pfColA. Destabilizing the pfColA by mutation revealed that the mutations that trigger higher dimerization are also the ones that facilitate complex formation, suggesting that a common conformational change might be involved.

Equilibrium and kinetic studies monitored by fluorescence anisotropy revealed that the Cai/pfColA association affinity lays in the micromolar range. It is difficult to estimate the physiological relevance of this affinity value as the native association does not happen in aqueous solution but rather in the restricted 2 dimensional liquid of the membrane. It seems obvious that calculated K_D, k_{on} and k_{off} should differ greatly from physiological ones, however semi-quantitative comparisons for different conditions and mutants would help to extract some mechanistic information. Both components, pfColA and Cai, are subjected to parallel homo association equilibria in DDM solution, which would compete with hetero-dimer formation. Specially pfColA dimerization shows to be favoured by the same conditions, detergents and mutants as the heterodimer. We hypothesise that a common conformational change is needed in both reactions It also indicated the possible existence of kinetic barriers involving homodimerization of the interacting partners that affects complex formation yields. This could be concluded from the observation that varying the concentration of Cai over a fixed amount of pfColA gives very different complex formation yields compared with performing the experiment in the opposite way. But further studies are necessary to confirm this hypothesis. We speculate that not all the Cai or Cai-GFP present in a given preparation

might be active in terms of binding capacity and partial detergent-denaturation might also take place. Nevertheless the efficiency of Cai as a potent pfColA inhibitor might not depend only on a high affinity association as it happens with immunity proteins of nuclease colicins (Wallis et al., 1995). The number of colicins that reach the inner membrane is believed to be largely dependent on the number of import sites (Duché et al., 1995). Provided that the immunity protein is able to neutralize the intruding colicin at every entry site the cell would be efficiently protected, specially taking into account that the receptor and forming binding domains remain attached to the translocation components even after the active domain has reached the inner membrane (Bénédetti et al., 1992; Duché, 2007) suggesting that the entry of additional colicins might be blocked (Zakharov et al., 2004).

Two extreme behaviours have emerged from the mutant analysis. Poorer binding is expected in those mutants affecting the interaction interface. Mutants K and KK are showing this behaviour in accordance with data from other authors (Espesset, 1994) and with the analysis of evolutionary couplings that point to H8-H9 as a binding hot-spot. In contrast, a series of mutants located in H6-H7 do show the opposite effect with higher Cai binding in competition experiments with wild type pfColA. Interestingly the same region shows up in pfColA proton conductance experiments. This may not be surprising after considering that pfColA activity implies substantial rearrangements of the protein and destabilizing mutations could facilitate conformational transitions. The effect is not unspecific, since many of the mutants are more destabilizing and do not affect proton flux, nor specific binding, (at least not directly involving the binding site). The fact that proton flux and Cai binding are affected similarly by mutations, either enhancing or inhibiting, seems to suggest that Cai binds to the pfColA open channel.

7.1 Conclusions

Taken together the information obtained from this study can contribute to a better understanding of toxin-antitoxin association in particular and α-helical membrane protein folding, oligomerization in general.

Specific conclusions of this thesis can be summarized as follows:

-Different techniques in the study of Cai require different solubilization conditions. There is no optimal solubilization method that satisfies the requirements of all the different techniques.

-Cai inhibits pfColA through formation of an inactive Cai/pfColA complex within the membrane.

-Cai/pfColA complex formed in DDM micelles has a 1:1 stoichiometry and remains highly stable once formed.

7.2 RESUMEN Y CONCLUSIONES

1. Introducción

Con el objetivo de avanzar en el análisis de las interacciones proteína-lípido y proteína-proteína en las membranas celulares se seleccionó un sistema modelo compuesto por el dominio formador de poros de la colicina A y su proteína de inmunidad Cai y se analizó su comportamiento *in vitro* mediante métodos bioquímicos y biofísicos. La proteína de inmunidad inhibe la formación de poros y subsecuente muerte celular provocada por la toxina mediante una interacción directa hélice-hélice (Nardi et al., 2001).

2. Cribado de condiciones para el estudio de la interacción Cai/pfColA en solución

Trabajar con proteínas de membrana en solución implica extraerlas del entorno lipídico para lo que generalmente se utilizan detergentes que son capaces de estabilizar las zonas hidrofóbicas de la proteína. Existen una serie de criterios a tener en cuenta a la hora de elegir el tipo de detergente para la extracción y solubilización: proteger contra la disociación de subunidades proteicas, evitar el desplegamiento, minimizar la exposición de hélices transmembrana al medio polar, valor de concentración micelar critica (cmc) bajo e la intercambiabilidad. Diferentes metodologías bioquímicas y espectroscópicas fueron utilizadas para determinar las condiciones óptimas para Cai en términos de solubilidad, monodispersidad y homogeneidad conformacional, con el objetivo de encontrar las condiciones en las cuales estudiar la interacción de Cai con pfColA.

El primer paso para poder estudiar la interacción de estas dos proteínas fue la puesta a punto del sistema de expresión y purificación de la proteína integral de membrana Cai. Para ello se obtuvieron diferentes construcciones mediante biología molecular. Por un lado se fusionó con la proteína verde fluorescente GFP en el C-terminal ya que esta estrategia ha demostrado ser muy útil para el seguimiento de la expresión por fluorescencia y subsecuente purificación de proteínas integrales de membrana (Drew et al., 2006). Por otro lado se fusionó con una cola de histidinas en el C-terminal simplificando así el proceso de purificación. Los mayores rendimientos de purificación de obtuvieron en la cepa bacteriana C41 (DE3) durante 16 h a 20 °C, solubilizando la fracción de membrana en el detergente dodecil-B-D maltopiranosido (DDM) y mediante cromatografía de afinidad a níquel seguida de cromatografía de tamizado molecular.

A continuación se pasó a evaluar el efecto de diferentes condiciones de la solución sobre la solubilidad y stabilidad de Cai. Los resultados de solubilidad seguidos por fluorescencia de GFP indicaron que el tampón fosfato estabiliza la proteína por encima de 50 mM y esto no se debe a un aumento de la fuerza iónica únicamente. La substitución del detergente DDM por un detergente que contiene fosfato tenía un efecto similar, sugiriendo que el entorno fosfolipídico en el que la proteína se encuentra en la célula es importante para su integridad conformacional. De hecho mediante resonancia magnética nuclear de ^{31}P se detectaron fosfolípidos en la muestra purificada de Cai. Siguiendo esta hipótesis se demostró que efectivamente la adición de una mezcla lipídica similar a la celular estabiliza la proteína detectado como una disminución de la accesibilidad de las cisteínas situadas en las hélices transmembrana.

Considerando que la adición de moléculas más polares sobre la proteína Cai solubilizada en el detergente DDM incrementaba la estabilidad se amplió el abanico de detergentes con el objetivo te optimizar la estabilidad de Cai. Entre los detergentes que se probaron aquellos más polares como LDAO o cargados como el lisofosfolípido oleoil-fosfatidilglicerol provocaron mayores tasas de solubilidad y muestras más monodispersas por cromatografía de tamizado molecular. Sin embargo estos detergentes más solubilizantes tienden a desestabilizar las interacciones proteína-proteína. Siendo más proclives a mantener la integridad de los oligómeros detergentes de la familia de los alkilglucósidos como el DDM u OG.

Por último, entre todas las metodologías utilizadas para estudiar la integridad conformacional de Cai una vez extraída de la membrana, la capacidad de preservar su capacidad de unión a la proteína a la que inhibe resultó ser la más informativa. La unión toxina-antitoxina únicamente ocurre en detergentes de la clase de los alkilglucósidos como DDM, DM, NM o OG como se demostró por entrecruzamiento químico.

Resulta interesante remarcar que el hecho de que una clase de detergentes permita la formación de complejo no es debido únicamente a su efecto sobre la conformación de Cai sino también sobre el dominio formador de poros pfColA. La colicina A soporta una flexibilidad conformacional inherente a su espectro funcional que incluye su secreción al medio como toxina soluble, su translocación a través de la membrana externa de la bacteria y su acción ionófora una vez insertada en la membrana interna. Estudiando las diferentes conformaciones que adopta pfColA en diferentes detergentes se vio que acorde con lo que pasa en la formación de complejo, los alkilglucósidos son los únicos que preservan la estructura terciaria de la proteína estudiado por dicroísmo circular en el cercano. EL mismo tipo de detergentes provoca la dimerización de la proteína pfColA seguida por entrecruzamiento químico.

3. Reconstitución funcional de complejo Cai/pfColA en vesículas lipídicas

El fragmento formador de poros de la colicina A, pfColA, forma poros en la membrana bacteriana lo que eventualmente conlleva la muerte celular. Las bacterias productoras son protegidas de la acción de la toxina mediante la expresión de la proteína de la inmunidad Cai que se encuentra integrada en la membrana interna. Con el objetivo de caracterizar la inhibición de esta actividad *in vitro*, se puso a punto un estudio funcional en vesículas lipídicas o LUVs (Large unilamelar vesicles). Se estudió la conductividad a protón inducida por pfColA y su inhibición por parte the Cai.

Para poder estudiar la inhibición de Cai sobre la actividad de pfColA primero se deben reconstituir ambas proteínas en los LUVs. Para monitorizar y cuantificar la reconstitución de pfColA se utilizó la transferencia de energía de fluorescencia (FRET) entre los triptófanos de la proteína y lípidos dansilados combinado con la separación de vesículas con o sin pfColA mediante cromatografía de tamizado molecular. Se demostró que el calentamiento de la muestra a 50 °C durante 10 min resulta ser un buen método de reconstitución aunque no se superó una tasa de reconstitución mayor del 20%. A efectos de maximizar la incorporación se ensayó el mutante de pfColA V119A el cual es conocido por pasar de la forma soluble a la de membrana más fácilmente. En este caso se obtuvieron rendimientos de incorporación cercanos al 90%. En cuanto a la reconstitución de Cai en LUVs, se añadió la proteína purificada en diferentes detergentes y se llevó a cabo una flotación en gradiente de sacarosa siendo el detergente LDAO el de mayor rendimiento de incorporación.

Para los ensayos de conductividad se utilizó la sonda rojo fenol encapsulado en LUVs y se indujo un potencial de membrana añadiendo valinomicina. La actividad de pfColA reconstituida en bicapas lipídicas resulto ser más selectiva a protones aunque otros cationes como sodio y litio también atraviesan el canal. El flujo de iones es unidireccional y dependiente de voltaje siendo linealmente dependiente a la concentración de pfColA en el rango de nano molar. En presencia de Cai reconstituida en liposomas la actividad de pfColA detectada como flujo de protones, se ve claramente disminuida. De la correlación entre la concentración de pfColA añadida y la magnitud del flujo de protones se deduce que la estequiometria de la interacción Cai/pfColA corresponde a una relación 1:1.

4. Co-expresión de Cai/pfColA *in vivo* y posterior aislamiento

Con el objetivo de estudiar la formación del complejo Cai/pfColA en el entorno nativo de la membrana celular se desarrolló un sistema de expresión in vivo. La proteína fue dirigida al periplasma mediante la fusión de un péptido señal que la dirige a este compartimiento para su subsiguiente inserción en la membrana interna. En el C-terminal de pfColA se fusionó la proteína fluorescente Cherry que conjuntamente con la fusión Cai-GFP permitió el seguimiento de la co-expresión y co-purificación. Diferentes condiciones de co-expresión fueron testadas siendo preferibles la cepa C43 (DE3) y la inducción por IPTG a baja densidad óptica (OD 0.2). El fraccionamiento celular reveló la co-localización de ambas proteínas en la membrana interna validando el sistema de co-expresión como plataforma para estudiar la interacción toxina-antitoxina en la membrana citoplasmática.

Una vez se consiguió expresar ambas proteínas en la membrana, se pasó a ensayar diferentes condiciones de solubilización para conseguir la extracción de un complejo intacto. Para ello se testaron diferentes detergentes en el proceso de purificación por cromatografía de afinidad a níquel. Se estudió el efecto del detergente sobre el complejo mediante geles de electroforesis SDS-PAGE de las fracciones de la cromatografía para detectar co-elución o al contrario disociación del complejo. Por otra parte se procedió a cargar las fracciones eluídas en geles nativos en los que se detectó el complejo como una banda que contiene tanto fluorescencia de Cherry como de GFP. De acuerdo con los resultados obtenidos en el primer capítulo, de todos los detergentes testados, solo los alkilglucósidos, en este caso DDM mantiene la integridad del complejo.

5. Estabilidad, afinidad y efecto de mutaciones en pfColA sobre el complejo Cai/pfColA

Una vez demostrado que el complejo Cai/pfColA puede ser co-expresado y aislado en detergente, nos propusimos estudiar las características bioquímicas de la interacción *in vitro*. Para ello se purificaron tanto la proteína pfColA en su forma soluble como Cai solubilizada y purifizada en DDM. Para determinar si las proteínas purificadas son capaces de interaccionar fuera de la membrana se utilizaron geles de electroforesis nativos en los que se titulaba pfColA-Cherry con concentraciones crecientes de Cai-GFP. Se demostró así que el complejo se puede formar *in vitro*, siendo el rendimiento de formación no mayor del 40%.

De esta manera se pudo pasar a purificar el complejo para deshacerse del exceso de ambas proteínas. El complejo muestra una gran estabilidad, manteniéndose unido después de varios pasos de

purificación. Para elucidar cual es la estequiometria del complejo se procedió a entrecruzar el complejo una vez purificado confirmándose lo que se había observado previamente en el ensayo funcional en LUVs, que se trata de un complejo 1:1.

El análisis conformacional indica que el complejo Cai/pfColA es una especie estable. La desnaturalización térmica y la accesibilidad de las cisteínas mostó que la unión a pfColA estabiliza a Cai. El estudio por dicroísmo circular en la región del cercano indicó que el complejo contiene un patrón de estructura terciaria distinto respecto a las proteínas por separado. Para obtener información de la afinidad entre Cai y pfCola se llevaron a cabo ensayos cinéticos de unión así como en equilibrio. Se utilizaron los geles nativos valiéndose de la detección de fluorescencia en gel combinados con anisotropía de fluorescencia.

Para los estudios cinéticos se marcaron las proteínas con diferentes fluoróforos extrínsecos, por un lado Cai se marcó con cumarina y pfColA por otro lado con fluoresceína. Se midió la constante de disociación mediante competición del complejo marcado con cumarina con un exceso molar de 20 de Cai no marcada. Para la constante de asociación se utilizaron tres concentraciones diferentes de Cai sin marcar que se añadieron a 1 µM de pfColA marcada con fluoresceína. La K_D del complejo medida en solución se encuentra en el rango de micromolar aunque mayores afinidades se esperan para la ineracción in vivo.

A continuación se ensayaron diferentes mutantes de pfColA en experimentos de competición en geles nativos y actividad medida como conducción de protón. Se observó que las mutaciones que impiden la unión a Cai son aquellos que presentan niveles más bajos de actividad en LUVs. En el otro extremo se encuentran mutantes que presentan una mayor unión a Cai y flujos superiores de protón. Esto sugiere que Cai une a pfColA en su estado de canal abierto. Se encontró que aquellos mutantes que son más propensos a formar complejo mejorando el rendimiento de formación de la proteína salvaje también tienden a formar más homodímero de pfColA en ciertos detergentes como DDM.

6. Conclusiones

En cuanto al efecto de diferentes condiciones de solubilización de las proteínas Cai y pfColA, aquellos detergentes con mayor poder de solubilización las interacciones proteína-proteína son más desfavorables y por lo tanto son los alkilglucósidos, menos solubilizantes, los que permiten la asociación nativa de Cai con pfColA.

El estudio funcional demostró que las dos proteínas pueden ser reconstituidas en una bicapa lipídica y ejercer su función, pfColA como conductora de protones y Cai mediante la inhibición de este flujo. Esta actividad resultó ser dosis dependiente, saturable y de la que se deduce un complejo nativo de estequioemtría 1:1.

En cuanto a la expresión in vivo, las proteínas Cai y pfColA pueden ser co-expresadas en el entorno fisiológico constituyendo una plataforma para el estudio de interacción de proteínas de membrana. El complejo expresado de esta forma puede ser aislado íntegramente en detergentes de la familia de los alkilglucósidos.

Por último, la formación del complejo es posible también en solución *in vitro* en DDM dando lugar a un complejo estable con una afinidad en el rango de micromolar. Mutaciones que resultan en menor actividad ionofórica también muestran menor capacidad de unión a Cai y viceversa lo que sugiere que Cai se une a pfColA en la conformación de canal abierto. La mutación de residuos que provocan mayor unión a Cai conlleva también mayores niveles de dimerización de pfColA en DDM. Esto sugiere que existe un cambio conformacional común implicado en ambos procesos.

CHAPTER 8

Bibliography

8. BIBLIOGRAPHY

Aisenbrey, C., Sudheendra, U.S., Ridley, H., Bertani, P., Marquette, A., Nedelkina, S., Lakey, J.H., and Bechinger, B. (2007). Helix orientations in membrane-associated Bcl-X(L) determined by 15N-solid-state NMR spectroscopy. Eur. Biophys. J. EBJ *37*, 71–80.

Alexandrov, A.I., Mileni, M., Chien, E.Y.T., Hanson, M.A., and Stevens, R.C. (2008). Microscale Fluorescent Thermal Stability Assay for Membrane Proteins. Structure *16*, 351–359.

Anderluh, G., and Lakey, J.H. (2008). Disparate proteins use similar architectures to damage membranes. Trends Biochem. Sci. *33*, 482–490.

Andersson, A.-S. (1996). Wild-type Escherichia coli Cells Regulate the Membrane Lipid Composition in a ``Window'' between Gel and Non-lamellar Structures. J. Biol. Chem. *271*, 6801–6809.

Andreoli, T.E., Tieffenberg, M., and Tosteson, D.C. (1967). The Effect of Valinomycin on the Ionic Permeability of Thin Lipid Membranes. J. Gen. Physiol. *50*, 2527–2545.

Baldwin, R.L. (1996). How Hofmeister ion interactions affect protein stability. Biophys. J. *71*, 2056.

Banerjee, P., Joo, J.B., Buse, J.T., and Dawson, G. (1995). Differential solubilization of lipids along with membrane proteins by different classes of detergents. Chem. Phys. Lipids *77*, 65–78.

Bañó-Polo, M., Baeza-Delgado, C., Orzáez, M., Marti-Renom, M.A., Abad, C., and Mingarro, I. (2012). Polar/Ionizable Residues in Transmembrane Segments: Effects on Helix-Helix Packing. PLOS ONE *7*, e44263.

Baty, D., Lloubes, R., Geli, V., Lazdunski, C., and Howard, S.P. (1987). Extracellular release of colicin A is non-specific. EMBO J. *6*, 2463.

Baty, D., Frenette, M., Lloubès, R., Geli, V., Howard, S.P., Pattus, F., and Lazdunski, C. (1988). Functional domains of colicin A. Mol. Microbiol. *2*, 807–811.

Bayramoglu, B., Toubiana, D., Vliet, S. van, Inglis, R.F., Shnerb, N., and Gillor, O. (2017). Bet-hedging in bacteriocin producing Escherichia coli populations: the single cell perspective. Sci. Rep. *7*, 42068.

Benedetti, H., Frenette, M., Baty, D., Knibiehler, M., Pattus, F., and Lazdunski, C. (1991). Individual domains of colicins confer specificity in colicin uptake, in pore-properties and in immunity requirement. J. Mol. Biol. *217*, 429–439.

Bénédetti, H., Lloubès, R., Lazdunski, C., and Letellier, L. (1992). Colicin A unfolds during its translocation in Escherichia coli cells and spans the whole cell envelope when its pore has formed. EMBO J. *11*, 441–447.

Benke, S., Roderer, D., Wunderlich, B., Nettels, D., Glockshuber, R., and Schuler, B. (2015). The assembly dynamics of the cytolytic pore toxin ClyA. Nat. Commun. *6*, 6198.

Berardi, M.J., Shih, W.M., Harrison, S.C., and Chou, J.J. (2011). Mitochondrial uncoupling protein 2 structure determined by NMR molecular fragment searching. Nature *476*, 109–113.

Berezin, C., Glaser, F., Rosenberg, J., Paz, I., Pupko, T., Fariselli, P., Casadio, R., and Ben-Tal, N. (2004). ConSeq: the identification of functionally and structurally important residues in protein sequences. Bioinforma. Oxf. Engl. *20*, 1322–1324.

Bibi, E., and Kaback, H.R. (1990). In vivo expression of the lacY gene in two segments leads to functional lac permease. Proc. Natl. Acad. Sci. *87*, 4325–4329.

Bishop, L.J., Bjes, E.S., Davidson, V.L., and Cramer, W.A. (1985). Localization of the immunity protein-reactive domain in unmodified and chemically modified COOH-terminal peptides of colicin E1. J. Bacteriol. *164*, 237–244.

Bligh, E.G., and Dyer, W.J. (1959). A rapid method of total lipid extraction and purification. Can. J. Biochem. Physiol. *37*, 911–917.

Blois, T.M., Hong, H., Kim, T.H., and Bowie, J.U. (2009). Protein Unfolding with a Steric Trap. J. Am. Chem. Soc. *131*, 13914–13915.

Böhme, S., Padmavathi, P.V.L., Holterhues, J., Ouchni, F., Klare, J.P., and Steinhoff, H.-J. (2009). Topology of the amphipathic helices of the colicin A pore-forming domain in E. coli lipid membranes studied by pulse EPR. Phys. Chem. Chem. Phys. *11*, 6770–6777.

Boon, T. (1971). Inactivation of Ribosomes In Vitro by Colicin E3. Proc. Natl. Acad. Sci. *68*, 2421–2425.

Böttcher, C., Gent, C.M., Fries, C., Böttcher, C.J.F., Pries, C., Böttcher, C.F.J., van Duijn, C.M., Bottcher, F., and Bötcher, C.J.F. (1961). A rapid and sensitive sub-micro phosphorus determination.

Bourdineaud, J.P., Boulanger, P., Lazdunski, C., and Letellier, L. (1990). In vivo properties of colicin A: channel activity is voltage dependent but translocation may be voltage independent. Proc. Natl. Acad. Sci. U. S. A. *87*, 1037–1041.

Bowie, J.U. (1997). Helix packing in membrane proteins1. J. Mol. Biol. *272*, 780–789.

Branigan, E., Pliotas, C., Hagelueken, G., and Naismith, J.H. (2013). Quantification of free cysteines in membrane and soluble proteins using a fluorescent dye and thermal unfolding. Nat. Protoc. *8*.

Braun, V., Patzer, S.I., and Hantke, K. (2002). Ton-dependent colicins and microcins: modular design and evolution. Biochimie *84*, 365–380.

Brunden, K.R., Uratani, Y., and Cramer, W.A. (1984). Dependence of the conformation of a colicin E1 channel-forming peptide on acidic pH and solvent polarity. J. Biol. Chem. *259*, 7682–7687.

Burkhard, P., Stetefeld, J., and Strelkov, S.V. (2001). Coiled coils: a highly versatile protein folding motif. Trends Cell Biol. *11*, 82–88.

Burn, P. (1988). Talking point Amphitropic proteins: a new class of membrane proteins. Trends Biochem. Sci. *13*, 79–83.

Burré, J., Wittig, I., and Schägger, H. (2009). Non-classical 2-D Electrophoresis. In Proteomics, J. Reinders, and A. Sickmann, eds. (Humana Press), pp. 33–57.

Butko, P., Huang, F., Pusztai-Carey, M., and Surewicz, W.K. (1996). Membrane Permeabilization Induced by Cytolytic δ-Endotoxin CytA from Bacillus thuringiensis var. israelensis. Biochemistry (Mosc.) *35*, 11355–11360.

Call, M.E., Schnell, J.R., Xu, C., Lutz, R.A., Chou, J.J., and Wucherpfennig, K.W. (2006). The structure of the zetazeta transmembrane dimer reveals features essential for its assembly with the T cell receptor. Cell *127*, 355–368.

Cao, Z., and Bowie, J.U. (2012). Shifting hydrogen bonds may produce flexible transmembrane helices. Proc. Natl. Acad. Sci. *109*, 8121–8126.

Cascales, E., Buchanan, S.K., Duche, D., Kleanthous, C., Lloubes, R., Postle, K., Riley, M., Slatin, S., and Cavard, D. (2007). Colicin Biology. Microbiol. Mol. Biol. Rev. *71*, 158–229.

Cavard, D., Lloubès, R., Morlon, J., Chartier, M., and Lazdunski, C. (1985). Lysis protein encoded by plasmid ColA-CA31. Gene sequence and export. Mol. Gen. Genet. MGG *199*, 95–100.

Cavard, D., Sauve, P., Heitz, F., Pattus, F., Martinez, C., Dijkman, R., and Lazdunski, C. (1988). Hydrodynamic properties of colicin A. Eur. J. Biochem. *172*, 507–512.

Chang, Y.-C., and Bowie, J.U. (2014). Measuring membrane protein stability under native conditions. Proc. Natl. Acad. Sci. *111*, 219–224.

Chattopadhyay, A., and Harikumar, K.G. (1996). Dependence of critical micelle concentration of a zwitterionic detergent on ionic strength: implications in receptor solubilization. FEBS Lett. *391*, 199–202.

Chen, Y.-H., and Yang, J.T. (1971). A new approach to the calculation of secondary structures of globular proteins by optical rotatory dispersion and circular dichroism. Biochem. Biophys. Res. Commun. *44*, 1285–1291.

Chin, C.N., and von Heijne, G. (2000). Charge pair interactions in a model transmembrane helix in the ER membrane. J. Mol. Biol. *303*, 1–5.

Choe, S., Bennett, M.J., Fujii, G., Curmi, P.M.G., Kantardjieff, K.A., Collier, R.J., and Eisenberg, D. (1992). The crystal structure of diphtheria toxin. Nature *357*, 216–222.

Choma, C., Gratkowski, H., Lear, J.D., and DeGrado, W.F. (2000). Asparagine-mediated self-association of a model transmembrane helix. Nat. Struct. Biol. *7*, 161–166.

Collins, E.S., Whittaker, S.B.-M., Tozawa, K., MacDonald, C., Boetzel, R., Penfold, C.N., Reilly, A., Clayden, N.J., Osborne, M.J., Hemmings, A.M., et al. (2002). Structural dynamics of the membrane translocation domain of colicin E9 and its interaction with TolB. J. Mol. Biol. *318*, 787–804.

Contreras, F.-X., Ernst, A.M., Wieland, F., and Brugger, B. (2011). Specificity of Intramembrane Protein-Lipid Interactions. Cold Spring Harb. Perspect. Biol. *3*, a004705–a004705.

Cooper, A. (2004). Biophysical Chemistry (The Royal Society of Chemistry).

Cordes, F.S., Bright, J.N., and Sansom, M.S.P. (2002). Proline-induced Distortions of Transmembrane Helices. J. Mol. Biol. *323*, 951–960.

Cosentino, K., Ros, U., and García-Sáez, A.J. (2016). Assembling the puzzle: Oligomerization of α-pore forming proteins in membranes. Biochim. Biophys. Acta BBA - Biomembr. *1858*, 457–466.

Crameri, A., Whitehorn, E.A., Tate, E., and Stemmer, W.P.C. (1996). Improved Green Fluorescent Protein by Molecular Evolution Using DNA Shuffling. Nat. Biotechnol. *14*, 315–319.

Cross, T.A., Sharma, M., Yi, M., and Zhou, H.-X. (2011). Influence of solubilizing environments on membrane protein structures. Trends Biochem. Sci. *36*, 117–125.

Cymer, F., von Heijne, G., and White, S.H. (2015). Mechanisms of Integral Membrane Protein Insertion and Folding. J. Mol. Biol. *427*, 999–1022.

Daley, D.O. (2008). The assembly of membrane proteins into complexes. Curr. Opin. Struct. Biol. *18*, 420–424.

Davies, J.K., and Reeves, P. (1975a). Genetics of resistance to colicins in Escherichia coli K-12: cross-resistance among colicins of group A. J. Bacteriol. *123*, 102–117.

Davies, J.K., and Reeves, P. (1975b). Genetics of resistance to colicins in Escherichia coli K-12: cross-resistance among colicins of group B. J. Bacteriol. *123*, 96–101.

Davies, J. T. (1957). A quantitative kinetic theory of emulsion type I. physical chemistry of emulsifying agent. Proc. Int. Congr. Surf. Act. 426–38.

Deprez, C., Blanchard, L., Guerlesquin, F., Gavioli, M., Simorre, J.-P., Lazdunski, C., Marion, D., and Lloubès, R. (2002). Macromolecular Import into Escherichia coli: The TolA C-Terminal Domain Changes Conformation When Interacting with the Colicin A Toxin. Biochemistry (Mosc.) *41*, 2589–2598.

Dobson, A., Cotter, P.D., Ross, R.P., and Hill, C. (2012). Bacteriocin Production: a Probiotic Trait? Appl. Environ. Microbiol. *78*, 1–6.

Dover, L.G., Evans, L.J.A., Fridd, S.L., Bainbridge, G., Raggett, E.M., and Lakey, J.H. (2000). Colicin Pore-Forming Domains Bind to *Escherichia Coli* Trimeric Porins †. Biochemistry (Mosc.) *39*, 8632–8637.

Doyle, D.A., Cabral, J.M., Pfuetzner, R.A., Kuo, A., Gulbis, J.M., Cohen, S.L., Chait, B.T., and MacKinnon, R. (1998). The Structure of the Potassium Channel: Molecular Basis of K+ Conduction and Selectivity. Science *280*, 69–77.

Drew, D., Fröderberg, L., Baars, L., and de Gier, J.-W.L. (2003). Assembly and overexpression of membrane proteins in Escherichia coli. Biochim. Biophys. Acta BBA - Biomembr. *1610*, 3–10.

Drew, D., Lerch, M., Kunji, E., Slotboom, D.-J., and de Gier, J.-W. (2006). Optimization of membrane protein overexpression and purification using GFP fusions. Nat. Methods *3*, 303–313.

Drew, D., Newstead, S., Sonoda, Y., Kim, H., von Heijne, G., and Iwata, S. (2008). GFP-based optimization scheme for the overexpression and purification of eukaryotic membrane proteins in Saccharomyces cerevisiae. Nat. Protoc. *3*, 784–798.

Duché, D. (2007). Colicin E2 Is Still in Contact with Its Receptor and Import Machinery When Its Nuclease Domain Enters the Cytoplasm. J. Bacteriol. *189*, 4217–4222.

Duché, D., Parker, M.W., González-Mañas, J.M., Pattus, F., and Baty, D. (1994a). Uncoupled steps of the colicin A pore formation demonstrated by disulfide bond engineering. J. Biol. Chem. *269*, 6332–6339.

Duché, D., Baty, D., Chartier, M., and Letellier, L. (1994b). Unfolding of colicin A during its translocation through the Escherichia coli envelope as demonstrated by disulfide bond engineering. J. Biol. Chem. *269*, 24820–24825.

Duché, D., Letellier, L., Géli, V., Bénédetti, H., and Baty, D. (1995). Quantification of group A colicin import sites. J. Bacteriol. *177*, 4935–4939.

Duché, D., Corda, Y., Géli, V., and Baty, D. (1999). Integration of the colicin A pore-forming domain into the cytoplasmic membrane of Escherichia coli1. J. Mol. Biol. *285*, 1965–1975.

Dunkel, S., Pulagam, L.P., Steinhoff, H.-J., and Klare, J.P. (2015). In vivo EPR on spin labeled colicin A reveals an oligomeric assembly of the pore-forming domain in E. coli membranes. Phys Chem Chem Phys *17*, 4875–4878.

Dunker, A.K., and Jones, T.C. (1978). Proposed knobs-into-holes packing for several membrane proteins. Membr. Biochem. *2*, 1–16.

Dyson, H.J., and Wright, P.E. (2005). Intrinsically unstructured proteins and their functions. Nat. Rev. Mol. Cell Biol. *6*, 197–208.

Eilers, M., Patel, A.B., Liu, W., and Smith, S.O. (2002). Comparison of helix interactions in membrane and soluble alpha-bundle proteins. Biophys. J. *82*, 2720–2736.

Espesset, D., Corda, Y., Cunningham, K., Bénédetti, H., Lloubès, R., Lazdunski, C., and Géli, V. (1994a). The colicin A pore-forming domain fused to mitochondrial intermembrane space sorting signals can be functionally inserted into the Escherichia coli plasma membrane by a mechanism that bypasses the Tol proteins. Mol. Microbiol. *13*, 1121–1131.

Espesset, D., Piet, P., Lazdunski, C., and Géli, V. (1994b). Immunity proteins to pore-forming colicins: structure-function relationships. Mol. Microbiol. *13*, 1111–1120.

Espesset, D., Duché, D., Baty, D., and Géli, V. (1996). The channel domain of colicin A is inhibited by its immunity protein through direct interaction in the Escherichia coli inner membrane. EMBO J. *15*, 2356–2364.

Evans, L.J.A., Goble, M.L., Hales, K.A., and Lakey, J.H. (1996). Different Sensitivities to Acid Denaturation within a Family of Proteins: Implications for Acid Unfolding and Membrane Translocation. Biochemistry (Mosc.) *35*, 13180–13185.

Fernández, C., and Wüthrich, K. (2003). NMR solution structure determination of membrane proteins reconstituted in detergent micelles. FEBS Lett. *555*, 144–150.

Fersht, A. (1999). Structure and mechanism in protein science: a guide to enzyme catalysis and protein folding (Macmillan).

Fiske, C.H., and Subbarow, Y. (1925). The Colorimetric Determination of Phosphorus. J. Biol. Chem. *66*, 375–400.

Fradin, C., Satsoura, D., and Andrews, D.W. (2009). Punching Holes in Membranes: How Oligomeric Pore-Forming Proteins and Lipids Cooperate to Form Aqueous Channels in Membranes. In Biomembrane Frontiers: Nanostructures, Models, and the Design of Life, Handbook of Modern Biophysics, p. 223.

Fredericq, P. (1964). [COLICINS AND COLICINOGENY]. Ann. Inst. Pasteur *107*, SUPPL:7-17.

Fukuda, H., Arai, M., and Kuwajima, K. (2000). Folding of green fluorescent protein and the cycle3 mutant. Biochemistry (Mosc.) *39*, 12025–12032.

Garavito, R.M., and Ferguson-Miller, S. (2001). Detergents as Tools in Membrane Biochemistry. J. Biol. Chem. *276*, 32403–32406.

Geertsma, E.R., Nik Mahmood, N.A.B., Schuurman-Wolters, G.K., and Poolman, B. (2008). Membrane reconstitution of ABC transporters and assays of translocator function. Nat. Protoc. *3*, 256–266.

Geli, V., and Lazdunski, C. (1992). An alpha-helical hydrophobic hairpin as a specific determinant in protein-protein interaction occurring in Escherichia coli colicin A and B immunity systems. J. Bacteriol. *174*, 6432–6437.

Geli, V., Baty, D., Crozel, V., Morlon, J., Lloubes, R., Pattus, F., and Lazdunski, C. (1986). A molecular genetic approach to the functioning of the immunity protein to colicin A. Mol. Gen. Genet. MGG *202*, 455–460.

Geli, V., Baty, D., and Lazdunski, C. (1988). Use of a foreign epitope as a “tag” for the localization of minor proteins within a cell: the case of the immunity protein to colicin A. Proc. Natl. Acad. Sci. U. S. A. *85*, 689–693.

Geli, V., Baty, D., Pattus, F., and Lazdunski, C. (1989). Topology and function of the integral membrane protein conferring immunity to colicin A. Mol. Microbiol. *3*, 679–687.

Géli, V., Koorengevel, M.C., Demel, R.A., Lazdunski, C., and Killian, J.A. (1992). Acidic interaction of the colicin A pore-forming domain with model membranes of Escherichia coli lipids results in a large perturbation of acyl chain order and stabilization of the bilayer. Biochemistry (Mosc.) *31*, 11089–11094.

Ghachi, M.E., Bouhss, A., Barreteau, H., Touzé, T., Auger, G., Blanot, D., and Mengin-Lecreulx, D. (2006). Colicin M Exerts Its Bacteriolytic Effect via Enzymatic Degradation of Undecaprenyl Phosphate-linked Peptidoglycan Precursors. J. Biol. Chem. *281*, 22761–22772.

Gilbert, R.J.C. (2016). Protein–lipid interactions and non-lamellar lipidic structures in membrane pore formation and membrane fusion. Biochim. Biophys. Acta BBA - Biomembr. *1858*, 487–499.

Gillor, O., Etzion, A., and Riley, M.A. (2008). The dual role of bacteriocins as anti- and probiotics. Appl. Microbiol. Biotechnol. *81*, 591–606.

Goñi, F.M. (2014). The basic structure and dynamics of cell membranes: An update of the Singer–Nicolson model. Biochim. Biophys. Acta BBA - Biomembr. *1838*, 1467–1476.

van der Goot, F.G., González-Mañas, J.M., Lakey, J.H., and Pattus, F. (1991). A “molten-globule” membrane-insertion intermediate of the pore-forming domain of colicin A. Nature *354*, 408–410.

Gordon, M., and Finkelstein, A. (2001). The Number of Subunits Comprising the Channel Formed by the T Domain of Diphtheria Toxin. J. Gen. Physiol. *118*, 471–480.

Gouaux, E. (1997). The long and short of colicin action: the molecular basis for the biological activity of channel-forming colicins. Structure *5*, 313–317.

Green, M.R., Sambrook, J., and Sambrook, J. (2012). Molecular cloning: a laboratory manual (Cold Spring Harbor, N.Y: Cold Spring Harbor Laboratory Press).

Greig, S.L., Radjainia, M., and Mitra, A.K. (2009). Oligomeric Structure of Colicin Ia Channel in Lipid Bilayer Membranes. J. Biol. Chem. *284*, 16126–16134.

Griffin, W. C. (1954). Calculation of HLB values of non-ionic surfactants. J. Cosmet. Sci. *5*, 249–256.

Groves, J.D., and Tanner, M.J.A. (1999). Topology studies with biosynthetic fragments identify interacting transmembrane regions of the human red-cell anion exchanger (band 3; AE1). Biochem. J. *344*, 687–697.

Guan, L., Smirnova, I.N., Verner, G., Nagamori, S., and Kaback, H.R. (2006). Manipulating phospholipids for crystallization of a membrane transport protein. Proc. Natl. Acad. Sci. U. S. A. *103*, 1723–1726.

Guidotti, G. (1972). Membrane Proteins. Annu. Rev. Biochem. *41*, 731–752.

Guihard, G., Boulanger, P., Bénédetti, H., Lloubés, R., Besnard, M., and Letellier, L. (1994). Colicin A and the Tol proteins involved in its translocation are preferentially located in the contact sites between the inner and outer membranes of Escherichia coli cells. J. Biol. Chem. *269*, 5874–5880.

Harris, N.J., and Booth, P.J. (2012). Folding and stability of membrane transport proteins in vitro. Biochim. Biophys. Acta BBA - Biomembr. *1818*, 1055–1066.

Harris, N.J., Findlay, H.E., Simms, J., Liu, X., and Booth, P.J. (2014). Relative Domain Folding and Stability of a Membrane Transport Protein. J. Mol. Biol. *426*, 1812–1825.

Hattori, M., Hibbs, R.E., and Gouaux, E. (2012). A Fluorescence-Detection Size-Exclusion Chromatography-Based Thermostability Assay for Membrane Protein Precrystallization Screening. Structure *20*, 1293–1299.

He, M.M., and Kaback, H.R. (1998). In vitro folding of a membrane protein: Effect of denaturation and renaturation on substrate binding by the lactose permease of Escherichia coli. Mol. Membr. Biol. *15*, 15–20.

von Heijne, G. (1989). Control of topology and mode of assembly of a polytopic membrane protein by positively charged residues. Nature *341*, 456–458.

von Heijne, G. (1992). Membrane protein structure prediction. J. Mol. Biol. *225*, 487–494.

Heim, R., and Tsien, R.Y. (1996). Engineering green fluorescent protein for improved brightness, longer wavelengths and fluorescence resonance energy transfer. Curr. Biol. *6*, 178–182.

Hessa, T., Kim, H., Bihlmaier, K., Lundin, C., Boekel, J., Andersson, H., Nilsson, I., White, S.H., and von Heijne, G. (2005a). Recognition of transmembrane helices by the endoplasmic reticulum translocon. Nature *433*, 377–381.

Hessa, T., White, S.H., and von Heijne, G. (2005b). Membrane insertion of a potassium-channel voltage sensor. Science *307*, 1427.

Hessa, T., Meindl-Beinker, N.M., Bernsel, A., Kim, H., Sato, Y., Lerch-Bader, M., Nilsson, I., White, S.H., and von Heijne, G. (2007). Molecular code for transmembrane-helix recognition by the Sec61 translocon. Nature *450*, 1026–1030.

Hirota, N., Goto, Y., and Mizuno, K. (1997). Cooperative α-helix formation of β-lactoglobulin and melittin induced by hexafluoroisopropanol. Protein Sci. *6*, 416–421.

Hoch, D.H., Romero-Mira, M., Ehrlich, B.E., Finkelstein, A., DasGupta, B.R., and Simpson, L.L. (1985). Channels formed by botulinum, tetanus, and diphtheria toxins in planar lipid bilayers:

relevance to translocation of proteins across membranes. Proc. Natl. Acad. Sci. U. S. A. *82*, 1692–1696.

Holm, L., and Sander, C. (1993). Structural alignment of globins, phycocyanins and colicin A. FEBS Lett. *315*, 301–306.

Hong, H. (2014). Toward understanding driving forces in membrane protein folding. Arch. Biochem. Biophys. *564*, 297–313.

Hong, H., Joh, N.H., Bowie, J.U., and Tamm, L.K. (2009). Chapter 8 Methods for Measuring the Thermodynamic Stability of Membrane Proteins. B.-M. in Enzymology, ed. (Academic Press), pp. 213–236.

Hong, H., Blois, T.M., Cao, Z., and Bowie, J.U. (2010). Method to measure strong protein–protein interactions in lipid bilayers using a steric trap. Proc. Natl. Acad. Sci. U. S. A. *107*, 19802–19807.

Hong, H., Chang, Y.-C., and Bowie, J.U. (2013). Measuring Transmembrane Helix Interaction Strengths in Lipid Bilayers Using Steric Trapping. Methods Mol. Biol. Clifton NJ *1063*, 37–56.

Hopf, T.A., Schärfe, C.P.I., Rodrigues, J.P.G.L.M., Green, A.G., Kohlbacher, O., Sander, C., Bonvin, A.M.J.J., and Marks, D.S. (2014). Sequence co-evolution gives 3D contacts and structures of protein complexes. eLife *3*, e03430.

Huang, K.S., Bayley, H., and Khorana, H.G. (1980). Delipidation of bacteriorhodopsin and reconstitution with exogenous phospholipid. Proc. Natl. Acad. Sci. U. S. A. *77*, 323–327.

Huang, K.S., Bayley, H., Liao, M.J., London, E., and Khorana, H.G. (1981). Refolding of an integral membrane protein. Denaturation, renaturation, and reconstitution of intact bacteriorhodopsin and two proteolytic fragments. J. Biol. Chem. *256*, 3802–3809.

Huster, D., Xiao, L., and Hong, M. (2001). Solid-State NMR Investigation of the Dynamics of the Soluble and Membrane-Bound Colicin Ia Channel-Forming Domain. Biochemistry (Mosc.) *40*, 7662–7674.

Ibañez de Opakua, A. (2011). Conformational equilibrium of the pore-forming domain of colicin A: implication in its mechanism of action.

Jakes, K.S., Kienker, P.K., Slatin, S.L., and Finkelstein, A. (1998). Translocation of inserted foreign epitopes by a channelforming protein. Proc. Natl. Acad. Sci. U. S. A. *95*, 4321–4326.

James, N., and Jameson, D. (2014). Steady-State Fluorescence Polarization/Anisotropy for the Study of Protein Interactions. In Fluorescence Spectroscopy and Microscopy, Y. Engelborghs, and A.J.W.G. Visser, eds. (Humana Press), pp. 29–42.

James, R., Kleanthous, C., and Moore, G.R. (1996). The biology of E colicins: paradigms and paradoxes. Microbiol. Read. Engl. *142 (Pt 7)*, 1569–1580.

Jameson, D., and Mocz, G. (2005). Fluorescence Polarization/Anisotropy Approaches to Study Protein-Ligand Interactions. In Protein-Ligand Interactions, G. Ulrich Nienhaus, and G.U. Nienhaus, eds. (Humana Press), pp. 301–322.

Jiang, Y., Lee, A., Chen, J., Ruta, V., Cadene, M., Chait, B.T., and MacKinnon, R. (2003). X-ray structure of a voltage-dependent K+ channel. Nature *423*, 33–41.

J. Miles, A., and A. Wallace, B. (2016). Circular dichroism spectroscopy of membrane proteins. Chem. Soc. Rev. *45*, 4859–4872.

Joh, N.H., Min, A., Faham, S., Whitelegge, J.P., Yang, D., Woods, V.L., and Bowie, J.U. (2008). Modest stabilization by most hydrogen-bonded side-chain interactions in membrane proteins. Nature *453*, 1266–1270.

Joh, N.H., Oberai, A., Yang, D., Whitelegge, J.P., and Bowie, J.U. (2009). Similar Energetic Contributions of Packing in the Core of Membrane and Water-Soluble Proteins. J. Am. Chem. Soc. *131*, 10846–10847.

Jungwirth, P., and Cremer, P.S. (2014). Beyond hofmeister. Nat. Chem. *6*, 261–263.

Kang, C., Tian, C., Sönnichsen, F.D., Smith, J.A., Meiler, J., George, A.L., Vanoye, C.G., Kim, H.J., and Sanders, C.R. (2008). Structure of KCNE1 and Implications for How It Modulates the KCNQ1 Potassium Channel. Biochemistry (Mosc.) *47*, 7999–8006.

Kienker, P., and Slatin, S. (2003). Colicin channels and protein translocation. In Pore-Forming Peptides and Protein Toxins, (CRC Press), pp. 102–131.

Kienker, P.K., Jakes, K.S., and Finkelstein, A. (2000). Protein Translocation Across Planar Bilayers by the Colicin Ia Channel-forming Domain Where Will It End? J. Gen. Physiol. *116*, 587–598.

Kienker, P.K., Jakes, K.S., and Finkelstein, A. (2008). Identification of Channel-lining Amino Acid Residues in the Hydrophobic Segment of Colicin Ia. J. Gen. Physiol. *132*, 693–707.

Kim, C., Schmidt, T., Cho, E.-G., Ye, F., Ulmer, T.S., and Ginsberg, M.H. (2011). Basic amino-acid side chains regulate transmembrane integrin signalling. Nature *481*, 209–213.

Kim, H.J., Howell, S.C., Van Horn, W.D., Jeon, Y.H., and Sanders, C.R. (2009). Recent advances in the application of solution NMR spectroscopy to multi-span integral membrane proteins. Prog. Nucl. Magn. Reson. Spectrosc. *55*, 335–360.

Kim, Y.C., Tarr, A.W., and Penfold, C.N. (2014). Colicin import into E. coli cells: A model system for insights into the import mechanisms of bacteriocins. Biochim. Biophys. Acta BBA - Mol. Cell Res. *1843*, 1717–1731.

Klaenhammer, T.R. (1988). Bacteriocins of lactic acid bacteria. Biochimie *70*, 337–349.

Klug, C.S., Su, W., Liu, J., Klebba, P.E., and Feix, J.B. (1995). Denaturant unfolding of the ferric enterobactin receptor and ligand-induced stabilization studied by site-directed spin labeling. Biochemistry (Mosc.) *34*, 14230–14236.

Koehler, J., Sulistijo, E.S., Sakakura, M., Kim, H.J., Ellis, C.D., and Sanders, C.R. (2010). Lyso-Phospholipid Micelles Sustain the Stability and Catalytic Activity of Diacylglycerol Kinase in the Absence of Lipids. Biochemistry (Mosc.) *49*, 7089–7099.

el Kouhen, R., Fierobe, H.P., Scianimanico, S., Steiert, M., Pattus, F., and Pagès, J.M. (1993). Characterization of the receptor and translocator domains of colicin N. Eur. J. Biochem. *214*, 635–639.

Kozlov, M.M., McMahon, H.T., and Chernomordik, L.V. (2010). Protein-driven membrane stresses in fusion and fission. Trends Biochem. Sci. *35*, 699–706.

Kramer, R.M., Shende, V.R., Motl, N., Pace, C.N., and Scholtz, J.M. (2012). Toward a Molecular Understanding of Protein Solubility: Increased Negative Surface Charge Correlates with Increased Solubility. Biophys. J. *102*, 1907–1915.

Krogh, A., Larsson, B., von Heijne, G., and Sonnhammer, E.L. (2001). Predicting transmembrane protein topology with a hidden Markov model: application to complete genomes. J. Mol. Biol. *305*, 567–580.

Krueger-Koplin, R.D., Sorgen, P.L., Krueger-Koplin, S.T., Rivera-Torres, I.O., Cahill, S.M., Hicks, D.B., Grinius, L., Krulwich, T.A., and Girvin, M.E. (2004). An evaluation of detergents for NMR structural studies of membrane proteins. J. Biomol. NMR *28*, 43–57.

Ladokhin, A.S., and White, S.H. (1999). Folding of amphipathic α-helices on membranes: energetics of helix formation by melittin1. J. Mol. Biol. *285*, 1363–1369.

Lakey, J.H., and Slatin, S.L. (2001). Pore-forming colicins and their relatives. Curr. Top. Microbiol. Immunol. *257*, 131–161.

Lakey, J.H., Baty, D., and Pattus, F. (1991). Fluorescence energy transfer distance measurements using site-directed single cysteine mutants. J. Mol. Biol. *218*, 639–653.

Lakey, J.H., Duche, D., Gonzáles-Mañas, J.-M., Baty, D., and Pattus, F. (1993). Fluorescence Energy Transfer Distance Measurements. J. Mol. Biol. *230*, 1055–1067.

Lakey, J.H., Parker, M.W., González-Mañas, J.M., Duché, D., Vriend, G., Baty, D., and Pattus, F. (1994). The role of electrostatic charge in the membrane insertion of colicin A. Eur. J. Biochem. *220*, 155–163.

Lakowicz, J. R. (2006). Principles of Fluorescence Spectroscopy (Boston, MA: Springer US).

Langosch, D., and Heringa, J. (1998). Interaction of transmembrane helices by a knobs-into-holes packing characteristic of soluble coiled coils. Proteins *31*, 150–159.

Lau, F.W., and Bowie, J.U. (1997). A Method for Assessing the Stability of a Membrane Protein. Biochemistry (Mosc.) *36*, 5884–5892.

Lazdunski, C.J., Bouveret, E., Rigal, A., Journet, L., Lloubès, R., and Bénédetti, H. (1998). Colicin Import into Escherichia coli Cells. J. Bacteriol. *180*, 4993–5002.

Lazzaroni, J.-C., Dubuisson, J.-F., and Vianney, A. (2002). The Tol proteins of Escherichia coli and their involvement in the translocation of group A colicins. Biochimie *84*, 391–397.

Lee, C., Kang, H.J., von Ballmoos, C., Newstead, S., Uzdavinys, P., Dotson, D.L., Iwata, S., Beckstein, O., Cameron, A.D., and Drew, D. (2013). A two-domain elevator mechanism for sodium/proton antiport. Nature *501*, 573–577.

Liebau, J., Pettersson, P., Zuber, P., Ariöz, C., and Mäler, L. (2016). Fast-tumbling bicelles constructed from native Escherichia coli lipids. Biochim. Biophys. Acta BBA - Biomembr. *1858*, 2097–2105.

Lin, J.-H., and Baumgaertner, A. (2000). Stability of a Melittin Pore in a Lipid Bilayer: A Molecular Dynamics Study. Biophys. J. *78*, 1714–1724.

Lindeberg, M., Zakharov, S.D., and Cramer, W.A. (2000). Unfolding pathway of the colicin E1 channel protein on a membrane surface1. J. Mol. Biol. *295*, 679–692.

Linton, E., Walsh, M.K., Sims, R.C., and Miller, C.D. (2012). Translocation of green fluorescent protein by comparative analysis with multiple signal peptides. Biotechnol. J. *7*, 667–676.

Lloubes, R., Baly, D., and Lazdunski, C. (1986). The promoters of the genes for colicin production, release and immunity in the ColA plasmid: effects of convergent transcription and Lex A protein. Nucleic Acids Res. *14*, 2621–2636.

London, E. (1992). How bacterial protein toxins enter cells: the role of partial unfolding in membrane translocation. Mol. Microbiol. *6*, 3277–3282.

London, E., and Khorana, H.G. (1982). Denaturation and renaturation of bacteriorhodopsin in detergents and lipid-detergent mixtures. J. Biol. Chem. *257*, 7003–7011.

Lundbäck, A.-K., van den Berg, S., Hebert, H., Berglund, H., and Eshaghi, S. (2008). Exploring the activity of tobacco etch virus protease in detergent solutions. Anal. Biochem. *382*, 69–71.

Lwoff, A., Jacob, F., Ritz, E., and Gage, M. (1952). [Induction of bacteriophage production and of a colicine by peroxides, ethyleneimines and halogenated alkylamines]. Comptes Rendus Hebd. Seances Acad. Sci. *234*, 2308–2310.

MacKenzie, K.R., Prestegard, J.H., and Engelman, D.M. (1997). A Transmembrane Helix Dimer: Structure and Implications. Science *276*, 131–133.

Maeda, H., Muroi, S., and Kakehashi, R. (1997). Effects of Ionic Strength on the Critical Micelle Concentration and the Surface Excess of Dodecyldimethylamine Oxide. J. Phys. Chem. B *101*, 7378–7382.

Mankovich, J.A., Lai, P.H., Gokul, N., and Konisky, J. (1984). Organization of the colicin Ib gene. Promoter structure and immunity domain. J. Biol. Chem. *259*, 8764–8768.

Marin, V.L., Bayburt, T.H., Sligar, S.G., and Mrksich, M. (2007). Functional Assays of Membrane-Bound Proteins with SAMDI-TOF Mass Spectrometry. Angew. Chem. Int. Ed Engl. *46*, 8796–8798.

Marley, J., Lu, M., and Bracken, C. (2001). A method for efficient isotopic labeling of recombinant proteins. J. Biomol. NMR *20*, 71–75.

Matsuzaki, K., Murase, O., Fujii, N., and Miyajima, K. (1996). An Antimicrobial Peptide, Magainin 2, Induced Rapid Flip-Flop of Phospholipids Coupled with Pore Formation and Peptide Translocation. Biochemistry (Mosc.) *35*, 11361–11368.

Mayer, L.D., Hope, M.J., and Cullis, P.R. (1986). Vesicles of variable sizes produced by a rapid extrusion procedure. Biochim. Biophys. Acta BBA - Biomembr. *858*, 161–168.

Meneses, P., and Glonek, T. (1988). High resolution 31P NMR of extracted phospholipids. J. Lipid Res. *29*, 679–689.

Merrill, A.R., Cohen, F.S., and Cramer, W.A. (1990). On the nature of the structural change of the colicin E1 channel peptide necessary for its translocation-competent state. Biochemistry (Mosc.) *29*, 5829–5836.

Mertens, N., Remaut, E., and Fiers, W. (1995). Tight transcriptional control mechanism ensures stable high-level expression from T7 promoter-based expression plasmids. Biotechnol. Nat. Publ. Co. *13*, 175–179.

Mileykovskaya, E., and Dowhan, W. (2000). Visualization of Phospholipid Domains in Escherichia coli by Using the Cardiolipin-Specific Fluorescent Dye 10-N-Nonyl Acridine Orange. J. Bacteriol. *182*, 1172–1175.

Mileykovskaya, E., and Dowhan, W. (2009). Cardiolipin Membrane Domains in Prokaryotes and Eukaryotes. Biochim. Biophys. Acta *1788*, 2084–2091.

Miller, D., Charalambous, K., Rotem, D., Schuldiner, S., Curnow, P., and Booth, P.J. (2009). In vitro Unfolding and Refolding of the Small Multidrug Transporter EmrE. J. Mol. Biol. *393*, 815–832.

Min, D., Jefferson, R.E., Bowie, J.U., and Yoon, T.-Y. (2015). Mapping the energy landscape for second-stage folding of a single membrane protein. Nat. Chem. Biol. *11*, 981–987.

Mitchinson, C., Wilderspin, A.F., Trinnaman, B.J., and Green, N.M. (1982). Identification of a labelled peptide after stoicheiometric reaction of fluorescein isothiocyanate with the Ca2+-dependent adenosine triphosphatase of sarcoplasmic reticulum. FEBS Lett. *146*, 87–92.

Mitra, K., Ubarretxena-Belandia, I., Taguchi, T., Warren, G., and Engelman, D.M. (2004). Modulation of the bilayer thickness of exocytic pathway membranes by membrane proteins rather than cholesterol. Proc. Natl. Acad. Sci. U. S. A. *101*, 4083–4088.

Moffat, J.C., Vijayvergiya, V., Gao, P.F., Cross, T.A., Woodbury, D.J., and Busath, D.D. (2008). Proton Transport through Influenza A Virus M2 Protein Reconstituted in Vesicles. Biophys. J. *94*, 434–445.

Montalbán-López, M., Sánchez-Hidalgo, M., Valdivia, E., Martínez-Bueno, M., and Maqueda, M. (2011). Are bacteriocins underexploited? Novel applications for old antimicrobials. Curr. Pharm. Biotechnol. *12*, 1205–1220.

Moon, C.P., Zaccai, N.R., Fleming, P.J., Gessmann, D., and Fleming, K.G. (2013). Membrane protein thermodynamic stability may serve as the energy sink for sorting in the periplasm. Proc. Natl. Acad. Sci. *110*, 4285–4290.

Mosbahi, K., Walker, D., Lea, E., Moore, G.R., James, R., and Kleanthous, C. (2004). Destabilization of the Colicin E9 Endonuclease Domain by Interaction with Negatively Charged Phospholipids IMPLICATIONS FOR COLICIN TRANSLOCATION INTO BACTERIA. J. Biol. Chem. *279*, 22145–22151.

Muga, A., Gonzalez-Manas, J.M., Lakey, J.H., Pattus, F., and Surewicz, W.K. (1993). pH-dependent stability and membrane interaction of the pore-forming domain of colicin A. J. Biol. Chem. *268*, 1553–1557.

Müller, G. (2000). Towards 3D structures of G protein-coupled receptors: a multidisciplinary approach. Curr. Med. Chem. *7*, 861–888.

Murail, S., Robert, J.-C., Coïc, Y.-M., Neumann, J.-M., Ostuni, M.A., Yao, Z.-X., Papadopoulos, V., Jamin, N., and Lacapère, J.-J. (2008). Secondary and tertiary structures of the transmembrane domains of the translocator protein TSPO determined by NMR. Stabilization of the TSPO tertiary fold upon ligand binding. Biochim. Biophys. Acta BBA - Biomembr. *1778*, 1375–1381.

Murata, K., Mitsuoka, K., Hirai, T., Walz, T., Agre, P., Heymann, J.B., Engel, A., and Fujiyoshi, Y. (2000). Structural determinants of water permeation through aquaporin-1. Nature *407*, 599–605.

Murray, D.T., Li, C., Gao, F.P., Qin, H., and Cross, T.A. (2014). Membrane Protein Structural Validation by Oriented Sample Solid-State NMR: Diacylglycerol Kinase. Biophys. J. *106*, 1559–1569.

Nardi, A., Slatin, S.L., Baty, D., and Duché, D. (2001). The C-terminal half of the colicin A pore-forming domain is active in vivo and in vitro11Edited by I. B. Holland. J. Mol. Biol. *307*, 1293–1303.

Natale, P., Brüser, T., and Driessen, A.J.M. (2008). Sec- and Tat-mediated protein secretion across the bacterial cytoplasmic membrane—Distinct translocases and mechanisms. Biochim. Biophys. Acta BBA - Biomembr. *1778*, 1735–1756.

Newman, M.J., Foster, D.L., Wilson, T.H., and Kaback, H.R. (1981). Purification and reconstitution of functional lactose carrier from Escherichia coli. J. Biol. Chem. *256*, 11804–11808.

Newstead, S., Ferrandon, S., and Iwata, S. (2008). Rationalizing α-helical membrane protein crystallization. Protein Sci. *17*, 466–472.

Nietlispach, D., and Gautier, A. (2011). Solution NMR studies of polytopic α-helical membrane proteins. Curr. Opin. Struct. Biol. *21*, 497–508.

Nilsson, I., and Heijne, G. von (1990). Fine-tuning the topology of a polytopic membrane protein: Role of positively and negatively charged amino acids. Cell *62*, 1135–1141.

Nury, H., Dahout-Gonzalez, C., Trézéguet, V., Lauquin, G., Brandolin, G., and Pebay-Peyroula, E. (2005). Structural basis for lipid-mediated interactions between mitochondrial ADP/ATP carrier monomers. FEBS Lett. *579*, 6031–6036.

Otzen, D.E. (2003). Folding of DsbB in Mixed Micelles: A Kinetic Analysis of the Stability of a Bacterial Membrane Protein. J. Mol. Biol. *330*, 641–649.

Padmavathi, P.V.L., and Steinhoff, H.-J. (2008). Conformation of the Closed Channel State of Colicin A in Proteoliposomes: An Umbrella Model. J. Mol. Biol. *378*, 204–214.

Parker, M.W., and Pattus, F. (1993). Rendering a membrane protein soluble in water: a common packing motif in bacterial protein toxins. Trends Biochem. Sci. *18*, 391–395.

Parker, M.W., Pattus, F., Tucker, A.D., and Tsernoglou, D. (1989). Structure of the membrane-pore-forming fragment of colicin A. Nature *337*, 93–96.

Pattus, F., Heitz, F., Martinez, C., Provencher, S.W., and Lazdunski, C. (1985). Secondary structure of the pore-forming colicin A and its C-terminal fragment. Eur. J. Biochem. *152*, 681–689.

Poget, S.F., and Girvin, M.E. (2007). Solution NMR of membrane proteins in bilayer mimics: Small is beautiful, but sometimes bigger is better. Biochim. Biophys. Acta BBA - Biomembr. *1768*, 3098–3106.

Pollard, T.D. (2010). A Guide to Simple and Informative Binding Assays. Mol. Biol. Cell *21*, 4061–4067.

Popot, J.L., and Engelman, D.M. (1990). Membrane protein folding and oligomerization: the two-stage model. Biochemistry (Mosc.) *29*, 4031–4037.

Popot, J.L., Trewhella, J., and Engelman, D.M. (1986). Reformation of crystalline purple membrane from purified bacteriorhodopsin fragments. EMBO J. *5*, 3039–3044.

Privé, G.G. (2007). Detergents for the stabilization and crystallization of membrane proteins. Methods *41*, 388–397.

Pugsley, A.P. (1988). The immunity and lysis genes of ColN plasmid pCHAP4. Mol. Gen. Genet. MGG *211*, 335–341.

Pulagam, L.P., and Steinhoff, H.-J. (2013). Acidic pH-Induced Membrane Insertion of Colicin A into E. coli Natural Lipids Probed by Site-Directed Spin Labeling. J. Mol. Biol. *425*, 1782–1794.

Qiu, X.Q., Jakes, K.S., Kienker, P.K., Finkelstein, A., and Slatin, S.L. (1996). Major transmembrane movement associated with colicin Ia channel gating. J. Gen. Physiol. *107*, 313–328.

Raetz, C.R. (1978). Enzymology, genetics, and regulation of membrane phospholipid synthesis in Escherichia coli. Microbiol. Rev. *42*, 614–659.

Raloff, J. (1998). Staging germ warfare in foods: Science harnesses bacteria to fend off food poisoning and spoilage. Sci. News *153*, 89–90.

Rath, P., Bousché, O., Merrill, A.R., Cramer, W.A., and Rothschild, K.J. (1991). Fourier transform infrared evidence for a predominantly alpha-helical structure of the membrane bound channel forming COOH-terminal peptide of colicin E1. Biophys. J. *59*, 516–522.

Raymond, L., Slatin, S.L., and Finkelstein, A. (1985). Channels formed by colicin E1 in planar lipid bilayers are large and exhibit pH-dependent ion selectivity. J. Membr. Biol. *84*, 173–181.

Read, J.A., and Duncan, R. (2011). Biophysical and functional assays for viral membrane fusion peptides. Methods San Diego Calif *55*, 122–126.

Renner, L.D., and Weibel, D.B. (2011). Cardiolipin microdomains localize to negatively curved regions of Escherichia coli membranes. Proc. Natl. Acad. Sci. *108*, 6264–6269.

Ricker, R.D., and Sandoval, L.A. (1996). Fast, reproducible size-exclusion chromatography of biological macromolecules. J. Chromatogr. A *743*, 43–50.

Riek, R.P., Rigoutsos, I., Novotny, J., and Graham, R.M. (2001). Non-α-helical elements modulate polytopic membrane protein architecture1. J. Mol. Biol. *306*, 349–362.

Rigaud, J.-L., and Lévy, D. (2003). Reconstitution of Membrane Proteins into Liposomes. B.-M. in Enzymology, ed. (Academic Press), pp. 65–86.

Rigaud, J.L., Bluzat, A., and Buschlen, S. (1983). Incorporation of bacteriorhodopsin into large unilamellar liposomes by reverse phase evaporation. Biochem. Biophys. Res. Commun. *111*, 373–382.

Riley, M.A., and Wertz, J.E. (2002). Bacteriocins: Evolution, Ecology, and Application. Annu. Rev. Microbiol. *56*, 117–137.

Rivera, A.M., and Boucher, H.W. (2011). Current Concepts in Antimicrobial Therapy Against Select Gram-Positive Organisms: Methicillin-ResistantStaphylococcus aureus, Penicillin-Resistant Pneumococci, and Vancomycin-Resistant Enterococci. Mayo Clin. Proc. *86*, 1230–1243.

Roman, E.A., and González Flecha, F.L. (2014). Kinetics and Thermodynamics of Membrane Protein Folding. Biomolecules *4*, 354–373.

Sanders, C.R., and Myers, J.K. (2004). Disease-Related Misassembly of Membrane Proteins. Annu. Rev. Biophys. Biomol. Struct. *33*, 25–51.

Santoro, M.M., and Bolen, D.W. (1988). Unfolding free energy changes determined by the linear extrapolation method. 1. Unfolding of phenylmethanesulfonyl .alpha.-chymotrypsin using different denaturants. Biochemistry (Mosc.) *27*, 8063–8068.

Schein, S.J., Kagan, B.L., and Finkelstein, A. (1978). Colicin K acts by forming voltage-dependent channels in phospholipid bilayer membranes. Nature *276*, 159–163.

Schendel, S.L., and Cramer, W.A. (1994). On the nature of the unfolded intermediate in the in vitro transition of the colicin E1 channel domain from the aqueous to the membrane phase. Protein Sci. Publ. Protein Soc. *3*, 2272–2279.

Schlebach, J.P., Kim, M.-S., Joh, N.H., Bowie, J.U., and Park, C. (2011). Probing Membrane Protein Unfolding with Pulse Proteolysis. J. Mol. Biol. *406*, 545–551.

Schlebach, J.P., Cao, Z., Bowie, J.U., and Park, C. (2012). Revisiting the folding kinetics of bacteriorhodopsin. Protein Sci. *21*, 97–106.

Schomburg, D., and Salzmann, M. (2013). Enzyme Handbook (Springer Science & Business Media).

Schramm, E., Olschläger, T., Tröger, W., and Braun, V. (1988). Sequence, expression and localization of the immunity protein for colicin B. Mol. Gen. Genet. MGG *211*, 176–182.

Sellman, B.R., Nassi, S., and Collier, R.J. (2001). Point mutations in anthrax protective antigen that block translocation. J. Biol. Chem. *276*, 8371–8376.

Senzel, L., Huynh, P.D., Jakes, K.S., John Collier, R., and Finkelstein, A. (1998). The Diphtheria Toxin Channel-forming T Domain Translocates Its Own NH2-Terminal Region Across Planar Bilayers. J. Gen. Physiol. *112*, 317–324.

Shinzawa-Itoh, K., Aoyama, H., Muramoto, K., Terada, H., Kurauchi, T., Tadehara, Y., Yamasaki, A., Sugimura, T., Kurono, S., Tsujimoto, K., et al. (2007). Structures and physiological roles of 13 integral lipids of bovine heart cytochrome *c* oxidase. EMBO J. *26*, 1713–1725.

Shokri, A., and Larsson, G. (2004). Characterization of the Escherichia coli membrane structure and function during fedbatch cultivation. Microb. Cell Factories *3*, 9.

Shu, X., Shaner, N.C., Yarbrough, C.A., Tsien, R.Y., and Remington, S.J. (2006). Novel Chromophores and Buried Charges Control Color in mFruits,. Biochemistry (Mosc.) *45*, 9639–9647.

Silverman, J.A., Mindell, J.A., Finkelstein, A., Shen, W.H., and Collier, R.J. (1994). Mutational analysis of the helical hairpin region of diphtheria toxin transmembrane domain. J. Biol. Chem. *269*, 22524–22532.

Slatin, S.L. (1988). Colicin E1 in planar lipid bilayers. Int. J. Biochem. *20*, 737–744.

Slatin, S.L., Qiu, X.-Q., Jakes, K.S., and Finkelstein, A. (1994). Identification of a translocated protein segment in a voltage-dependent channel. Nature *371*, 158–161.

Slatin, S.L., Nardi, A., Jakes, K.S., Baty, D., and Duché, D. (2002). Translocation of a functional protein by a voltage-dependent ion channel. Proc. Natl. Acad. Sci. *99*, 1286–1291.

Slatin, S.L., Finkelstein, A., and Kienker, P.K. (2008). Anomalous Proton Selectivity in a Large Channel: Colicin A †. Biochemistry (Mosc.) *47*, 1778–1788.

Slatin, S.L., Duché, D., and Baty, D. (2010). Determinants of the Proton Selectivity of the Colicin A Channel. Biochemistry (Mosc.) *49*, 4786–4793.

Šmajs, D., Doležalová, M., Macek, P., and Žídek, L. (2008). Inactivation of colicin Y by intramembrane helix-helix interaction with its immunity protein: Helix-helix interaction between colicin Y and Cyi. FEBS J. *275*, 5325–5331.

Sobko, A.A., Kotova, E.A., Antonenko, Y.N., Zakharov, S.D., and Cramer, W.A. (2006). Lipid Dependence of the Channel Properties of a Colicin E1-Lipid Toroidal Pore. J. Biol. Chem. *281*, 14408–14416.

Sobko, A.A., Rokitskaya, T.I., and Kotova, E.A. (2009). Histidine 440 controls the opening of colicin E1 channels in a lipid-dependent manner. Biochim. Biophys. Acta BBA - Biomembr. *1788*, 1962–1966.

Sobko, A.A., Kovalchuk, S.I., Kotova, E.A., and Antonenko, Y.N. (2010). Induction of lipid flip-flop by colicin E1 - a hallmark of proteolipidic pore formation in liposome membranes. Biochem. Biokhimiia *75*, 728–733.

Song, H.Y., and Cramer, W.A. (1991). Membrane topography of ColE1 gene products: the immunity protein. J. Bacteriol. *173*, 2935–2943.

Sonoda, Y., Newstead, S., Hu, N.-J., Alguel, Y., Nji, E., Beis, K., Yashiro, S., Lee, C., Leung, J., Cameron, A.D., et al. (2011). Benchmarking Membrane Protein Detergent Stability for Improving Throughput of High-Resolution X-ray Structures. Structure *19*, 17–25.

Spach, G. (1983). Physical chemistry of transmembrane ion motions: proceedings of the 36th international meeting of the Société de Chimie physique, Paris, 27 September - 1 October 1982 (Amsterdam: Elsevier).

Subburaj, Y., Cosentino, K., Axmann, M., Pedrueza-Villalmanzo, E., Hermann, E., Bleicken, S., Spatz, J., and García-Sáez, A.J. (2015). Bax monomers form dimer units in the membrane that further self-assemble into multiple oligomeric species. Nat. Commun. *6*, 8042.

Tanford, C. (1968). Protein Denaturation. In Advances in Protein Chemistry, M.L.A. C.B. Anfinsen John T. Edsall and Frederic M. Richards, ed. (Academic Press), pp. 121–282.

Taylor, R.M., Zakharov, S.D., Heymann, J.B., Girvin, M.E., and Cramer, W.A. (2000). Folded State of the Integral Membrane Colicin E1 Immunity Protein in Solvents of Mixed Polarity †. Biochemistry (Mosc.) *39*, 12131–12139.

Thomas, J.D., Daniel, R.A., Errington, J., and Robinson, C. (2001). Export of active green fluorescent protein to the periplasm by the twin-arginine translocase (Tat) pathway in Escherichia coli. Mol. Microbiol. *39*, 47–53.

Thuduppathy, G.R., Terrones, O., Craig, J.W., Basañez, G., and Hill, R.B. (2006). The N-Terminal Domain of Bcl-xL Reversibly Binds Membranes in a pH-Dependent Manner. Biochemistry (Mosc.) *45*, 14533–14542.

Ulmschneider, M.B., Ulmschneider, J.P., Freites, J.A., Heijne, G. von, Tobias, D.J., and White, S.H. (2017). Transmembrane helices containing a charged arginine are thermodynamically stable. Eur. Biophys. J. 1–11.

Umbreit, J.N., and Strominger, J.L. (1973). Relation of Detergent HLB Number to Solubilization and Stabilization of D-Alanine Carboxypeptidase from Bacillus subtilis Membranes. Proc. Natl. Acad. Sci. U. S. A. *70*, 2997–3001.

Unterreitmeier, S., Fuchs, A., Schäffler, T., Heym, R.G., Frishman, D., and Langosch, D. (2007). Phenylalanine Promotes Interaction of Transmembrane Domains via GxxxG Motifs. J. Mol. Biol. *374*, 705–718.

Valiyaveetil, F.I., Zhou, Y., and MacKinnon, R. (2002). Lipids in the structure, folding, and function of the KcsA K+ channel. Biochemistry (Mosc.) *41*, 10771–10777.

Verardi, R., Traaseth, N.J., Masterson, L.R., Vostrikov, V.V., and Veglia, G. (2012). Isotope Labeling for Solution and Solid-State NMR Spectroscopy of Membrane Proteins. Adv. Exp. Med. Biol. *992*, 35–62.

Vitrac, H., Bogdanov, M., and Dowhan, W. (2013). Proper Fatty Acid Composition Rather than an Ionizable Lipid Amine Is Required for Full Transport Function of Lactose Permease from Escherichia coli. J. Biol. Chem. *288*, 5873–5885.

W A Cramer, J B Heymann, S L Schendel, B N Deriy, F S Cohen, P A Elkins, and Stauffacher, and C.V. (1995). Structure-Function of the Channel-Forming Colicins. Annu. Rev. Biophys. Biomol. Struct. *24*, 611–641.

Wagner, S., Bader, M.L., Drew, D., and de Gier, J.-W. (2006). Rationalizing membrane protein overexpression. Trends Biotechnol. *24*, 364–371.

Wagstaff, K.M., Dias, M.M., Alvisi, G., and Jans, D.A. (2005). Quantitative Analysis of Protein–Protein Interactions by Native Page/Fluorimaging. J. Fluoresc. *15*, 469–473.

Walian, P., Cross, T.A., and Jap, B.K. (2004). Structural genomics of membrane proteins. Genome Biol. *5*, 215.

Wallis, R., Moore, G.R., James, R., and Kleanthous, C. (1995). Protein-protein interactions in colicin E9 DNase-immunity protein complexes. 1. Diffusion-controlled association and femtomolar binding for the cognate complex. Biochemistry (Mosc.) *34*, 13743–13750.

Walshaw, J., and Woolfson, D.N. (2003). Extended knobs-into-holes packing in classical and complex coiled-coil assemblies. J. Struct. Biol. *144*, 349–361.

Walther, D., Eisenhaber, F., and Argos, P. (1996). Principles of helix-helix packing in proteins: the helical lattice superposition model. J. Mol. Biol. *255*, 536–553.

Wang, Z., Wong, N.C., Cheng, Y., Kehl, S.J., and Fedida, D. (2009). Control of voltage-gated K+ channel permeability to NMDG+ by a residue at the outer pore. J. Gen. Physiol. *133*, 361–374.

Weckström, K. (1985). Aqueous micellar systems in membrane protein crystallization. Partial miscibility of a nonionic surfactant in the presence of salt or polyethylene glycol. FEBS Lett. *192*, 220–224.

Werner, K., Richter, C., Klein-Seetharaman, J., and Schwalbe, H. (2008). Isotope labeling of mammalian GPCRs in HEK293 cells and characterization of the C-terminus of bovine rhodopsin by high resolution liquid NMR spectroscopy. J. Biomol. NMR *40*, 49–53.

Westheimer, F. (1987). Why nature chose phosphates. Science *235*, 1173–1178.

White, S.H., and Wimley, W.C. (1999). MEMBRANE PROTEIN FOLDING AND STABILITY: Physical Principles. Annu. Rev. Biophys. Biomol. Struct. *28*, 319–365.

White, G.F., Racher, K.I., Lipski, A., Hallett, F.R., and Wood, J.M. (2000). Physical properties of liposomes and proteoliposomes prepared from Escherichia coli polar lipids. Biochim. Biophys. Acta BBA - Biomembr. *1468*, 175–186.

Wikström, M., Kelly, A.A., Georgiev, A., Eriksson, H.M., Klement, M.R., Bogdanov, M., Dowhan, W., and Wieslander, Å. (2009). Lipid-engineered Escherichia coli Membranes Reveal Critical Lipid Headgroup Size for Protein Function. J. Biol. Chem. *284*, 954–965.

Williamson, I.M., Alvis, S.J., East, J.M., and Lee, A.G. (2002). Interactions of phospholipids with the potassium channel KcsA. Biophys. J. *83*, 2026–2038.

Wimley, W.C., and White, S.H. (1996). Experimentally determined hydrophobicity scale for proteins at membrane interfaces. Nat. Struct. Biol. *3*, 842–848.

Wimley, W.C., Creamer, T.P., and White, S.H. (1996). Solvation energies of amino acid side chains and backbone in a family of host-guest pentapeptides. Biochemistry (Mosc.) *35*, 5109–5124.

Wittig, I., and Schägger, H. (2005). Advantages and limitations of clear-native PAGE. PROTEOMICS *5*, 4338–4346.

Wittig, I., Karas, M., and Schägger, H. High Resolution Clear Native Electrophoresis for In-gel Functional Assays and Fluorescence Studies of Membrane Protein Complexes.

Wu, Y., Sui, S.-F., and Wu, Y. (1999). Conformational changes of urea-denatured colicin E1 induced by phospholipid membranes. J. Pept. Res. *53*, 477–485.

Yu, D., Wowor, A.J., Cole, J.L., and Kendall, D.A. (2013). Defining the Escherichia coli SecA Dimer Interface Residues through In Vivo Site-Specific Photo-Cross-Linking. J. Bacteriol. *195*, 2817–2825.

Zakharov, S.D., and Cramer, W.A. (2002a). Insertion intermediates of pore-forming colicins in membrane two-dimensional space. Biochimie *84*, 465–475.

Zakharov, S.D., and Cramer, W.A. (2002b). Colicin crystal structures: pathways and mechanisms for colicin insertion into membranes. Biochim. Biophys. Acta BBA - Biomembr. *1565*, 333–346.

Zakharov, S.D., Rokitskaya, T.I., Shapovalov, V.L., Antonenko, Y.N., and Cramer, W.A. (2002). Tuning the membrane surface potential for efficient toxin import. Proc. Natl. Acad. Sci. *99*, 8654–8659.

Zakharov, S.D., Eroukova, V.Y., Rokitskaya, T.I., Zhalnina, M.V., Sharma, O., Loll, P.J., Zgurskaya, H.I., Antonenko, Y.N., and Cramer, W.A. (2004). Colicin Occlusion of OmpF and TolC Channels: Outer Membrane Translocons for Colicin Import. Biophys. J. *87*, 3901–3911.

Zakharov, S.D., Sharma, O., Zhalnina, M.V., and Cramer, W.A. (2008). Primary Events in the Colicin Translocon: FRET Analysis of Colicin Unfolding Initiated by Binding to BtuB and OmpF. Biochemistry (Mosc.) *47*, 12802–12809.

Zhang, Y.L., and Cramer, W.A. (1992). Constraints imposed by protease accessibility on the trans-membrane and surface topography of the colicin E1 ion channel. Protein Sci. Publ. Protein Soc. *1*, 1666–1676.

Zhang, Y.L., and Cramer, W.A. (1993). Intramembrane helix-helix interactions as the basis of inhibition of the colicin E1 ion channel by its immunity protein. J. Biol. Chem. *268*, 10176–10184.

Zhang, X.Y.-Z., Lloubès, R., and Duché, D. (2010a). Channel Domain of Colicin A Modifies the Dimeric Organization of Its Immunity Protein. J. Biol. Chem. *285*, 38053–38061.

Zhang, Y., Li, C., Vankemmelbeke, M.N., Bardelang, P., Paoli, M., Penfold, C.N., and James, R. (2010b). The crystal structure of the TolB box of colicin A in complex with TolB reveals important differences in the recruitment of the common TolB translocation portal used by group A colicins. Mol. Microbiol. *75*, 623–636.

Zoonens, M., Comer, J., Masscheleyn, S., Pebay-Peyroula, E., Chipot, C., Miroux, B., and Dehez, F. (2013). Dangerous Liaisons between Detergents and Membrane Proteins. The Case of Mitochondrial Uncoupling Protein 2. J. Am. Chem. Soc. *135*, 15174–15182.